Modelling Carbonate and Sulphide Scales in Sour Systems

Giulia Ness

Submitted for the degree of Doctor of Philosophy

Heriot-Watt University

Institute of Petroleum Engineering

School of Energy, Geoscience, Infrastructure and Society

September 2019

ABSTRACT

Carbonate and sulphide scales are pH-dependent inorganic deposits that often form in oil and gas wells posing a significant threat to production efficiency, system integrity, fluid quality and production safety. Despite the frequent occurrence of these scales, their prediction and mitigation still present numerous challenges, particularly in the case of sulphides. This work is aimed at laying out and addressing these challenges to ultimately improve field scale management programs.

Carbonate and sulphide scales are directly coupled together and differ from other inorganic scales because they are intimately linked to the in-situ concentration of carbon dioxide (CO_2) and hydrogen sulphide (H_2S), which influence the local pH and availability of reactive species.

Pressure-volume-temperature (PVT) and scale prediction calculations must be combined to accurately model three phase component distributions and to determine the scaling risk profile from reservoir to separator conditions. Although some commercial software integrates these two sets of calculations, these packages are usually more targeted to one or the other applications; i.e. either oil/gas PVT or aqueous phase chemistry.

This work defines a rigorous step-by-step procedure (workflow) which allows us to obtain carbonate and sulphide scale prediction profiles from commonly available field data using any choice of PVT and scale prediction software. The capability of decoupling PVT and scale prediction software offered by this workflow (as opposed to using an integrated software package) enabled a thorough study of the impact of field measurements and software choice on the final pH-dependent scale prediction results.

The newly developed workflow was also applied to two real field case scenarios to show how it can be used to answer key operational questions.

To my husband Paul.

AKNOWLEDGMENTS

The last four years have certainly been the happiest and most intense years of my life, rich of life changing events.

During this time, Professor Ken Sorbie was a lot more than just a PhD supervisor. Ken offered me the perfect PhD project, allowed me to tap into his deep knowledge and wisdom, challenged me to achieve greater results, supported me when I most needed it and created a work environment which allowed me to succeed professionally whilst pursuing my dream to build a family. For this I am deeply grateful. It has been an honour to be one of his students and I am truly thankful for all he has done for me.

A special thank you goes to Professor Eric MacKay for all his support and encouragement during these years. The outstanding team Ken and Eric have built is a reflection of the great men they are.

Although it will be a long time before she can read this, I want to thank my daughter Rebecca for being such a good baby and allowing me to get plenty of sleep during the writing up phase. You are my sunshine.

Finally, my deepest gratitude goes to my husband who is also my greatest supporter of all. Paul believed in me when I did not, he patiently put up with the challenges of a commuting partner, he somehow managed the emotional highs and lows of his Italian wife and provided relentless support, patience and love during this time. Paul, this PhD thesis is as much yours as it is mine.

“Whatever is good and perfect is a gift coming down to us from God our Father, who created all the lights in the heavens.” James 1:17.

Research Thesis Submission

Name*:*			
School:			
Version: *(i.e. First, Resubmission, Final)*		Degree Sought:	

Declaration

In accordance with the appropriate regulations I hereby submit my thesis **and I** declare that:

1. The thesis embodies the results of my own work and has been composed by myself
2. Where appropriate, I have made acknowledgement of the work of others
3. The thesis is the correct version for submission and is the same version as any electronic versions submitted*.
4. My thesis for the award referred to, deposited in the Heriot-Watt University Library, should be made available for loan or photocopying and be available via the Institutional Repository, subject to such conditions as the Librarian may require
5. I understand that as a student of the University I am required to abide by the Regulations of the University and to conform to its discipline.
6. I confirm that the thesis has been verified against plagiarism via an approved plagiarism detection application e.g. Turnitin.

* *Please note that it is the responsibility of the candidate to ensure that the correct version of the thesis is submitted.*

Signature of Candidate*:*		Date:	

Submission

Submitted By *(name in capitals):*	
Signature of Individual Submitting:	
Date Submitted:	

For Completion in the Student Service Centre (SSC)

Limited Access	Requested	Yes		No		Approved	Yes		No	
E-thesis Submitted (mandatory for final theses)										
Received in the SSC by *(name in capitals):*				Date:						

TABLE OF CONTENTS

NOMENCLATURE

Capital Letters

ANP	Alba Northern Platform
API	American Petroleum Institute
BOPD	Barrel Oil Per Day
BS&W	Basic Sediment and Water
BWPD	Barrel Water Per Day
C_0	Total Initial Charge
C_i	Concentration of Component *i*
CPA	Cubic Plus Association
EOS	Equation of State
FVF	Formation Volume Factor
FW	Formation Water
GOR	Gas Oil Ratio
GWR	Gas Water Ratio
H	Henry's Constant
HA	General Organic Acid
HWU	Heriot-Watt University
ICP	Inductively Coupled Plasma
IW	Injection Water
K_{GO}	Gas/Oil Partition Coefficient
K_{GW}	Gas/Water Partition Coefficient
K_i	Thermodynamic Equilibrium Constant
K_{ij}	Binary Interaction Coefficients
K_{OW}	Oil/Water Partition Coefficient
K_{sp}	Solubility Product
$K_{VL,i}$	Vapour/Liquid Partition Coefficient of Component *i*
MDI	Maximum Dissolved Iron
M_i	Mass Component *i*
MSE	Check SCALECHEM
MW	Molecular Weight
NACE	National Association of Corrosion Engineers
OIW	Oil in Water
PI	Productivity Index
PVT	Pressure-Volume-Temperature
PW	Produced Water
Q_i	Produced Water Rate
ROV	Relative Oil Volume
SG	Standard Gravity
SI	Scaling Index
SRB	Sulphate Reducing Bacteria
SRK	Reddlich-Kwong Equation of State modified by Soave
SRK	Saturation Ratio
SW	Sea Water

T	Temperature
T_c	Critical Temperature
VLE	Vapour Liquid Equilibrium
WAG	Water Alternating Gas
Z	Compressibility Factor

Lower Case Letters

a_i	Activity of component i
eH	Oxidation/reduction potential
f_i	fugacity of component i
k_1	Rate Constant
m_i	Molarity of component i
p	Pressure
p_c	Critical Pressure
w_i	Molar fraction of component i in water phase
x_i	Molar fraction of component i in oil phase
y_i	Molar fraction of component i in gas phase
z_i	Molar fraction of component i in mixed feed

Greek Letters

β	Vapour mole fraction
β_2	Stability Constant
γ_i	Activity coefficient of component i
φ_i	Fugacity coefficient of component i

LISTS OF TABLES

LIST OF FIGURES

PUBLICATIONS

Peer-Reviewed Publications

Ness, G., K. S. Sorbie. 2018. The Impact of Field Measurements and Data Handling Procedures on Carbonate and Sulphide Scale Predictions. SPE Production & Operations.

Verri, G. et al. 2017. Iron Sulphide Scale Management in High H_2S and CO_2 Carbonate Reservoirs. SPE Production & Operations 32 (03): 305-313.

Verri, G., K. S. Sorbie, D. Silva. 2017. A rigorous general workflow for accurate prediction of carbonate and sulphide scaling profiles in oil and gas wells. Journal of Petroleum Science and Engineering 156: 673-681.

Verri, G. et al. 2017. A New Approach to Combined Sulphide and Carbonate Scale Predictions Applied to Different Field Scenarios. SPE Production & Operations.

Conference Papers

Ness, G. et al. 2019. The Impact of H2S on Carbonate Scaling risk. A Field Case Study. Proc., SPE International Conference on Oilfield Chemistry, Galveston, TX, SPE-193583-MS.

Ness, G., K. S. Sorbie. 2018. Rigorous Carbonate and Sulphide Scale Predictions: What Really Matters? Proc., SPE International Oilfield Scale Conference and Exhibition, Aberdeen, Scotland, UK, SPE-190726-MS. **KEYNOTE**

Ness, G., K. S. Sorbie. 2018. Carbonate and Sulphide Scale Predictions in Oil and Gas Wells. Proc., Oilfield Chemistry Symposium, Geilo, Norway.

Verri, G., K. S. Sorbie. 2017. The Impact of Field Measurements, Data Handling Procedures and Software Selection on Carbonate and Sulphide Scale Predictions. Proc., SPE Symposium: Production Enhancement and Cost Optimisation, Kuala Lumpur, Malaysia, SPE-189218-MS.

Verri, G., K. S. Sorbie. 2017. Iron Sources in Sour Wells: Reservoir Fluids or Corrosion? Proc., NACE Corrosion, New Orleans, USA, C2017-8998.

Verri, G. et al. 2017. A New Approach to Combined Sulphide and Carbonate Scale Predictions Applied to Different Field Scenarios. Proc., SPE International Conference on Oilfield Chemistry, Montgomery, Texas, USA, SPE-184514-MS.

Conference Posters

Ness, G., K. S. Sorbie 2017. The Impact of Reservoir Souring on Calcium Carbonate Scaling Risk. London, UK: Energy Institute.

Verri, G. et al. 2016. Iron Sulphide Scale Management in High H_2S and CO_2 Carbonate Reservoirs. Proc., SPE International Oilfield Scale Conference and Exhibition, Aberdeen, Scotland, UK, SPE-179871-MS.

Chapter 1 – INTRODUCTION

1.1 OILFIELD SCALE BACKGROUND

Produced water from oil and gas wells contains a variety of minerals which can be dissolved at given conditions or precipitate out if the solution becomes supersaturated. The precipitation of these ions is called mineral scale deposition. This process depends on the aqueous fluid composition and also on temperature, pressure and solution pH. Mineral scale formation is one of the key flow assurance challenges in oil and gas production and operations. Dissolved minerals that are in equilibrium at reservoir conditions before being produced, can precipitate as inorganic scale in the production system due to mixing of incompatible fluids (e.g. well producing from two different zones with two different water compositions), because of changes in temperature and pressure (also called auto-scaling) or because of water evaporation which concentrates ions in solution causing super saturation conditions (Vetter and Farone, 1987, Jasinski et al., 1998, Olajire, 2015).

The formation of scale deep in the reservoir is not considered a problem in oil and gas production and operations. However, scale deposition in the near wellbore region, injection or production tubing, topside equipment etc. poses a significant threat to production efficiency since it can cause near-well formation damage, flow restrictions, solids accumulation in vessels, fluid quality problems and in some scenarios it can be a threat to safe production and operations.

Common oilfield scales can be classified as “pH-independent” or “pH-dependent” scales (Olajire, 2015). The first category includes sulphates, principally barium, strontium, and calcium sulphate, while the second category refers mainly to carbonate

and sulphide scales. The main focus of this research is on pH-dependent carbonate and sulphide scales which include calcium carbonate ($CaCO_3$), iron carbonate ($FeCO_3$) and iron sulphide (FeS).

The two strategies used to address oilfield scale problems are scale prevention and scale removal. Prior to designing a control strategy for oilfield scales, it is important to establish if scale is indeed present in the system, where in the production system it may deposit and what impact it has on production. This information is required to establish what approach should be taken to prevent and/or remove scale and what results can be expected once the treatment is implemented.

Some of the main questions to answer prior to designing a treatment for oilfield scales include:

- What type of scale has formed or is predicted to form and at what level of "severity"?
- Where is the scale forming/predicted to form (tubing, wellhead, chokes, topside equipment)?
- What problems is it causing (i.e. corrosion, flow restrictions, water quality, O/W separation, well plugging)?
- Given the well completions and configuration of the production system, what options are available for removal/prevention of these pH dependent scales?

1.2 pH DEPENDENT SCALES

Unlike other types of inorganic scales, carbonates and sulphides are directly associated with the in-situ concentrations of acid gases such as carbon dioxide (CO_2) and hydrogen

sulphide (H_2S), which both influence the local pH and the availability of reactive species. Hence, predicting the formation of pH- dependent scales requires a full calculation of all hydrocarbon and aqueous phases present to determine the distribution and speciation of CO_2 and H_2S in the system. This is done by combining pressure/volume/temperature (PVT) calculations with an aqueous phase model to describe aqueous phase chemical reactions.

Several commercially available software packages combine PVT calculations with aqueous phase scale prediction models, but such packages are more targeted to aqueous systems and have very limited hydrocarbon capabilities. Likewise, PVT modelling software focusing on the hydrocarbon phase does not usually fully model the aqueous phase or can only predict a limited number of scales/complexes. Moreover, within each type of software it is often possible to select a large number of different Equations of State (EOS), activity models, equilibrium parameters etc., which may ultimately impact the final carbonate and sulphide scale prediction profile.

The equations describing the carbonate/sulphide coupled system have been known for a long time but there remain some critical challenges in the prediction of pH dependent scales which are addressed here.

This was work originally focused on the study of iron sulphide (FeS) scale formation and the challenges associated with FeS scale predictions in oil and gas wells, and this is why a large section of this chapter refers to iron sulphide scale. However, it soon became evident that pH dependent scales are strongly linked together and one cannot be studied in isolation when dealing with real field scenarios. Hence, carbonate scales had to be included in the research work to improve sulphide scale predictions since the level of CO_2 in the aqueous phase is the main determinant of pH. At the start of this work, it

was assumed that carrying out carbonate scale predictions was a well-established and routinely practiced activity and that clear methods to run these calculations were available in the literature. This turned out ***not*** to be the case and it was clear that there was still much confusion on both carbonate and sulphide scale predictions. In order to improve iron sulphide scale predictions, it was necessary to improve ***carbonate*** scale predictions first and this is why the calculations and field studies described in this work largely refer to carbonate scale.

1.3 OBJECTIVES

The long term goal of this project is to obtain reliable carbonate and sulphide scale predictions which allow to implement the correct scale management strategy and prevent or reduce scale related problems in oil and gas operations.

To achieve this goal, the two main objectives of this work are (i) to define and address the key challenges associated with carbonate and sulphide scale predictions, and (ii) to apply these new findings to real field scenarios in order to improve the scale management program.

It emerged from this work that there are three key categories of data and procedures that must be correctly gathered and used in order to obtain reliable carbonate and sulphide scale predictions:

- ✓ Data handling procedures;
- ✓ Field Measurements;
- ✓ Software, equations and parameters choice.

To address the problem of using commonly available field data to correctly calculate scale prediction profiles (data handling procedures challenge), a rigorous scale prediction workflow was developed (Chapter 3); this will later be referred to as the "Heriot-Watt University (HWU) scale prediction workflow". This general workflow for carbonate and sulphide scale predictions can be applied using *any* commercial PVT and *any* scale prediction software. However, like all software and procedures it provides more reliable results when users have a good understating of the data and equations that are used. Critical judgment of output data is also needed when using even the more established commercial packages as errors and inaccuracies may be hidden inside "black box" software. The HWU scale prediction workflow was validated by taking a perfect numerical example where "the answer" was known and then reconstructed the full topside-downhole-topside scaling calculation cycle to obtain the (known) scaling profile.

The Heriot-Watt scale prediction workflow was applied to two different field scenarios (a Middle East gas/condensate well (Chapter 4) and a North Sea oil well (Chapter 5)) to demonstrate how this rigorous procedure is a fundamental tool for reliable carbonate and sulphide scale predictions. The results obtained help explain important field findings and answer key questions related to the scale management program of these wells.

The impact of errors or uncertainty of field measurements was investigated by running sensitivity studies in a wide range of scenarios to establish which field data is truly critical in carbonate and sulphide scale predictions. This is described in Chapter 6.

In addition, the effect of choosing different software, equations and parameters for carbonate and sulphide scale predictions was investigated and is described in Chapter 7.

Finally, a summary of the whole thesis and a number of research issues for future work are proposed in Chapter 8.

Chapter 2– LITERATURE REVIEW

2.1 CARBONATE AND SULPHIDE SCALES IN OIL AND GAS SYSTEMS

2.1.1 Calcium Carbonate Scale Formation Mechanism

Calcium carbonate scale ($CaCO_3$) is one of the most common types of inorganic deposits found in oil and gas production (Vetter and Farone, 1987). The precipitation of $CaCO_3$ can be caused by two different mechanisms:

- mixing of incompatible fluids in the wellbore or topside;
- "auto-scaling process" where changes in temperature and pressure in the system cause a change in dissolved acid gases concentration and create a scale forming environment.

The chemical equations (in the aqueous phase) that govern the formation of calcium carbonate are shown in Equation (2.1) through (2.5).

$$H_2O \leftrightarrow OH^- + H^+ \tag{2.1}$$

$$CO_2 + H_2O \leftrightarrow H_2CO_3 \tag{2.2}$$

$$H_2CO_3 \leftrightarrow H^+ + HCO_3^- \tag{2.3}$$

$$HCO_3^- \leftrightarrow CO_3^{2-} + H^+ \tag{2.4}$$

$$Ca^{2+} + CO_3^{2-} \rightarrow CaCO_3(s) \tag{2.5}$$

These equations clearly show how the concentration of carbonates CO_3^{2-} and consequently the precipitation of carbonate scale is influenced by pH. The more

dissolved CO_2 in the system, the lower the pH and amount of $CaCO_3$ precipitate. If other pH dependent species such as H_2S and organic acids are introduced in the system they will also influence carbonate scale precipitation and this is described in Section 2.2.

Calcium carbonate ($CaCO_3$) is one of the most important scale forming minerals in oil and gas production. Most reservoir waters contain relatively high concentrations of Ca^{2+} and whilst these are in equilibrium with the dissolved CO_2 at reservoir temperature and pressure. However, depressurisation of the system when fluids are produced causes CO_2 loss (to other phases, gas and oil), pH increases and consequently $CaCO_3$ precipitation occurs. Tertiary recovery techniques such as CO_2 water alternating gas (WAG) can make this issue far greater by lowering the reservoir fluids pH and dissolving more carbonates at reservoir temperature and pressure which will precipitate once they enter the producing well (Silva, 2017).

There are three main anhydrous crystalline polymorphs of calcium carbonate and these are: calcite, aragonite and vaterite.

Vaterite is some 2.5 times more soluble in water than aragonite and 3.7 times more soluble than calcite. Consequently during normal scale formation there is no driving tendency to vaterite precipitation and calcite is the commonly observed form (Brankling et al., 2001). Although calcite has the greatest thermodynamic stability at ambient conditions, the thermodynamically less stable aragonite and/or vaterite may be stabilised under certain conditions of temperature and in the presence of other ions (Friedman and Schultz, 1994). For example, the presence of magnesium ion favours the precipitation of aragonite instead of calcite (Nancollas and Sawada, 1982).

The solubility product defined in Equation (2.6) (where $[Ca^{2+}]$ and $[CO_3^{2-}]$ are the concentrations of calcium and carbonate respectively) is shown in Figure 2.1 for calcite, aragonite and vaterite (Krauskopf, 1995). The temperature dependence of the calcite solubility product is also shown in Equation (2.7) where *t* is the temperature in Celsius (Panthi, 2003).

$$K_{sp(CaCO_3)} = [Ca^{2+}] \times [CO_3^{2-}] \tag{2.6}$$

$$pK_{sp(CaCO_3)} = 0.01183 \times t + 8.03 \tag{2.7}$$

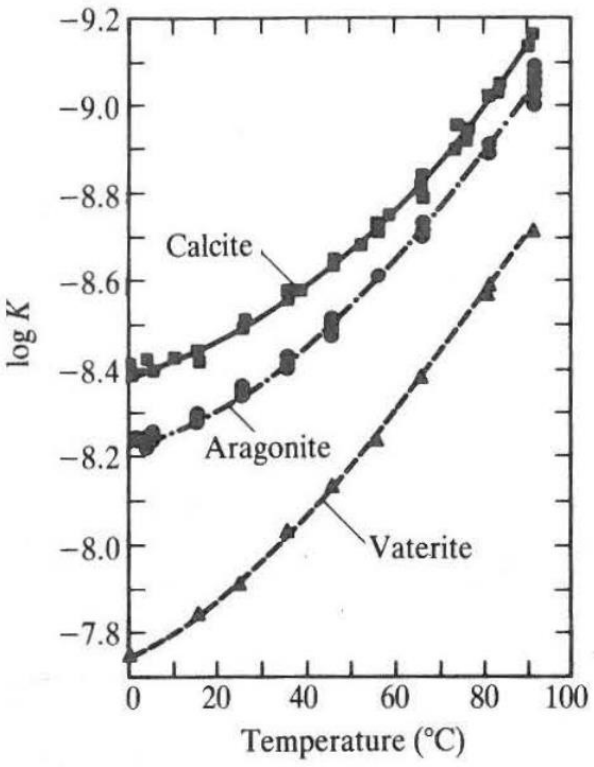

Figure 2.1: Change with temperature of the solubility products of three polymorphs of $CaCO_3$.

Unlike iron sulphide, calcium carbonate scale has been widely investigated in the context of oil and gas operations and many field studies are available in the literature. The reason for including calcium carbonate (and iron carbonate) in this research work is

because all pH dependent scales must be studied together but iron sulphide is the main focus of this research and so the literature review will focus mainly on this type of scale.

2.1.2 Iron Carbonate Scale (Siderite)

Iron carbonate is included in this study as it is a pH dependent scale like calcium carbonate and iron sulphide. The formation of iron carbonate is shown in Equation (2.8).

$$Fe^{2+} + CO_3^{2-} \rightarrow FeCO_{3(s)} \qquad (2.8)$$

Although iron carbonate is part of this study for completeness and all the scale prediction software used include calculations for $FeCO_3$, none of the scenarios investigated in the field examples studied show $FeCO_3$ precipitation. This is because the compositional "window" for iron carbonate formation in sour systems is very limited.

In a sour system containing Fe^{2+} if the water pH is sufficiently high to precipitate $CaCO_3$, FeS will also precipitate. In the same system, iron carbonate precipitates only when $H_2S_{(aq)}$ is the limiting reagent in FeS formation. If Fe^{2+} is the limiting reagent, it will also be consumed as FeS and $FeCO_3$ will not form. This is shown in a general example in Figure 2.2 where the initial Fe^{2+}=100 mg/l at 65°C and 10 bar and the total dissolved sulphides vary to show when different scales form.

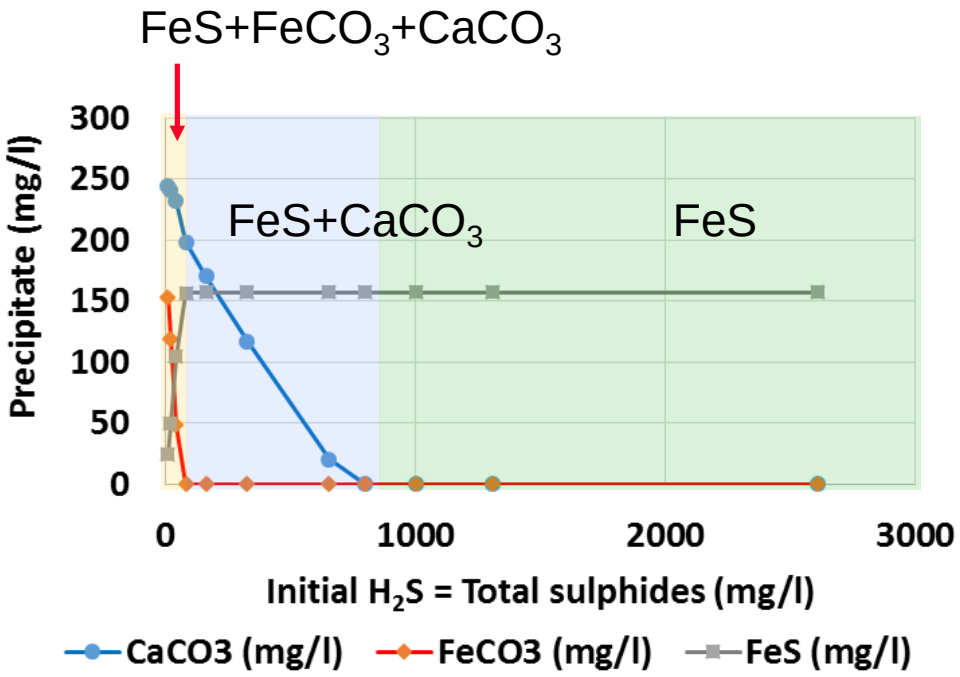

Figure 2.2: Example of $FeS+FeCO_3+CaCO_3$ co-precipitation at 65°C and 10 bar.

Although these conclusions are based on thermodynamics only, the kinetics of FeS precipitation are very fast (see Section 2.1.4) and do not change the outcome of this combined scale precipitation (Woollam et al., 2011, Sun et al., 2006).

2.1.3 Iron Sulphide Scale Formation Mechanism

Unlike carbonate scales which are a common type of inorganic deposit in oil and gas wells and have been widely researched in the past decades, sulphide scales in the oilfield used to be referred to as "exotic scale" due to their less prominent presence in oilfield environments. However, in recent years, sulphide scales – in particular iron sulphide (FeS) - have become a much more routinely reported type of deposit in many fields and this can be attributed to a number of factors as follows:

- Secondary and tertiary recovery methods are being applied in aging fields to improve overall productivity. These methods often involve injection of water (liquid or steam) which stimulates the proliferation of sulphate reducing bacteria

(SRBs) in various regions of the reservoir. These bacteria are responsible for biogenic souring (H_2S generation by SRBs).

- New high pressure, temperature and salinity fields (HP/HT/HS) present significant challenges including the presence of high levels of Fe, Zn and Pb in the reservoir fluids. These can precipitate to form FeS, ZnS and PbS, even in the presence of low levels of H_2S posing a threat to well productivity and system integrity.

- Development of shale gas and oil requires hydraulic fracturing of well ("frakking") which is achieved by pumping very large volumes of water in the well at pressure above fracture pressure. This water can be treated but normally still carries a number of contaminants which can cause near wellbore and formation souring.

- The more strict environmental regulations around the globe have made safe water disposal and water recycling a key focus for the industry. Re-injecting produced water (PWRI) can posed a real threat to injectors and disposal wells both in terms of H_2S and solids generation and formation damage.

Iron sulphide scale forms from the reaction between hydrogen sulphide and ferrous iron. In sour systems, iron is normally only present as Fe^{2+} because of the highly reducing conditions (low Eh) in an oil reservoir. In oxidising environments (high Eh), Fe^{3+} would be formed which would react with H_2S to form elemental sulphur (Amend et al., 2004).

The formation of a generic FeS species can be represented by Equation (2.9), (2.10) or (2.11) which are linked through the H_2S speciation equations (see Section 2.2.2).

$$Fe^{2+} + S^{2-} \rightarrow FeS\,(s) \quad (2.9)$$

$$Fe^{2+} + HS^{-} \rightarrow FeS \downarrow + H^{+} \quad (2.10)$$

$$Fe^{2+} + H_2S \rightarrow FeS \downarrow + 2H^{+} \quad (2.11)$$

As with many other crystalline materials, "iron sulphide" has a number of natural polymorphic forms some with rather different stoichiometry. *However, the complexity of iron sulphide formation reactions and the limited data available makes it a controversial topic of discussion among oilfield chemists. Therefore a more detailed review on this subject is provided here.*

Several iron sulphide forms can be present in oilfield scale deposits each with variable solubility in acid. The more common iron sulphide species and their main characteristics are listed in Table 2.1.

Parameter	***Mackinawite***	***Marcasite***	***Pyrite***	***Pyrrhotite***	***Troilite***	***Greigite***
Chemical Formula	Fe_9S_8	FeS_2	FeS_2	Fe_7S_8	FeS	Fe_3S_4
Crystalline Structure	Tetragonal	Orthorhombic	Cubic	Monoclinic	Hexagonal	Cubic
Colour	Bronzy	Tin-White	Brassy Yellow	Bronze Yellow	Light Greyish	-
Hardness	Soft	6-6.5	6-6.5	3.5-4.5	3.5-4.5	-
Density (g/cm3)	4.30	4.875	5.013	4.69	4.85	-
Solubility in Acids	Fast	Slow and difficult	Slow and difficult	Moderate	Rapid and easy	-

Table 2.1: Iron sulphide species common in the oil industry and their solubility in mineral acid (Nasr-El-Din and Al-Humaidan, 2001, Rickard and Luther, 2007).

It is thought that the first iron sulphide scale formed under oilfield conditions is a nano-particulate phase of disordered mackinawite (Wolthers et al., 2005).

A study of iron monosulphide (FeS) formation has shown that in the first few seconds of the reaction an intermediate product/cluster forms as a precursor to condensed iron sulphide structures. Different clusters such as $FeSH^+$ have been identified but it is not clear precisely which one forms under different conditions (Lewis, 2010).

The first condensed iron sulphide phase to form from aqueous Fe-S clusters is mackinawite (FeS) (Rickard and Luther, 2007). There has been much debate regarding the precursor form of crystallised mackinawite. In the past, researchers reported the formation of a precursor amorphous phase to crystalline mackinawite which transforms into crystalline mackinawite after a few days of exposure to an H_2S environment (Rickard, 1989). However, more recent work shows that the first iron sulphide precipitate is a phase which has been described as “disordered mackinawite” and it is not amorphous but has a nanocrystalline structure, 2-5nm in size with long range tetragonal order (Wolthers et al., 2005). Extended X-Ray absorption fine structure (EXAFS) and rapid flow techniques show that this material develops after 1-10ms after mixing cation and anion solutions (Rickard and Luther, 2007). Disordered mackinawite is potentially electroactive but its size poses a challenge to the differentiation between clusters, dissolved complexes and nanoparticles.

The overall proposed process of mackinawite formation is shown in Figure 2.3 although the times shown are temperature dependent.

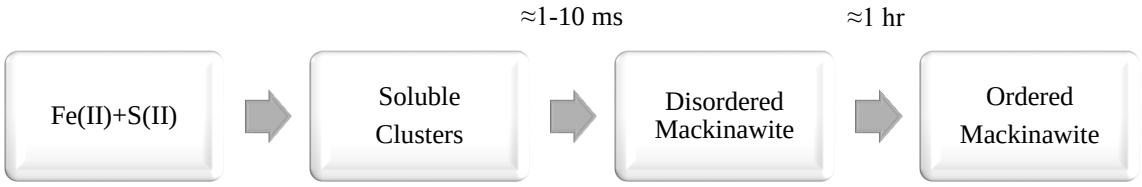

Figure 2.3: Proposed process of mackinawite formation (Rickard and Luther, 2007)

The structure of freshly precipitated material is very sensitive to small changes in pH, minor amounts of atmospheric oxygen and slight oxidation during freeze-drying. This material is also fine grained and aggregated making it difficult to characterise (Csákberényi-Malasics et al., 2012).

Pyrite (cubic FeS_2) is the most common sulphide mineral in Earth surface environments. Mackinawite is normally referred to as a precursor to pyrite formation. It could be a precursor in high Fe systems in the sense that it forms far more rapidly than pyrite. However, it is not a precursor in the sense that it is a *necessary* prerequisite for pyrite formation. It has also been demonstrated that the transformation from mackinawite to pyrite is not a solid state transformation but a dissolution/precipitation mechanism (Rickard and Luther, 2007).

Mechanistically, it has been demonstrated that pyrite formation in low-temperature aqueous solution involves the formation of a dissolved [FeS] transition intermediate and that the suppression of such intermediates can inhibit pyrite formation. This is different from the soluble iron sulphide form described for mackinawite formation (Rickard and Luther, 2007).

Rickard and Luther (2007) describe in much detail the challenges associated with the study of pyrite formation and the specific conditions chosen for lab experiments. It is important to remember that the work they reviewed applies primarily to marine

environments and that conditions found in oil and gas systems are of course significantly different. Hence, the experimental results and understanding currently available are not sufficient to allow better predictions of pyrite formation in oil and gas systems.

Equations (2.9), (2.10), (2.11) describe the formation of a generic form of iron sulphide. However, a more specific mechanism proposed for the precipitation of iron sulphide suggests that Equation (2.10) competes with the reaction and condensation shown in Equation (2.12) (Rickard, 1995).

$$Fe^{2+} + 2HS^{-} = Fe(HS)_{2\,(s)} \rightarrow FeS_{(s)} + H_2S \qquad (2.12)$$

Although Rickard interprets the $Fe(HS)_2$ as a solid phase because it can be collected in the outflow of his experiments and because it supports the lack of evidence for $Fe(HS)_2$ complex in solution, there is no actual proof that $Fe(HS)_2$ is indeed a solid. Rickard & Luther (2007) later refer to this intermediate species as aqueous iron-sulphide complexes and suggest that the complex formed is $Fe(SH)^+$ rather than $Fe(HS)_2$ (Rickard and Luther, 2007).

Separate experimental findings suggest the same competing reaction mechanism with the formation of soluble iron sulphide species which are not pH dependant (Davison et al., 1999). The formation of such species would explain the experimental results shown in Figure 2.4 where Fe(II) represents the total concentration of soluble forms of iron.

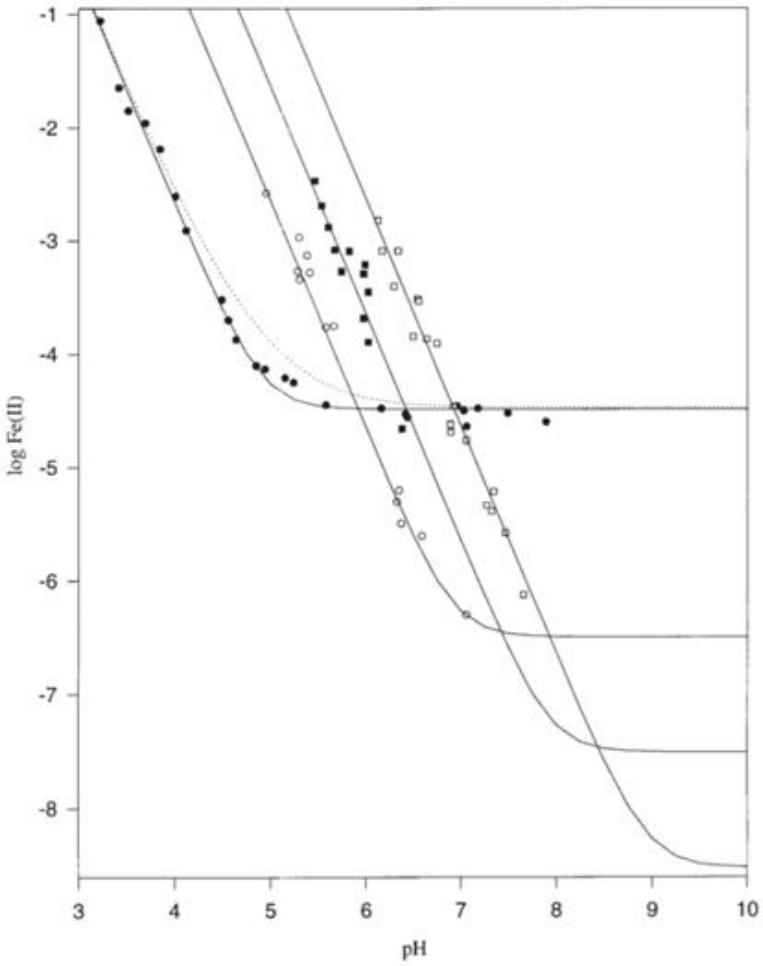

Figure 2.4: Plot of log Fe(II) vs pH at 20C for partial pressure of H2S 0.1MPa (black dot), 0.00097MPa (white dot), 0.000095MPa (black square) and 0.0000093MPa (white square). The solid lines are calculated using MINTEQ (Royal Institute of Technology, 2013).

For low H_2S partial pressures (0.001, 0.0001 and 0.00001 MPa) all the data lie on single lines with slopes of -2 indicating that the only soluble Fe(II) species present is Fe^{2+} because Fe^{2+} is directly proportional to $(aH^+)^2$ as per Equation (2.13) which shows the temperature dependence of the solubility product (K_{sp}) for Equation (2.11). This is also illustrated in Figure 2.5.

$$K_{sp} = \frac{[Fe^{2+}][H_2S]}{[H^+]^2} = 10^{\left(\frac{2848.779}{T_k}\right)-6.347} \qquad (2.13)$$

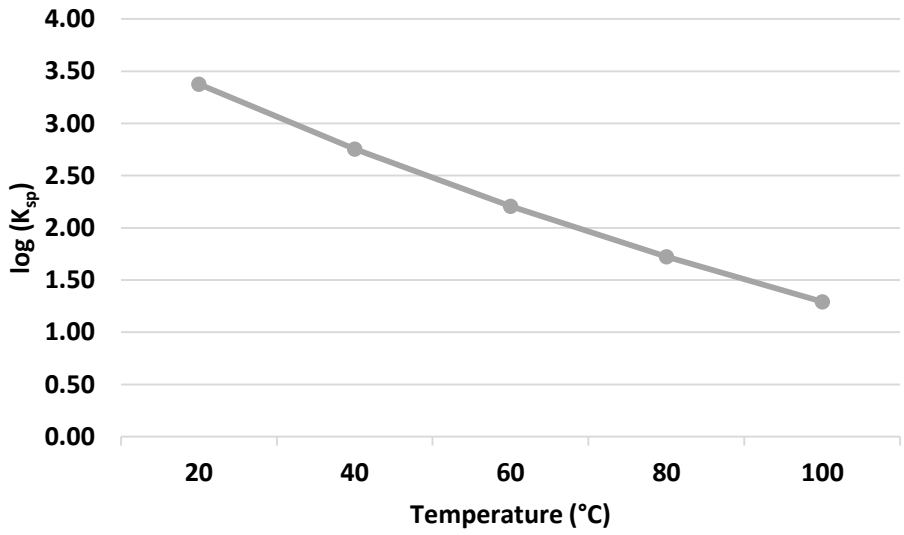

Figure 2.5: Temperature dependence of FeS solubility product.

At higher H_2S partial pressure (0.1MPa) this linearity is observed up to pH=4.7. Above this pH the measured concentration of soluble iron Fe(II) is independent of pH suggesting that a dissolved iron sulphide species is forming. $Fe(HS)_2$ could be the species causing this behaviour but others are also proposed as potential soluble forms of iron sulphide (also proposed $Fe(HS)^+$). The formation of $Fe(HS)_2$ can be represented by the cumulative stability constant β_2 as per Equation (2.14).

$$\beta_2 = \frac{[Fe(HS)_2]}{[Fe^{2+}][HS^-]^2} \qquad (2.14)$$

When solving Equation (2.14) together with the set of equations described in Section 2.2, it is possible to qualitatively reproduce the experimental results shown above. This is shown in Figure 2.6 where the variation of Total Fe(II), Fe^{2+} and $Fe(HS)_2$ with pH is plotted for a system at 20°C and H_2S = 0.1 MPa (corresponding to ≈3900 ppm total sulphides in water).

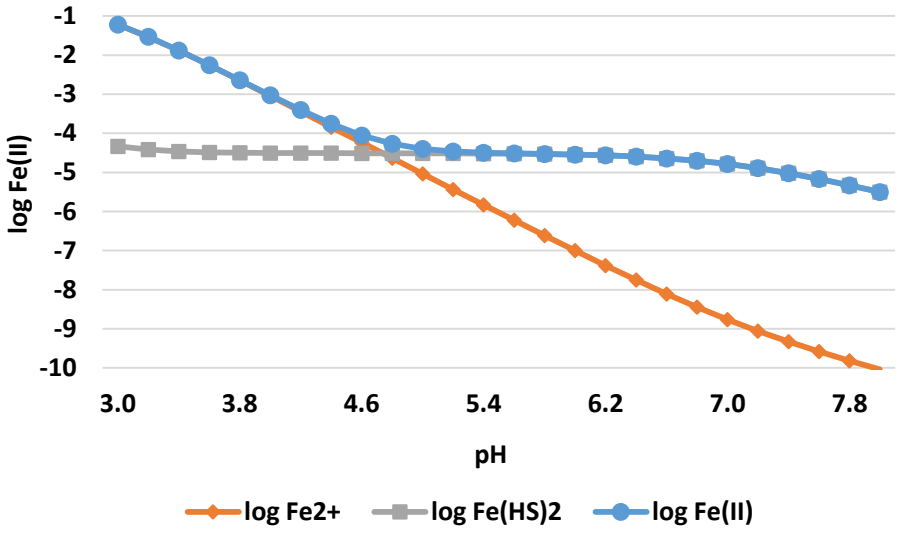

Figure 2.6: Concentration of Fe(II), Fe^{2+} and $Fe(HS)_2$ at variable pH at 20°C and H_2S = 0.1MPa.

The trend corresponding to the total Fe(II) for pH=3-6 seems to match the experimental results of Figure 2.4 well. However, at higher pH a second drop in Fe(II) levels is predicted suggesting that a pH dependent form of iron sulphide is precipitating again. Looking carefully at the 0.1MPa results in Figure 2.4, it can be seen that the last two experimental points seem to depart from the predicted horizontal line as seen in Figure 2.6. However, the data currently available is not sufficient to validate these calculations.

The presence of soluble iron sulphide species poses some important challenges in sulphide scale predictions.

The first challenge is associated with the uncertainty around the chemical equations that regulate soluble iron sulphide formation. What species form and what is their equilibrium constant? If this information was available and reliable it could be readily implemented in a scale prediction software to account for these species. Some commercial software already have this capability (e.g. ScaleChem predicts the formation of $FeSH^+$) but the reliability of the thermodynamic data supporting these predictions is dependent upon good experimental data which is still limited.

Another challenge is related to the analysis of dissolved iron in dissolved waters. It has already been discussed how sampling and analysis of Fe^{2+} in sour waters can be highly unreliable (NACE, 2012) but the presence of dissolved iron sulphide species poses an additional problem to this measurements. Just like colloidal FeS, iron that is present as soluble iron species would be measured as free iron Fe^{2+} in ICP measurements and wrongly used in scale predictions.

2.1.4 Kinetics of Iron Sulphide Scale Precipitation

The kinetics and mechanism of mackinawite formation in aqueous solutions at low temperatures is pH dependent and involves the two competing reactions shown in Equation (2.10) and (2.11) (Rickard and Luther, 2007).

For the reaction between Fe^{2+} and H_2S (Equation (2.11)), a rate constant log $k_1 = 7 \pm 1$ $l \cdot mol^{-1} \cdot s^{-1}$ is provided by Rickard and Luther (2007) for Equation (2.15) where $a_{Fe^{2+}}$ and a_{H_2S} are the activities of Fe^{2+} and H_2S respectively.

$$\frac{\partial FeS}{\partial t} = k_1 \times a_{Fe^{2+}} \times a_{H_2S} \tag{2.15}$$

At 25°C and low sulphide concentrations the kinetics of the first step shown in Equation (2.12) are described by Equation (2.16) (Rickard, 1995) where a_{HS^-} is the activity of HS^- and $k_2 = 10^{13}$ $l^2 \cdot mol^{-2} \cdot s^{-1}$:

$$\frac{\partial Fe(HS)_2}{\partial t} = k_2 \times a_{Fe^{2+}} \times a_{HS^-}^2 \tag{2.16}$$

The reaction between Fe^{2+} and H_2S in the H_2S pathway and the formation of $Fe(HS)_2$ in the bisulphide pathway are fast reactions and they are pH and sulphide concentration dependent. This is due to the speciation of H_2S at different pH described in Figure 2.7.

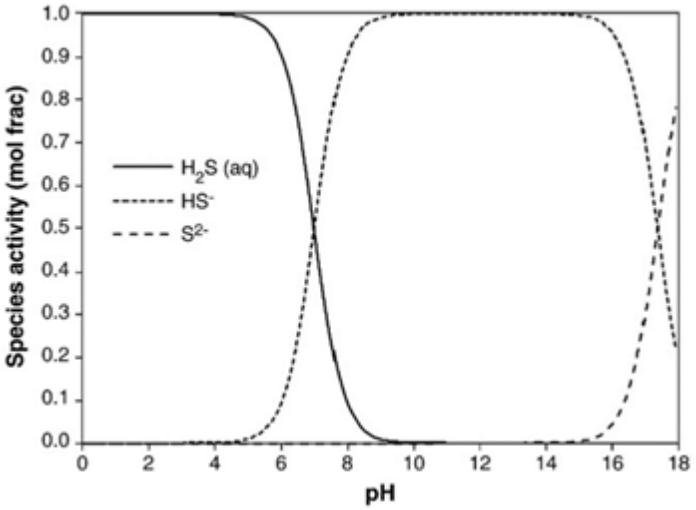

Figure 2.7: pH dependence of sulphide speciation. (Lewis, 2010).

The condensation of $Fe(HS)_2$ is a relatively slow reaction and probably not the only one that can occur. The presence of $Fe(HS)_2$ or other aqueous iron sulphide complexes may constitute an important factor for further reactions such as pyrite formation but this is still not clear and more studies are required.

Kinetic equations for the transformation of mackinawite to other crystalline forms are not available in the literature.

It is clear that the above information is far from sufficient to include kinetics in the prediction of iron sulphide precipitation. Scale prediction software as described in Section 2.2.2 are therefore limited to thermodynamic calculations and based on the above discussion on soluble iron sulphide species, these thermodynamic equations may also have some limitations.

2.1.5 Iron Sulphide Crystal Forms in Oil and Gas Wells

The nature of the iron sulphide scale deposit in a gas, oil or water well is dependent on multiple factors, and a number of observations on these deposits have been reported:

- **Well type.** Water wells show more dense and adhesive iron sulphide deposits which can protect the base metal from corrosion while gas wells normally have more porous and non-adhesive iron sulphide deposits which do not protect the base metal quite as efficiently (Nasr-El-Din and Al-Humaidan, 2001).

- **Scale aging**. Disordered Mackinawite is the first form of sulphide scale to form in aqueous environments and over time it may react to form more stable sulphide phases such as ordered mackinawite, greigite and ultimately pyrite or pyrrhotite. Aging of this scale and high temperatures change the reactivity of the scale which becomes more stable, sulphur rich and harder to remove (Wolthers et al., 2003).

- **Well depth**. An example of scale compositional changes with well depth is shown in Figure 2.8 (Wang et al., 2013a). However, these changes will be different for each well depending on H_2S and CO_2 partial pressures, temperature, flow regime and other factors which can change the in situ scale precipitation. In this example, scale thickness increases with well depth and iron sulphide scales are dominant at all depth above 9,300 ft. Pyrrhotite is the most abundant iron sulphide phase followed by troilite. The amount of mackinawite decreases with the well depth and is rarely found at depth >6,000 ft. Interestingly, siderite (FeCO3) was also present at all depths.

Depth	560 ft.	1280 ft.	2000 ft.	4000 ft.	6800 ft.	7560 ft.	9320 ft.
Iron Sulfides	86%	69%	72%	66%	75%	65%	0%
Mackinawite	*29%*	*24%*	*16%*	*2%*	*0%*	*1%*	*0%*
Pyrrhotite	*41%*	*28%*	*33%*	*60%*	*65%*	*58%*	*0%*
Troilite	*16%*	*13%*	*20%*	*4%*	*10%*	*6%*	*0%*
Gerigite	*0%*	*4%*	*3%*	*0%*	*0%*	*0%*	*0%*
Iron (Oxyhydr)Oxides	6%	10%	6%	4%	12%	16%	98%
Akaganeite	*6%*	*8%*	*6%*	*4%*	*8%*	*12%*	*82%*
Goethite	*0%*	*2%*	*0%*	*0%*	*0%*	*0%*	*0%*
Hibbingite	*0%*	*0%*	*0%*	*0%*	*4%*	*4%*	*16%*
Carbonates	8%	21%	22%	30%	13%	17%	0%
Siderite	*8%*	*21%*	*22%*	*8%*	*5%*	*5%*	*0%*
Aragonite	*0%*	*0%*	*0%*	*22%*	*8%*	*12%*	*0%*
Others	0%	0%	0%	0%	0%	2%	2%
Halite	*0%*	*0%*	*0%*	*0%*	*0%*	*2%*	*0%*
Rokuhnite	*0%*	*0%*	*0%*	*0%*	*0%*	*0%*	*2%*

Figure 2.8: Example of scale compositional changes at different well depth (Wang et al., 2013a).

- **Scale layer and mixed scale formation.** The scale composition varies from layers closer to the metal surface of the tubing to the scale in contact with the fluid stream. Normally sulphur rich scale dominates the outer layer in contact with the fluid stream while mackinawite is the main scale type in layers close to the metal surface. Different scale thickness is also found along the tubing. Figure 2.9 shows the appearance of scale near the pipe wall and on the flow side. A second important factor is the influence of other inorganic scales which can precipitate together with sulphides and form a heterogeneous deposit. Figure 2.10 gives an example of layered compositional changes at two well depths (Wang et al., 2013a). The layer next to the pipe consisted primarily of iron oxide (akaganeite). The flow side layers at 4,000 ft and 6,800 ft. had only pyrrhotite and troilite (sulphur rich iron sulphides). A small amount of mackinawite was also present in the middle layer at 4,000 ft.

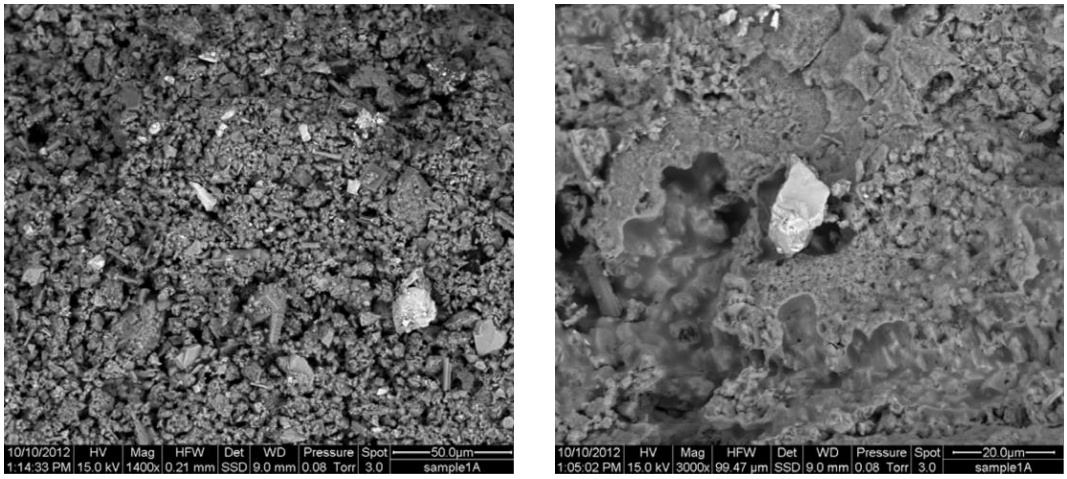

Figure 2.9: Composite scale appearance in the flow side (1) and the pipe side (2)

Depth	4000 ft.			6880 ft.		
Layer	Tube Side	Middle	Flow Side	Tube Side	Middle	Flow Side
Iron Sulfides	0%	88%	100%	0%	0%	100%
Mackinawite	*0%*	*6%*	*0%*	*0%*	*0%*	*0%*
Pyrrhotite	*0%*	*71%*	*92%*	*0%*	*0%*	*88%*
Troilite	*0%*	*11%*	*8%*	*0%*	*0%*	*12%*
Iron (Oxyhydr)Oxides	91%	0%	0%	78%	87%	0%
Akaganeite	*88%*	*0%*	*0%*	*70%*	*87%*	*0%*
Goethite	*3%*	*0%*	*0%*	*0%*	*0%*	*0%*
Hibbingite	*0%*	*0%*	*0%*	*8%*	*0%*	*0%*
Carbonates	6%	12%	0%	0%	13%	0%
Siderite	*6%*	*0%*	*0%*	*0%*	*13%*	*0%*
Aragonite	*0%*	*12%*	*0%*	*0%*	*0%*	*0%*
Others	3%	0%	0%	22%	0%	0%
Halite	*2%*	*0%*	*0%*	*0%*	*0%*	*0%*
Rokuhnite	*0%*	*0%*	*0%*	*22%*	*0%*	*0%*
Barite	*1%*	*0%*	*0%*	*0%*	*0%*	*0%*

Figure 2.10: Example of layered scale composition at two different well depths (Wang et al., 2013a).

There are some important points to keep in mind when studying and predicting the formation of different crystal forms of iron sulphide:

1. Kinetics play a key role in iron sulphide precipitation and transformation of iron sulphide deposits but because of limited studies and since many other factors influence these reactions in the field, at this point it is not possible to implement reliable kinetic calculations in scale predictions;

2. Reactions at field conditions are not always at equilibrium and some less stable forms of iron sulphide (i.e. mackinawite) may be present rather than being all converted to more stable precipitates (i.e pyrite);

3. Individual solubility prodcuts are not available for all iron sulphide scales;

4. Precipitation reactions occurring in bulk solutions differ from those occurring at the surface and surface chemistry. This is particularly relevant for iron sulphide when the source of iron is from corrosion mechanisms. Although many lab studies have been conducted to investigate the formation of sulphide scales on metal surfaces, the results are not always sufficient to describe field conditions where other factors play an important role. More information on surface iron sulphide formation is provided in Section 2.1.7.

Because of these major challenges, all commercial scale prediction software are based on thermodynamic calculations only and calculate the global minimum of Gibbs free energy for the system to predict the formation of different forms of iron sulphide. However, production fluids are not usually at equilibrium and scale prediction software often gives users the option to "switch off" the formation of more stable precipitates in the system. The decision to do so is arbitrary, but normally based on field findings and common knowledge of which iron sulphide forms are usually present. Pourbaix diagrams (Eh/pH diagrams) can be used to better understand this process (Verink Jr., 2011).

In oil reservoirs and in the producer wells, the system tends to be highly reducing. Thus, another important parameter for iron sulphide deposition is the system electrochemical potential, eH. The electrochemical potential needs to be low for reduced sulphur species (i.e. H_2S and HS^-) to be present and therefore have the ability to form sulphide scales.

Also, the principal iron species at low eH (more reducing conditions) is Fe^{2+} and at high eH (more oxidising conditions) is Fe^{3+}. The Pourbaix diagram at 25°C and 1 bar for sulphur species in water is shown in Figure 2.11.

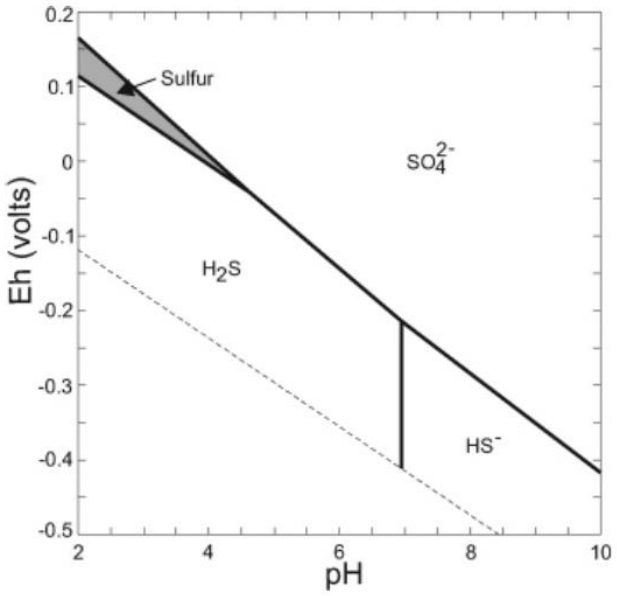

Figure 2.11: pH-Eh diagram for stable sulphur species in aqueous solution (25 °C, 1 bar total pressure, ∑(S)=10-3) (Rickard and Luther, 2007).

Although most oilfield systems are anoxic, even small changes in electrochemical potential can have an impact on scale formation (Wylde, 2014).

The construction of eH/pH stability diagrams including all forms of iron sulphide shows which forms are most stable at defined conditions. These are expected to be formed after a sufficiently long equilibration time in their respective domains of eh and pH. Precursors to these stable forms can be identified by removing the latter from eH/pH diagrams and drawing a new diagram. An example of this process is show in Figure 2.12 where stable pyrite and troilite have been removed to show that marcasite and mackinawite are metastable iron sulphide species (Anderko and Shuler, 1997).

An important point is that it is clear from the above results that an unambiguous prediction of a given form of FeS cannot be made for given field conditions. The thermodynamically most stable form (pyrite or troilite) is always predicted and it is only possible to obtain the metastable forms (marcasite or mackinawite) by deliberately supressing one or both of these more stable forms. Hence, such a calculation would not be a true "prediction" but would be more of a "decision".

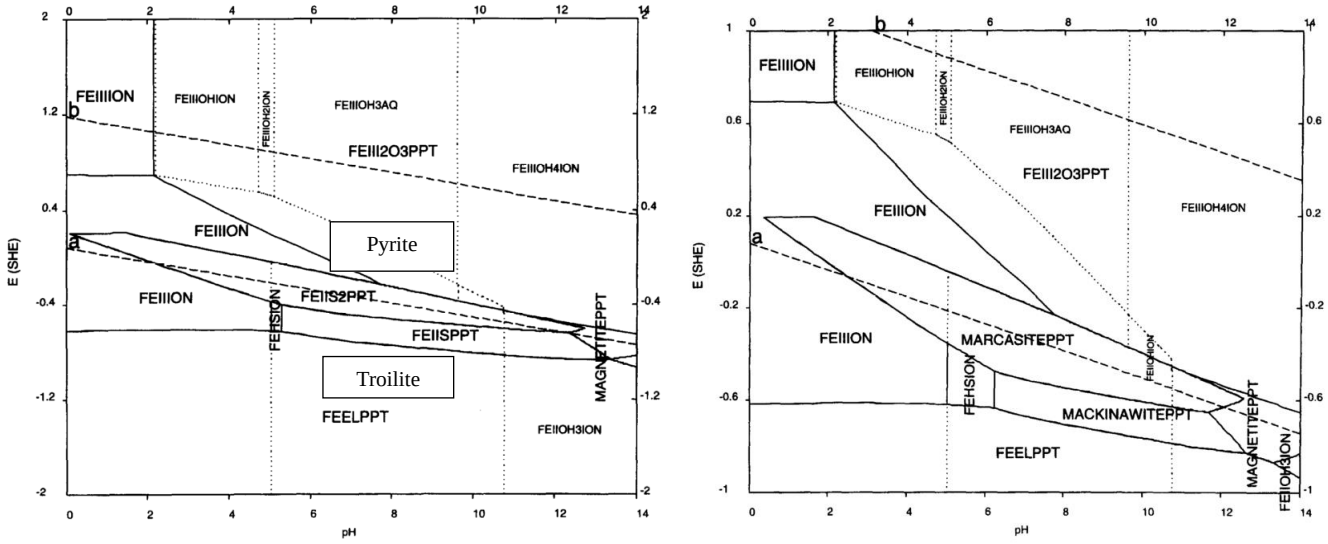

Figure 2.12: eH/pH diagrams for all forms of iron sulphide (1) and after excluding pyrite and troilite (2) (Anderko and Shuler, 1997).

2.1.6 Problems Caused by Iron Sulphide Scale in Oil and Gas Wells

Iron sulphide scale represents a serious threat to oil and gas system integrity, field productivity, fluid (oil and water) quality and health and safety in the field.

In most fields where iron sulphide forms, iron is the limiting reagent in the formation of iron sulphide because H_2S is usually present in excess. Hence, it is the source of iron and not the amount of hydrogen sulphide in the produced fluids that most commonly determines the amount of scale formed (Ford et al., 1992).

The perceived but often real difficulty in mitigating iron sulphide problems, causes most operators to take a reactive approach to the problem by relying on scale removal methods. Unfortunately, these methods can cause further issues in the system, they can be expensive and not always work effectively. More information is provided in Section 2.4.

The main problems caused by iron sulphide scale in oil and gas wells are:

- **Corrosion**. Iron sulphides scale can be a product of corrosion itself but it can also cause further corrosion issues in the system. Under deposit corrosion can happen as a results of layers of sulphide scales forming on pipes but also due to iron sulphides precipitating out of solution and depositing at the bottom of vessels and pipelines. It is commonly believed that a passive film of iron sulphide scale can form and protect against further corrosion. This can be true for uniform sulphide layers not subject to erosion and which do not allow transport of electrons from the pipe to the produced fluids (Kvarekval et al., 2003). Different studies show how some iron sulphide films which are formed can be relatively easy to remove and may be unstable under high flow rate conditions (Banaś et al., 2007). Localised corrosion processes may be accelerated in the area where iron sulphide is not present as this becomes a small anodic area compared to a large cathodic surface (iron sulphide coated). Porous deposits also provide only partial corrosion deposit as they allow electron transfer between bulk fluid and the metal pipe (Svenningsen et al., 2009).

- **Emulsions**. As solid particles in the system, small iron sulphides crystals have a tendency to collect at the oil/water interface and stabilize emulsion bands.

- **Water quality - Produced water re-injection**. Produced water re-injection is commonly used in onshore fields to dispose of produced water or in offshore facilities to maintain reservoir pressure and minimize water disposal overboard. If the water contains iron sulphides scale, these particles can contribute to increased injection pressure due to near well formation plugging. Iron sulphides particles are also very oleophilic and can transport oil in the water injection system causing further injectivity problems and making removal treatments more complicated as the scale becomes oil coated.

- **Water quality – Overboard**. Due to the high oil affinity of iron sulphide particles, this scale contributes to increase Oil in Water (OIW) which is highly regulated by environmental agencies. Exceeding the OIW peak reading or the yearly oil discharge tonnage can translate into significant fines and ultimately platform shut down.

- **Water quality – Water recycling**. The increased issues related to water usage and water management in the oil and gas industry require that more produced water is recycled and reused in operations such as hydraulic fracturing ("frakking"). If this water is contaminated with sulphide scales it may cause problems in newly drilled or stimulated wells.

- **Oil quality**. The presence of iron sulphide stabilises the oil/water interface making it more difficult to obtain low Basic Sediment and Water (BS&W) (Brownlee et al., 2000).

- **Formation damage**. Formation damage normally occurs during acid jobs when spent acid carrying high levels of dissolved iron and other contaminants reaches

the near wellbore where iron re-precipitates out due to the higher pH (Garzon et al., 2007).

- **Tubing restrictions**. Dense and adhesive iron sulphide deposits can restrict and ultimately plug production tubing and topside pipes. The flow restriction has an impact on production rates and ultimately productivity efficiency. Iron sulphide was also found to plug gas lift mandrels when sour gas is used for lifting water that contains iron (Nasr-El-Din et al., 2001).

- **Health and safety**. Iron sulphides releases hydrogen sulphides during acid dissolution and this poisonous gas can reach very high concentrations if much scale is dissolved. Moreover, certain forms of iron sulphides can be pyrophoric and have the potential to cause severe fires if not well managed.

Unlike other types of scale, iron sulphide not only impacts oil production but has a direct influence on system integrity (corrosion) and is a health and safety hazard. Hence, special measures must be put in place to better control the formation of these deposits rather than relying on scale removal.

2.1.7 Iron Sulphide as Corrosion Product

The study of FeS as corrosion product is a vast topic investigated by many research groups around the world and it is beyond the scope of this study to provide a detailed analysis of the problem. However, since many fields around the world experience corrosion related FeS precipitation it is important to provide a brief overview on the subject and include a few relevant references for further investigation.

The main sources of iron in oil and gas systems are reservoir rocks, drilling fluids, some proppants in hydraulic fracturing, “normal” corrosion of any metal tubulars or

components and "additional" corrosion due to acid stimulation treatments (Ramachandran et al., 2015a, Ma et al., 2016). Corrosion is certainly one of the main causes of iron sulphide precipitation in sour wells and topside equipment and corrosion prediction models for CO_2/H_2S systems attempt to describe this mechanism.

As previously mentioned, the precipitation of iron sulphide and conversion to different crystalline forms is strongly dependent on kinetics but these processes are not fully understood. Despite the relative abundance of experimental data, the uncertain mechanism of H_2S corrosion makes it difficult to develop a model for kinetics of iron sulphide layer formation and further to predict the corrosion rate of mild steel, particularly in real oilfield conditions.

Various researchers have proposed different mechanisms for CO_2/H_2S corrosion and iron sulphide formation on mild steel surfaces (Sun and Nešić, 2009). There seems to be a consensus that a mackinawite layer forms first on the surface as a product of H_2S corrosion and that other crystalline forms such as pyrite and pyrrhotite form only at elevated temperatures (over 150°C), probably because kinetics of the transformation reactions are accelerated at higher temperature (Gao et al., 2017, Sun et al., 2006).

The formation of an inner layer of iron oxide (probably magnetite Fe_3O_4) at high temperatures in oxygen free systems is also reported. The proposed reaction mechanism is shown in Equation (2.17) (Gao et al., 2017, Ramachandran et al., 2015b).

$$3Fe^{2+}_{(aq)} + 4H_2O \rightarrow Fe_3O_{4(s)} + 8H^+ + 2e^- \qquad (2.17)$$

It is common belief amongst industry experts that a layer of iron sulphide on the metal surface protects against further steel corrosion, particularly against CO_2 corrosion. This

is supported by experimental results which show lower corrosion rates for a system containing CO_2 and H_2S compared to a CO_2 only scenario (Zheng et al., 2015a). Whilst this may be true in some cases, there are other mechanical, chemical and electrochemical reactions that can accelerate corrosion in the presence of an iron sulphide layer. These include under deposit corrosion, cracking of the iron sulphide film, hydrogen penetration into the steel and others (Sun and Nešić, 2009).

Two different mechanisms have been proposed to describe the formation of mackinawite on carbon steel in a CO_2/H_2S environment. The first one is the formation of a solid adherent mackinawite layer through a "solid-state" corrosion reaction as shown in Equation (2.18**)**. This mechanism supports the theory of inward diffusion of sulphide species through the mackinawite layer to progress the reaction (Sun and Nešić, 2009).

$$Fe_{(S)} + H_2S \rightarrow FeS_{(s)} + H_2 \tag{2.18}$$

The second proposed mechanism is based on one anodic reaction (dissolution of Fe from the steel surface) shown in Equation (2.19) and four cathodic reactions (reduction of H^+ ions, direct reduction of aqueous H_2S, H_2CO_3 and H_2O) as shown in Equation (2.20) through (2.23) (Zheng et al., 2015a).

$$Fe_{(s)} \rightarrow Fe^{2+}_{(aq)} + 2e^- \tag{2.19}$$

$$2H^+_{(aq)} + 2e^- \rightarrow H_{2(g)} \tag{2.20}$$

$$2H_2S_{(aq)} + 2e^- \rightarrow H_{2(g)} + 2HS^-_{(aq)} \tag{2.21}$$

$$2H_2CO_{3(aq)} + 2e^- \rightarrow H_{2(g)} + HCO^-_{3(aq)} \quad (2.22)$$

$$2H_2O + 2e^- \rightarrow H_{2(g)} + OH^-_{(aq)} \quad (2.23)$$

This second mechanism supports the theory of Fe^{2+} diffusion through an iron sulphide layer to react with sulphide species and form iron sulphide.

Depending on which mechanism and experimental data the CO_2/H_2S corrosion model is based upon, corrosion rate results will be different, leaving a degree of uncertainty in oilfield corrosion prediction.

The rigorous calculation of aqueous phase properties such as dissolved CO_2 and H_2S, pH and alkalinity proposed in this work to study bulk phase scale precipitation provides important input data for the calculation of corrosion rates in the same way that understanding corrosion rates can be useful to estimate the "available" iron concentration for iron sulphide scale formation.

The interactive nature of corrosion modelling and sulphide scale predictions shows how these processes would ideally be studied in combination through the use of an "all-in-one" corrosion, PVT and scale prediction software. However, this important step forward would require a greater understanding of thermodynamics and kinetics that link corrosion and bulk precipitation mechanisms.

2.1.8 Pyrophoric Behaviour of FeS

Pyrophoric (self-combusting) sulphide ores represent a major hazard in the mining industry and a number of studies have been published to investigate the exothermic oxidation mechanism and predict the likelihood of deposit self-combustion (Zhao et al., 2011)

In oil and gas systems, sulphur containing scales such as pyrite and pyrrhotite may also produce pyrophoric materials and may require particular care during handling (Belzile et al., 2004, Murphy and Strongin, 2009).

An oxidative reaction occurs when pyrophoric scales are in an environment containing water vapour and a sufficient concentration of dissolved oxygen to trigger the reaction. This oxidation reaction is highly exothermic and if the rate at which heat is generated is higher than the rate of heat removal by conduction or convection the temperature can increase and reach self-ignition conditions. If hydrocarbons are present in the deposit these may also ignite heating equipment to temperatures close to 1500°C (Plellis, 2012).

In oil and gas system there are several critical points where pyrophoric scale may pose a more significant threat. These include:

- Crude oil tanks
- Sour water tanks
- Vessels in sour service (i.e. inlet separators, pig receiver and launchers)
- Marine tankers and barges
- Portable tanks
- Storage legs in offshore platforms

Possible mitigation methods for pyrophoric sulphides include:

- Preventing the formation of pyrophoric materials by controlling/preventing iron sulphide scale formation.

- Using inert gas such as nitrogen or carbon dioxide to keep oxygen out of the system when possible.

- Chemical neutralisation of pyrophoric deposits by using potassium permanganate wash, although this method has been unsuccessful in some cases (Plellis, 2012).

- Spraying tank/container with aqueous H_2S scavenger and sulphide dissolvers (e.g. in a formulated package for the specific application).

2.1.9 Elemental Sulphur in Sour Gas Wells

It is well known that sulphur is soluble in sour gas and often precipitates during production if temperature and pressures decrease (Brunner et al., 1988).

Elemental sulphur can precipitate in the tubing causing flow restrictions (Tang et al., 2011) and/or within the reservoir as the pressure is reduced causing formation damage (Fadairo et al., 2012). In addition, sulphur can cause significant corrosion problems (Fang et al., 2011) which need to be controlled with the use of appropriate corrosion inhibitor chemistries. Such precipitated elemental sulphur may interact with existing deposits of FeS, however we have not found published work showing this to be the case. A more comprehensive study of elemental sulphur precipitation is beyond the scope our work.

2.2 THE PREDICTION OF pH DEPENDENT SCALES

The prediction of carbonate and sulphide scales is very closely related to the correct determination of partitioning and speciation of CO_2 and H_2S which affect (and are

affected by) pH, alkalinity and the availability of reactive species (Olajire, 2015, Kan and Tomson, 2010, Kaasa and Ostvold, 1997, Vetter and Farone, 1987).

The three thermodynamic processes to account for when predicting carbonate and sulphide scales are:

- Partitioning of molecular CO_2 and H_2S between gas, oil and water;
- Speciation of molecular CO_2 and H_2S in water (to HCO_3^-, CO_3^{2-}, HS^- and S^{2-});
- Reaction between cations (e.g. Ca^{2+}, Fe^{2+}) and anions (e.g. HCO_3^- and HS^-) to form scale and complexes.

This is schematically shown in Figure 2.13. A generic organic acid (HA) is also included.

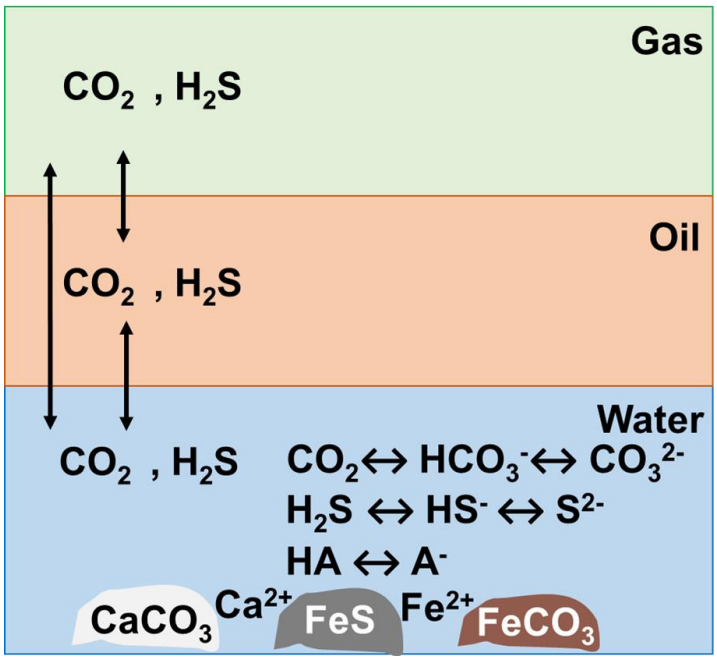

Figure 2.13: Schematic representation of carbonates and sulphides partitioning, speciation and precipitation.

The first mechanism is modelled by carrying out thermodynamic PVT calculations (Pedersen and Christensen, 2007, Danesh, 1998). These are normally based on the use of a cubic equation of state (EOS) but in the presence of polar compounds such as water, different EOS and mixing rules must be used (see Section 2.2.1).

The second and third chemical processes above can be described using a scale prediction model.

2.2.1 PVT Calculations

All the systems investigated in this work are considered to be at equilibrium. Hence, the fugacity of each component *i* (the "tendency" of a molecule to leave from one phase to another) must be equal throughout all the phases in a heterogeneous system (Equation (2.24)) (Danesh, 1998).

$$f_i^{(1)} = f_i^{(2)} = f_i^{(3)} = \cdots = f_i^{(\theta)} \tag{2.24}$$

Where $f_i^{(\theta)}$ = fugacity of component *i* in phase θ.

The ratio of fugacity to pressure (P) is defined as the fugacity coefficient ϕ. For example, the fugacity coefficient of component *i* in the gas phase in a multicomponent system can be written as in Equation (2.25) where y_i is the molar fraction of component *i* in the gas phase.

$$\phi_i^V = \frac{f_i^V}{P \times y_i} \tag{2.25}$$

The fugacity coefficient of a compound in a mixture can be calculated from Equation (2.26) or equivalent Equation (2.27) (Kontogeorgis and Folas, 2009).

$$RT\ ln\phi_i = RT\frac{f_i^{(\theta)}}{P \times y_i} = \int_V^{\infty}\left[\left(\frac{\partial p}{\partial n_i}\right)_{T,V,n_{j\neq i}} - \frac{RT}{V}\right]dV - RT\ \ln\left(\frac{PV}{RT}\right) \quad (2.26)$$

$$RT\ ln\phi_i = RT\frac{f_i^{(\theta)}}{P \times y_i} = \int_0^{P}\left(\overline{V}_i - \frac{RT}{P}\right)dP \quad (2.27)$$

An Equation of State (EOS) which can be expressed as functions of P (V,T) or V (P, T) is applied to determine the fugacity coefficient of Equation (2.26) or (2.27) which is then used to calculate each component's molar fraction.

Cubic EOS, in particular Peng-Robinson (PR), are the most commonly used for hydrocarbon systems but many other types of EOS exist and Figure 2.14 shows a possible classification of EOS (Silva, 2017).

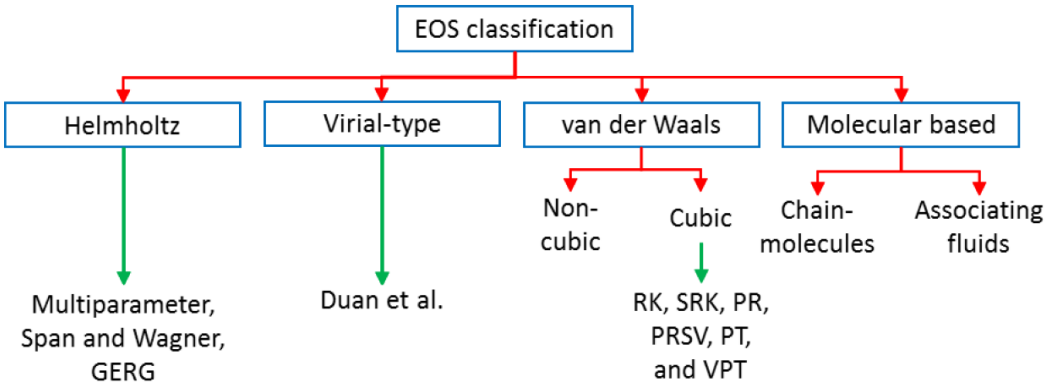

Figure 2.14: Classification of EOS (Silva, 2017).

Examples of classical cubic EOSs are shown in Figure 2.15 (Kontogeorgis and Folas, 2009).

EoS	Equation	Energy and co-volume parameters	Critical Compressibility factor
van der Waals[3] (vdW)	$P = \frac{RT}{V-b} - \frac{a}{V^2}$	$a = \frac{27}{64}\frac{(RT_c)^2}{P_c}$ $b = \frac{1}{8}\frac{RT_c}{P_c}$	$Z_c = 0.375$
Redlich–Kwong[4] (RK)	$P = \frac{RT}{V-b} - \frac{a}{V(V+b)\sqrt{T}}$	$a = 0.427\,48\frac{(R^2T_c^{2.5})}{P_c}$ $b = 0.086\,64\frac{RT_c}{P_c}$	$Z_c = 0.333$
Soave–Redlich-Kwong (SRK)	$P = \frac{RT}{V-b} - \frac{a(T)}{V(V+b)}$	$a_c = 0.427\,48\frac{(RT_c)^2}{P_c}$ $b = 0.086\,64\frac{RT_c}{P_c}$	$Z_c = 0.333$
Soave[5]		$a(T) = a_c\left[1 + m(1-\sqrt{T_r})\right]^2$ $m = 0.48 + 1.574\omega - 0.176\omega^2$	
Peng–Robinson (PR)	$P = \frac{RT}{V-b} - \frac{a(T)}{V(V+b)+b(V-b)}$	$a_c = 0.457\,24\frac{(RT_c)^2}{P_c}$ $b = 0.077\,80\frac{RT_c}{P_c}$	$Z_c = 0.307$
Peng and Robinson[6]		$a(T) = a_c\left[1 + m(1-\sqrt{T_r})\right]^2$ $m = 0.374\,64 + 1.542\,26\omega$ $-0.269\,92\omega^2$	

Figure 2.15: The most important cubic EOSs and the "classical" way of estimating their parameters (based on critical point and vapour pressures) (Kontogeorgis and Folas, 2009) .

Numerous textbooks and publications (Kontogeorgis and Folas, 2009, Firoozabadi, 1999, Pedersen and Christensen, 2007) describe the various EOS, their applicability and main limitations. The study of EOS and PVT calculations is a broad topic which some researchers spend an entire career investigating. However, it is not the goal of this work to provide a detailed study of EOS and PVT calculations but rather to determine their impact on scale predictions, with particular focus on the commercially available options for these calculations.

PVT Calculations for Polar Compounds

This work is aimed at improving the prediction of carbonate and sulphide scale formation in oil and gas wells. Since it is fundamental to correctly describe the water phase behaviour in scale prediction calculations, more information on the topic is here provided.

Water is an important component of reservoir and produced fluids. It can be present as connate water, free formation water or be injected in the reservoir for pressure support/enhanced oil recovery.

In many cases hydrocarbon fluids are studied independently of the water phase because the water-hydrocarbon mutual solubility is considered small. However, there are field scenarios where neglecting the water-hydrocarbon mutual solubility can cause large errors. An example is shown in Figure 2.16 for North Sea black oil at 293K where the oil bubble point pressure decreases quite significantly as the water cut increases (Danesh, 1998). While formation water is believed to be in equilibrium with reservoir hydrocarbons, injected water that is not originally in equilibrium with the reservoir will dissolve oil light ends causing an increase in bubble point pressure. Moreover, at high water cut, a significant fraction of the produced gas can be released by the water phase and this must be accounted for when measuring topside flow rates.

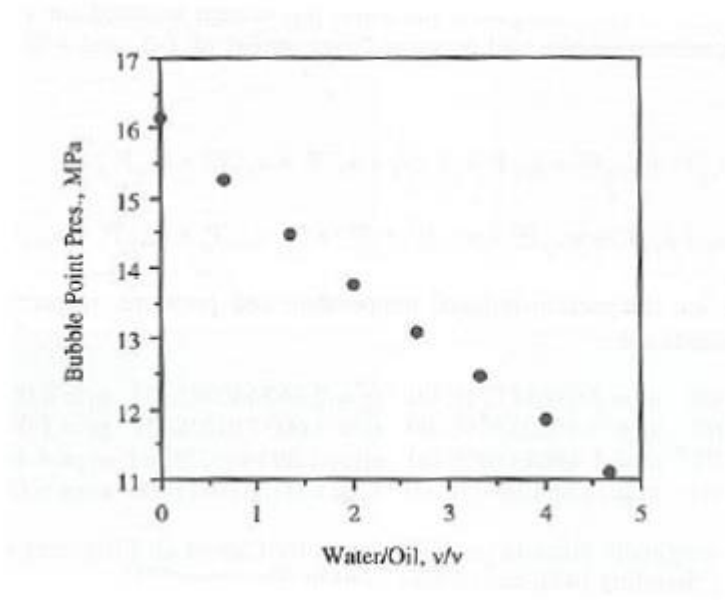

Figure 2.16: Variations of bubble point pressure contacted with fresh water (Danesh, 1998).

Water is the main phase to be characterised for scale predictions and the distribution of components such as CO_2 and H_2S between all phases present in the system is key to obtain meaningful results.

A cubic equation of state with classical a-parameter mixing rule is based on the assumption that molecules are randomly distributed in each phase (Pedersen and Christensen, 2007). This assumption does not apply for water dissolved in hydrocarbon phases because the behaviour of water-hydrocarbon mixtures is complicated by the association between water molecules. This behaviour is caused by the polarity of water molecules and various models have been proposed to describe these polar interactions.

In conventional applications where water-hydrocarbon mutual solubility is small, simple empirical correlations can be used to estimate the water phase properties (Danesh, 1998).

To describe phase equilibria of complex associating systems (those which contain compounds capable of hydrogen bonding) a common approach is to use the Cubic Plus

Association (CPA) (Kontogeorgis and Folas, 2010b). CPA combines a classical simple EOS (i.e. SRK) with an association term such as that one described by the Statistical Associating Fluid Theory (SAFT).

The cubic plus association (CPA) model is based on the concept that there are two contributions to the compressibility factor Z: the first one comes from chemical interactions between the polar molecules (formation of dimers) and is indicated as Z^{ch}; the second one comes from physical interactions, it is indicated as Z^{ph} and is the one calculated using the selected EOS (Firoozabadi, 1999). The final equation is shown in Equation (2.28).

$$Z = Z^{ch} + Z^{ph} - 1 \tag{2.28}$$

Empirical correlations have been proposed for Z^{ch} (dos Santos et al., 2015, Kontogeorgis and Folas, 2010a).

Equation (2.28) is reduced to a conventional EOS when water is not present.

Other empirical correlations such as the "asymmetric/non-random" mixing rules and the "Huron and Vidal" mixing rule have also been proposed (Kontogeorgis and Folas, 2010b).

Equation (2.26) and (2.27) are in principle suitable to describe all types of fluid phases, conditions and mixtures of any number of components. In practice, certain equilibria types are often more conveniently described with activity coefficient models (i.e. Pitzer model, NRTL, UNIQUAC, etc.) which are useful to represent deviations from ideality. This is particularly true for polar phases such as aqueous phases (Kaasa and Ostvold, 1998).

Equation (2.29) shows how the fugacity of each component can be calculated using activity coefficients.

$$\gamma_i = \frac{f_i^L}{f_i^0 \times x_i} \tag{2.29}$$

Where γ_i, f_i^0 and x_i are the activity coefficient of component *i* in the liquid phase, the standard state fugacity of component *i* in the mixture and the molar fraction of component *i* in the liquid phase.

The standard state fugacity of component *i* in the mixture is given by Equation (2.30) where v_i^∞ is the partial molar volume of component *i* at infinite dilution.

$$\left(\frac{\partial \ln f_i^0}{\partial p}\right)_T = \frac{v_i^\infty}{RT} \tag{2.30}$$

Henry's law is used to define f_i^L as shown in Equation (2.31) where $H_{i,j}$ is Henry's constant for component *i* in solvent *j*.

$$H_{i,j} = \lim_{x_i \to 0} \frac{f_i^L}{x_i} \tag{2.31}$$

Finally, Equation (2.30) is integrated from the solvent vapour pressure to the working pressure resulting in Equation (2.32).

$$f_i^L = \gamma_i x_i H_{i,j} exp \int_{P_{vp}}^{P} \frac{v_i^\infty}{RT} dP \tag{2.32}$$

Different commercial software (PVT only or integrated PVT and scale predictions) use different approaches to describe the water phase: some use a conventional cubic EOS (which is clearly not the correct approach); some have implemented various EOS which the user can select from; others use so called "modified" EOS where the parameters

have been fitted to match a set of specific experimental data; finally some use Henry's law (the activity coefficient approach) to calculate the aqueous phase composition.

This variability shows the need for experimental data matching and tuning of the relevant parameters. Unfortunately, most oil and gas fields do not have the necessary measurements required for data matching and predefined EOS parameters are normally used.

Flash Calculations

A flash calculation (or PT-flash process) is run using a PVT software to determine the number of phases present at a given temperature and pressure, the molar amount and the molar composition of each phase. This is schematically shown in Figure 2.3 (Pedersen and Christensen, 2007) where z_i, y_i and x_i are the component mole fractions in the initial feed, gas and oil respectively and β is the vapour mole fraction.

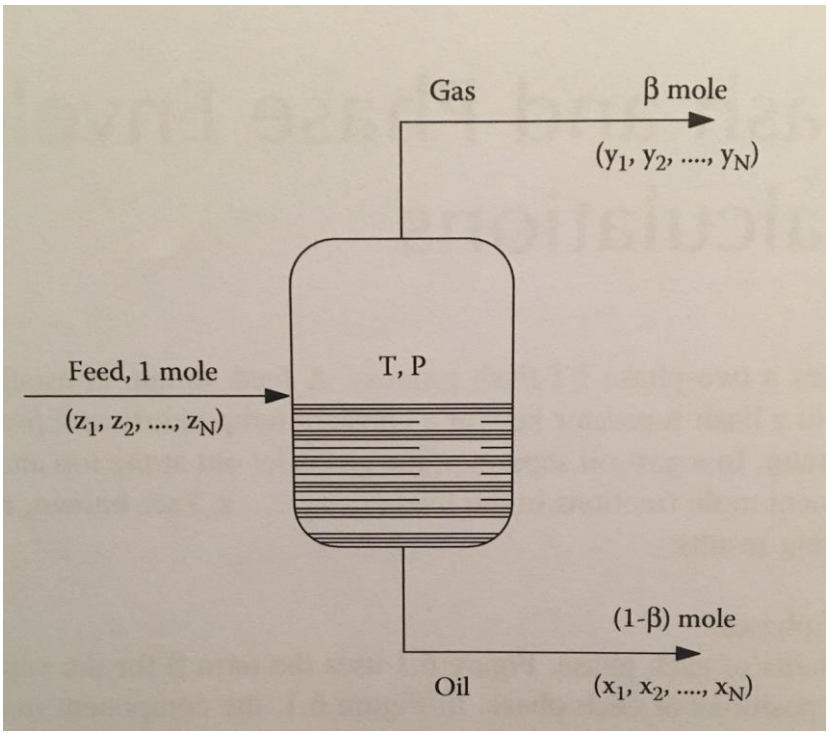

Figure 2.17: Principle of PT-flash process for a hydrocarbon reservoir fluid mixture.

The determination of the number of phases is accomplished by carrying out a stability test (Pedersen and Christensen, 2007) which is based on the calculation of the minimum Gibbs free energy (G) for the resulting system (Gibbs free energy of the mixture compared to that one of separate phases).

$K_{VL,i}$ is the equilibrium ratio (or partition coefficient) of the mole fraction of component *i* between the vapour (V) and liquid (L) phase (Equation (2.33)) and at equilibrium it can also be written as the ratio of fugacity coefficients (ϕ_i) from Equation (2.24**)** and (2.25) .

$$K_{VL,i} = \frac{y_i}{x_i} = \frac{\theta_i^L}{\theta_i^V} \tag{2.33}$$

If two or more phases are present, the Rachford-Rice equation (Equation (2.34)) is used to determine their compositions using an iteration process.

$$F(\beta) = \sum_{i=1}^{N} \frac{z_i(K_{VL,i} - 1)}{1 + \beta(K_{VL,i} - 1)} = 0 \tag{2.34}$$

An initial estimate (guess) of the K-factors is used to calculate the vapour mole fraction β. New estimates of the phase mole fractions can be made using Equation (2.35) and (2.36) and the fugacity coefficients of these new compositions are calculated using an EOS. A new K-factor estimate is obtained to calculate a new β and the process repeated until convergence. For some systems it may be necessary to use different techniques to ensure convergence and reduce computing time (Pedersen and Christensen, 2007).

$$y_i = \frac{z_i K_{VL,i}}{1 + \beta(K_{VL,i} - 1)} \tag{2.35}$$

$$x_i = \frac{z_i}{1 + \beta(K_{VL,i} - 1)} \tag{2.36}$$

Partition Coefficients

The equilibrium ratio or partition coefficient K_{AB}, is defined as the ratio of the concentrations of a species in two immiscible phases (A and B) at equilibrium, and it represents the relative solubility of this species between these two phases. A partition coefficients for each component present in the system is obtained from flash calculations in PVT software.

Two key components in carbonate and sulphide scale predictions are CO_2 and H_2S and their partitioning in a gas/oil/water system depends on (Vetter et al., 1987):

- Temperature (T) and pressure (p)
- Concentration in feed
- Brine composition
- Oil composition
- Three phase relative volumes

In a 3 phase system there are 3 partition coefficients, as shown schematically in Figure 2.18:

- A gas/oil partition coefficient, K_{GO}
- A gas/water partition coefficient, K_{GW}
- An oil/water partition coefficient, K_{OW}

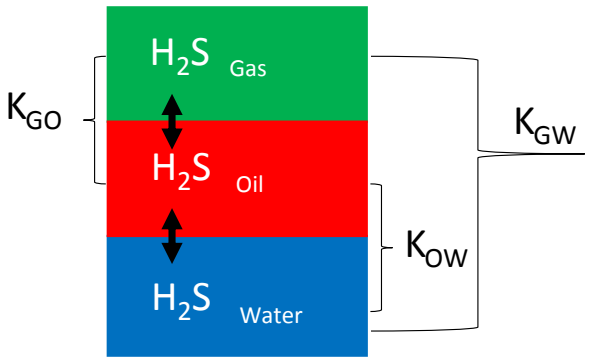

Figure 2.18: Partition coefficients for a gas/oil/water system.

The mole fraction of component *i* in the gas, oil and water phases is denoted as y_i, x_i and w_i respectively and the corresponding partition coefficients are $K_{GO} = (y_i/x_i)$; $K_{GW} = (y_i/w_i)$ and $K_{OW} = (x_i/w_i)$. It can be seen that there are actually only ***two*** independent partition coefficients since clearly from above, $K_{OW} = (K_{GW} / K_{GO})$.

Partition coefficients should be expressed in mole fraction. For example, the gas/water partition coefficient of H_2S is described as in Equation (2.37).

$$K_{GW,H_2S} = \frac{\frac{mol\ H_2S_{(G)}}{mol\ G}}{\frac{mol\ H_2S_{(W)}}{mol\ W}} \tag{2.37}$$

However, in the oil industry other units such as ppm and mol/l are also used and it is important to convert all partition coefficient values to the same units before running any results comparison (Burger et al., 2013).

2.2.2 Scale Prediction Calculations – Aqueous Electrolyte Model

The PVT equations described in Section 2.2.1 allow us to calculate the distribution of components between all phases present at the given T and p point and the relative volume and mole fraction of each phase.

This information is used in an aqueous electrolyte model to calculate the concentration of all reactive species in the aqueous phase and to predict the formation of scale.

These aqueous phase calculations are based on solving a system of nonlinear equations consisting of:

i. Acid equilibria reactions;

ii. Mineral precipitation reactions;

iii. Conservation of mass;

iv. Electrical neutrality of solutions.

Acid equilibria reactions. The acid equilibria reactions include the self-ionization of water and the speciation in solution of carbon, sulphur, and organic acids (here assumed to be a generic organic acid) as shown in Equations (2.38) through (2.44). They also include the corresponding thermodynamic equilibrium constants shown in Equations (2.45) through (2.51) where K_i, m_i, and γ_i are respectively the thermodynamic equilibrium constant, the molarity (mol/l) and activity coefficient of component *i*.

$$H_2O \leftrightarrow OH^- + H^+ \tag{2.38}$$

$$CO_2 + H_2O \leftrightarrow H_2CO_3 \tag{2.39}$$

$$H_2CO_3 \leftrightarrow H^+ + HCO_3^- \tag{2.40}$$

$$HCO_3^- \leftrightarrow CO_3^{2-} + H^+ \tag{2.41}$$

$$H_2S \leftrightarrow HS^- + H^+ \tag{2.42}$$

$$HS^- \leftrightarrow S^{2-} + H^+ \tag{2.43}$$

$$HA \leftrightarrow A^- + H^+ \tag{2.44}$$

$$K_{H_2O} = (m_{OH^-} \times m_{H^+})(\gamma_{OH^-} \times \gamma_{H^+}) \tag{2.45}$$

$$K_{CO_2,1} = \frac{m_{H_2CO_3}}{m_{CO_2}} \frac{\gamma_{H_2CO_3}}{\gamma_{CO_2}} \tag{2.46}$$

$$K_{CO_2,2} = \frac{m_{H^+} \times m_{HCO_3^-}}{m_{H_2CO_3}} \frac{\gamma_{H^+} \times \gamma_{HCO_3^-}}{\gamma_{H_2CO_3}} \tag{2.47}$$

$$K_{CO_2,3} = \frac{m_{H^+} \times m_{CO_3^{2-}}}{m_{HCO_3^-}} \frac{\gamma_{H^+} \times \gamma_{CO_3^{2-}}}{\gamma_{HCO_3^-}} \tag{2.48}$$

$$K_{H_2S,1} = \frac{m_{HS^-} \times m_{H^+}}{m_{H_2S}} \frac{\gamma_{HS^-} \times \gamma_{H^+}}{\gamma_{H_2S}} \tag{2.49}$$

$$K_{H_2S,2} = \frac{m_{H^+} \times m_{S^{2-}}}{m_{HS^-}} \frac{\gamma_{H^+} \times \gamma_{S^{2-}}}{\gamma_{HS^-}} \tag{2.50}$$

$$K_{HA} = \frac{m_{H^+} \times m_{A^-}}{m_{HA}} \frac{\gamma_{H^+} \times \gamma_{A^-}}{\gamma_{HA}} \tag{2.51}$$

Mineral precipitation reactions. This work focuses on the prediction of $CaCO_3$, $FeCO_3$ and FeS formation described by Equations (2.52), (2.53) and (2.54) with corresponding solubility products in Equations (2.55), (2.56) and (2.57). However, additional chemical equilibrium equations can be included for pH-independent scales such as $BaSO_4$ and $CaSO_4$, for the formation of complexes and other soluble species such as $FeSH^+$ and calcium bicarbonate ion ($Ca(HCO_3)^+$) and for the formation of other crystalline forms of these scale such as pyrite and pyrrhotite. As many of these equations as necessary can be included in this system of nonlinear equations providing an equilibrium constant (or solubility product for solids) is available.

$$Ca^{2+} + CO_3^{2-} \rightarrow CaCO_3(s) \tag{2.52}$$

$$Fe^{2+} + CO_3^{2-} \rightarrow FeCO_3(s) \tag{2.53}$$

$$Fe^{2+} + S^{2-} \rightarrow FeS\,(s) \tag{2.54}$$

$$K_{sp,CaCO_3} = m_{Ca^{2+}}\, m_{CO_3^{2-}}\, \gamma_{Ca^{2+}}\, \gamma_{CO_3^{2-}} \tag{2.55}$$

$$K_{sp,FeCO_3} = m_{Fe^{2+}}\, m_{\,CO_3^{2-}}\, \gamma_{Fe^{2+}}\, \gamma_{CO_3^{2-}} \tag{2.56}$$

$$K_{sp,2}(FeS) = m_{Fe^{2+}}\, m_{S^{2-}}\, \gamma_{Fe^{2+}}\, \gamma_{S^{2-}} \tag{2.57}$$

The sulphide related Equations (2.42), (2.43) and (2.54) can be re-written into Equations (2.58) or (2.59) with solubility products $K_{sp,1}$ and K_{sp} respectively and the correlations between solubility products are shown in Equation (2.60) and (2.61). Hence, the solubility product of iron sulphide can be described as K_{sp}, $K_{sp,1}$ or $K_{sp,2}$ depending on which chemical equation it refers to.

$$Fe^{2+} + HS^- \rightarrow FeS \downarrow + H^+ \tag{2.58}$$

$$Fe^{2+} + H_2S \rightarrow FeS \downarrow + 2H^+ \tag{2.59}$$

$$K_{sp,1} = \frac{m_{Fe^{2+}} \times m_{HS^-}}{m_{H^+}} \frac{\gamma_{Fe^{2+}} \times \gamma_{HS^-}}{\gamma_{H^+}} = \frac{K_{sp,2}}{K_{H_2S,2}} \tag{2.60}$$

$$K_{sp} = \frac{m_{Fe^{2+}} \times m_{H_2S}}{(m_{H^+})^2} \frac{\gamma_{Fe^{2+}} \times \gamma_{H_2S}}{(\gamma_{H^+})^2} = \frac{K_{sp,1}}{K_{H_2S,1}} \tag{2.61}$$

Reliable iron sulphide scale prediction are strongly related to the iron sulphide solubility product and to the H_2S dissociation constants. These values are temperature dependent and whilst many results have been published for room temperature conditions (Table 2.2), few data are available at higher temperatures and pressures. For this reason, discrepancies between scale prediction results obtained using different software packages are likely. It must also be noted that whilst values for $K_{H2S,1}$ reported by different authors are in good agreement, there is a large degree of uncertainty around the second dissociation constant $K_{H2S,2}$ (7 orders of magnitude variation) (Sun et al., 2008).

Reference	K_{sp}	$K_{sp,1}$	$K_{sp,2}$	$K_{H2S,1}$	$K_{H2S,2}$
(Dean, 1999)	-	-	6.30E-18	-	-
(Sun et al., 2008)	1.63E+03			9.63E-08 (average)	1.33E-13 (average)
(Davison, 1991)		2.51E-04			
(Ning et al., 2013)		1.12E-03			
		2.82E-04			
		1.15E-03			
		1.70E-04			
		3.16E-04			
(Davison et al., 1999)	2.77E+04	1.00E-03			
(Rickard, 2006)	3.16E+03 (23°C)	3.16E-04 (23°C)			

Table 2.2: Literature values for FeS solubility products and H_2S dissociation constants at 25°C.

Equation (2.62) describes the temperature dependence of iron sulphide solubility as K_{sp} whilst Equations (2.63) through (2.66) and Equations (2.67) and (2.68) describe the temperature dependence of $K_{H2S,1}$ and $K_{H2S,2}$ respectively (T is the temperature in Kelvin (Sun et al., 2008).

$$K_{sp} = 10^{\left(\frac{2848.779}{T_k}\right)-6.347} \tag{2.62}$$

$$K_{H_2S,1} = K_{H_2O} \times 10^{\left(19.84+\frac{930.8}{T}-2.8\ln(T)\right)} \tag{2.63}$$

$$K_{H_2S,1} = 10^{-\left(32.55+\frac{1519.44}{T}-15.672\ln(T)+0.02722\times T\right)} \tag{2.64}$$

$$K_{H_2S,1} = 10^{-\left(15.345-0.045676\times T+5.9666\times 10^{-5}\times T^2\right)} \tag{2.65}$$

$$K_{H_2S,1} = 10^{\left(782.43945+0.361261\times T-1.6722\times 10^{-4}\times T^2-\frac{20565.7315}{T}-142.741722\ln(T)\right)} \tag{2.66}$$

$$K_{H_2S,2} = 10^{\left(\frac{31286}{T}+94.9734\ln(T)-0.097611\times T-2.17087\times 10^{6}\times T^2-607.722\right)} \tag{2.67}$$

$$K_{H_2S,2} = 10^{-\left(23.93-0.030446\times T+2.4831\times 10^{-5}\times T^2\right)} \tag{2.68}$$

An example is presented here to determine the variability of iron sulphide solubility product at 25°C, 80°C and 120°C and the calculated values are compared to results obtained using the commercial software ScaleChem (MSE). These values are important to explain some of the findings for the gas/condensate well example in Chapter 4.

The iron sulphide K_{sp} shown in Table 2.3 is calculated at 25°C, 80°C and 120°C using Equation (2.62) whilst $K_{H2S,1}$ and $K_{H2S,2}$ are the minimum, maximum and average values obtained from Equation (2.63) through (2.68). $K_{sp,1}$ and $K_{sp,2}$ are calculated using Equation (2.69) and (2.70) which are derived from Equation (2.60) and (2.61) (the minimum and maximum values are obtained using the minimum and maximum $K_{H2S,1}$ and $K_{H2S,2}$). Table 2.3 also shows $K_{sp,2}$, $K_{H2S,1}$ and $K_{H2S,2}$ from ScaleChem (MSE) at 25°C, 80°C and 120°C. These values are printed out by the software whilst $K_{sp,1}$ and K_{sp} are calculated from Equations (2.69) and (2.70).

$$K_{sp,1} = K_{sp} \times K_{H_2S,1} \tag{2.69}$$

$$K_{sp,2} = K_{sp,1} \times K_{H_2S,2} \tag{2.70}$$

	25°C				
	K_{sp}	$K_{sp,1}$	$K_{sp,2}$	$K_{H2S,1}$	$K_{H2S,2}$
Lit. Minimum	-	1.52E-04	9.64E-20	9.29E-08	6.36E-16
Lit. Average	1.63E+03	1.65E-04	1.66E-19	1.01E-07	1.01E-15
Lit. Maximum	-	1.71E-04	2.38E-19	1.05E-07	1.39E-15
ScaleChem	5.48E+03	5.98E-04	5.99E-18	1.09E-07	1.00E-14
	80°C				
	K_{sp}	$K_{sp,1}$	$K_{sp,2}$	$K_{H2S,1}$	$K_{H2S,2}$
Lit. Minimum	-	1.17E-05	1.80E-19	2.21E-07	1.54E-14
Lit. Average	5.29E+01	1.54E-05	6.25E-19	2.92E-07	4.05E-14
Lit. Maximum	-	1.88E-05	1.23E-18	3.55E-07	6.57E-14
ScaleChem	7.61E+02	2.14E-04	5.42E-17	2.81E-07	2.53E-13
	120°C				
	K_{sp}	$K_{sp,1}$	$K_{sp,2}$	$K_{H2S,1}$	$K_{H2S,2}$
Lit. Minimum	-	1.96E-06	1.30E-19	2.46E-07	6.64E-14
Lit. Average	7.98E+00	2.66E-06	1.53E-18	3.33E-07	5.76E-13
Lit. Maximum	-	3.04E-06	3.30E-18	3.82E-07	1.08E-12
ScaleChem	2.79E+02	9.17E-05	1.02E-16	3.28E-07	1.12E-12

Table 2.3: Calculated FeS solubility products and H_2S dissociation constants at 25°C, 80°C and 120°C from literature (Lit.) and ScaleChem.

Some key observations from the data shown in Table 2.3 are:

- The iron sulphide solubility product K_{sp} decreases as temperature increases indicating that FeS is less soluble at higher temperatures (Figure 2.19 for average literature values).

- On the other hand, $K_{H2S,1}$ and $K_{H2S,2}$ increase with increased temperature but this effect is more significant for $K_{H2S,2}$ (Figure 2.19 for average literature values).

- $K_{sp,1}$ is dependent on K_{sp} and $K_{H2S,1}$ and like K_{sp} it decreases as temperature increases (Figure 2.20).

- However, $K_{sp,2}$ increases as temperature increases because of the temperature effect of $K_{H2S,2}$ used to calculate $K_{sp,2}$ (Figure 2.20). Hence, depending on which

equation is used to describe the iron sulphide solubility product, the temperature dependent trend is different.

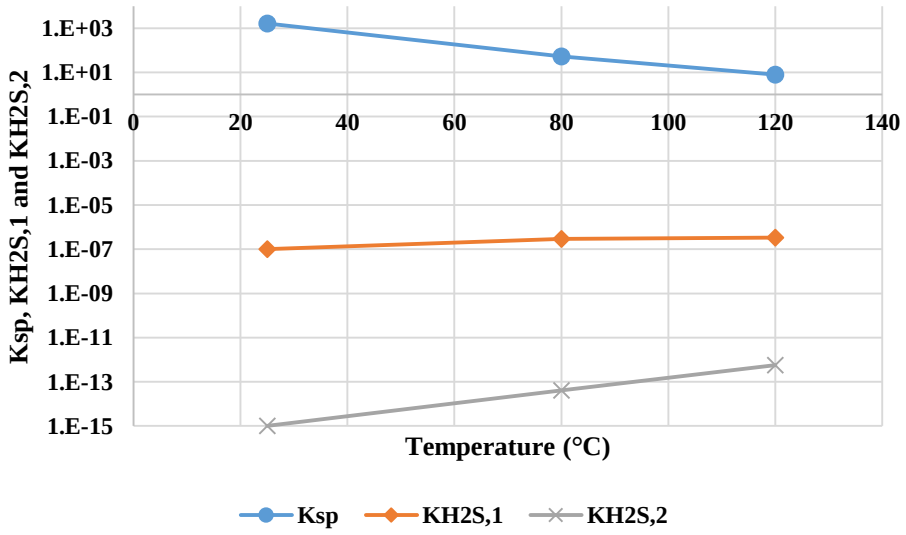

Figure 2.19: K_{sp}, $K_{H2S,1}$ and $K_{H2S,2}$ temperature dependence.

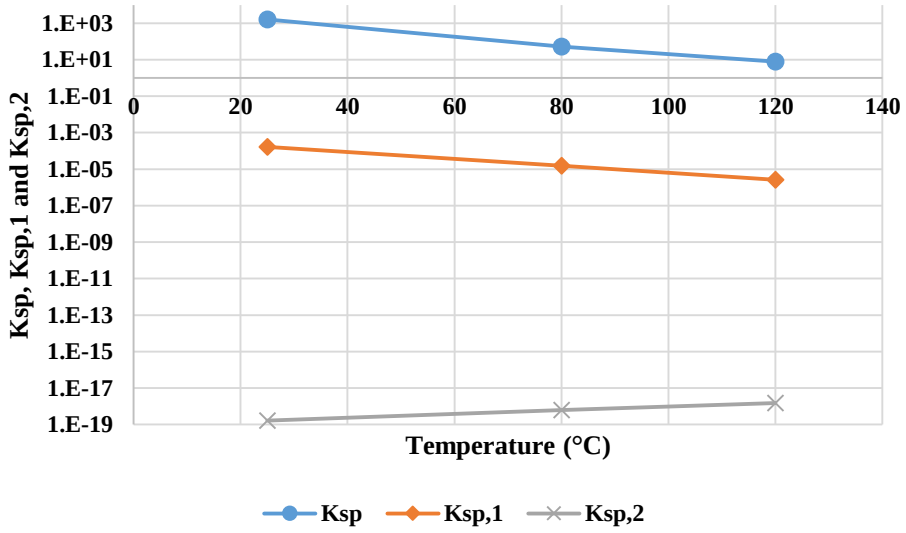

Figure 2.20: K_{sp}, $K_{sp,1}$ and $K_{sp,2}$ temperature dependence.

- Whilst $K_{H2S,1}$ values calculated from different equations are in good agreement (resulting in similar $K_{sp,1}$ values), there are up to two orders of magnitude difference for the calculated $K_{H2S,2}$ resulting in a significant variation of $K_{sp,2}$.

- There are two orders of magnitude difference for $K_{sp,2}$ between the published data and ScaleChem (MSE) results (Figure 2.21). This difference also affects $K_{sp,1}$ and K_{sp} and it is more significant at higher temperature (Figure 2.22 and Figure 2.23). These results do not confirm the validity of one over another but the significant discrepancy is likely explained by the use of a different set of experimental data in ScaleChem which is not in agreement with the reported published values. These results have important implications in the calculation of Maximum Dissolved Iron (MDI) shown in Section 3.4 and in the determination of FeS precipitation.

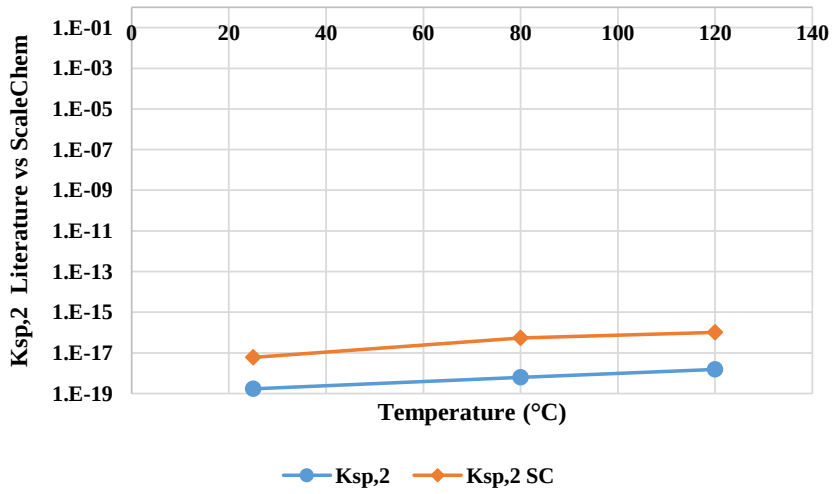

Figure 2.21: Calculated $K_{sp,2}$ from literature vs ScaleChem.

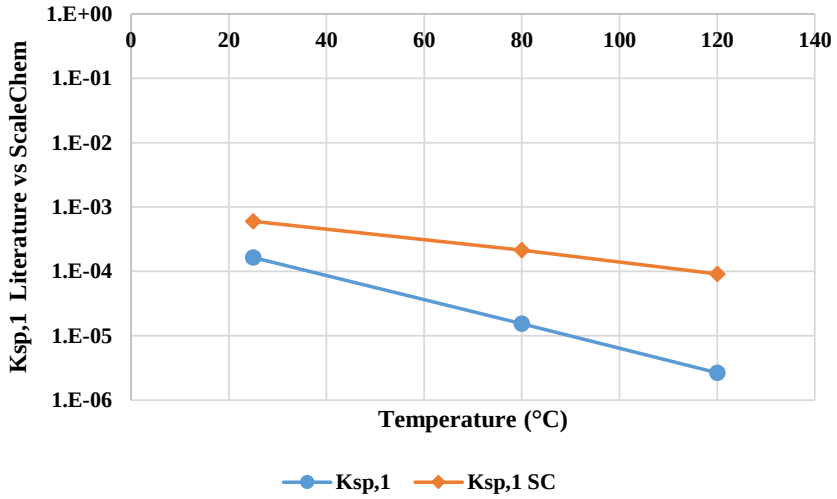

Figure 2.22: Calculated $K_{sp,1}$ from literature vs ScaleChem.

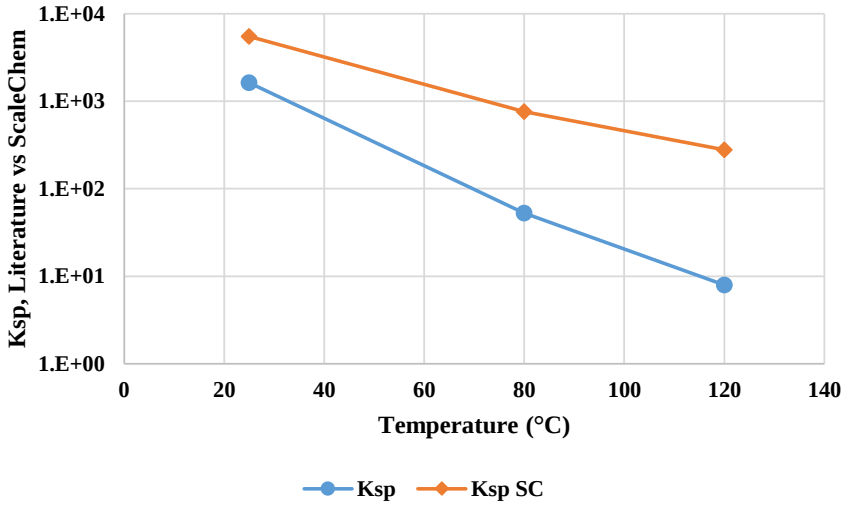

Figure 2.23: Calculated K_{sp} from literature vs ScaleChem.

Conservation of mass and electrical neutrality of solutions. The conservation of mass is shown in Equations (2.71) through (2.75) while the condition of electroneutrality is described by Equation (2.76) where V is the volume of aqueous solution and C_0 is the initial total system charge.

$$\left(m_{CO_2(0)} + m_{HCO_3^-(0)} + m_{CO_3^{2-}(0)}\right)V = \left(m_{CO_2} + m_{HCO_3^-} + m_{CO_3^{2-}}\right)V + n_{CaCO_3} + n_{FeCO_3} \quad (2.71)$$

$$\left(m_{H_2S(0)} + m_{HS^-(0)} + m_{S^{2-}(0)}\right)V = \left(m_{H_2S} + m_{HS^-} + m_{S^{2-}}\right)V + n_{FeS} \quad (2.72)$$

$$m_{Ca^{2+}(0)}V = m_{Ca^{2+}}V + n_{CaCO_3} \quad (2.73)$$

$$m_{Fe^{2+}(0)}V = m_{Fe^{2+}}V + n_{FeCO_3} + n_{FeS} \quad (2.74)$$

$$(m_{HA(0)} + m_{A^-(0)})V = (m_{HA} + m_{A^-})V \quad (2.75)$$

$$C_0 = 2m_{Ca^{2+}} + 2m_{Fe^{2+}} + m_{H^+} - m_{OH^-} - m_{HCO_3^-} - 2m_{CO_3^{2-}} - m_{HS^-} - 2m_{S^{2-}} - m_{A^-} \quad (2.76)$$

Numerical methods such as Newton-Raphson, Broyden and finite difference can be used to solve this system of nonlinear equations.

This set of equations is implemented in commercial scale prediction software which calculate scaling tendencies as well as the resulting full aqueous composition. Scaling tendencies are expressed in terms of Saturation Ratio (SR) or Scaling Index (SI) for each scale type (Kaasa, 1998). These are shown for the $CaCO_3$ example in Equation (2.77) and (2.78).

$$SR = \frac{m_{Ca^{2+}} \times m_{CO_3^{2-}}}{K^0_{sp,CaCO_3}} \quad (2.77)$$

$$SI = log\frac{m_{Ca^{2+}} \times m_{CO_3^{2-}}}{K^0_{sp,CaCO_3}} \quad (2.78)$$

Scale forms when SR>1 (or SI>0) while the system is at equilibrium for SR= 1 (SI=0) and under saturated for SR<1 (or SI<0). The mass of scale predicted to precipitate is also calculated.

Finally, an important property of aqueous systems relevant to inorganic scale formation is alkalinity (Kaasa and Ostvold, 1997). The total (or titration) alkalinity of a natural

water sample can be regarded as a measure of the proton deficit of the solution relative to an arbitrarily defined zero level of protons (Dickson, 1981). Equation (2.79) describes alkalinity for a system containing carbonates, sulphides and organic acids (generic form indicated as HA). However, other chemical species contributing to alkalinity (such as borate) must be included in the calculation if present in oilfield waters.

$$Alkalinity = m_{OH^-} + m_{HCO_3^-} + 2\,m_{CO_3^{2-}} + m_{HS^-} + 2\,m_{S^{2-}} + m_{A^-} - m_{H^+} \qquad (2.79)$$

It is clear from Equation (2.79) that bisulphides (HS^-) can be very important in the determination of alkalinity and must be correctly included in pH dependent scale predictions. Understanding this correlation is fundamental to explain the results shown in Chapter 6 where the impact of variable HS^- concentration is investigated.

Number of calculation steps. A variable number of T and p points from reservoir to separator can be selected for carbonate and sulphide scale predictions. At each point it is possible to:

- "Remove" the precipitated scale from the system assuming that equilibrium is reached and precipitation occurs. Depending on the number of selected points, the local scale precipitation curve can look significantly different as the example in Figure 2.24 shows. If taken to the extreme, this scenario will produce an almost flat curve which represents a system where equilibrium is reached at every infinitely small step. This does not represent real field scenarios and raises the question of how many steps should be chosen for scale predictions;

- Scale is "carried through" from one point to the next and a cumulative scale precipitation curve is obtained. This curve is the same regardless of how many T and p steps have been selected as shown in Figure 2.25. This curve represents

the maximum amount of scale that can form at each selected T and p point if no scale precipitates upstream of that point (which can happen if equilibrium is not reached and supersaturation occurs). Hence, it represents the worst case scenario. This approach also allows to account for scale re-dissolution and it is the recommended one.

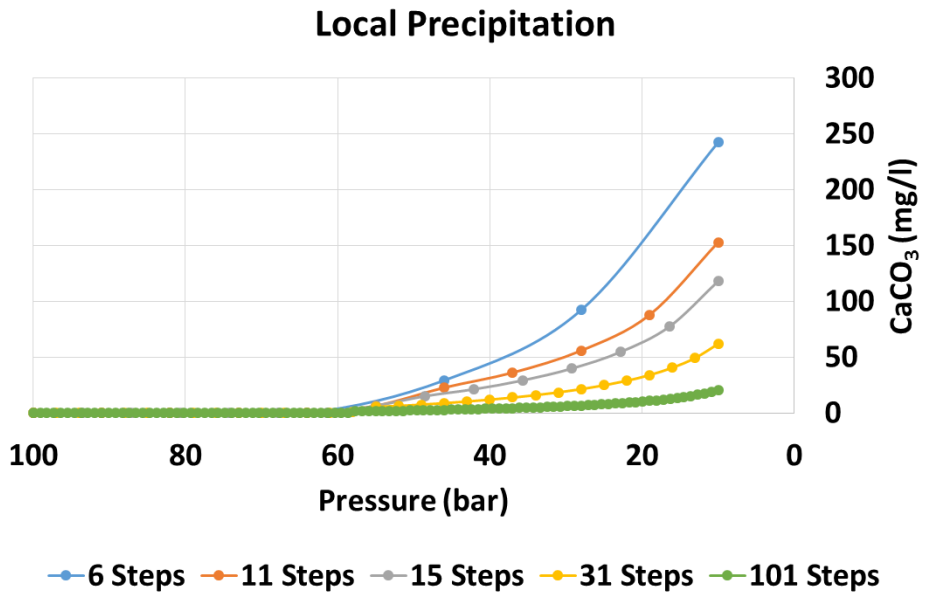

Figure 2.24: Example of local precipitation curve for 6, 11, 15, 31 and 101 T and p steps.

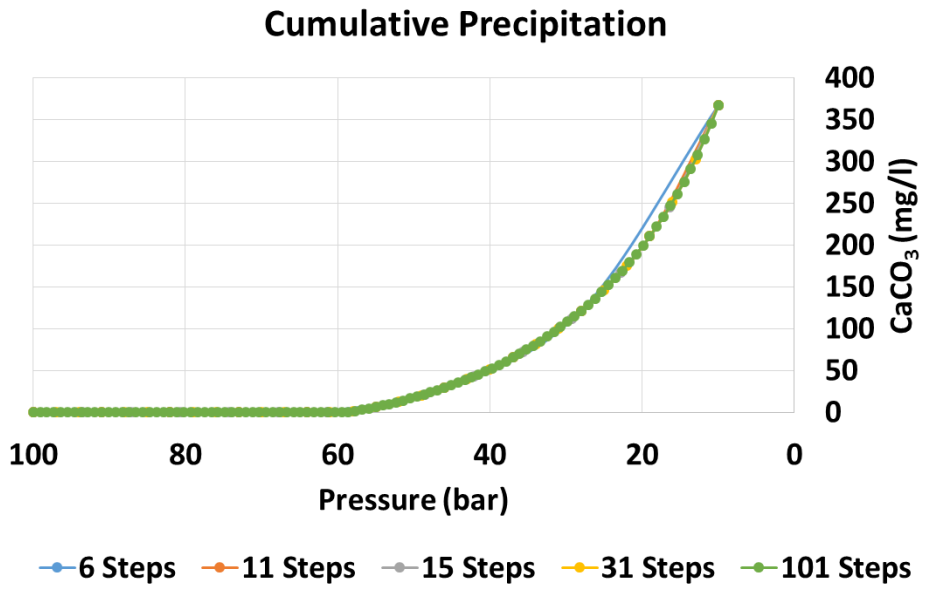

Figure 2.25: Example of cumulative precipitation curve for 6, 11, 15, 31 and 101 T and p steps.

2.3 CARBONATE AND SULPHIDE SCALE PREDICTION CHALLENGES

There are three key categories of data and procedures that must be correctly gathered and used in order to obtain reliable carbonate and sulphide scale predictions. These categories are:

- Data handling procedures;
- Field measurements;
- Software, equations and parameter choice.

2.3.1 Data Handling Procedures

The commonly available "raw" field data is not always the data input required in PVT and aqueous phase model software for the prediction of carbonate and sulphide scales. Hence, there are additional calculation steps (usually iterative steps) which have to be included in the scale prediction procedure to ensure the results are representative of the system investigated. This is described in more detail in Section 3.3 where a rigorous procedure for carbonate and sulphide scale prediction is clearly outlined.

Addition of water to hydrocarbon PVT modelling. In many cases, hydrocarbons are studied independently of the water phase because for a dry oil the water-hydrocarbon mutual solubility is considered small. However, there are field scenarios where neglecting the water-hydrocarbon mutual solubility can cause large errors (Danesh, 1998). While formation water is believed to be in equilibrium with reservoir hydrocarbons, injected water that is not originally in equilibrium with the reservoir will dissolve oil light ends causing a decrease in bubble point pressure. Moreover, at high water cut, a large fraction of the produced gas can be released by the water phase and this must be accounted for when measuring topside flow rates. Finally, if PVT

calculations exclude water and the resulting gas phase is used to obtain water phase CO_2 and H_2S without the correct three phase mass balance calculations, this can lead to large errors. Hence, the input oil and gas compositions (or the total feed) in PVT software must include the correct percentage of water to accurately model the system.

Experimental PVT data regression – tuning Equation of State (EOS). For some gas/condensate and light hydrocarbons it is possible to use the default component properties given by the selected PVT software. However, when component lumping is performed and particularly in the case of heavy oils this can lead to large errors in the final CO_2 and H_2S partitioning which ultimately impacts the pH dependent scale predictions. The properties of pseudo-components (i.e. C_{7+}) vary significantly in different oils and it is important to tune EOS using experimental PVT data to obtain the correct GOR and ultimately a better estimate of CO_2 and H_2S three phase distribution. Indeed, for carbonate/sulphide scale prediction, the most important quantities to come from the phase behaviour are the effective *partition coefficients* of the CO_2 and H_2S between the various (oil, water, gas) phases as discussed in Chapter 7 (Burger et al., 2013). These quantities may be difficult to predict *a priori* for a complex oil and may need to be "overwritten" (i.e. directly input by the user replacing the PVT calculation values) if reliable experimental data is available or if the quantities calculated by the PVT software are "unreasonable".

Use of correct CO_2 and H_2S concentration for oil and gas phases. Experimental PVT data is normally acquired at the early stage of production and refers only to the hydrocarbon phase of a specific well. In addition to including the correct water concentration to the oil and gas (or total feed) composition, CO_2 and H_2S concentrations must also be adjusted. The total three phase CO_2 concentration may change over time

and be different for various wells in the field. Likewise, the H_2S concentration is likely to increase over time in fields where biogenic souring occurs (Johnson et al., 2017). The variation of total water, CO_2 and H_2S concentration for a specific well requires the "reconstruction" of the total PVT feed (or the oil and gas composition) from more recent and representative surface field measurements. Simply using the original hydrocarbon composition for these values can lead to errors, particularly in the calculation of 3 phase total sulphides due to the high H_2S solubility in oil.

Aqueous total carbonates and sulphides vs molecular CO_2 and H_2S. It is important to distinguish between aqueous molecular CO_2 and H_2S and aqueous total carbonates and sulphides. The former is the concentration of molecular CO_2 and H_2S in equilibrium with the gas phase CO_2 and H_2S (vapour/liquid equilibrium, VLE). The latter is the total concentration of water phase carbonate and sulphide species including CO_2, HCO_3^-, CO_3^{2-}, H_2S, HS^- and S^{2-}. This distinction is important to understand the data input/output of some scale prediction models and it is also important when running VLE calculations followed by scale predictions. The final aqueous CO_2 and H_2S concentration must always be the one in equilibrium with the gas phase so all the equations must be solved together or appropriate iterations carried out.

Representative reservoir water composition. If only the original FW is produced from the reservoir and there are no changes to the water composition, the equilibrated FW can be used as starting point for wellbore scale prediction calculations. However, when the field is water flooded (e.g. sea water injection) or produced water is re-injected into the reservoir, the water entering the wellbore will have a significantly different composition from the original formation water (frequently this is a mixture of the injection water (IW) and original FW although some reservoirs may also have more

than one FW). Moreover, reservoir souring will have an impact on dissolved species including CO_2, HCO_3^-, CO_3^{2-}, H_2S, HS^-, $S^{2-}$and SO_4^{2-} (Burger and Jenneman, 2009). Hence, it is essential to reconstruct a representative *current* "near wellbore" reservoir water to use for our scale predictions (see Section 3.2). This composition will most likely change over time and may need to be recalculated for more accurate scale predictions. If a reservoir model is coupled to predict compositional changes of produced water, these results can also be used as a starting point to forecast future well scaling potential.

2.3.2 Field Measurements

Rigorous and robust sampling and analysis procedures are necessary to obtain reliable input data for scale prediction models. If reliable input data is not available, it is consequently not possible to trust the output results and sensitivity studies may be required.

Aqueous iron (Fe^{2+}). Iron can be present in sour water as free Fe^{2+} or precipitated iron scales such as FeS and $FeCO_3$. Note that Fe^{3+} is not expected to be present in sour water because it is a strong oxidant and would react with H_2S to give Fe^{2+} and molecular sulphur (Amend et al., 2004).We distinguish between total iron count and dissolved iron count (NACE, 2012) the former obtained by ICP on an acid digested sample while the latter is usually obtained by ICP on a "freshly collected" sample and theoretically accounts only for the free iron present in the water as Fe^{2+}. However, FeS can be present in colloidal form and pass through the 0.45μm filters used in the sample preparation procedure causing higher "dissolved iron" readings (Al-Harbi et al., 2018). There are also additional challenges associated with sampling of sour waters for iron count analysis and these are widely recognized in the oil industry and are described in a

NACE Standard Practice document (NACE, 2012). In this document, it is stated that "iron counts from fluids containing dissolved sulphides are not reliable because of precipitation of iron sulphide that may deposit on metal surfaces as well as remain suspended in solution". Hence, the majority of iron count measurements in produced fluids may be inaccurate and misleading. This is not to say that such reported iron level data is "useless"; for example, if a high dissolved iron level is measured and the Fe^{2+} concentration is inconsistent with the solution conditions from thermodynamic modelling, then this may tell us that corrosion is occurring somewhere upstream of the sampling point and appearing in the sample. But such cases (common in oil and gas fields) must be carefully interpreted.

pH: It is very well known that water pH is highly dependent on dissolved CO_2 concentration and examples of this were shown in previous publications (Verri and Sorbie, 2017b). When samples are collected, the pressure and temperature changes (which have already occurred at the sampling point) cause variations of CO_2 concentration and the measured pH is different from the "true" value in the system. In-situ and in-line pH measurements are sometimes used to overcome these challenges but these techniques are expensive, not always reliable and are rarely available for routine produced water samples. In many cases, CO_2 and alkalinity measurements are used instead but these can also be impacted by the sampling and analysis procedures.

Alkalinity, bicarbonates (HCO_3^-) and bisulphides (HS^-): The important difference between alkalinity and bi-carbonates in sweet systems is extensively described in the literature (Kaasa and Ostvold, 1997). However, in sour wells HS^- contributes to the total water alkalinity as shown in Equation (2.79). The titration, used to determine alkalinity, will also include HS^- ions which can represent a large fraction of the total alkalinity

depending on the relative CO_2/H_2S concentration and water pH. In addition, since the data measured from produced fluids is the "true" final value, it is necessary to make sure that the *final* calculated water chemistry (in scale prediction software) matches the measured value and not that the measured value is set as the "initial" concentration (initial data input). The same applies to all water ions and to the final pH. Some scale prediction software include the formation of species such as $CaHCO_3^+$, $MgHCO_3^+$, etc. and if present these must all be included in the alkalinity calculations.

Gas phase CO_2 and H_2S: Gas phase CO_2 and H_2S concentrations are two of the most critical measurements for carbonate/sulphide scale prediction because they are used to calculate the aqueous CO_2 and H_2S concentrations and (in some cases) to reconstruct water pH. It is important to collect CO_2 and H_2S gas phase readings for each individual well and not rely on commingled gas samples. It is also key to obtain these readings from a sample point where the gas phase is at equilibrium with the oil and water phase because all the equations used in PVT and scale prediction software are referred to equilibrium. This sample point should ideally be the test separator gas outlet and the sample should be collected only when the well flow through the separator has stabilized and equilibrium conditions are reached.

Calcium (Ca^{2+}) concentration and other ions: The original reservoir formation water (FW) composition can be acquired during the appraisal stage of a field. This FW composition is important for several scaling calculations such as assessing barium sulphate deposition on mixing with sea water (SW). However, for carbonate and sulphide scale prediction, the composition of near wellbore reservoir water will generally be different from the original FW and change gradually over the life of the field due to factors such as water injection, in situ mixing, reservoir geochemistry,

pressure drop in the reservoir, reservoir souring, etc. Representative (changing) downhole samples from producing wells are difficult and expensive to obtain and we rely on real-time surface data for the vast majority of field scale calculations. The surface produced brine may already have undergone some scaling reactions and its ion composition will be different from the water that "left the reservoir". Particularly for Ca^{2+}, the produced brine composition is used to reconstruct the downhole version of this same aqueous fluid element. Moreover, if calcium carbonate scale is likely to precipitate after sampling due to the depressurization which causes loss of CO_2 and increase in pH, the measured Ca^{2+} will not represent the "true" Ca^{2+} in the system. In addition if active scale inhibitor is present, this may prevent $CaCO_3$ precipitation and produce an over saturated water chemistry. Finally, other factors such as contamination from drilling and completion fluids can affect the formation and produced water samples and provide misleading field data. Brine salinity is also important in carbonate and sulphide scale predictions but this is addressed in the "Software, equations and parameters choice" – salting out effect.

2.3.3 Software, Equations and Parameters Choice

In all PVT and scale prediction models, there are a number of equations and parameters which can be changed at the user's discretion. Often software users default to the same choice of equations and parameters although, without sufficient understanding of the implications associated with these variables, it is difficult to adjust them to describe specific field scenarios.

When developing a software package, there is always a conflict between making it easy for users to run and offering the right level of flexibility on various parameters and equations. Users more familiar with and interested in water chemistry (i.e. scale

predictions) are usually less familiar with PVT calculations whilst expert PVT users are not normally involved in detailed aqueous phase scale prediction modelling and often neglect the aqueous phase in their calculations (or treat it in a simplified manner e.g. by simply considering "salinity" in their model). For this reason many integrated PVT + scale prediction software packages compromise on one or the other part of the package.

Assuming the correct procedure for the prediction of pH dependent scale precipitation is followed, there are numerous variables associated with the choice of software, equations and parameters for both the PVT and aqueous phase models which will influence the final pH dependent scale prediction results. These variables are listed in Table 2.4.

PVT Model	***Aqueous Phase Model***
Equation of State (EOS)	Activity model (e.g. Pitzer)
Mixing rule	Solubility products
Component properties (T_c, p_c, etc.)	Equilibrium constants
Binary interaction coefficients (K_{ij})	Complexes and other species
Henry's law constant	
Salting out coefficient	
Experimental database – oils, T and p	Experimental database – brines, T and p

Table 2.4: Variables in PVT and aqueous phase models which have an impact in the pH dependent scale predictions.

Despite the large number of equations, parameters and other modelling options available in PVT software, all these variables ultimately lead to calculating just ***two*** key pieces of information for the system, as follows:

- Three phase volume and mole distributions at the various values of temperature (T) and pressure (p);

- CO_2 and H_2S partition coefficients K_{OW}, K_{GW} and K_{GO}.

The final scale prediction results can be accurate only when these values are accurate irrespective of how they are obtained. This also means that if we knew these values *a priori* (from direct experiment, for example) and fixed them in our calculations, the choice of PVT software, EOS etc. would be irrelevant; we could simply use these K-values in our aqueous model and use the phase data for material balance, and we would obtain accurate answers.

This information will become important in later chapters (Chapter 7) where the extent of the impact of software and EOS choice on partition coefficients is thoroughly investigated.

Volume and Mole Phase Distribution. To obtain good results for the mole phase distribution at variable T and p, the information and tools required are reliable PVT experimental data, a full PVT software with choice of EOS and the capabilities for data regression to adjust the EOS accordingly. Reservoir and production engineers are normally those who deal with this type of work more frequently and can provide a good PVT model for the *hydrocarbon phase* to be used a starting point for scale predictions. A classification of the various EOS is shown in Figure 2.14 but hydrocarbon PVT modelling can be a complex science and it is beyond the scope this work to describe all EOS models and when each one should be used. However, this work focuses on systems containing water (and other polar components such as CO_2 and H_2S) for the study of scale predictions, it is well known that cubic equations of state such as Peng Robinson do not describe these systems correctly. Hence, using a more appropriate EOS (e.g. cubic plus association, CPA) is strongly recommended to obtain more physically reliable results. If the PVT model is tuned by someone who is only interested in the

hydrocarbon phase and does not rigorously account for polar components, the errors associated with using that specific PVT model in scale predictions can be significant.

CO_2 and H_2S Partition Coefficients. The definition of partition coefficients is given in Section 2.2.1 and their variability when using different software, EOS and other input parameters is calculated in Section 7.2. CO_2 and H_2S partition coefficients affect the solubility of CO_2 and H_2S in the aqueous phase at various T and p in the system and ultimately impact pH dependent scale predictions. However, only reliable experimental data for three phase CO_2 and H_2S concentration can provide the "correct" partition coefficients and confirm which of the modelling results is true.

2.4 IRON SULPHIDE PREVENTION, INHIBITON AND SCALE REMOVAL

Ultimately the reason for running scale prediction calculations is to prevent whenever possible the formation of deposits which have a negative impact on oil and gas production and operations. This is not always possible and the treatment strategy for iron sulphide scale (and similarly for carbonate scales) reflects this challenge. There are three different approaches to dealing with iron sulphide scale in oil and gas wells: prevention, inhibition and removal (see Figure 2.26). Normally, a combination of these methods is required to effectively control irons sulphide scale in the oilfield (Przybylinski, 2001).

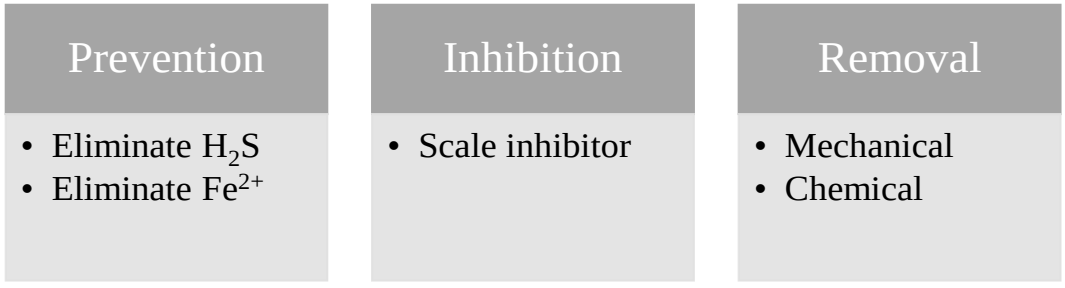

Figure 2.26: Strategies to control iron sulphide scale in oil and gas fields.

If one of the two elements forming iron sulphide (H_2S and Fe^{2+}) can be removed or reduced to a sufficiently low level, the sulphide scale formation can be prevented or greatly reduced. Alternatively, sulphide scale can be managed by chemically or mechanically removing deposits that have formed. Finally, the most pursued albeit difficult way of preventing iron sulphide problems is to inhibit its formation using an effective scale inhibitor.

2.4.1 Iron Sulphide Scale Prevention

The two elements needed to form iron sulphide are Fe^{2+} and H_2S in water. Therefore, if one of these components is removed from the system, then FeS will obviously not form.

In most field scenarios it is not practically possible to completely remove one of these elements. However, there are cases where the control of H_2S and/or Fe^{2+} is sufficient to reduce the scale risk to a minimum level which is operationally acceptable. H_2S and Fe^{2+} removal are also key for combined mitigation and removal strategies, such as acid removal as discussed in the iron sulphide removal section below.

Eliminate H_2S

The sources of hydrogen sulphide in the oilfield can be divided in three main categories (Nasr-El-Din and Al-Humaidan, 2001):

- Biotic (biogenic): generated by sulphate reducing bacteria (SRB).
- Abiotic: thermochemical sulphur reduction, thermal hydrolysis of organic sulphur compounds, or hydrolysis of metal sulphides.
- Decomposition of thread sealants and chemical containing sulphide during drilling operations (minor impact).

Hydrogen sulphide generation can occur in different parts of the system and the mitigation approach depends on the source, location and severity the problem. An example is shown in Figure 2.27.

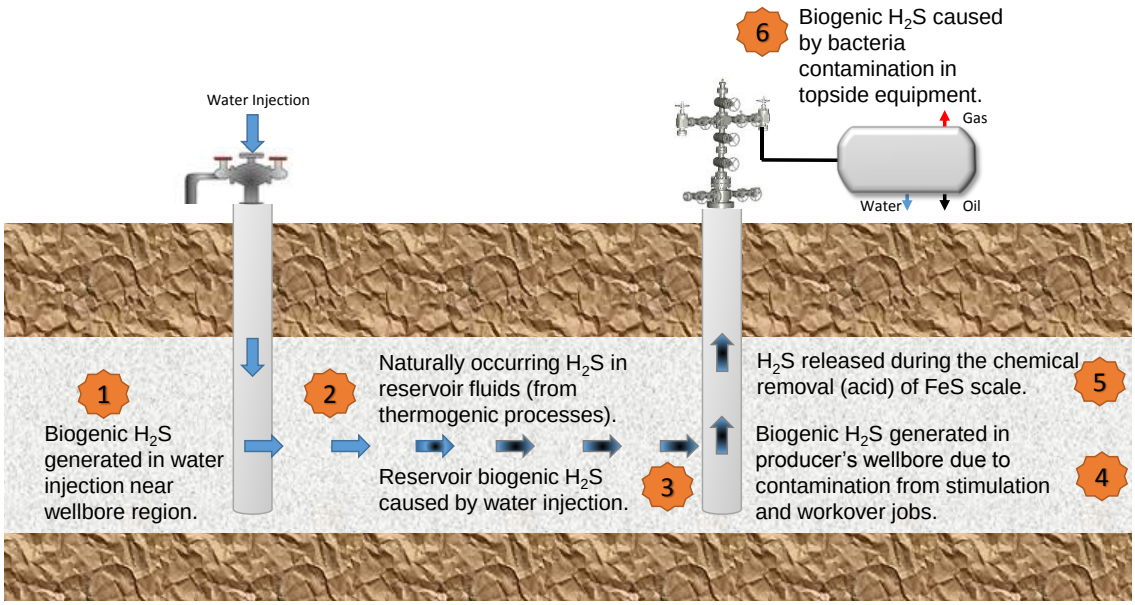

Figure 2.27: Schematic of H_2S common generation points and likely causes.

Some key factors to account for when addressing the sulphide problem are:

- H_2S source (biogenic, thermogenic)
- H_2S levels in every fluid phase (current and projected over the field life)
- Potential treatment points (upstream or downstream of the Fe^{2+} source)
- Other operational constraints (i.e. chemical volumes and on site availability)
- Treatment cost
- Environmental impact

It is beyond the scope of this work to review H_2S treatments in oil and gas systems (scavengers and biocides) but a large number of papers have been published on this

subject (Coombe et al., 2013, Aften and Roberts, 2011, Wylde et al., 2008, Al-Humaidan and Nasr-El-Din, 1999).

Eliminate Fe^{2+}

Before considering how iron can be removed from the system, it is important to understand what the sources of iron in the system are. The nature of the iron source will determine in many cases how removal should be tackled.

The absence of iron in the formation brines does not preclude the formation of iron scale in the system (Wylde and Winning, 2004). The main sources of iron in oil and gas systems are reservoir rocks, drilling fluids, some proppants in hydraulic fracturing, "normal" corrosion of any metal tubulars or components and "additional" corrosion due to acid stimulation treatments (Ramachandran et al., 2015a, Ma et al., 2016).

In some cases, the change in the reservoir recovery process may lead to some additional iron in solution as in an EOR process such as CO_2/WAG. For example, BP have reported increased dissolved iron levels during low salinity water injection and attributed this phenomenon to iron being the bridging ion between clay and naphthenic acids. These bridging ions come back with the produced water as part of the low salinity process (Sheng, 2013).

Evaluating the source of iron in the system is not always straightforward. Some research claims that it is possible to identify the source of iron by looking at the scale composition. If the metal contains manganese, manganese should also be found in the scale deposit (Nasr-El-Din and Al-Humaidan, 2001). However, manganese can be present as MnS clusters in the metal and remain stable at those conditions or dissolve

and stay in solution with the produced fluids. Manganese Mn^{2+} analysis in produced fluids is very common to assess corrosion problems albeit the Fe^{2+}/ Mn^{2+} ratio becomes rather unreliable in a system containing H_2S (Bahadori, 2014). The presence of Mn^{2+} in the produced water is a proof that at least some manganese does not precipitate with other scale. No evidence of scale containing manganese has been found in the literature.

When the main source of iron is corrosion, implementing a corrosion mitigation program rather than scale inhibition treatment is normally the most successful and cost effective approach to prevent FeS formation and prevent or limit system integrity problems.

If dissolved iron is naturally present in reservoir fluids or if sour wells are commingled with Fe^{2+} containing brines, iron chelators can be used to bind with the metal, change its reactivity and prevent the reaction with H_2S and formation of FeS.

Iron chelators are also usually preferred over more aggressive albeit more commonly used chemicals such as mineral acids for scale dissolution. A list of common iron chelators is presented in Table 2.5 (Wylde, 2014).

Chemical Name	**Acronym**
Ethylenediamine-tetra-acetic acid	EDTA
Diethylene-triamine-penta-acetic acid	DTPA
Hydroxyethylene-diamine-tetra-acetic acid	HEDTA
Nitilotriacetic acid	NTA
THPS and Modified THPS	THPS
Citric acid, Acetic acid, Glycolic acid	

Table 2.5: Iron chelating chemicals.

Although chelating agents have very high binding constants with both Fe^{3+} and Fe^{2+}, these values are often reported for the fully deprotonated species at a high pH value (Wang et al., 2013a). This makes chelating agents rather less effective for use in normal lower pH production fluids since they are less dissociated and their binding constants are lower, and thus they are less effective. This poses a particular high challenge when these chelators are deployed as additives in acid jobs. As an example, experimental data has shown that EDTA, a common chelating agent, is in the completely unionized, mono-ionized and di-ionized form at acid return pH suggesting that it will not protect all the coordination sites of the metal to prevent FeS deposition (Brezinski, 1999). Despite their wide spread use to mitigate iron sulphide deposition, laboratory testing suggests that EDTA and NTA are not effective at acid flowback conditions (pH=3) and can form a white solid due to full protonation of the chemical. In addition, EDTA-Fe complexes have been proven to be unstable for temperatures above 250°F at 500psi (Brezinski, 1999). However, at pH=5 and T=70°C both NTA and EDTA have shown good inhibition performance at substoichiometric concentration (Ko et al., 2019).

Iron chelators can be injected in the system continuously at low concentrations to control sulphide scale precipitation and they are sometimes used in conjunction with surfactants to penetrate the oil layer (barrier) common in iron sulphide deposits which are generally found to be oil wet (Wylde, 2014).

2.4.2 Iron Sulphide Scale Inhibition

As mentioned in previous Sections, the first iron sulphide scale formed under oilfield conditions is a nano-particulated phase of disordered mackinawite (Wolthers et al., 2005). This is not an amorphous solid but has a long tetragonal crystalline structure.

Inhibition may be very hard due to the low solubility and fast kinetics of mackinawite formation but crystal growth can be chemically controlled (Okocha et al., 2018).

Scale inhibitor efficiency tests are run routinely for sulphides and other inorganic scales. Defining the correct criteria for "successful" results is a key part of scale inhibitor selection and this strongly applies to sulphide scales. The sub microscopic size of disordered mackinawite crystals suggests that chemical treatments may not technically "inhibit" iron sulphide formation but rather "control" it and prevent crystal growth by a chelation or steric stabilisation effect. Chelation is a common method for managing iron sulphide problems. Nevertheless, keeping iron is solution in one part of the system may cause more problems downstream and may not be a viable option in all cases.

Since disordered mackinawite is very reactive and very difficult to inhibit, some researches have been focusing on dispersing these initial long range crystalline structures and keep them in solution while stopping further growth. This method may be good to prevent solid precipitation and accumulation in vessels but can have a detrimental effect on emulsions and water quality. Hence, test methods and success criteria should be determined based on system requirements.

Amongst the most studied chemistries for sulphide scale inhibition are polymeric scale inhibitors. Polymers have been found to be far more effective than phosphonate based chemicals at preventing ZnS and PbS deposition which can sometimes occur in conjunction with FeS scale (Jordan et al., 2000). Laboratory tests and one field application show how different polymeric scale inhibitors were screened and selected to prevent ZnS and PbS scale precipitation (Lopez et al., 2005). A different study shows

that a higher scale inhibitor concentration may be required to inhibit ZnS and PbS compared to carbonate and sulphate scales (Collins and Jordan, 2003).

A product with undisclosed chemistry was found to be effective for iron sulphide dispersion in a field trial to tackle oil/water interface problems. Calcium levels and solution pH also had an impact on the chemical performance (Lehmann and Firouzkouhi, 2008).

Interesting results have been published on the development of a new polymeric chemical for FeS, ZnS and PbS inhibition which was optimised by altering different monomers to obtain the most effective final blend (Savin et al., 2014). Although these products are defined as iron sulphide inhibitors by the authors, it is clear from test results run in the laboratory that iron sulphide does indeed form (black water) but the crystal size is controlled and remains suspended even after centrifugation (Wylde et al., 2017). The suggested mechanism illustrated in Figure 2.28 is that amide bonds in the copolymer seeded metal sulphide crystals via electrostatic interaction. The metal/sulphide crystal can then grow within the polymer structure until steric resistance stops growth still keeping this structure in solution (Wylde et al., 2015).

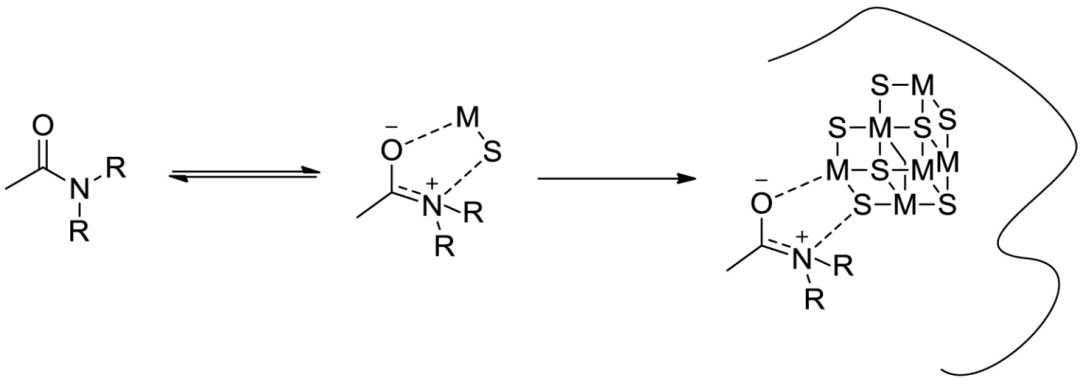

Figure 2.28: proposed mechanism for iron sulphide inhibition of a new copolymer molecule

Although these chemistries are claimed to be extremely effective and sometimes "revolutionary", it is important to remember that inhibition efficiencies are strongly dependent on specific field scenarios and that a chemical selection study should always be undertaken prior to implementing a chemical treatment.

2.4.3 Iron Sulphide Scale Removal

Sulphide scales have extremely low solubility products which makes them hard to remove once they form. To understand how these compare to more common oilfield scales, solubility products for carbonate, sulphate and sulphide scales are shown in Table 2.6 (Dean, 1999).

Mineral	**Solubility Product (Ksp)**
Calcium carbonate (calcite, $CaCO_3$)	3.36×10^{-9}
Iron carbonate ($FeCO_3$)	3.13×10^{-11}
Barium sulphate (barite, $BaSO_4$)	1.08×10^{-10}
Iron sulphides (FeS)	6.3×10^{-18} ($K_{sp,2}$)
Zinc sulphide (sphalerite, ZnS)	$1.6 \times 10^{-24} – 2.5 \times 10^{-22}$
Lead sulphide (galena, PbS)	8×10^{-28}

Table 2.6: Solubility product constants for a selection of common inorganic mineral scales and sulphide scales found in oil and gas production at 25°C.

Due to the numerous challenges associated with iron sulphide inhibition and prevention and to the limited amount of research conducted on this topic, many operators still rely on scale removal treatments as a mean of managing iron sulphide scale problems in the field (Wylde et al., 2016).

Despite scale removal treatments being common in the oilfield, they present a number of challenges and in some cases significant drawbacks which include corrosion, release of toxic H_2S in the system, secondary deposition and others.

Moreover, the scale aging process changes the sulphide crystalline structure and its solubility in acid. Aged sulphide scales normally contain larger amounts of acid insoluble components like marcasite, pyrite and pyrrhotite and they are more challenging to remove with simple chemical treatments. Scale composition can also be different in different sections of the well. These changes in scale composition highlights the need for extensive scale deposit sampling to draw the right conclusions about scale solubility and the help selecting an effective clean out method.

When removing sulphide scale deposits there a number of factors to consider:

- Remove scale which often contains more than one type of deposit
- High dissolution capacity at system conditions (i.e. downhole p and T)
- Keep corrosion at minimal levels
- Minimise amount of toxic gas (H_2S) evolved in the system
- Prevent scale re-precipitation
- Do not cause formation damage
- Cost-effective treatment
- Operationally doable treatment

Sulphide scale removal treatments can be divided in three categories:

- Mechanical
- Chemical
- Mechanical + Chemical

Mechanical clean-up is normally performed on acid insoluble sulphide scales. It can then be followed by a chemical treatment to completely remove the more soluble scale deposits which are found closer to the metal surface (i.e. tubing).

The most common mechanical clean out methods are scale milling and coiled tubing abrasive jet cleaning. New methods currently under investigation also include a fluidic oscillation technology (Leal et al., 2007) and the use of ultrasonic waves (Kunanz et al., 2014).

Some of the challenges encountered in mechanical scale removal particularly in deep high pressure wells include: high annulus velocities required for lifting out scale particles, need for killing the well using heavy mud, more than one coiled tubing runs may be necessary for effective scale removal, jet pressure limitations (Mirza and Prasad, 1999).

The most common chemical scale removal products are shown in Figure 2.29 (Wylde et al., 2016).

Property	INHIBITED 7.5% HCl	ORGANIC ACIDS	THPS	ACROLEIN
Loading	Excellent but does not work on some polymorphs	Poor	Okay but affected by high pressure	Okay performance
Kinetics	Excellent 1-3 hr	Slow c.24 hr	Slow c.24 hr	Slow c.24 hr
Ecotox	Corrosion inhibitor component is poor	Good	Toxic	Deadly
Application	Easy to moderate Sometimes pre-flush required	Moderate Pre-flush required/surfactants	Easy to moderate Pre-flush sometimes required	Moderate always require a preflush and specialized equipment
Corrosivity	Still corrosive at high temperature	Moderate	Moderate	Low
Secondary deposition	High risk as non-chelating	Low risk	No risk	No risk
H_2S Evolution	Very high	Medium	High	Very low
Handling	High risk	Risks (low pH)	Risk (skin corrosive)	Gas – very challenging
Effective on $CaCO_3$	√	√	X	X
Effective on $CaSO_4$	√	X	X	X

Figure 2.29: Key features, benefit and shortcomings of the most common types of iron sulphide dissolver chemistries used in the oil and gas industry.

The dissolution kinetics are temperature and chemical dependent so preliminary lab tests on field scale samples are always recommended prior to treatment deployment.

Hydrochloric acid is the most common product used for chemical scale removal and it is used in conjunction with other chemicals to tackle different issues encountered during acid sulphide dissolution. The main drawbacks of acid treatments are corrosivity and hydrogen sulphide generation from the scale dissolution. Moreover, acid scale removal treatments could introduce Fe^{3+} as a contaminant of the acid or a product of metal corrosion when the top protective iron sulphide layer is removed. This Fe^{3+} is very unstable in the presence of H_2S and may react quickly to form elemental sulphur which is very hard to dissolve and can only be removed using expensive organic acids (Walker et al., 1990).

If acid soluble scale is suspected to be present in the well, an acid clean out job is required prior to acid stimulation. In fact, the first acid pumped into the well will be spent to remove the sulphide and carbonate scale present in the tubing and near wellbore. This spent acid will also contain large amounts of dissolved iron which is likely to re-precipitate once the acid reaches the carbonate reservoir and its pH is further increased. If this fluid is not pumped out of the well but pushed in the formation as part of an acid stimulation job, it can cause significant formation damage and negatively affect production rates (Ford et al., 1992).

One subject not discussed in most of the literature on acid treatments for sulphide scale removal is related to asphaltic oils. Asphaltenes are naturally present in some oils and they can become unstable at low pH or in the presence of certain chemicals causing the formation of rigid film emulsions. This slimy material can reduce well productivity, cause severe topside separation issues and sometimes completely stop well flow (Jacobs and Thorne, 1986). Hence, acid treatments may not be a viable option for wells producing asphaltic oils or may require additional control measures.

A second commonly used sulphide scale dissolver is THPS which works using a chelation mechanism. Some additives like ammonium salt and phosphate significantly improve THPS sulphide scale dissolution performance. The dissolution efficiency of THPS was tested against 20% HCl showing comparable performance for the 20% THPS + 4% ammonium chloride blend while THPS alone did not give particularly good performance (Gilbert et al., 2002).

Further studies on THPS dissolution capabilities against iron sulphide capabilities are also available. However, most of these studies are conducted at relatively low pressures

and when pressure is increased the dissolution efficiency of THPS declines significantly (Wang et al., 2013b).

An additional chemistry proven to be effective for iron sulphide scale removal and for scavenging H_2S is Acrolein (Salma, 2000). This is an extremely reactive chemistry which only forms CO_2 and H_2O as reaction products. Unfortunately it is also very toxic and difficult to handle leaving numerous concerns amongst operators who may consider using it. Nevertheless, it is probably the most effective chemistry currently available and it has the least negative impact on the system.

A polymer based chemistry has been proposed as a non-acidic alternative to acid treatments (Wang et al., 2013b). However, the lab data is very limited and there is no field study to support these findings.

A carboxylate copolymer was found to perform well in lab tests and in one field application (Wylde et al., 2016).

A combination of two dissolver products simply named as Fluid A and Fluid B was tested on Ghawar field scale samples showing a reasonable dissolution performance for some forms of iron sulphide (Hajj et al., 2015). However, this treatment caused the formation of elemental sulphur which represented almost 15% of the sample in the leftover solids. As previously mentioned, elemental sulphur is insoluble in hydrochloric acid and can only be removed using expensive organic acids.

2.5 SUMMARY AND CONCLUSIONS

This literature review covers the basics of pH dependent scale predictions and describes in some detail the challenges associated with field studies of carbonate and sulphide scales.

Although this review was initially focused solely on sulphide scales, it is clear now that these cannot be investigated in isolation and carbonates must also be included in the discussion. This is because there is a strong interdependence between system properties such as pH, alkalinity etc. which are impacted by CO_2 and H_2S concentrations and ultimately affect both carbonates and sulphides precipitation.

Nevertheless, a larger section of this review is dedicated to iron sulphide scale because its prediction and treatment in the field present numerous additional challenges compared to carbonates.

The critical review of published work presented here clearly identifies the top big issues associated with the study of carbonate and sulphide scales in oil and gas wells:

1. The aqueous iron chemistry must be properly studied and resolved for oil and gas produced waters. Not only the field measurement of dissolved iron is unreliable in sour systems but the potential presence of soluble iron species brings more uncertainty around the actual water chemistry composition to be used for scale predictions. Do these soluble iron species form at field conditions? If they do, which species are they and do they really affect the final scale prediction results? Fe^{2+} is normally present in relatively small concentrations suggesting that any soluble or colloidal species may play an

important role in FeS scale precipitation but studies at field conditions must be undertaken to answer these important questions.

2. Introducing kinetic equations to describe iron sulphide precipitation and transformation to different crystalline forms is the only way to run actual scale predictions rather than simply matching field findings. At present, only thermodynamic data is available and it is by "suppressing" more stable FeS forms that less stable forms (more likely to precipitate at field conditions) are predicted. The discussion of introducing kinetics in oilfield scale predictions (including carbonates) has been ongoing for many years but the large number of variables linked to such calculations (time, temperature, H_2S exposure, fluids composition etc.) and the lack of experimental data for systems that mimic real field conditions mean that reliable kinetic calculations are not possible at this stage. When the composition of precipitated scale is known it is possible to include/exclude different FeS forms to match scale predictions to field data. But forward predictions are completely arbitrary when the same process is used. Software users must then be aware that increasing the complexity of calculations without supporting them with reliable data and parameters will simply introduce more uncertainty to scale prediction results and further limit their reliability.

3. The partitioning of acid gases CO_2 and H_2S between gas, oil and water directly impacts CO_2 and H_2S availability in the aqueous phase which controls carbonate and sulphide scale precipitation. Hence, the choice of EOS, parameters and indeed of PVT software plays a pivotal role in the final pH dependent scale predictions which require a good understanding of these variables.

4. Too often scale prediction software are used as a black box without a good understanding of the calculations run in the background or without questioning the reliability of the parameters used. An example was shown for the mackinawite solubility product calculated by ScaleChem which was found to be very different to some of the published data. Another example is the distinction between alkalinity and bicarbonates which becomes particularly important in the case of sour waters. The correct use of field data is then critical for reliable scale predictions but results between different software could differ significantly depending on the database of experimental data implemented.

5. Corrosion and scale prediction modelling of iron sulphide are strongly linked together through the $CO_{2(aq)}$ and $H_2S_{(aq)}$, the in-situ pH and Fe^{2+} availability. Therefore, it is clear that a powerful modelling tool would include PVT, aqueous phase (bulk) and corrosion equations together rather than running these calculations separately. When all reaction mechanisms are considered simultaneously it is often possible to get an overall picture of the problem and explain field findings which are sometimes hard to describe using individual tools.

6. The field treatment of FeS is more challenging than other scales, particularly in the case of inhibition. There are currently limited options on the market for iron sulphide scale inhibition and since completely stopping the formation of mackinawite is not possible due to its fast kinetics of precipitation, these products tend to keep iron sulphide dispersed in colloidal form. Hence, when implementing an iron sulphide scale treatment, the entire production process

must be considered to avoid simply “moving” the problem to a different part of the system.

It is clear that new relevant experimental data is necessary to move forward on some of these issues and improve the current common knowledge on sulphide scale predictions.

However, this work aims at addressing some of the challenges described above by:

- clearly defining a step-by-step procedure for carbonate and sulphide scale predictions using commonly available field data and any commercial PVT and scale prediction software;
- reviewing the impact of field measurement errors, choice of different software and parameters on final scale predictions;
- applying these methods to two very different field scenarios to address key operational questions.

Chapter 3– CARBONATE AND SULPHIDE SCALE PREDICTION PROCEDURE: THE WORKFLOW

3.1 INTRODUCTION

This Chapter lays out the core part of this research work which is the development of a rigorous procedure (workflow) for carbonate and sulphide scale predictions.

Although some carbonate scale prediction methods were published in the past (McCartney et al., 2014, Fleming et al., 2007) these methods are specific to the field case investigated, they are software dependent, they rely on limited integrated PVT software and they cannot be used as a general procedure for carbonate and sulphide scale predictions in oil and gas wells.

Some major operators (e.g. BP, Shell) have in-house proprietary procedures and it is not the aim of this work to discredit these procedures which we do not have access to and cannot review.

What makes this workflow different from any other scale prediction procedure is that:

- It is publicly available. This means that it has been tested and reviewed by many experts and improved over the course of this PhD project (this version is the most recent update) and that it can be used by anyone who has experience in pH-dependent scale predictions.

- It is not software specific. This procedure can be applied using any scale prediction and PVT software overcoming many of the limitations of commercial integrated software and can be used by any company who has access to any PVT and aqueous phase model (integrated or not);

- It is not field specific. Is this truly a general procedure? In short yes, it is. In practice every field scenario is different and although the general headings of each step apply, the individual calculations differ from case to case. Moreover, some steps (i.e. the Ca^{2+} recombination from separator to reservoir) may not be necessary depending on which input data is available. On the other hand, more technically challenging scenarios (e.g. gas lift, multiple zone production, etc.) will need additional steps to be included. Hence, this is a guiding methodology which must be made specific to each field scenario investigated by competent scientists and engineers who understand the chemistry and mechanics of the problem.

Carbonate and sulphide scale predictions are more complex than another inorganic scale (e.g. $BaSO_4$, $SrSO_4$, etc.) since the formation of these scales is very closely coupled with the CO_2 and H_2S partitioning between gas, oil and water (Olajire, 2015). For this reason, at each point in the system, it is essential to obtain in-situ 3 phase (oil/water/gas) CO_2 and H_2S distributions by running pressure/volume/temperature (PVT) calculations and then using these results in a mineral scale prediction model. The mineral scales which may form in this system are mainly calcium carbonate ($CaCO_3$), iron sulphide (FeS) and iron carbonate (siderite, $FeCO_3$) although other coupled scales and complexes can also form.

Some commercial software (i.e. ScaleChem (OLI, 2016) and MultiScale (Expro, 2015)) combine these calculations into one single package but packages more targeted to aqueous systems have limited hydrocarbon capabilities while full PVT software packages (i.e. Winprop (CMG, 2017) and PVTsim (Calsep, 2015)) focus primarily on the hydrocarbon phase and have limited capabilities for scale predictions and

calculations of water phase properties. Finally, the input data required for these software is not all commonly available (e.g. all phase compositions at the same temperature and pressure/sample point) and a rigorous step-by-step procedure is necessary to reconstruct the correct values.

The oil industry is quite divided regarding surface and subsurface work, and most models focus primarily on the hydrocarbon phase or the water phase. To close this gap, an integrated workflow (step-by-step procedure) which combines any full PVT software with any scale prediction software to use field data to generate carbonate and sulphide scale prediction profiles from the reservoir to the first stage of separation has been developed in this work. With the correct modifications to include changes in stream flows and total mass balance, the workflow can also be applied downstream of the first stage of separation. Although a few operator and service companies have proprietary internal procedures to run such calculations, prior to this work being conducted, there was no published (an publicly available) comprehensive step-by-step procedure to clearly show how to go from commonly available field data to scale prediction profile from the reservoir to the separator. This procedure is of great benefit to fully "unpack" and describe all the factors impacting pH-dependent scale predictions, to correctly utilise all the available data and ultimately to be able to integrate the use of any chosen PVT software with any aqueous phase model eliminating the limitations described above.

This chapter describes a procedure or workflow (and not a new code) based on a compositional phase behaviour model which can in principle be applied to any field scenario providing that the PVT model is tuned to the selected system data and an appropriate aqueous mineral scale prediction code is available. If any mineral deposition

occurs, then the total fluid composition is adjusted to account for this, and the subsequent compositions are affected.

This workflow will be referred to as the “Heriot-Watt scale prediction workflow” or “HWU scale prediction workflow” in the rest of the document.

The thermodynamic and chemical process involved in these calculations are described in Section 2.2.

3.2 WATER CHEMISTRY RECOMBINATION

Before describing the scale prediction workflow, it is important to review the basic thermodynamic principles needed to recalculate the reservoir water composition which produces the measured topside water chemistry.

NOTE. In this work, “reservoir water composition” is referred to the fully equilibrated reservoir water just about to enter the near wellbore area and not to water deeper in the reservoir where other geochemical reactions may take place and not have reached equilibrium yet.

The chemical changes that water undergoes from the reservoir to the first stage of separation are caused by temperature and pressure changes, gas vaporization, water condensation/evaporation, scale precipitation, wax and asphaltene precipitation etc. Hence, the water composition measured at separator can differ very significantly from the water present at reservoir conditions. An example of three different waters in an oil and gas well is shown in Figure 3.1

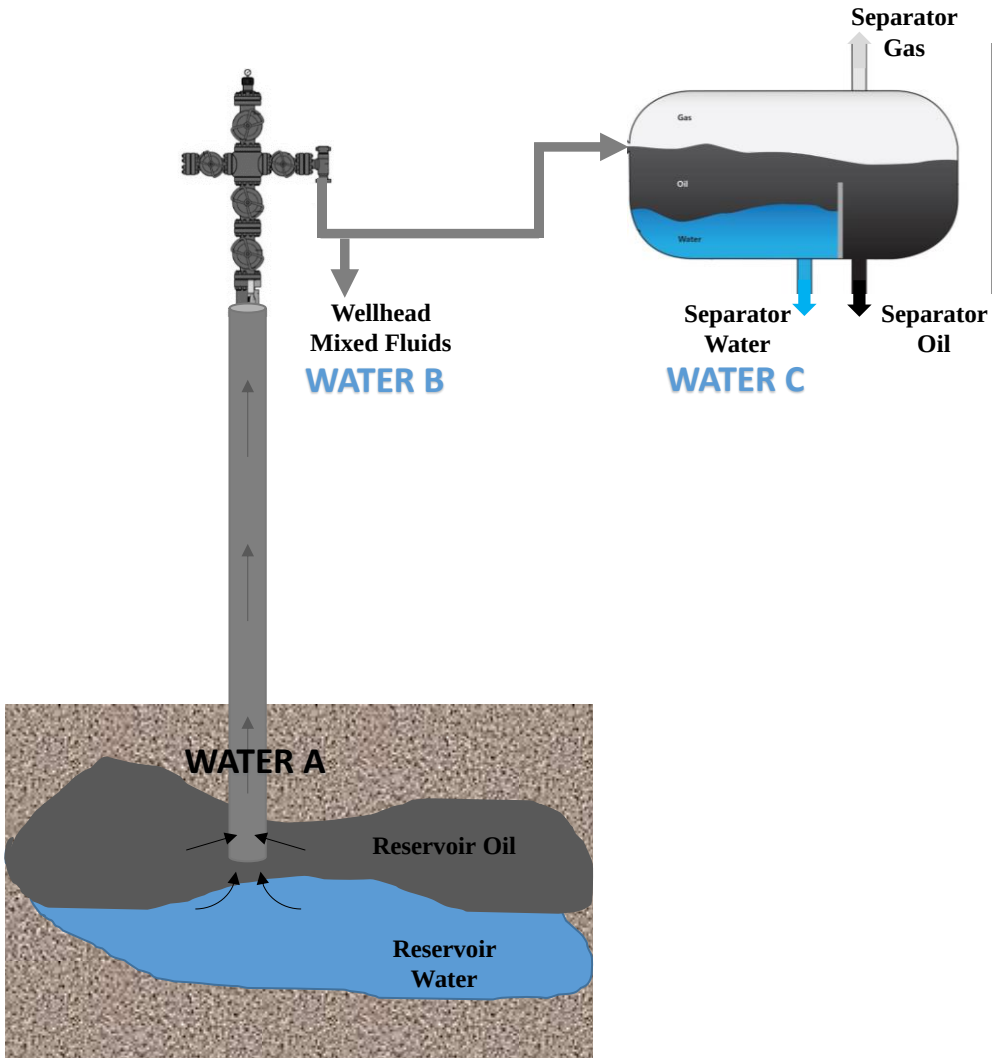

Figure 3.1: Schematic of water changes in an oil and gas well.

Sometimes, the original reservoir formation water (FW) composition (Figure 3.2) is used as the reservoir water composition and start point for scale prediction calculations in the later life of the well. This FW composition is important for several scaling calculations such as assessing barium sulphate deposition on mixing with sea water (SW). However, for carbonate and sulphide scale predictions, the composition of near wellbore reservoir water is generally different from the original FW and changes gradually over the life of the field due to factors such as water injection, in situ mixing, reservoir geochemistry, pressure drop in the reservoir, reservoir souring, etc.

Representative (changing) downhole samples from producing wells are difficult and expensive to obtain and scale calculations rely on routinely collected surface samples. The surface produced brine may already have undergone some scaling reactions and its ion composition will be different from the water that "left the reservoir".

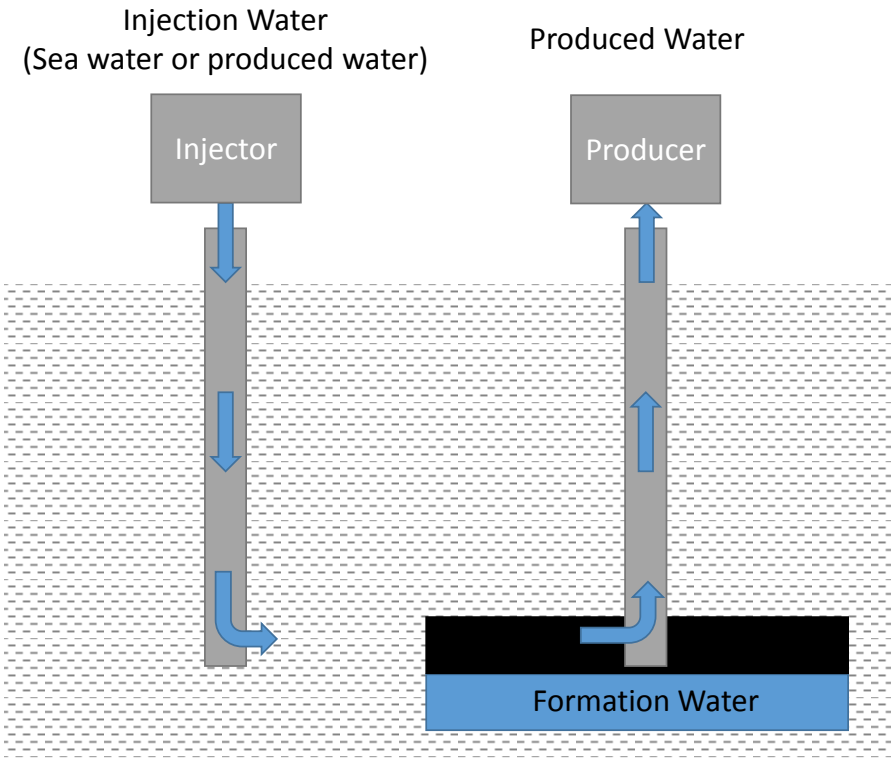

Figure 3.2: Injection water (IW), formation water (FW) and produced water (PW) schematic.

Gas vaporization, water condensation/evaporation, wax and asphaltene precipitation can be modelled by running the correct PVT calculations as shown in this Chapter for the HWU Workflow. However, if carbonate and sulphide scales precipitate somewhere along the system between the reservoir and the separator, the measured topside Ca^{2+}, Fe^{2+} and alkalinity can be significantly different from downhole values and the reservoir composition must be recalculated.

Other challenges in reconstructing downhole water composition include but are not limited to:

- Wells producing from multiple zones and/or non-homogeneous reservoirs. This scenario requires additional information on downhole water compositions and production data.

- Scale precipitation at the point of sampling due to depressurization, loss of CO_2 and increase in pH, producing a Ca^{2+} measurement which is not representative of the "true" Ca^{2+} concentration in the system.

- Presence of active scale inhibitor in the system which prevents $CaCO_3$ precipitation and produces an over saturated water chemistry.

- Various sources of produced water contamination such as drilling and completion fluids, stimulation treatment chemicals etc.

These scenarios must be investigated on an individual basis and likely require a scenario mapping approach.

3.2.1 Derivation of Equilibrium Equation

The charge balance Equation **(3.1)** can be combined with the alkalinity Equation **(3.2)**to produce Equation **(3.3)**.

$$C_0 = 2m_{Ca^{2+}} + 2m_{Fe^{2+}} + m_{H^+} - m_{OH^-} - m_{HCO_3^-} - 2m_{CO_3^{2-}} - m_{HS^-} - 2m_{S^{2-}} - m_{A^-} \quad (3.1)$$

$$Alkalinity = m_{OH^-} + m_{HCO_3^-} + 2\,m_{CO_3^{2-}} + m_{HS^-} + 2\,m_{S^{2-}} + m_{A^-} - m_{H^+} \quad (3.2)$$

$$\frac{Alkalinity}{(2m_{Ca^{2+}} + 2m_{Fe^{2+}})} = 1 \quad (3.3)$$

The precipitation of $CaCO_3$, $FeCO_3$ and FeS anywhere between the reservoir and separator changes the system alkalinity as well as the concentration of Ca^{2+} and/or Fe^{2+} depending on which scale forms. Nevertheless, Equation (3.3) is valid anywhere in the system where equilibrium is reached so Equations (3.4) and (3.5) are also valid. By subtracting the separator alkalinity to the reservoir alkalinity and multiplying by the corresponding water volume (to account for water volume changes due to condensation/evaporation) we obtain Equation (3.6) where "n" is the absolute number of moles.

NOTE: chlorides are normally used to balance the total charge in a water chemistry analysis. The total number of moles of chlorides does not change from reservoir to separator and can be cancelled out. If NaCl precipitates, Na^+ must be included in the equation but for every mole of Na^+ removed, one of mole of Cl^- is also removed so the net effect is zero.

$$\frac{(Alkalinity)_{separator}}{(2m_{Ca^{2+}} + 2m_{Fe^{2+}})_{separator}} = 1 \tag{3.4}$$

$$\frac{(Alkalinity)_{reservoir}}{(2m_{Ca^{2+}} + 2m_{Fe^{2+}})_{reservoir}} = 1 \tag{3.5}$$

$$(n_{Alkalinity_{res.}} - n_{Alkalinity_{sep.}}) = 2[(n_{Ca^{2+}} + n_{Fe^{2+}})]_{res.} - 2[(n_{Ca^{2+}} + n_{Fe^{2+}})]_{sep.} \tag{3.6}$$

It follows that the ratio between the alkalinity change and the (Ca^{2+} + Fe^{2+}) change from reservoir to separator is also equal to 2 as shown in Equation (3.7).

$$\frac{(n_{Alkalinity_{res.}} - n_{Alkalinity_{sep.}})}{(n_{Ca^{2+}} + n_{Fe^{2+}})_{res.} - (n_{Ca^{2+}} + n_{Fe^{2+}})_{sep.}} = 2 \quad (3.7)$$

Equation **(3.7)** is not a constraint in the calculation of reservoir water composition if the chosen aqueous phase software automatically adjusts Ca^{2+} and HCO_3^- in the reservoir equilibration process with $CaCO_3$ rock. However, if the software fixes the final number of moles of Ca^{2+} to the input value, this equation must be used to ensure the number of moles of Ca^{2+} is adjusted correctly.

3.2.2 Applying Reservoir Equilibrium

The method used to calculate the reservoir water composition from topside water chemistry involves re-equilibrating the topside (separator) 3 phase full compositions and flow rates with calcium carbonate rock at reservoir temperature and pressure. The $CaCO_3$ that precipitates between the reservoir and the separator is re-dissolved at reservoir conditions (equilibrium) providing the equilibrated reservoir water chemistry. This method is used automatically in commercial software such as ScaleChem but it is also applied in the HWU scale prediction workflow that uses separate PVT and aqueous phase models.

The data input required for these calculations includes full three phase compositions at the point of sampling (i.e. separator) which are normally not directly available. Hence, it is not possibly to simply “plug in” available data but these compositions must be calculated by using the correct procedure (see workflow description) which normally involves a series of steps and iteration processes.

3.3 THE WORKFLOW

The design of a rigorous step-by-step procedure for carbonate and sulphide scale predictions can be divided into two main parts (Figure 3.3) (Verri et al., 2017a).

Part 1. **From separator to reservoir**: reconstruct reservoir water chemistry from commonly available surface data. This part of the workflow also provides the cumulative scale precipitation from reservoir to separator.

Part 2. **From reservoir to separator**: this part of the workflow is used to obtain a scale prediction profile from reservoir to separator using the reconstructed reservoir water chemistry.

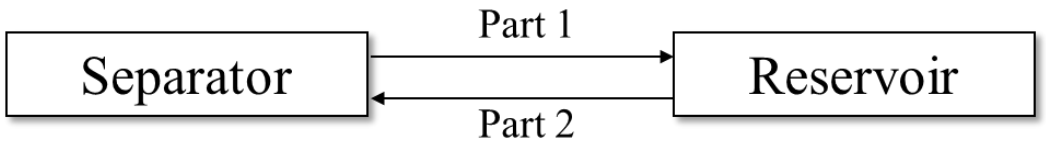

Figure 3.3: Schematic of workflow Part 1 and Part 2.

NOTE. Due to the uncertainty associated with water soluble iron measurement in sour systems (NACE, 2012) the following workflow is run assuming initial Fe^{2+}=0. By combining the water chemistry results calculated suing this workflow and the concept of Maximum Dissolved Iron (MDI) (Verri and Sorbie, 2017b) it is possible to investigate iron sulphide formation. If sulphides are not present, Fe^{2+} can be treated just like an additional cation, and the same procedure used below for Ca^{2+} can be applied with the addition of Fe^{2+}.

3.3.1 Part 1: From Separator to Reservoir

The recombination process to obtain the reservoir water composition from surface water chemistry can be divided into six steps and is shown in Figure 3.4.

The data required to run these steps includes separator temperature (T) and pressure (p), reservoir T and p; well flow rates, well gas CO_2 and H_2S concentration measured at separator conditions, produced water chemistry from separator sample and original hydrocarbon PVT. This data is commonly available for most wells.

Note that this workflow is an improved version of the one previously published (Verri et al., 2017a) and it ensures that the mass balance for both carbonates and sulphides is correct.

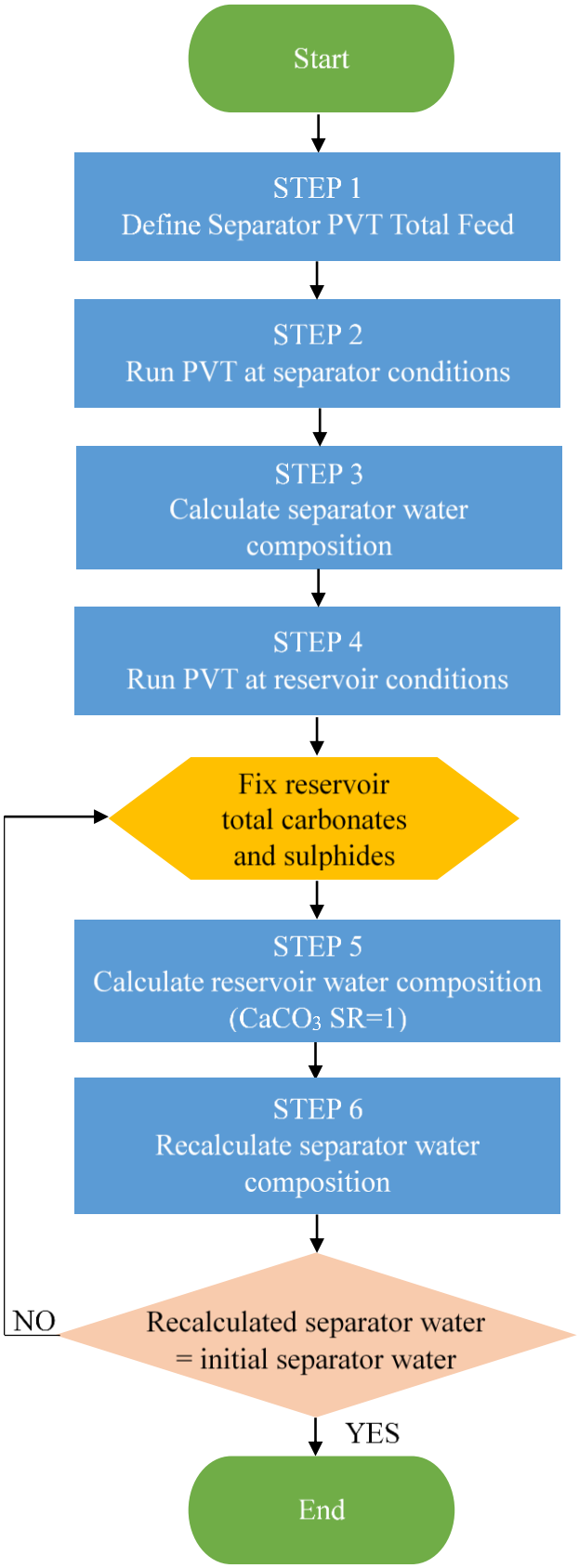

Figure 3.4: Workflow Part 1 - Steps 1 through 6 for the calculation of reservoir water composition from separator water chemistry.

Step 1. Define PVT Total Feed. The PVT total feed is the composition of the combined phases (hydrocarbon, aqueous, CO_2 rich and all others) present in the system. The PVT total feed may change from reservoir to separator if paraffin and asphaltenes precipitate/dissolve or if reactions involving CO_2 and H_2S occur in the water phase (e.g. $CaCO_3$ precipitation/dissolution).

The total feed must include all components present in the system, and it is particularly important to add the correct amount of total water, CO_2 and H_2S present in the system. These values change over time and must be adjusted if conditions change (i.e. water injection, reservoir souring).

PVT experimental data usually provides the hydrocarbon composition only whilst water, CO_2 and H_2S concentrations must be adjusted accordingly. The PVT experimental data is used for data regression to adjust EOS parameters and match the experimental hydrocarbon behaviour with model results.

On the other hand, the procedure to correctly adjust water, CO_2 and H_2S concentration in the total feed depends on what information is available and on which fluids are being studied. In Chapter 4 and Chapter 5 these calculations are described for a gas/condensate well and for a black oil (Verri et al., 2017b, Verri et al., 2017c).

In all scenarios, whether this workflow or a commercial integrated PVT + scale prediction software is used, some important checks may be carried out to ensure that the total feed is calculated correctly. These include but are not limited to:

- Ensure that the total feed flashed at standard conditions gives the correct gas-oil-ratio (GOR). For high water cut wells, the gas-water-ratio (GWR) also plays an

important role and the total feed flashed at standard conditions must produce a gas volume equal to GOR + GWR.

- If the separator is close to equilibrium conditions (sufficient retention time), the total feed flashed at separator conditions should give the correct gas/oil/water ratio as well as the field measured CO_2 and H_2S gas phase concentration (assuming these field measurements are reliable for the scenario investigated).

Step 2. Run PVT Calculations at Separator Conditions. Using the calculated total PVT feed from Step 1, run PVT flash calculations at separator temperature and pressure.

This step calculates the gas, oil and water molecular CO_2 and H_2S concentrations at separator conditions as well as the three-phase relative volume and mole distributions of all phases. Figure 3.5 schematically illustrates the parameters calculated in Step 2 for CO_2 and the same applies to each component present in the system.

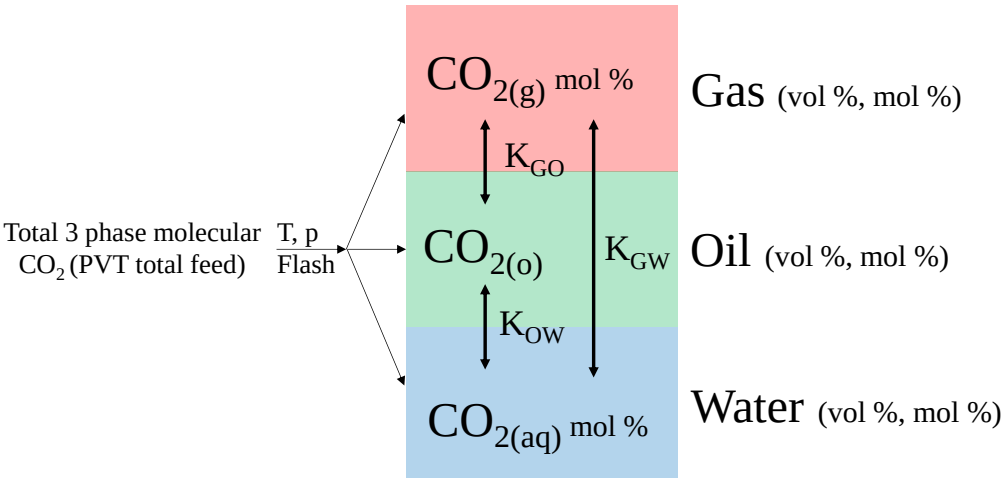

Figure 3.5: Results of PVT flash for CO_2 at given T and p.

The calculated separator gas phase CO_2 and H_2S concentrations and the oil, gas and water relative flow rates should match the measured values if equilibrium is achieved in the separator.

Having obtained the three-phase relative flow rates and mole %, it is possible to calculate the total number of moles of oil + gas + water in the system as well as the total moles of carbonates and sulphides at separator conditions.

This total number of moles does not account for other aqueous species such as HCO_3^-, CO_3^{2-}, HS^- and S^{2-} which influence changes in molecular three phase CO_2 and H_2S total moles when temperature and pressure change (from reservoir to separator) and when scale precipitates or dissolves. In gas/condensate wells, low water cut wells or high CO_2/H_2S wells the contribution of HCO_3^-, CO_3^{2-}, HS^- and S^{2-} to the total number of moles of carbonates and sulphides is negligible when compared to the number of moles in the three phase system. Hence, we can assume that the total PVT feed is the same at reservoir and separator conditions.

However, in higher water cut wells or low CO_2/H_2S scenarios, the aqueous phase reactions significantly impact total carbonates and sulphides in the system and cause a change in the PVT total feed from reservoir to separator. The iteration process required to account for this effect is described in Step 4 and 5.

Step 3. Calculate Separator Water Compositions. The full aqueous phase composition includes HCO_3^-, CO_3^{2-}, HS^- and S^{2-} as well as the calculation of pH. Some PVT software packages only consider the partitioning of molecular CO_2 and H_2S between oil, gas and water but do not calculate CO_2 and H_2S speciation (to HCO_3^-, CO_3^{2-}, HS^- and S^{2-}) or pH. Others include the aqueous phase model too but usually have limited capabilities on one or the other part of the software package.

An aqueous phase model is required to obtain the full water composition and when this model is separate from the PVT software package, the correct iteration procedure must be used to integrate the two. Hence, the fundamental importance of this workflow.

All aqueous phase models have an "initial" set of input values which are used to calculate the "final" equilibrium conditions.

In Step 3 of the workflow, the *final* aqueous molecular CO_2 and H_2S concentrations are fixed to the values calculated from the PVT flash (Step 2) while the *final* alkalinity (or pH) and Ca^{2+} concentration are fixed to the measured field values. If $CaCO_3$ is expected to precipitate at separator conditions, the aqueous phase can be equilibrated with $CaCO_3$ instead of fixing the final pH or alkalinity (this is discussed further in Section 6.2.3).

The initial conditions (CO_2, H_2S and alkalinity/pH) are adjusted until the fixed final conditions are obtained. The results of this calculation fully define the concentration of all species in the aqueous phase and the pH at separator temperature and pressure.

Step 4. Run PVT Calculations at Reservoir Conditions. The separator PVT total feed calculated in Step 1 is flashed at reservoir temperature and pressure to calculate the three phase volume and mole distribution.

As mentioned in Step 2, in reality the PVT total feed changes from reservoir to separator and it is impacted by reactions in the aqueous phase ($CaCO_3$, FeS and $FeCO_3$ precipitation and dissolution which impact the total molecular CO_2 and H_2S moles in the system) and by the precipitation of paraffin and asphaltenes (which is not considered in this work).

The precipitation and dissolution of pH dependent scales in the system has a negligible impact on the total moles of all components in the system. Hence, using the same PVT

total feed at reservoir and separator is good to calculate the three phase volume and mole distribution of gas/oil/water.

On the other hand, the same aqueous phase reactions can have a significant impact on the total moles of molecular CO_2 and H_2S in the system and consequently change the total PVT feed. Step 5 describes how to correct for this change which is negligible only if the water cut is low and/or the CO_2 and H_2S concentrations are high.

Step 5. Calculate Reservoir Water Composition. This step requires the integration of results from different software (separate PVT and aqueous phase model) using two iteration processes to ensure the correct mass balance of components in all three phases.

The interdependence of PVT results and aqueous phase model results is schematically shown in Figure 3.6 for $CaCO_3$ and FeS scale (where "Reservoir total carbonates" = "Separator total carbonates" + $CaCO_3\downarrow$ and "Reservoir total sulphides" = "Separator total sulphides" + $FeS\downarrow$).

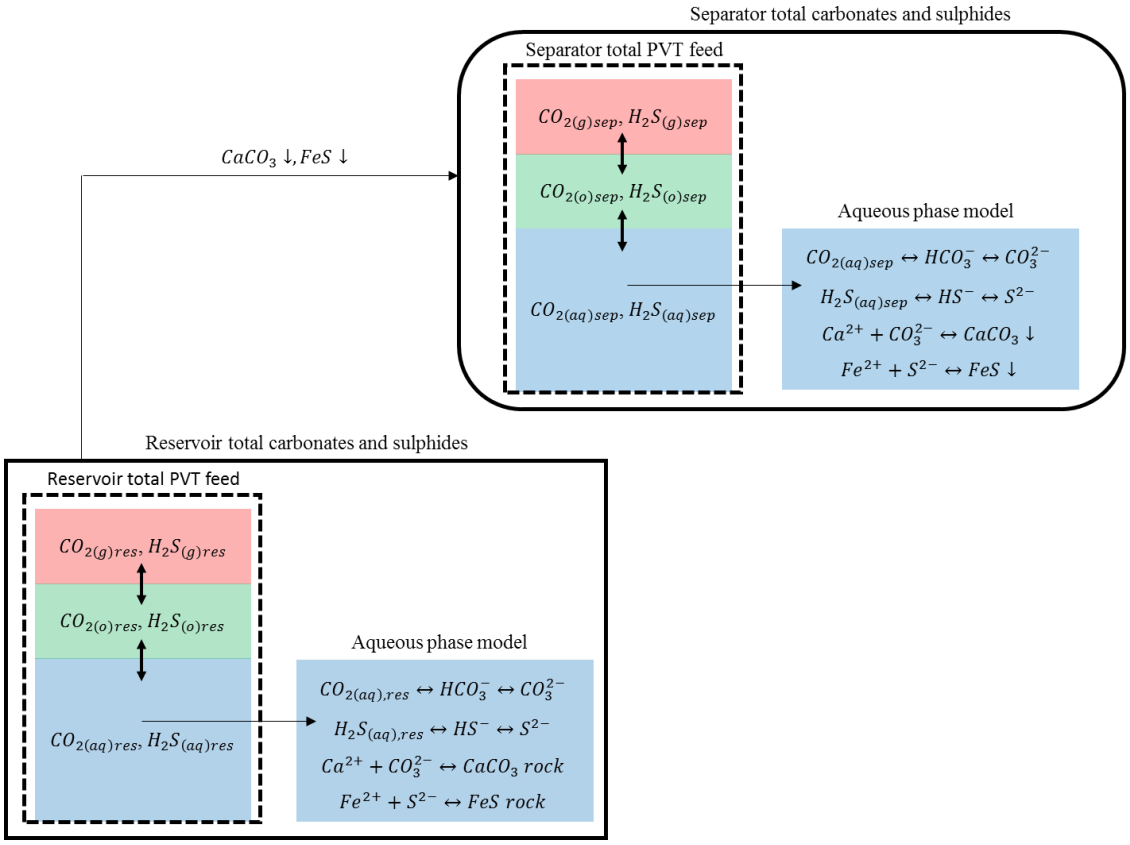

Figure 3.6: Graphic representation of reservoir and separator three phase total carbonates and sulphides and interdependence between PVT and aqueous phase model results.

System constraints to calculate the reservoir water compositions:

I. The reservoir fluids are equilibrated with $CaCO_3$ (SR=1) on the assumption that some $CaCO_3$ rock is present in the formation. If different types of rock (e.g. pyrite) are present in the reservoir, they must be included in the equilibration process.

II. For the general workflow, the total number of moles of reservoir carbonates and sulphides must be initially fixed and for the first iteration these are fixed to the same values calculated at separator conditions. If any scale precipitates in the separator or upstream of the separator, the recalculated separator water chemistry (Step 6) will not match the originally calculated water composition

(Step 3) and in the second iteration the reservoir carbonates and sulphides are adjusted to include any precipitated scale. More than one iteration may necessary to have <1% difference in recalculated water chemistry.

III. The input water chemistry for the aqueous phase model is the separator water chemistry with concentrations adjusted for the aqueous phase volume change from separator to reservoir (due to condensation/evaporation processes). However, when fluids go from surface to reservoir pressure, more CO_2 and H_2S dissolve in the aqueous phase and to account for this effect the input molecular CO_2 and H_2S are adjusted until the final calculated total carbonates and total sulphides match the target value (constraint II).

The output of this simulation provides the full reservoir water chemistry.

Step 6. Recalculate Separator Water Composition. Using the reservoir water chemistry calculated in Step 5 as data input for the aqueous phase model (adjusted for water volume changes from reservoir to separator), the separator water chemistry is recalculated by adjusting the input molecular CO_2 and H_2S until the output total carbonates and sulphides match the reservoir value.

If this recalculated separator water composition differs from the one calculated in Step 3, the originally fixed reservoir total carbonates and sulphides have to be adjusted in Step 5 and Step 5 and 6 repeated.

Simplified Workflow for Low Water Cut and High CO_2/H_2S Wells. In the case of low water cut wells or wells producing high CO_2 and H_2S, the majority of CO_2 and H_2S moles is found in the hydrocarbon phase. Hence, changes in molecular CO_2 and H_2S in

the aqueous phase due to scale precipitation/dissolution have a negligible impact on the total PVT feed.

Therefore, the same PVT total feed calculated for separator conditions can be flashed to determine the aqueous molecular CO_2 and H_2S concentrations at any other point in the system from reservoir to separator.

The aqueous molecular CO_2 and H_2S concentrations at reservoir conditions are calculated in Step 4 and fixed in Step 5 instead of the total carbonates and sulphides (constraint II). The recalculated separator water (Step 6) should match the original composition (Step 3) without any iteration process.

3.3.2 Part 2: From Reservoir to Separator

In Part 1 of the workflow the separator and reservoir full water compositions are calculated along with the cumulative $CaCO_3$ scale predictions at separator temperature and pressure.

If scale predictions are required for any other T and p point upstream of the separator, Part 2 of the workflow describes the procedure to do so. This is shown in Figure 3.7.

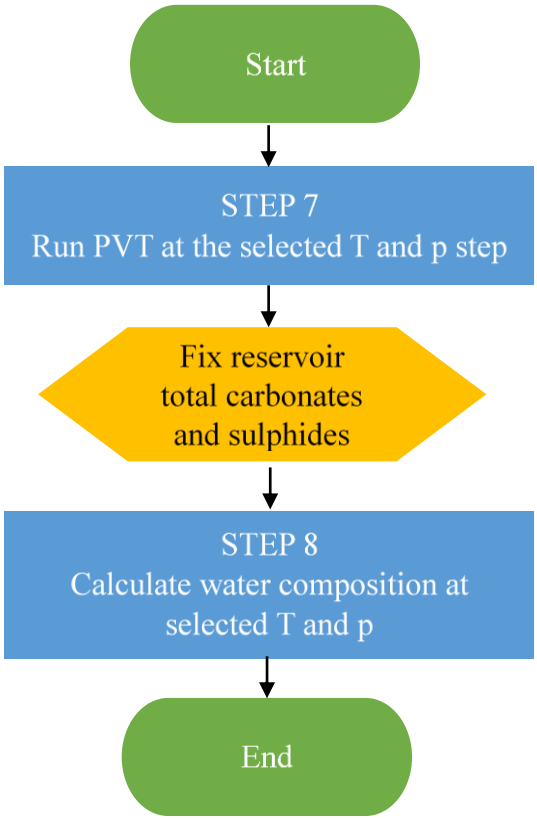

Figure 3.7: Workflow Part 2 - Steps 6 through 8 for the calculation of a scale prediction profile from the reservoir to the separator.

Step 7. Run PVT at Selected T and p Step. The separator PVT total feed calculated in Step 1 is flashed at the given temperature and pressure to calculate the three phase volume and mole distribution.

As mentioned in Step 2, in reality the PVT total feed changes from reservoir to separator and it is impacted by reactions in the aqueous phase and by the precipitation of paraffin and asphaltenes (which is not considered in this work).

The precipitation and dissolution of pH dependent scales in the system has a negligible impact on the total moles of all components in the system. Hence, using the same PVT total feed from reservoir to separator is good to calculate the three phase volume and mole distribution of gas/oil/water.

Step 8. Calculate Water Composition at Selected T and p Step. System constraints to calculate the water compositions at selected T and p:

I. The total number of moles of reservoir carbonates and sulphides is fixed to the value calculated in Part 1 of the workflow (the final one obtained after the iteration process). These total moles of carbonates and sulphides do not change along the system but any scale precipitate must be included in the calculations.

II. The input water chemistry for the aqueous phase model is the reservoir water chemistry but with concentrations adjusted for the aqueous phase volume change from reservoir to the selected point in the system (due to condensation/evaporation processes). However, to account for the repartitioning of gas at different T and p, the input molecular CO_2 and H_2S are adjusted until the final calculated total carbonates and total sulphides match the target value (constraint I).

The output of this simulation provides the full water chemistry at selected T and p as well as the predicted scale precipitation at that point.

3.4 MAXIMUM DISSOLVED IRON (MDI)

In most fields, iron is the limiting reagent in the formation of iron sulphide (i.e. H_2S is usually present in excess). Hence, it is the source of iron and not the amount of hydrogen sulphide in the produced fluids that most commonly determines the amount of scale formed (Ford et al., 1992).

Some reservoirs contain iron minerals and produced waters contain variable levels of Fe^{2+} concentrations (Warren and Smalley, 1994). In other cases, it is corrosion processes of various types that are the main iron source for the precipitation of iron

sulphide scale. Once FeS precipitates, it may be very difficult to understand the main source of iron which caused this precipitate to form, thus making it challenging to design a mitigation strategy that tackles the right issue.

To address some of these questions, the concept of "Maximum Dissolved Iron" (MDI) is introduced (Verri and Sorbie, 2017b). The MDI concentration is the highest Fe^{2+} concentration which can be present in the given water at defined temperature (T), pressure (p) and aqueous phase composition ($[CO_2]_{aq}$, $[H_2S]_{aq}$), before any iron scale precipitates. This does not necessarily correspond to the true in-situ Fe^{2+} concentration but it represents the upper limit of iron that is stable in aqueous solution. When the concept of MDI is applied to *reservoir* fluids, the maximum dissolved iron represent the highest concentration of naturally occurring Fe^{2+} that can potentially be carried into the well and the production system from reservoir fluids. Any additional iron found in the wellbore and topside must be of different origin and may be caused by:

- Corrosion mechanisms (Svenningsen et al., 2009, Woollam et al., 2011, Standlee et al., 2011, Zheng et al., 2015b);
- Acid jobs which cause additional corrosion and dissolution and re-precipitation of iron scales (Garzon et al., 2007);
- Iron containing proppants (Ma et al., 2016);
- "Colloidal" (more likely long-range crystal) iron sulphide possibly coming from reservoir fluids. The small size of initially formed iron sulphide found in other studies could support this theory (Al-Harbi et al., 2018).

The concept of maximum dissolved iron is directly related to iron sulphide solubility: where iron sulphide solubility is low, the maximum dissolved iron (Fe^{2+} in equilibrium

with FeS) will also be low. By calculating the maximum dissolved iron trends from downhole to the separator, it is possible to obtain a good indication of how the scaling tendencies change, throughout the production system. The calculated MDI can also be compared to the field measurements of Fe^{2+} to evaluate the extent of the various corrosion and scaling mechanisms in the system. However, sampling and analysis of iron in sour waters can be challenging and lead to inaccurate results (NACE, 2012).

3.5 SUMMARY AND CONCLUSIONS

A rigorous carbonate and sulphide scale prediction workflow was developed to go from commonly available field data to scale prediction profiles using any PVT and scale prediction software.

This detailed procedure can be applied to any oil and gas system and is a fundamental tool for the field studies carried out as part of this research and shown in Chapter 4 and Chapter 5 and for the sensitivity studies described in Chapter 6 and Chapter 7.

Although some companies have proprietary internal procedures for predicting pH-dependent scales, the Heriot-Watt scale prediction workflow is the first published step-by-step procedure for rigorous carbonate and sulphide scale predictions.

The challenge of unreliable iron field measurements for scale predictions was also addressed and the concept of maximum dissolved iron (MDI) developed. This is applied in Chapter 4 and Chapter 5 to investigate the source of iron in sulphide scale and to explain some important field findings.

This Chapter is a more detailed and improved version of previously published work (Verri et al., 2017a, Verri and Sorbie, 2017b).

Chapter 4– FIELD EXAMPLE 1: MIDDLE EAST GAS/CONDENSATE WELL

4.1 INTRODUCTION

The Permian Khuff formation containing gas condensate is wide-spread in the Middle East, with major deposits in Qatar, Iran, Saudi Arabia, Bahrain and Abu Dhabi (Whitson and Kuntadi, 2005). The Khuff formation in the Ghawar field in Saudi Arabia is divided into four units designated in order of increasing age as A, B, C and D (Rahim et al., 2010, Cole et al., 2003). Well UTMN-598 investigated in this study produces from Khuff C.

The Khuff formation is described as a fine-to-coarse crystalline dolomite with some interbeds of limestone and anhydrite (Whitson and Kuntadi, 2005). Some zones contain pyrite but this is only restricted to thin intervals. The reservoir temperature ranges from 126°C to 157°C, wells produce both sweet and sour gas (2-7% H_2S) with CO_2 content between 2% and 4%.

The main goal of this field study was to prove whether the iron contained in iron sulphide scale deposits present in well UTMN-598 originated from reservoir fluids or from corrosion/other sources. To answer this question it was necessary to calculate reliable reservoir aqueous phase CO_2 and H_2S compositions which could then be used to calculate a full water chemistry in equilibrium with the carbonate rock and determine the stability of dissolved iron using the Maximum Dissolved Iron (MDI) concept (Section 3.4). Since only topside gas phase readings were available, the newly developed HWU workflow was used to obtain downhole CO_2 and H_2S three phase concentrations.

4.2 WELL DATA

The first point to note in this study is the extremely limited amount of data available and the unreliability of some information given. A number of assumptions had to be made to overcome this issue, and these are discussed below.

Reservoir and separator temperature and pressure, GOR and gas phase CO_2 and H_2S concentrations for UTMN-598 are listed in Table 4.1.

Reservoir Temperature (°C)	146
Separator Temperature (°C)	33
Reservoir Pressure (bar)	314
Separator Pressure (bar)	8
GOR (std m3/sep m3)	3223
Separator $CO_{2(g)}$ (mol %)	3.28
Separator $H_2S_{(g)}$ (mol %)	5.77

Table 4.1: UTMN-598 field data.

The selected temperature and pressure points are given in Table 4.2.

Depth (ft)	Temperature (°C)	Pressure (bar)
Separator	33	8
Wellhead	56	160
1000	92	167
2000	99	174
3000	101	182
4000	110	189
5000	115	197
6000	117	204
7000	126	212
8000	128	219
9000	137	226
10000	138	234
10500	139	237
11000	143	241
11500	146	245
Reservoir	146	314

Table 4.2: Temperature and pressure points used in this study.

The formation water composition was not available for this reservoir; it appeared that no accurate and reliable measurements were made of the formation water composition by the operating company.

Only two separator water samples shown in Table 4.3 were provided for UTMN-598. Although the presence of Ca^{2+} and Mg^{2+} suggests that formation water enters the wellbore, these water samples are incomplete and highly unreliable and are believed to have been taken immediately after acid stimulation treatments rather than during normal well operation. Moreover, there is no consistency in the measured compositions making it unlikely that the given ion concentrations come from formation water. Hence, for the purpose of this work two different reservoir water chemistry scenarios were investigated:

1. Only condensed water is equilibrated with $CaCO_3$ at reservoir conditions. This equates to the lowest possible reservoir Ca^{2+} concentration for the calculated CO_2 and H_2S reservoir levels;

2. The reservoir Ca^{2+} concentration is set to 8,000 mg/l which represents the highest measured concentration in produced water samples.

Date	***Na^+***	***K^+***	***SO_4^{2-}***	***Ca^{2+}***	***Mg^{2+}***
	(mg/l)	(mg/l)	(mg/l)	(mg/l)	(mg/l)
08/09/2007	199	43	87	847	223
04/03/2010	2817	N/A	55	8060	2620

Table 4.3: UTMN-598 separator water samples.

PVT experimental results of downhole hydrocarbon samples were not available for this well and indeed for this field. Moreover, topside hydrocarbon compositions were also not available for UTMN-598 so the separator condensate and gas compositions of UTMN-1842 producing from the same part of the Khuff reservoir had to be used for

this work. The separator gas and condensate compositions for UTMN-1842 are shown in Table 4.4 where the relative density and molecular weight of the C_{12+} fraction are 0.8369 and 206 respectively. The separator $CO_{2(g)}$ and $H_2S_{(g)}$ concentrations for UTM-598 are different from those of UTMN-1847 and they were changed from 2.31 and 8 mol % to 3.28 and 5.77 mol % respectively to match those shown in Table 4.1 (the final composition was normalised to 100 and the other components prorated).

	Separator Oil UTMN 1842	**Separator Gas UTMN 1842**	**Separator Gas Adjusted UTMN-598**
H_2S	1.49	8.00	5.77
CO_2	0.06	2.31	3.28
N_2	0.11	8.93	9.05
CH_4	2.37	69.8	70.78
C_2H_6	0.54	6.00	6.08
C_3H_8	1.40	2.31	2.34
IC_4	0.73	0.39	0.40
NC_4	1.94	0.78	0.79
IC_5	1.58	0.32	0.32
NC_5	2.19	0.33	0.33
FC_6	6.91	0.45	0.46
FC_7	12.51	0.30	0.30
FC_8	13.82	0.08	0.08
FC_9	15.14	0	0
FC_{10}	11.44	0	0
FC_{11}	6.85	0	0
C_{12+}	20.92	0	0

Table 4.4: UTMN-1842 separator hydrocarbon compositions and UTMN-598 adjusted separator gas composition.

4.3 PROCEDURE AND RESULTS

The Heriot-Watt scale prediction workflow is applied here to allow the integration of a full PVT software (in this case Winprop (CMG, 2017)) with a commercial aqueous phase software (ScaleChem (OLI, 2016)) to obtain carbonate scale predictions for UTMN-598. However, the procedure is simplified because the scenarios investigated

do not require the separator to reservoir water chemistry recombination for Ca^{2+}. All the workflow steps and results are described below.

4.3.1 Step 1: Define PVT Total Feed

Based on the available data for this gas/condensate wells, the calculation of the total feed is divided into two steps: (i) separator recombination to obtain the hydrocarbon total feed followed by (ii) the water addition step.

The separator recombination is carried out using a PVT software suite and requires the well test data at separator conditions shown in Table 4.4 as well as the GOR shown in Table 4.1. The ratio of oil and gas volumes needs to be converted to a molar ratio using the densities of the two streams. The calculated recombined fluid composition is therefore sensitive to the values assigned to the oil and gas densities which are normally calculated from the equation of state (EOS). While the EOS based gas density is reliable, the EOS calculated oil phase density is generally not as accurate (CMG, 2017). If an experimentally determined value for the oil density or oil specific gravity is available it can be entered directly but this information was not provided for UTMN-598. The software used for these PVT calculations is Winprop and the EOS Peng-Robinson 1978 (Robinson and Peng, 1978).

After calculating the hydrocarbon feed to the separator (Table 4.5) which also represents the hydrocarbons leaving the reservoir, water is added to obtain the total feed.

Using the same PVT software, it is possible to add a variable mole percent of water to the hydrocarbon feed until the final total composition produces the correct relative volume of free water when flashed at given pressure and temperature conditions.

To estimate the total amount of water produced from a gas/condensate well, where water condensation/evaporation is non-negligible and the volume of produced water at separator is usually erratic and hard to measure, it is advised to define the condition at which gas leaves the reservoir rather than fixing a separator produced water volume. Three case scenarios are identified:

1. Gas leaving the reservoir is saturated with water. To obtain this condition, water is added to the total feed until saturated gas is obtained at reservoir conditions (since only saturated gas enters the wellbore).

2. Gas leaving the reservoir is under saturated. If the degree of under saturation is known, this can be reproduced in the total feed. Produced gas can be under saturated if the flow rate at which it travels in the reservoir is too fast to allow gas/water equilibrium to be reached.

Gas leaving the reservoir is saturated and free water (formation water) is also produced. The total PVT feed is calculated assuming saturated gas but the volume of formation water coming into the wellbore is added to the mass balance in scale prediction calculations. Saturated gas is expected to be produced from UTMN-598 whilst there is uncertainty around the production of formation water due to the lack of reliable produced water rates and samples.

The calculated UTMN-598 hydrocarbon feed and total feed are shown in Table 4.5.

	Hydrocarbon Feed UTMN 598	Total Feed UTMN 598
H_2S	5.60	5.45
CO_2	3.15	3.07
N_2	8.69	8.57
CH_4	68.02	67.10
C_2H_6	5.86	5.29
C_3H_8	2.30	2.12
IC_4	0.41	0.44
NC_4	0.84	0.86
IC_5	0.37	0.33
NC_5	0.41	0.34
FC_6	0.72	0.50
FC_7	0.79	0.60
FC_8	0.63	0.57
FC_9	0.61	0.59
FC_{10}	0.46	0.44
FC_{11}	0.28	0.27
C_{12+}	0.84	0.81
H_2O	-	2.64

Table 4.5: Calculated hydrocarbon feed and total feed for UMTN-598.

4.3.2 Step 2: Run PVT Calculations at Each Selected T and p Point

The scale prediction workflow is simplified in this field example because the reservoir water composition is not reconstructed from topside samples. Hence, some steps described in Chapter 3 are not necessary.

The calculated total feed shown in Table 4.5 is flashed at each selected T and p point from Table 4.2. The distribution of condensate/gas/water along the wellbore is shown in Figure 4.1 when only saturated gas is produced (no formation water entering the wellbore), a zoom-in on the liquid distribution is shown in Figure 4.2 whilst the calculated molecular $CO_{2(aq)}$ and $H_2S_{(aq)}$ from reservoir to separator are plotted in Figure 4.3.

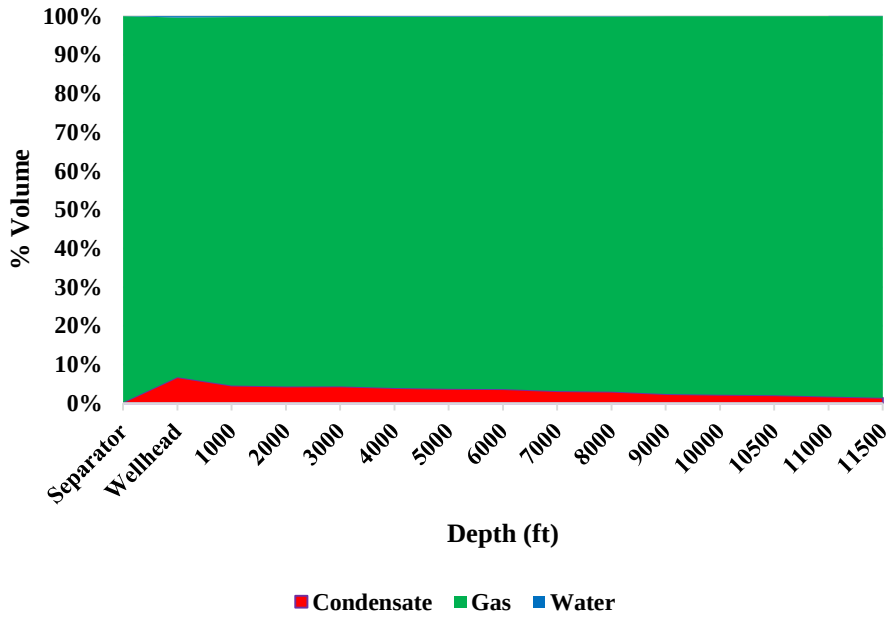

Figure 4.1: Condensate/gas/water volume % distribution along the wellbore for UTMN-598.

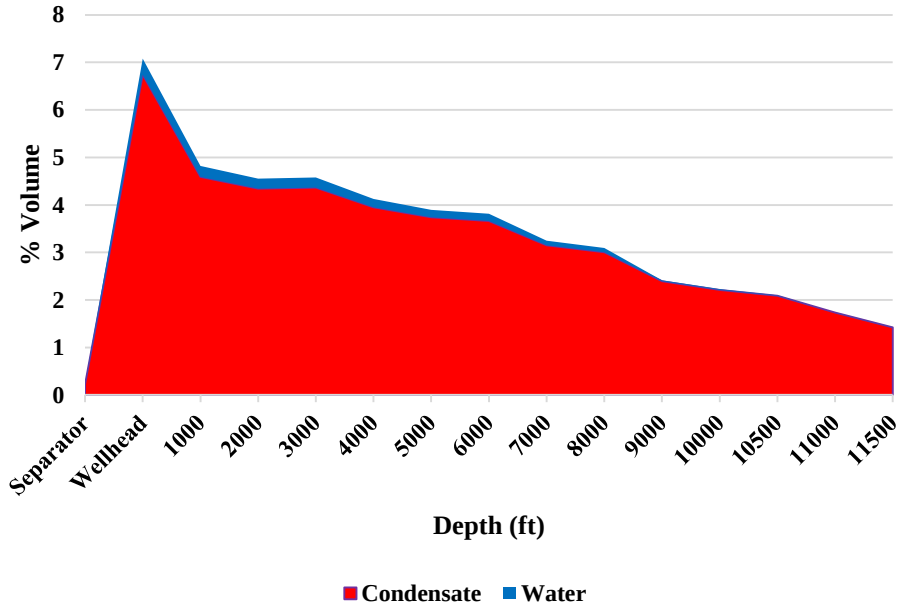

Figure 4.2: Condensate/water volume % distribution along the wellbore for UTMN-598.

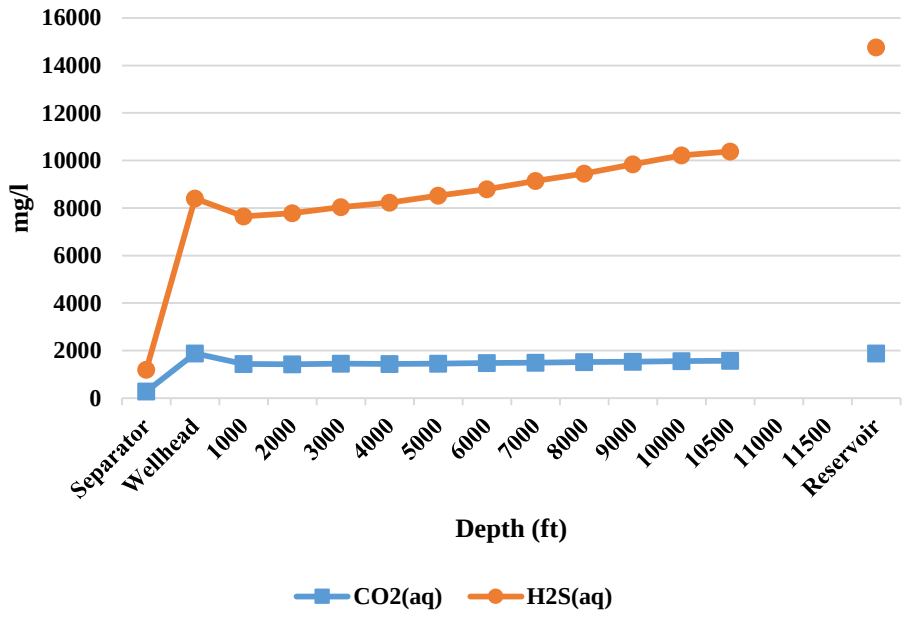

Figure 4.3: Aqueous CO_2 and H_2S concentration trends for UTMN-598.

4.3.3 Step 3. Calculate Reservoir Water Composition

In Step 2 the concentration of molecular CO_2 and H_2S in the aqueous phase at reservoir T and p were calculated.

Since the formation water composition is not available and the produced water chemistry data is limited and unreliable, two scenarios are investigated in this work:

1. Only condensed water is equilibrated with $CaCO_3$ at reservoir conditions. This equates to the lowest possible reservoir Ca^{2+} concentration for the calculated reservoir CO_2 and H_2S;

2. The reservoir Ca^{2+} concentration is set to 8,000 mg/l which represents the highest measured concentration in produced water samples.

Using a scale prediction software (ScaleChem) the initial total carbonates and sulphides introduced as CO_2 and H_2S are equilibrated with $CaCO_3$ and adjusted until the resulting molecular $CO_{2(aq)}$ and $H_2S_{(aq)}$ match those calculated with flash calculations. In scenario

2 the initial Ca^{2+} concentration is adjusted until the final Ca^{2+} concentration is equal to 8,000 mg/l. The resulting reservoir water chemistry for scenario 1 and 2 is shown in Table 4.6. These compositions are used in Section 4.3.5 to calculate the Maximum Dissolved Iron (MDI).

	Scenario 1	**Scenario 2**
CO_2 (mg/l)	1,877	1,877
H_2S (mg/l)	14,762	14,762
HCO_3^- (mg/l)	122	142
HS^- (mg/l)	923	713
Ca^{2+} (mg/l)	600	8000
pH	5.16	4.95

Table 4.6: Calculated reservoir water composition for UTMN-598 in scenario 1 and 2.

An important observation is that the majority of the *alkalinity* level comes from bisulphides (HS^-) and not from bicarbonates (HCO_3^-) due to the high H_2S concentration in the system. This shows the importance of clearly distinguishing between bicarbonate measurements and alkalinity measurements in produced water, if representative samples become available.

The buffering effect of $CaCO_3$ (equilibrium with carbonate rock) keeps the pH around 5 despite the high CO_2 concentration.

4.3.4 Step 3. Calculate Water Composition at Each Selected T and p Point

Using the $CO_{2(aq)}$ and $H_2S_{(aq)}$ calculated in Step 2, the full water chemistry was calculated at each selected T and p point shown in Table 4.2.

The decision was made by the operator to consider only condensed water in the wellbore and to not include formation water. For this reason the addition of CO_2 and H_2S has no impact on the alkalinity which remains equal to zero (see Section 6.2.4). If

formation water is produced, it is expected to be a very small fraction of the total produced water and to have a negligible impact on the final water composition.

The pH and concentration of $CO_{2(aq)}$, $H_2S_{(aq)}$, HCO_3^- and HS^- calculated at each T/p step are shown in Table 4.7 (water starts condensing at 10,500 ft and that is why there no data available for 11,000 and 11,500 ft).

Depth	**$CO_{2(aq)}$**	**$H_2S_{(aq)}$**	**HCO_3^-**	**HS^-**	**pH**
ft	**mg/l**	**mg/l**	**mg/l**	**mg/l**	
Separator	277	1197	2.16	1.77	4.05
Wellhead	1880	8404	5.65	6.25	3.54
1000	1440	7644	3.39	7.84	3.52
2000	1425	7786	3.08	8.13	3.51
3000	1449	8043	3.02	8.33	3.50
4000	1434	8231	2.65	8.61	3.49
5000	1450	8518	2.47	8.84	3.49
6000	1473	8789	2.41	9.01	3.48
7000	1484	9141	2.10	9.23	3.47
8000	1510	9451	2.05	9.40	3.47
9000	1530	9839	1.77	9.53	3.46
10000	1562	10220	1.75	9.71	3.46
10500	1575	10379	1.73	9.78	3.45
11000	N/A	N/A	N/A	N/A	N/A
11500	N/A	N/A	N/A	N/A	N/A
Reservoir	1877	14762	146.64	1024.79	5.22

Table 4.7: Calculated water chemistry for UMTN-598 at selected T and p points.

The water pH is plotted in Figure 4.4.

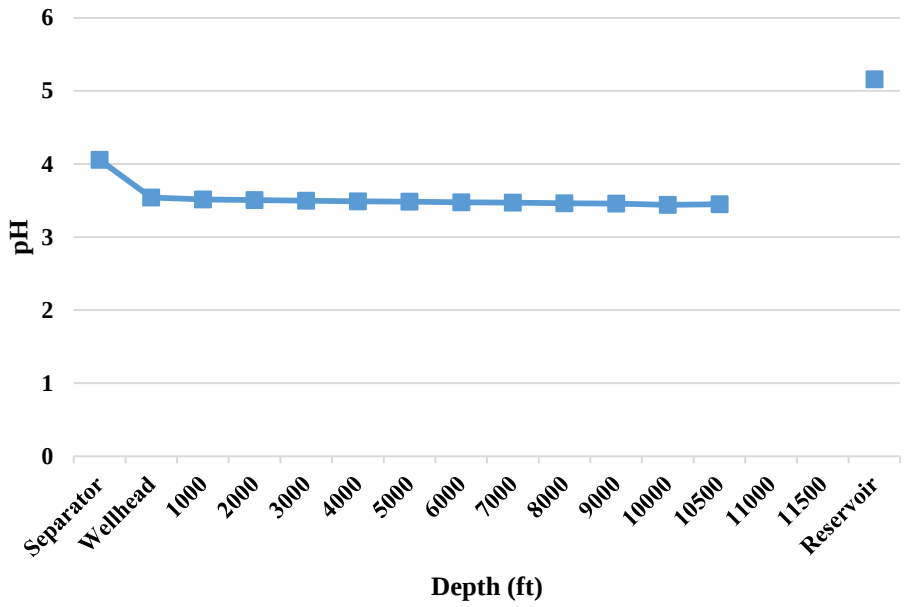

Figure 4.4: Calculated pH for UTMN-598.

Whilst the buffering effect of carbonate rock at reservoir conditions keeps the water pH above 5 despite the high CO_2 concentration, the pH of wellbore condensed water drops to ≈3.5 because $CaCO_3$ is not present and the alkalinity is zero.

It was reported by the operator that internal tubing corrosion was found to be more significant in the lower joints of the well and this could be explained by a combination of high temperature and low pH. Using the calculated $CO_{2(aq)}$ and $H_2S_{(aq)}$ and water pH it is possible to improve the corrosion predictions for UTMN-598 but a full corrosion assessment is beyond the scope of this work. Indeed, the aqueous phase pH and compositions which are calculated quite accurately here (within our assumptions) would actually provide ***input*** for a corrosion model.

The increase in pH at separator conditions is due to the repartitioning of CO_2 to the gas phase and the drop in $CO_{2(aq)}$.

4.3.5 Step 4. Calculate Maximum Dissolved Iron (MDI)

The Maximum Dissolved Iron (MDI) concentration is the highest Fe^{2+} concentration which can be present at defined temperature (T), pressure (p) and aqueous phase composition ($CO_{2(aq)}$ and $H_2S_{(aq)}$) before any iron scale precipitates (Verri and Sorbie, 2017b) (see Section 3.4). If the concept of MDI is applied to reservoir conditions, it can provide some information on whether iron in its soluble form can be stable in reservoir fluids. If it can, Fe^{2+} is potentially produced with reservoir fluids into the wellbore but if MDI = 0 (or very low, say <0.1mg/L) at reservoir conditions any iron precipitated in the production system will come from a different source (e.g. corrosion).

UTMN-598 reservoir MDI for scenario 1 and 2 is shown in Table 4.8 whilst the wellbore MDI trend calculated using the condensed water chemistry data shown in Table 4.7 is shown in Figure 4.5.

	Scenario 1	**Scenario 2**
MDI (mg/l)	1.2	2.3

Table 4.8: UTMN-598 reservoir MDI for scenario 1 and 2.

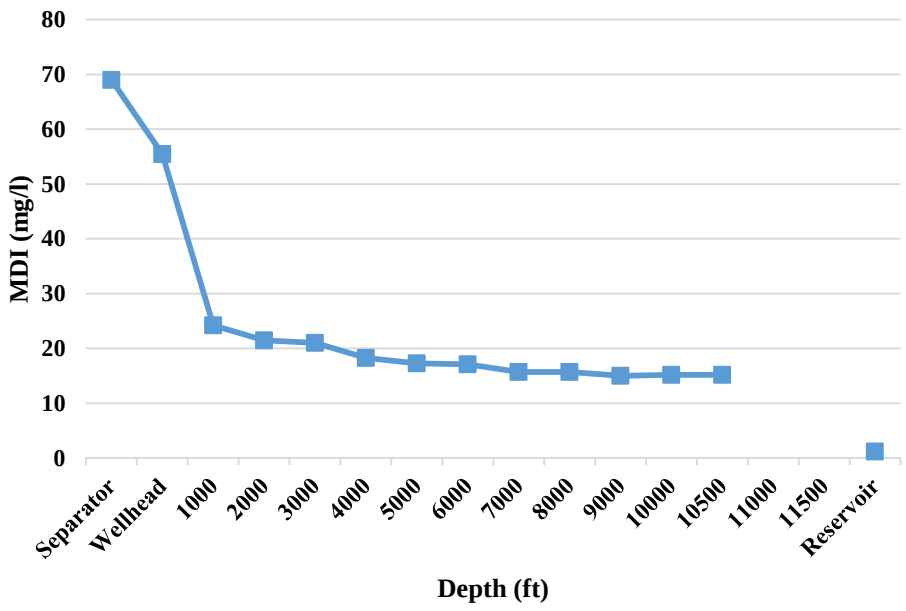

Figure 4.5: Calculated MDI for UTMN-598.

The reservoir MDI is predicted to be 1.2 mg/l (in the case of condensed water) or 2.3 mg/l (if reservoir Ca^{2+} = 8,000 mg/l) indicating that a small amount of Fe^{2+} could be present in the reservoir fluids in equilibrium with FeS rock (this MDI is calculated for the Fe^{2+}/mackinawite equilibrium). It is not clear if formation water enters the wellbore but if it does the flow rate is expected to be <10 barrels/day. Although these predictions show that formation water could carry a very small amount of Fe^{2+}, the likely amount of precipitated FeS is negligible due to the low water rate. Hence, Fe^{2+} coming from formation water cannot be the source of FeS deposits found in the wellbore.

MDI increases in the wellbore and reaches a maximum of 69 mg/l at separator conditions where the lower temperature and sulphide concentration allow more Fe^{2+} to be stable in solution.

Scale deposits are only found in the bottom joints of the tubing which confirms these MDI predictions that show a higher potential for FeS precipitation downhole as a results of higher temperature and aqueous sulphide concentration.

These calculated MDI values are different from previously published work (Verri et al., 2017b) which shows that Fe^{2+} is definitely not present at reservoir conditions (reservoir MDI =0). The results are plotted in Figure 4.6.

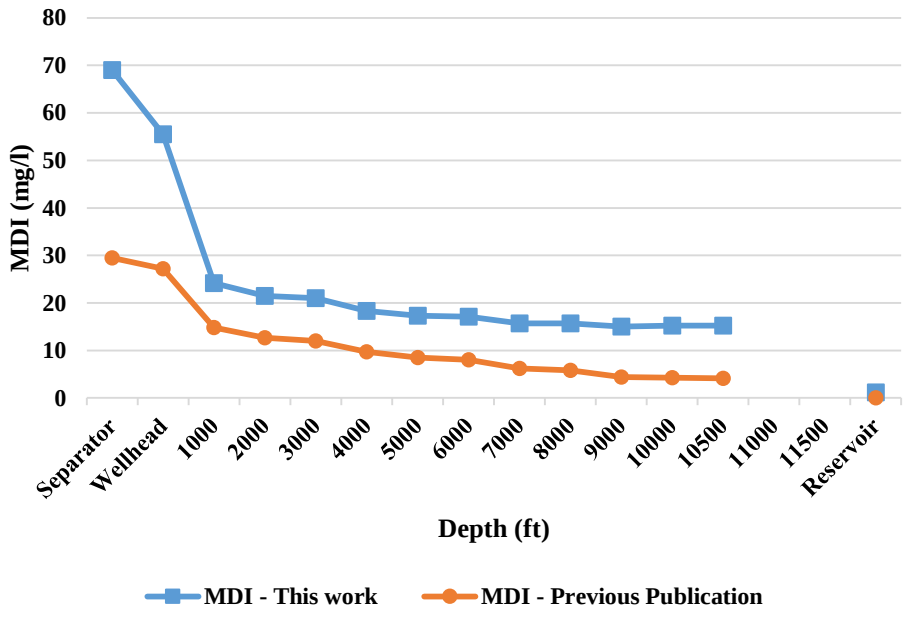

Figure 4.6: Comparison between UMTN-598 MDI calculated using ScaleChem (this work) and using the in-house HWU scale prediction code (previous publication).

The reason for this discrepancy lies in the software selection. Whilst previous results were obtained using the in-house HWU scale prediction code which implements the published data shown in Section 2.2.2, the results presented in this Chapter are obtained using ScaleChem which calculates a higher solubility product for mackinawite (Table 2.3). The different mackinawite solubility is the reason for the different (higher) MDI values shown in Figure 4.6.

4.4 CONCLUSIONS

This study on a gas/condensate well was carried out in order to determine the source of iron causing the high level of iron sulphide precipitation along the wellbore in this region of the Khuff field.

A simplified version of the Heriot-Watt scale prediction workflow was applied to determine the full water chemistry at reservoir conditions and at various selected T and

p points in the well. Once the full water chemistry was calculated, the MDI concept was applied to study where in the well Fe^{2+} is stable in its soluble form.

Some key findings from this work:

- Reservoir pH is calculated to be over 5 because of the buffering effect of carbonate rock. However, the condensed water along the wellbore does not contain any calcium carbonate and the high CO_2 concentration brings the water pH down to ≈3.5. The combination of high downhole temperatures and low pH are likely to be the reason for higher corrosion rates seen in the lower tubing joints of this well.
- The calculated reservoir MDI is 1.2÷2.3 mg/l suggesting that a small concentration of free iron (Fe^{2+}) can be stable at reservoir conditions If any formation water is produced it can potentially bring a small amount of Fe^{2+} into the wellbore but this cannot be the main source of Fe in wellbore FeS scale given the small produced water rates and the severity of the observed problem.
- These reservoir MDI results are in contrast with previously published work which showed that Fe^{2+} is not stable in this reservoir even when "milder" scaling conditions such as lower $H_2S_{(aq)}$ or higher $CO_{2(aq)}$) are tested. The reason for this discrepancy is to be found in the different scale prediction software used which implement a different mackinawite solubility product. ScaleChem uses a solubility product which is more than one order of magnitude higher than that used in the HWU scale prediction code providing a higher solubility value for FeS. It is difficult to establish which of these two results is correct because the experimental database used is different. However, according to published data shown in Section 2.2.2 it is more likely that the mackinawite solubility

calculated in ScaleChem is too high and that true MDI values are lower than those reported in Figure 4.5.

- The small reservoir MDI combined with a likely overestimated mackinawite solubility product in ScaleChem, suggest that the concentration of Fe^{2+} which could potentially be produced from the reservoir is too small to be the cause of FeS scale formation in UMTN-598. Hence, the main iron source in the precipitated FeS is not reservoir fluids but more likely the result of corrosion processes, acid job dissolution/re-precipitation mechanisms or contamination from other fluids. Thus, we believe that the original conclusion, i.e. that essentially no (very low) free Fe^{2+} comes from the reservoir, still holds.
- The MDI concentration increases in the wellbore and is higher at lower temperatures closer to surface conditions. This means that FeS is more likely to precipitate downhole (providing that there is Fe^{2+} availability) and that high concentrations of Fe^{2+} can be measured from separator samples despite a very high H_2S concentration. These findings are in agreement with field observations which show that scale is present only in the lower tubing joints of UTMN-598.

This Chapter is a more detailed and improved version of previously published work (Verri et al., 2017b).

Chapter 5 - FIELD EXAMPLE 2: NORTH SEA OIL WELL

5.1 INTRODUCTION

This chapter illustrates a field application of the Workflow described in Chapter 3 and clearly shows how each step is applied, what results are obtained and how they are used to address key operational questions.

The Alba field operated by Chevron is located in the UK central North Sea in Block 16/26 approximately 225 km NE of Aberdeen. The field was discovered 1984 with first oil in production in late 1994. The reservoir is of earliest Late Eocene age and comprises a series of stacked high density turbidite sands which are unconsolidated in nature (Mackay et al., 1998). The platform (ANP) was installed as a minimum facilities module in the North of the field exporting oil by a floating storage unit (FSU). Reservoir pressure in the Alba field is supported by sea-water injection (Paulo et al., 2001) which has been the cause of gradual reservoir souring until 2010 (Evans and Dunsmore, 2006) when an increasing number of wells started showing significant levels of H_2S.

Some platform wells have been experiencing an unexplained gradual and steady decline in well productivity index (PI) and different studies were carried out by the Flow Assurance and Scale Team (FAST) at Heriot-Watt University to investigate the potential causes of this productivity issue.

Two main potential problems were identified: scale squeeze treatment placement issues and inorganic scale (barite and carbonate) precipitation on sand screens acting as “cement” to consolidate sand and reduce productivity.

This chapter addresses the second challenge. While barite scale issues are well understood in this field and have been addressed for many years, past studies on the Alba field suggested that carbonate scale was not a risk factor for these producing wells. This work aims at accurately determining the calcium carbonate scale risk factor for one key Alba platform well (ANP 70), the potential impact calcium carbonate deposition has had on well productivity and what role H_2S may have been playing on calcite scale formation in recent years.

5.2 WELL PI AND CHEMICAL TREATMENT HISTORY

The well investigated in this study (ANP 70) was drilled in 2016, it is a high water cut (82%) deviated well producing 19.4 °API oil. The well is completed with sand screens and does not have artificial lift. The produced $H_2S_{(g)}$ trend for ANP 70 is shown in Figure 5.1 where the prominent spike in December 2016 was caused by an acid stimulation treatment (discussed later in the text).

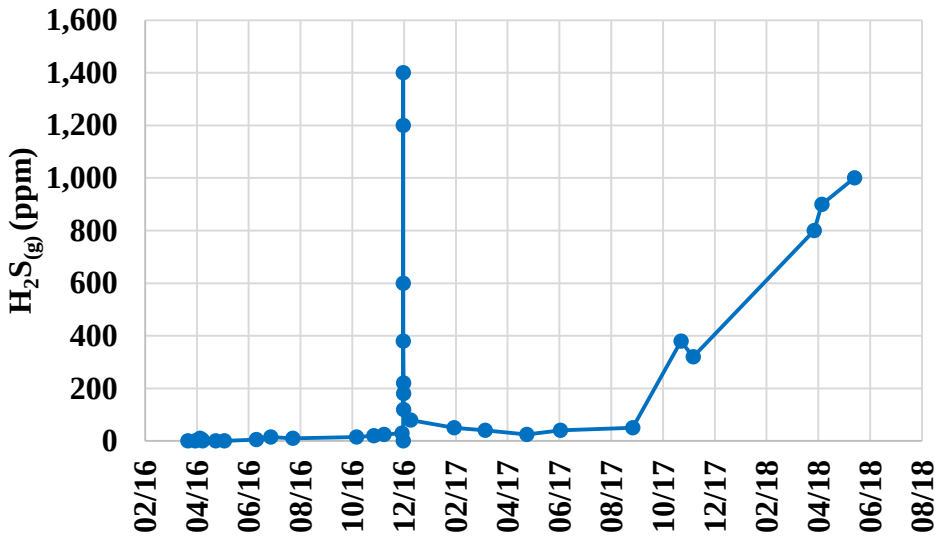

Figure 5.1: ANP 70 separator $H_2S_{(g)}$ trend.

The well PI is shown over time in Figure 5.2 where three distinctive regions can be identified:

1. An initial PI spike caused by the well clean-up from drilling and completion materials (acid stimulation job) followed by a natural PI drop when the well is brought online (this behaviour is seen in all other platform wells where the same completion and clean-up procedure were used);

2. A gradual but stead PI loss which was recovered after a formic acid stimulation job (12/16);

3. A second gradual and steady PI loss which has not yet been reversed.

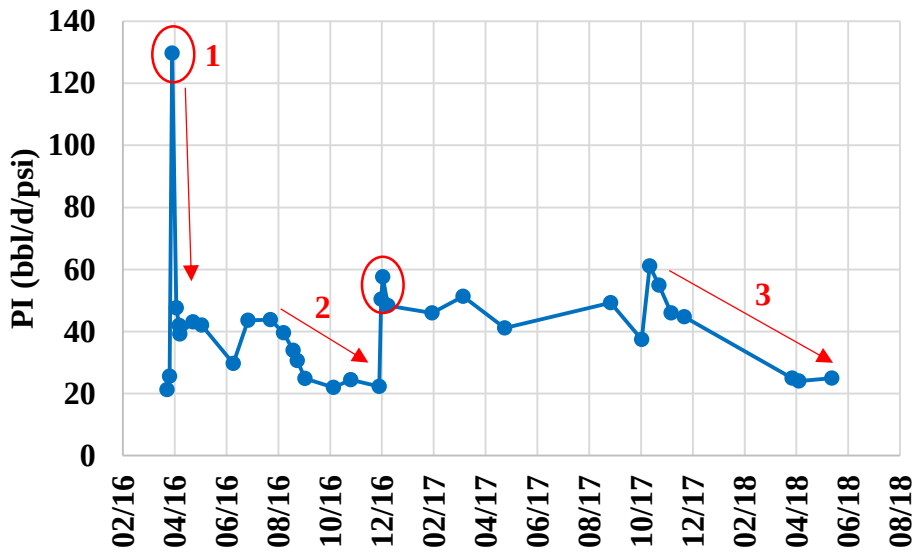

Figure 5.2: PI trend for ANP 70.

ANP 70 was also squeezed with scale inhibitor in 2016 following the clean-up treatment (pre-emptive scale squeeze) and subsequently in December 2017. The main aim of these treatments was to prevent $BaSO_4$ deposition. To better understand the impact of the formic acid stimulation treatment performed in December 2016, the flowback Ca^{2+}, Fe^{2+}, Si, $CO_{2(g)}$ and $H_2S_{(g)}$ are plotted in Figure 5.3.

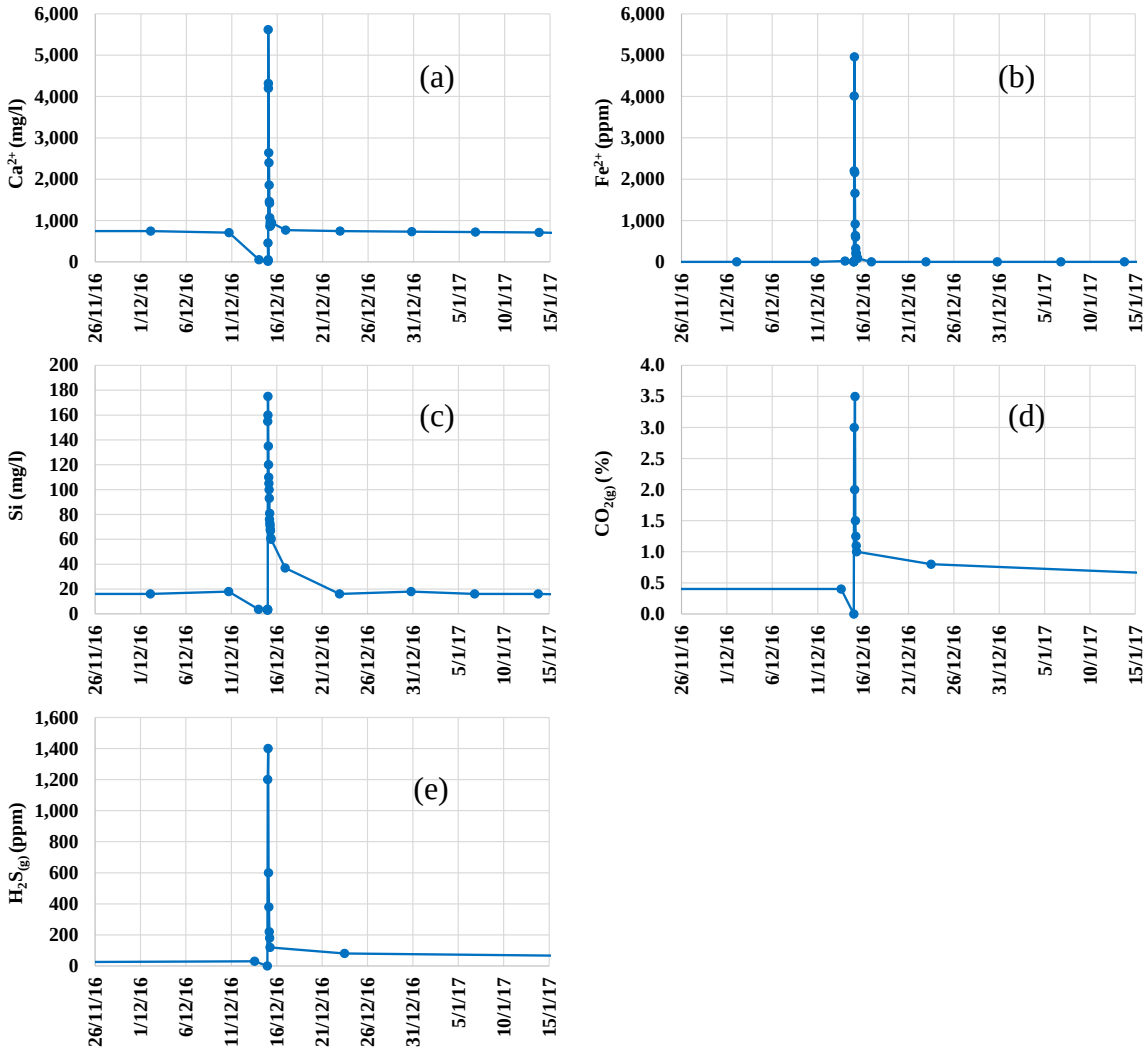

Figure 5.3: Formic acid flowback data (a) Ca^{2+}, (b) Fe^{2+}, (c) Si, (d) $CO_{2(g)}$, (e) $H_2S_{(g)}$.

These results suggest that:

- $CaCO_3$ dissolution occurred as both Ca^{2+} and $CO_{2(g)}$ concentrations were high in the flowback samples. See calculations below for an estimate of the amount of dissolved $CaCO_3$.

- Sand fines were dislodged and detected in the water ICP analysis (increased silica concentration). The percentage of solids was also higher in 3 of the filtered water samples.

- FeS scale was also dissolved because both Fe^{2+} and $H_2S_{(g)}$ concentrations spiked in the flowback samples. This FeS is likely to come from corrosion products present on the production tubing and completion materials.

The approximate mass of $CaCO_3$ (ΔM) dissolved in the acid stimulation job can be estimated by summing the various ΔM_i produced over the stages of the job as follows:

$$\Delta M = \sum \Delta M_i = \sum Q_i \times (C_i - C_0) \times \Delta t_i \quad (5.1)$$

where Qi is the produced water rate, Ca^{2+} concentration is C_i and the background produced value of Ca^{2+} is C_0. The results are shown in Table 5.1.

	C_i (Ca^{2+})	**Δt_i**	**Q (m^3/d)**	**ΔM_i**
	mg/l	min	m3/d	kg
15/12/2016 00:30	5620	-	-	-
15/12/2016 00:45	4320	15	535	7.2
15/12/2016 01:00	4200	15	535	0.7
15/12/2016 02:00	2640	60	535	34.8
15/12/2016 02:30	2400	30	535	2.7
15/12/2016 03:00	1860	30	535	6.0
15/12/2016 03:30	1460	30	535	4.5
15/12/2016 04:00	1420	30	535	0.4
15/12/2016 04:30	1070	30	535	3.9
15/12/2016 05:00	860	30	535	2.3
15/12/2016 05:30	950	30	535	-1.0
15/12/2016 06:00	880	30	535	0.8
15/12/2016 06:30	900	30	535	-0.2
15/12/2016 07:00	915	30	535	-0.2
15/12/2016 07:30	955	30	535	-0.4
15/12/2016 08:30	925	60	535	0.7
15/12/2016 09:15	950	45	535	-0.4
16/12/2016 22:00	770	2187	535	146.3
Total				208.0

Table 5.1: Mass of $CaCO_3$ dissolved during acid stimulation.

In this stimulation treatment, 82.7 bbl of 10% formic acid (relative density 1.1) were used. This equates to ≈ 31 kmol of acid which could theoretically dissolve over 15 kmol of $CaCO_3$ (if all acid reacted with $CaCO_3$). According to the Ca^{2+} flowback calculation above, our estimate shows that only ≈ 200 kg (around 2 kmol) of $CaCO_3$ were dissolved suggesting poor chemical treatment efficiency or "oversized" acid pill which removed all $CaCO_3$ (the latter is unlikely based on scale prediction results shown in the following paragraphs).

After discarding other possible causes of PI loss as part of previous work conducted on this field, based on the flowback samples, on the PI improvement caused by this acid stimulation job and on the slow but steady further PI drop, the hypothesis put forward is the following: *A small amount of carbonate scale had been slowly depositing in the near wellbore region (probably on the sand screens) acting as a consolidating agent with sand to restrict the flow of reservoir fluids into the wellbore*. A similar process of carbonate precipitation to provoke sand consolidation has been proposed by other researchers (van der Star et al., 2017) as a method for sand control. In that study, the carbonate precipitation was not caused by carbonate auto-scaling (Silva et al., 2018) but was induced by microbial activity. Nevertheless, the concept of sand "cementing" by carbonate scale is the same. Indeed one of the key questions for such a treatment is whether it would restrict the flow and cause PI losses, as appears to be the case for ANP 70 where carbonate scale is naturally occurring and not induced.

Finally, it is important to remember that this well was also scale squeezed to protect against $BaSO_4$ deposition and the chemical used (a sulphonated copolymer) should also have been effective in preventing $CaCO_3$ precipitation. The fact that $CaCO_3$ was indeed present in the well (proven by the acid stimulation results) supports the idea that there is

a placement issue when bullheading chemical treatments into this well. This problem has been investigated by other colleagues at HWU and is beyond the scope of this work.

To test the hypothesis of sand consolidation caused by $CaCO_3$ precipitation, carbonate scale predictions were carried out using two different PVT software and investigating 4 different production scenarios. The results of these calculations are presented below.

5.3 ALBA WELL DATA

A schematic representation showing the sample points and scale prediction points for ANP 70 is shown in Figure 5.4; these are the reservoir, the near-wellbore, the wellhead and the separator.

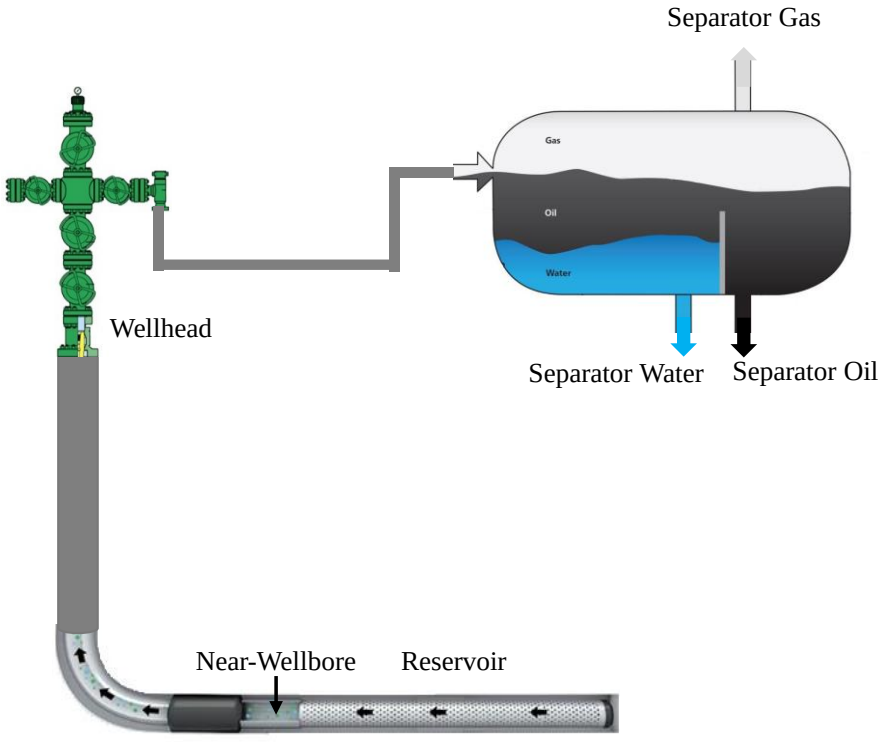

Figure 5.4: ANP 70 sample points and scale prediction points.

The given field data is listed in Table 5.2 and Table 5.3. Table 5.2 shows commonly available field data which includes temperatures, pressures, separator gas phase CO_2 and H_2S concentration and separator rates (a water and oil rate are given whilst the gas

rate will be calculated from the PVT based on GOR). Table 5.3 lists the main ions present in the separator produced water and used in these scale predictions.

Reservoir Temperature (°C)	78
Near-Wellbore Temperature (°C)	78
Wellhead Temperature (°C)	40
Separator Temperature (°C)	40
Average Reservoir Pressure (bar)	212
Near-Wellbore Pressure (bar)	159
Wellhead Pressure (bar)	25
Separator Pressure (bar)	7
Separator Oil Rate (BOPD)	1449
Separator Water Rate (BWPD)	6603
Separator $CO_{2(g)}$ (mol %)	0.6
Separator $H_2S_{(g)}$ (mol %)	0.08

Table 5.2: ANP 70 field data

Na^+	K^+	SO_4^{2-}	Ca^{2+}	Mg^{2+}	Ba^{2+}	Sr^{2+}
(mg/l)	(mg/l)	(mg/l)	(mg/l)	(mg/l)	(mg/l)	(mg/l)
11390	195	1730	550	930	0.78	13

Table 5.3: ANP 70 separator water chemistry.

The original PVT data is summarized in Table 5.4 through Table 5.9. Table 5.4 and Table 5.5 show the main hydrocarbon composition and C^{7+} properties of a sample of Alba oil taken from one of the first wells drilled. This is considered representative of the whole field but the CO_2 and H_2S concentrations need to be changed when calculating the total PVT feed as they differ in every well whilst H_2O must be added to obtain the total PVT feed (STEP 1 of the workflow).

Component	**Mole %**
CO_2	0.16
N_2	0.11
CH_4	39.87
C_2H_6	1.42
C_3H_8	0.3
IC_4	0.07
NC_4	0.11
IC_5	0.06
NC_5	0.04
FC_6	0.28
C_{7+}	57.58

Table 5.4: Original PVT Hydrocarbon composition.

C_{7+} *MW*	373
C_{7+} *SG*	0.9365

Table 5.5: C_{7+} Properties.

Table 5.6 through Table 5.9 show the hydrocarbon properties and raw PVT data of Alba oil which will be used for the data regression to optimize PVT parameters (interaction coefficients as well as C^{7+} critical pressure and temperature, molecular weight and volume shift).

API @ Standard Conditions	19.4
Residual Oil SG @ Standard Conditions	0.9367
Saturation Pressure (bar)	161.87
GOR (scf/bbl)	243

Table 5.6: Additional hydrocarbon properties.

Pressure (bar)	**Oil FVF (m^3/sm^3)**	**GOR (sm^3/sm^3)**	**Oil SG**	**Gas Z Factor**	**Gas FVF (m^3/sm^3)**	**Gas SG**
161.87	1.124	43.28	0.8612			
125.12	1.106	33.84	0.8689	0.9	0.00888	0.573
83.75	1.087	23.15	0.8773	0.912	0.01344	0.573
42.38	1.067	12.11	0.8866	0.942	0.02743	0.577
21.70	1.058	6.41	0.8903	0.964	0.05483	0.585
11.36	1.053	3.38	0.8925	0.979	0.1064	0.599
1.01	1.046	0	0.8954			0.675

Table 5.7: Differential liberation test results.

Pressure (bar)	Experimental ROV	Oil Density
345.76	0.985	874.3
311.29	0.9876	872
276.81	0.9902	869.7
242.34	0.9929	867.4
221.65	0.9946	865.9
207.86	0.9958	864.9
194.07	0.997	863.8
187.18	0.9976	863.3
180.28	0.9982	862.7
173.39	0.9989	862.2
166.49	0.9995	861.6
161.87	1	861.2

Table 5.8: Constant composition expansion test results.

	Sat. Pressure	Sep #1	Sep #2	Sep #3	Stock Tank
Pressure (bar)	161.87	9.01	1.50	1.01325	1.01325
Temperature (°C)	77.78	70	95	40	15.56
GOR (std m3/std m3)	N/A	40.8	2.5	0	0
Oil FVF (m3/sm3)	1.125	N/A	N/A	N/A	N/A
Oil API	N/A	N/A	N/A	N/A	19.4

Table 5.9: Separator test results (Sep=separator).

5.4 PROCEDURE

The following calculations were carried out to investigate the severity of the carbonate scaling problem in well ANP 70:

- Carbonate scale predictions using current produced fluid compositions, run by applying the HWU scale prediction workflow (updated version of (Verri et al., 2017a)) with the Winprop PVT package and the ScaleChem aqueous phase model;

- Carbonate scale predictions using current produced fluid compositions, run with the automated ScaleChem software (PVT + aqueous phase model) to test the impact of different PVT software on the scaling potential results;

- Carbonate scale predictions using different historical produced fluid compositions to evaluate the changes in scaling risk over time;

- Carbonate scale predictions using current produced fluid compositions with the exception of H_2S to investigate the impact of reservoir souring on the scaling potential;

- Calculation of Maximum Dissolved Iron (MDI) to investigate FeS formation; the MDI concept is explained in (Verri and Sorbie, 2017b).

5.4.1 Workflow Application: Winprop (PVT) + ScaleChem

The Heriot-Watt scale prediction workflow is applied here to allow the integration of a full PVT software (in this case Winprop (CMG, 2017)) with a commonly used aqueous phase software (ScaleChem (OLI, 2016)) to obtain carbonate scale predictions for ANP 70. The various steps in the procedure are explained to provide a clear example of how our workflow is applied to a real system.

STEP 1: Define PVT total feed. The Winprop PVT software was used for this calculation step and the selected Equation of State (EOS) was the Peng-Robinson EOS (1978). The original PVT experimental data was input into Winprop and a given set of parameters was optimized to match the experimental data. The parameters selected for this data regression process are C_{7+} critical pressure, critical temperature, molecular weight and volume shift as well as the interaction coefficients of all components. This optimization process is run automatically by Winprop and the optimized results for GOR are shown in Figure 5.5.

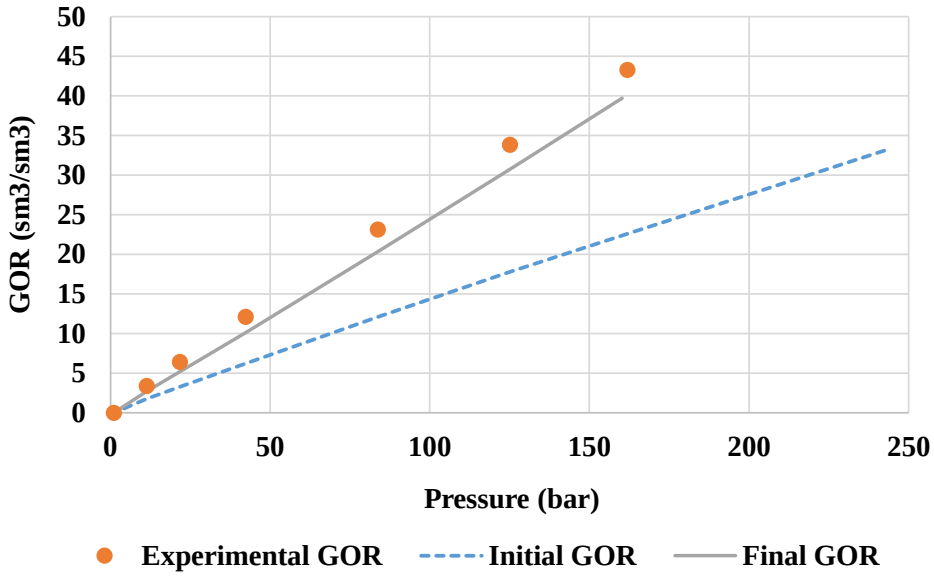

Figure 5.5: GOR optimization with experimental data regression (from differential liberation data).

Once the EOS properties and other PVT parameters are optimized to match experimental PVT data, the original hydrocarbon feed (Table 5.4) must be adjusted to include water, H_2S (this field was sweet at the time of the PVT tests) and correct CO_2 to the field measured value. These components were adjusted until a flash calculation of the new feed provides the measured CO_2 and H_2S gas phase concentrations at separator, as well as the measured oil and water flow rates. The recalculated PVT total feed and the results of the flash calculations at separator temperature and pressure are shown in Table 5.10. The values highlighted in yellow match the measured field data.

	Original HC Feed mol%	New Total Feed mol%	Separator Water mol%	Separator Oil mol%	Separator Gas mol%
H_2S	0	0.0014	0.00070	0.022	0.084
CO_2	0.16	0.00598	0.00157	0.082	0.609
N_2	0.11	0.00169	0.00002	0.005	0.269
CH_4	39.87	0.61125	0.01134	2.819	95.186
C_2H_6	1.42	0.02177	0.00579	0.254	2.271
C_3H_8	0.3	0.0046	0.00207	0.093	0.280
IC_4	0.07	0.00107	0.00038	0.041	0.052
NC_4	0.11	0.00169	0.00054	0.075	0.075
IC_5	0.06	0.00092	0.00018	0.062	0.026
NC_5	0.04	0.00061	0.00011	0.045	0.015
FC_6	0.28	0.00429	0.00038	0.384	0.055
C_{7+}	57.58	0.88277	0.00000	94.327	0.000
H_2O	0	98.46195	99.97693	1.792	1.077
Phase Volume %			40.778	8.835	50.387
Phase Mole %			98.461	0.936	0.603
Molar Volume (l/mol)			0.01817	0.41408	3.66706

Table 5.10: Original hydrocarbon feed, recalculated total PVT feed for ANP 70 and results of flash calculations at separator temperature and pressure.

STEP 2: Run PVT calculations at separator conditions. The results of PVT flash at separator temperature and pressure are shown in Table 5.10.

STEP 3: Calculate separator water composition. The ScaleChem aqueous phase model (aqueous phase only) was used for this calculation. The separator water composition shown in Table 5.3 was used as data input but the initial Ca^{2+}, $CO_{2(aq)}$ and $H_2S_{(aq)}$ were adjusted until the final equilibrated water met the following requirements:

- Output Ca^{2+} = 550 mg/l (to match measured separator concentration);
- Output $CO_{2(aq)}$ = 38.03 mg/l (this value was calculated from the PVT flash results at separator T and p (Table 5.10);

- Output $H_2S_{(aq)}$ = 13.10 mg/l (this value was calculated from the PVT flash results at separator T and p (Table 5.10);

- Since $CaCO_3$ was believed to precipitate at separator conditions, the water is saturated with $CaCO_3$. If this information was not available, we would need to fix the final pH or alkalinity to calculate the resulting water chemistry.

The resulting separator water chemistry is shown in Table 5.11.

NOTE: this is a simplified composition because many more soluble species such as $CaHCO_3^+$, $MgHCO_3^+$ and others are predicted to form. These species are accounted for when calculating total Ca^{2+}, Mg^{2+} etc. and alkalinity.

Ca^{2+}	***CO_2***	***H_2S***	***HCO_3^-***	***HS^-***	***pH***	***Alkalinity***
(mg/l)	(mg/l)	(mg/l)	(mg/l)	(mg/l)	(mg/l)	(mg/l) HCO_3^-
550	38	13	256	16	6.7077	410

Table 5.11: Calculated separator water chemistry (simplified).

From the PVT results in Table 5.10, the oil/water and gas/water partition coefficients for CO_2 and H_2S are derived and used to calculate three phase total carbonates and total sulphides. These results are shown in Table 5.12.

K_{OW} (CO_2)	***K_{GW} (CO_2)***	***K_{OW} (H_2S)***	***K_{GW} (H_2S)***	***Total Carbonates***	***Total Sulphides***
(mol fr./ mol fr.)	(mol fr./ mol fr.)	(mol fr./ mol fr.)	(mol fr./ mol fr.)	(mol)	(mol)
51.93	388.20	30.81	119.63	10,019	1,328

Table 5.12: Separator CO_2 and H_2S partition coefficients and calculated total carbonates and sulphides.

These total carbonates do not account for any precipitated $CaCO_3$ along the system but they are fixed as initial value for calculating the reservoir water composition (Step 5 below).

STEP 4: Run PVT calculations at reservoir conditions. The results of PVT flash at reservoir temperature and pressure are shown in Table 5.13. The reservoir pressure is above bubble point and a gas phase is not present.

	Total Feed mol%	**Reservoir Water mol%**	**Reservoir Oil mol%**	**K_{OW} (mol fr./ mol fr.)**	**K_{GW} (mol fr./ mol fr.)**
H_2S	0.0014	0.00114	0.01919	16.83	#N/A
CO_2	0.00598	0.00351	0.17623	50.21	#N/A
N_2	0.00169	0.00029	0.09757		
CH_4	0.61125	0.13452	33.46098		
C_2H_6	0.02177	0.0141	0.55061		
C_3H_8	0.0046	0.00275	0.13214		
IC_4	0.00107	0.00044	0.04492		
NC_4	0.00169	0.00061	0.07609		
IC_5	0.00092	0.00019	0.05126		
NC_5	0.00061	0.00011	0.03532		
FC_6	0.00429	0.0004	0.27258		
C_{7+}	0.88277	0	61.71105		
H_2O	98.46195	99.84194	3.37207		
Phase Volume %		81.3366	18.6634		
Phase Mole %		98.5695	1.4305		
Molar Volume (l/mol)		0.0184	0.29085		

Table 5.13: Results of flash calculations at reservoir temperature and pressure.

STEP 5: Calculate reservoir water composition. ScaleChem aqueous phase model (aqueous phase only) was used for this calculation. The full separator water composition (simplified composition shown in Table 5.11) was adjusted for water volume changes from separator to reservoir and used as data input. The initial $CO_{2(aq)}$ and $H_2S_{(aq)}$ are adjusted until the final equilibrated water met the following requirements:

- Output total carbonates = 10,019 mol (to match calculated separator value)
- Output total sulphides = 1,328 mol (to match calculated separator value)

- Since some carbonates are present in the reservoir rock, the water was saturated with $CaCO_3$.

The resulting simplified reservoir water chemistry is shown in Table 5.14.

Ca^{2+}	CO_2	H_2S	HCO_3^-	HS^-	pH	Alkalinity
(mg/l)	(mg/l)	(mg/l)	(mg/l)	(mg/l)	(mg/l)	(mg/l) HCO_3^-
547	82	17	296	21	6.3956	419

Table 5.14: Initially calculated reservoir water chemistry (simplified).

STEP 6: Recalculate separator water composition. ScaleChem aqueous phase model (aqueous phase only) was used for this calculation. The full reservoir water composition (simplified composition shown in Table 5.14) was adjusted for water volume changes from reservoir to separator and used as data input. The initial $CO_{2(aq)}$ and $H_2S_{(aq)}$ were adjusted until the final equilibrated water met the following requirements:

- Output total carbonates = 10,019 mol (to match reservoir value)
- Output total sulphides = 1,328 mol (to match reservoir value)

The resulting simplified separator water chemistry, the original separator water chemistry and the percent difference is shown in Table 5.15.

The predicted cumulative $CaCO_3$ precipitation is 15 mg/l and SR = 1.25.

	Recalculated Separator Water	Original Separator Water	Absolute Difference (%)
Ca^{2+}	549	550	0.23%
CO_2	37	38	2.43%
H_2S	13	13	0.51%
HCO_3^-	253	256	1.12%
HS^-	16	16	0.83%
pH	6.7136	6.7077	0.09%
Alkalinity	406	410	0.96%

Table 5.15: Recalculated and original separator water chemistry and absolute difference.

Although the difference between original and recalculated separator water chemistry is minor, a second iteration calculation is run to improve results accuracy.

STEP 5 - ITERATION 2: Calculate reservoir water composition. The calculations in this step are identical to those of Step 5 but now the total carbonates are fixed to 10,177 mol which is the initial separator value (10,019 mol) plus the cumulative $CaCO_3$ scale predicted to precipitate (15 mg/l). The resulting simplified reservoir water chemistry is shown in Table 5.16.

Ca^{2+}	CO_2	H_2S	HCO_3^-	HS^-	*pH*	*Alkalinity*
(mg/l)	(mg/l)	(mg/l)	(mg/l)	(mg/l)	(mg/l)	(mg/l) HCO_3^-
549	85	17	300	21	6.3898	423

Table 5.16: Calculated reservoir water chemistry - Iteration 2 (simplified).

STEP 6 - ITERATION 2: Recalculate separator water composition. The calculations in this step are identical to those of Step 6 but now the total carbonates are fixed to 10,177 mol.

The resulting simplified separator water chemistry, the original separator water chemistry and the percent difference is shown in Table 2.1. Since the recalculated separator matches the initial composition, no further iterations are necessary.

The predicted cumulative $CaCO_3$ precipitation is 15 mg/l and SR = 1.25.

	Recalculated Separator Water	**Original Separator Water**	**Absolute Difference (%)**
Ca^{2+}	550	550	0.00%
CO_2	38	38	0.02%
H_2S	13	13	0.02%
HCO_3^-	256	256	0.01%
HS^-	16	16	0.01%
pH	6.7078	6.7077	0.00%
Alkalinity	410	410	0.01%

Table 5.17: Recalculated and original separator water chemistry. Iteration 2.

STEP 7: Run PVT at near-wellbore and wellhead T and p. The results of PVT flash at near-wellbore and wellhead temperature and pressure are shown in Table 5.18.

	Total Feed mol%	Wellbore Water mol%	Wellbore Oil mol%	Wellhead Water mol%	Wellhead Oil mol%	Wellhead Gas mol%
H_2S	0.0014	0.0011	0.0219	0.00096	0.02807	0.03473
CO_2	0.00598	0.00342	0.18118	0.00288	0.14716	0.33985
N_2	0.00169	0.00028	0.09776	0.00006	0.01964	0.2933
CH_4	0.61125	0.12897	33.6331	0.03912	9.67509	97.45571
C_2H_6	0.02177	0.01361	0.58031	0.01076	0.46245	1.33124
C_3H_8	0.0046	0.00271	0.13423	0.00276	0.12437	0.12837
IC_4	0.00107	0.00043	0.04516	0.00046	0.05007	0.02316
NC_4	0.00169	0.0006	0.07636	0.00064	0.08865	0.03267
IC_5	0.00092	0.00019	0.05113	0.0002	0.06663	0.0108
NC_5	0.00061	0.00011	0.03521	0.00011	0.0468	0.00622
FC_6	0.00429	0.0004	0.27117	0.00037	0.37763	0.02199
C_{7+}	0.88277	0	61.32549	0	87.19209	0
H_2O	98.46195	99.8482	3.54699	99.94169	1.72134	0.32196
Phase Volume %		81.231	18.769	67.1467	14.699	18.1543
Phase Mole %		98.5605	1.4395	98.5004	1.0124	0.4872
Molar Volume (l/mol)		0.01843	0.29163	0.01816	0.38677	0.99276

Table 5.18: Results of flash calculations at near-wellbore and wellhead temperature and pressure.

STEP 8: Calculate water composition at wellbore and wellhead T and p. The ScaleChem aqueous phase model (aqueous phase only) was used for this calculation.

The full reservoir water composition (simplified composition shown in Table 5.16) is adjusted for water volume changes from reservoir to near-wellbore and wellhead conditions respectively and used as data input. The initial $CO_{2(aq)}$ and $H_2S_{(aq)}$ are adjusted until the final equilibrated water meets the following requirements:

- Output total carbonates = 10,177 mol (to match reservoir value)
- Output total sulphides = 1,328 mol (to match reservoir value)

The resulting near-wellbore and wellhead water chemistry (simplified), the $CaCO_3$ scale predictions and partition coefficients are shown in Table 5.19.

	Near-Wellbore Water Chemistry	**Wellhead Water Chemistry**	**Separator Water Chemistry**
Ca^{2+} (mg/l)	542	556	550
CO_2 (mg/l)	85	65	38
H_2S (mg/l)	17	19	13
HCO_3^- (mg/l)	285	274	256
HS^- (mg/l)	17	15	16
pH	6.39	6.49	6.71
Alkalinity (eq. HCO_3^- mg/l)	405	429	410
$CaCO_3$ (SR)	1.16	0.64	1.25
$CaCO_3$ (mg/l)-cumulative	14	0	15
K_{OW} (CO_2)	52.98	51.10	51.93
K_{GW} (CO_2)	#N/A	118.00	388.20
K_{OW} (H_2S)	19.91	29.24	30.81
K_{GW} (H_2S)	#N/A	36.18	119.63

Table 5.19: Simplified near-wellbore, wellhead and separator water chemistry, $CaCO_3$ scale predictions and partition coefficients.

The first thing to note is that the CO_2, H_2S bisulphides and bicarbonates concentration does not change significantly form near-wellbore to separator despite the considerable pressure drop. This is because water represents 82% of the total fluid and the number of CO_2 and H_2S moles released into the hydrocarbon phase have a small impact on the final aqueous phase composition. Note that there is a 100 barrel water volume change (evaporation) from near-wellbore to separator and this impacts the concentrations (mg/l) shown in Table 5.19.

A small concentration of $CaCO_3$ scale (14 mg/l) is predicted to precipitate in the near wellbore whilst no scale is forming at wellhead conditions (or $CaCO_3$ precipitated upstream and carried up the wellbore could potentially re-dissolve if equilibrium is reached). Since the values reported in Table 5.19 refer to cumulative $CaCO_3$ scale, the

$CaCO_3$ predicted at separator (15 mg/l) is almost entirely from near-wellbore precipitation if the scale is carried through the system rather than precipitated in situ.

5.4.2 Simplified Procedure: Automated ScaleChem Calculations (Integrated PVT + Aqueous Phase Model)

To compare the results obtained using the HWU Workflow with Winprop PVT, additional calculations were carried out using ScaleChem for both the PVT and the aqueous phase model. However, the software requires some data input that is not readily available and for this reason the separator oil and gas compositions calculated with Winprop (Table 5.10) are used as data input for ScaleChem together with the measured separator water chemistry of Table 5.3. The input Ca^{2+}, $CO_{2(aq)}$ and $H_2S_{(aq)}$ are adjusted until the output separator Ca^{2+}, $CO_{2(g)}$ and $H_2S_{(g)}$ match measured values. The procedure used in ScaleChem is schematically shown in Figure 5.6.

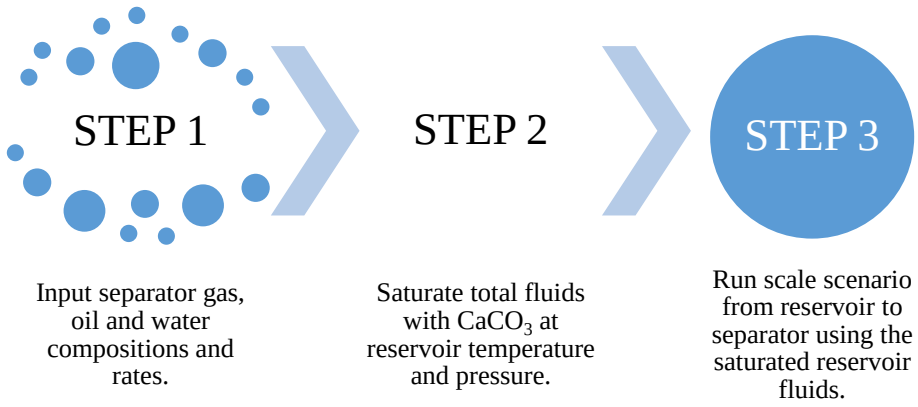

Figure 5.6: Procedure for automated ScaleChem scale predictions (integrated PVT and aqueous phase model).

The output simplified water chemistry, scale predictions and partition coefficients at reservoir, near-wellbore, wellhead and separator conditions is shown in Table 5.20.

	Reservoir Water Chemistry	Near-Wellbore Water Chemistry	Wellhead Water Chemistry	Separator Water Chemistry
Ca^{2+}	556	549	564	550
CO_2	95	96	67	37
H_2S	16	16	18	12
HCO_3^-	315	301	285	252
HS^-	19	18	14	15
pH	6.4	6.4	6.5	6.7
$CaCO_3$ *(SR)*	1	1.12	0.69	1.34
$CaCO_3$ *(mg/l)-cumulative*	0	13	0	34
K_{OW} (CO_2)	34.58	36.12	33.51	33.93
K_{GW} (CO_2)	#N/A	#N/A	120.85	399.63
K_{OW} (H_2S)	31.74	32.98	37.42	38.04
K_{GW} (H_2S)	#N/A	#N/A	40.07	129.15

Table 5.20: Simplified reservoir, near-wellbore, wellhead and separator water chemistry, $CaCO_3$ scale predictions and partition coefficients obtained using ScaleChem integrated PVT and aqueous phase model.

5.5 RESULTS COMPARISON

The carbonate scale prediction results obtained with the HWU workflow using Winprop PVT and with the automated ScaleChem process (ScaleChem PVT) are shown in Figure 5.7 for $CaCO_3$ saturation ratio (SR) and Figure 5.8 for $CaCO_3$ mass (mg/l). *All these results refer to cumulative $CaCO_3$ precipitation.*

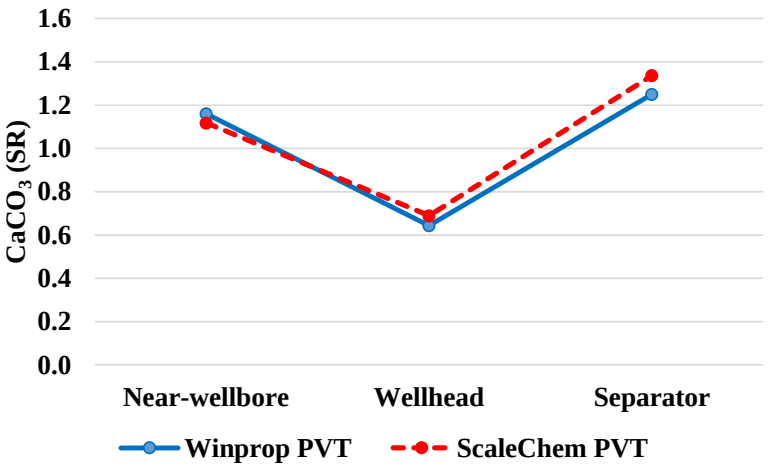

Figure 5.7: Comparison between $CaCO_3$ SR calculated using Winprop PVT and ScaleChem PVT for ANP 70.

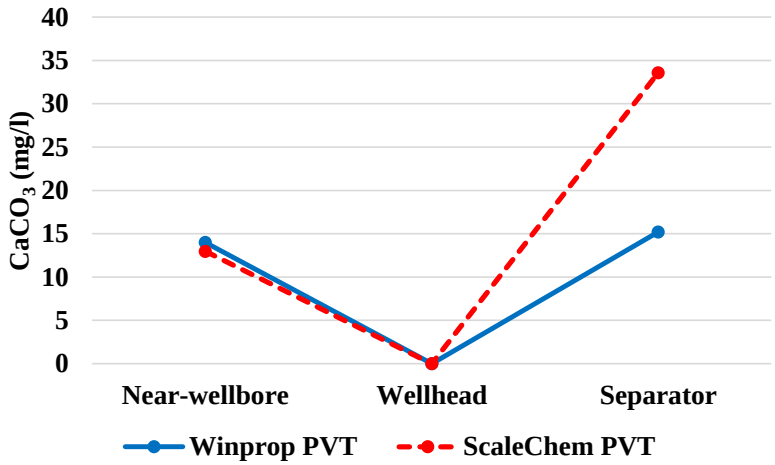

Figure 5.8: Comparison between $CaCO_3$ mass calculated using Winprop PVT and ScaleChem PVT for ANP 70.

Although both scenarios predict a really mild calcium carbonate problem and the results are similar, ScaleChem PVT predicts more $CaCO_3$ precipitation at separator conditions for Well A and can be considered the worst case scenario. Hence, ScaleChem PVT is used for the additional calculations shown in Paragraph 5.6.

NOTE. Thermodynamically, SR<1 at wellhead conditions means that if $CaCO_3$ precipitates upstream of that point and is carried through the system, at wellhead T and p it will re-dissolve (providing the kinetics allow it to). However, $CaCO_3$ would then re-precipitate at separator conditions where SR>1.

5.6 CALCIUM CARBONATE SCALE PREDICTION TIMELINE AND EFFECT OF H_2S

The results shown in Paragraph 0 are obtained using the most recent produced water and gas chemistry data. However, some of the produced fluids properties (e.g. water cut, H_2S content, etc.) have changed over time and it is important to understand how this has affected the carbonate scaling potential of ANP 70. Moreover, one of the key questions

to answer is whether H_2S is playing an important role in $CaCO_3$ precipitation or if it has a small or negligible effect in this well.

To answer this question, four different scenarios were investigated. The data used for each scenario are summarized in Table 5.21. Scenario 1, 2 and 3 account for changes in fluid properties over time whereas Scenario 4 is a hypothetical case where H_2S is removed from Scenario 3 to test its impact on $CaCO_3$ predictions. Scenario 1 refers to the fluids produced just before the first PI decline in August 2016 (Figure 5.2); scenario 2 takes into account fluids composition just before the H_2S started increasing steeply in September 2017, whilst scenario 3 is representative of the more recent produced fluid compositions including H_2S.

	Date	**Oil rate**	**Water rate**	**Gas rate**	**Gas H_2S**	**Gas CO_2**	**Separator Ca^{2+}**
		m3/d	m3/d	m3/d	mol %	mol %	mg/l
Scenario 1	Aug 2016	849	536	5862	0	0.3	640
Scenario 2	Sept 2017	315	1523	2171	0	0.5	625
Scenario 3	Apr 2018	230	1050	1588	0.08	0.6	550
Scenario 4	Apr 2018	230	1050	1588	0	0.6	550

Table 5.21: Produced fluid rates and compositions for Scenarios 1-4.

The automated ScaleChem PVT + aqueous phase model was used for these calculations because it provides "worst case scenario" results (more $CaCO_3$ precipitation than Winprop PVT) and because it provides a faster way to run multiple scenarios and compare trends.

The carbonate scale prediction results for scenarios 1-3 are shown in Figure 5.9 for $CaCO_3$ saturation ratio (SR) and Figure 5.10 for $CaCO_3$ mass (mg/l).

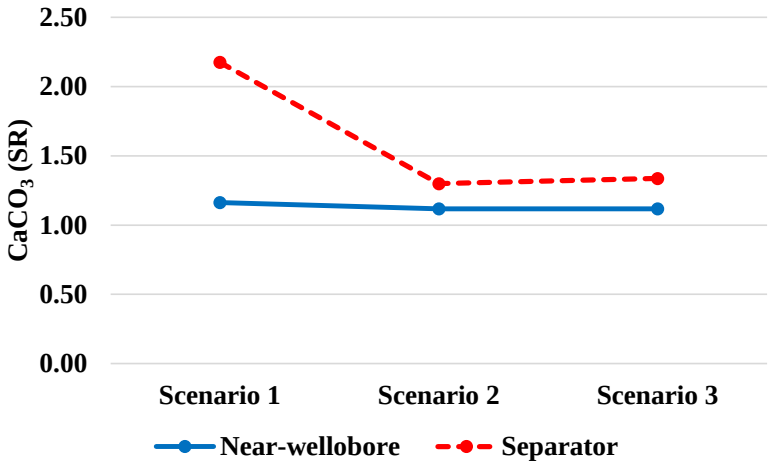

Figure 5.9: $CaCO_3$ SR at near-wellbore and separator conditions for scenarios 1-3.

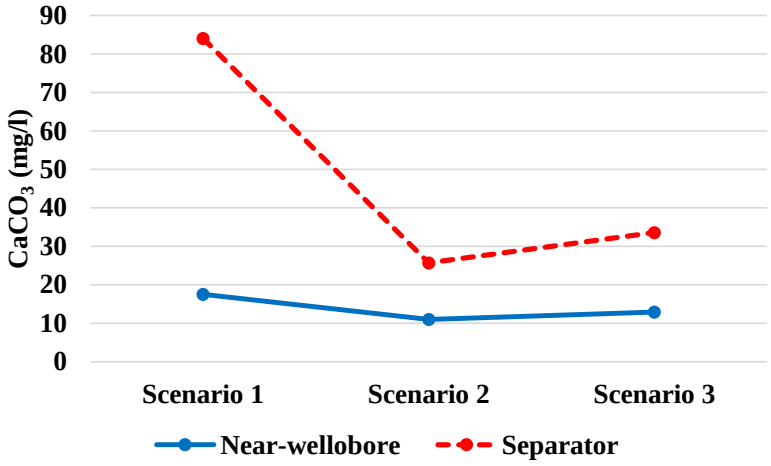

Figure 5.10: Cumulative $CaCO_3$ (mg/l) at near-wellbore and separator conditions for scenarios 1-3.

These results show a very mild carbonate scale problem in ANP 70 with more scale predicted to precipitate at separator conditions rather than in the near-wellbore region. Moreover, the carbonate scaling potential was more significant when the well was first brought online and produced lower water cut fluids (scenario 1). Based on common oilfield standards, this scaling problem may be considered to be either very mild or negligible. However, the positive impact of the acid job carried out in ANP 70 and the clear correlation between dissolved $CaCO_3$ and improved PI suggests that $CaCO_3$ is indeed precipitating in the near-wellbore region despite the low predicted saturation

ratio and it is causing a negative impact on production. The original hypothesis was that some $CaCO_3$ precipitation (to be quantified by these calculations) may have been acting as a "cementing" agent to consolidate sand on the screens and near wellbore region causing a loss in well productivity. This hypothesis still holds in light of the results obtained here, and there is a better way to present these results for ANP 70 that can clarify this statement. Instead of plotting the concentration (in mg/l) of precipitated $CaCO_3$, Figure 5.11 shows the cumulative daily mass of calcite precipitation obtained using the water production rate associated with each scenario. Only the near-wellbore region results are shown since the productivity loss is caused by obstructions in this part of the well. Scenario 4 is also shown to explain the impact of H_2S on carbonate scale predictions for ANP 70.

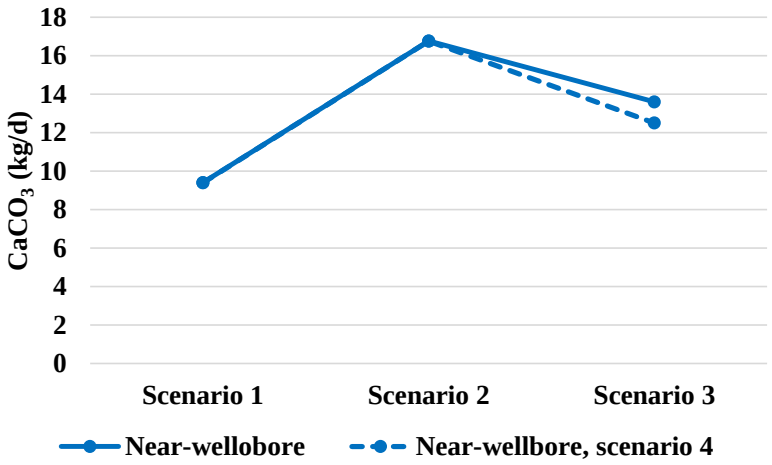

Figure 5.11: Predicted daily $CaCO_3$ precipitation in the near wellbore region for scenarios 1-4.

The daily cumulative $CaCO_3$ increases from scenario 1 to scenario 2 because of the increased water production rates whereas the opposite happens from scenario 2 to 3. The comparison between scenario 3 and 4 shows that H_2S plays a minor role in the carbonate scaling potential for ANP 70 compared to the water cut changes and overall water production rates. Comparing scenarios 3 (with H_2S) and 4 (no H_2S), we see that the presence of H_2S has a slightly "negative" (increasing) effect on calcite deposition. It

is explained in detail in Section 6.2.4 that H_2S can in fact either decrease or increase the amount of calcite deposition depending on the CO_2/H_2S ratio; here it turns out to be slightly negative.

The main conclusion from these scaling calculations comes from the actual cumulative amounts of calcite deposition in the near well region in scenarios 3 and 4. If the kinetics of the calcite deposition process allow this scale to form, and the well is not properly treated with scale inhibitor, then over 14 kg/d of $CaCO_3$ (or over 5 tonne/year) will precipitate out in the sand screens. This quantity of scale is certainly sufficient to gradually obstruct production over time and produce the kind of PI trend observed in this well. Thus, the answers to our earlier questions are: yes, the predicted calcite problem is mild but is sufficient in terms of depositional mass rate of calcite to cause a PI decline in well ANP70. However, the additional souring of the reservoir has only led to a minor increase in the severity of this calcite scaling problem.

5.7 IRON SULPHIDE SCALE PREDICTIONS AND MDI

So far all calculations and results have focused on carbonate scale predictions only. The reason behind it is that the concept of Maximum Dissolved Iron (MDI) as explained in Section 3.4 is used to investigate iron sulphide (mackinawite) scale predictions and the full water chemistry must be firstly calculated at each selected point.

The calculated MDI for the reservoir, near wellbore, wellhead and separator full water chemistries shown in Table 5.20 is given in Table 5.22.

	Reservoir	**Near-Wellbore**	**Wellhead**	**Separator**
MDI (mg/l)	<0.1	<0.1	0.14	<0.1

Table 5.22: Reservoir, near-wellbore, wellhead and separator MDI calculated for the full water chemistries obtained with Winprop PVT.

These results demonstrate that:

- Dissolved Fe^{2+} is not stable at the given reservoir conditions (MDI <0.1 mg.l) and if iron was present in the reservoir, it would be in solid form (i.e. pyrite, pyrrhotite, etc.);

- The source of Fe^{2+} in any iron sulphide precipitated in the wellbore or at separator is from corrosion processes and not from reservoir fluids (since the reservoir cannot produce levels of Fe^{2+} above 0.1 mg/l) ;

- If Fe^{2+} becomes available anywhere in the system (through corrosion processes or other external sources), it will be precipitated as FeS. However, depending on the size of the crystals/colloidal species formed it may be carried through the system by the mobile fluids or it be deposited locally;

- Localized corrosion rate, kinetics of FeS formation and crystal growth as well as transformation in other polymorphs will determine where FeS forms and deposits. An underlying low level of ≈0.7 mg/l Fe^{2+} (recorded as dissolved iron but more likely a colloidal form of iron sulphide which is detected in ICP analysis) in the produced water suggests that corrosion in the well is ongoing and some corrosion products are carried through the system. Moreover, the spike in Fe^{2+} and $H_2S_{(g)}$ levels in the acid stimulations job flowback suggest that corrosion products (including FeS) were dissolved from the tubing and/or sand screens during this treatment. The extent of the CO_2 and sour corrosion problem should be studied separately and using the correct corrosion prediction tools.

5.8 CONCLUSIONS

This study was carried out to address the issue of whether there was enough of a downhole calcite scaling problem in Alba well ANP 70 to explain the observed PI decline in this well, as an example of several other similar wells in Alba. The secondary question addressed was to assess if the fact that Alba had gradually soured over several years from its initially sweet state had made the calcite problem significantly worse. For this purpose, the explicit steps in the workflow procedure are explained in some detail as examples which will help the oilfield chemistry community to better predict such scales. In particular, the careful coupling of a good PVT model with an aqueous scale prediction model is central to this process.

The specific conclusions from this study are as follows:

i. The (downhole) carbonate scaling potential of well ANP 70 was quite mild in terms of the SR and the amount of carbonate (in mg/l) expected;

ii. When converted to the mass of calcium carbonate deposition over time, then a maximum value of ~14kg/day (5 tonnes/year) could potentially be deposited. This quantity would be sufficient to cause the observed PI loss vs. time in well ANP 70;

iii. The previous conclusion is supported by the field observations from a formic acid stimulation job completed in December 2016, which suggest that scale deposition did indeed occur in the near wellbore region. The estimated mass of $CaCO_3$ removed in the formic job was ≈200 kg;

iv. Taking the scale prediction and acid stimulation data together then this suggests that: (a) the efficiency of that stimulation job was low and more $CaCO_3$ scale is

still present downhole and/or (b) kinetics only allow for a smaller amount of scale to precipitate and/or (c) the produced water is partially inhibited thanks to the scale inhibitor squeeze treatments. However, even if only a fraction of this predicted $CaCO_3$ forms on the sand screens, it could act as a "cementing" agent to consolidate sand and cause problems to the well productivity;

v. The presence of H_2S on the calcium carbonate scaling tendency had a very slightly deleterious effect (calcite deposition increased) but the magnitude of this was very minor in this case; in other cases it can be much more significant (Verri and Sorbie, 2017a);

vi. For these scaling calculations for ANP 70, choosing Winprop PVT or ScaleChem PVT had a negligible effect on the final carbonate scale predictions.

It should be noted that given the minor scaling potential for $CaCO_3$, inhibiting this scale should not be a challenge. Scale inhibitor squeeze treatments have been applied to manage barium sulphate formation in well ANP 70 (and other Alba wells) using sulphonated copolymer scale inhibitor, and this should prevent such a mild carbonate problem. However, related studies have indicated that this well may have a placement issue when squeeze treatments are bull-headed (rather than carried out using coiled tubing). This may explain why $CaCO_3$ is seen in this well despite the scale inhibitor squeeze treatments carried out. As a recommendation from this work, a second acid stimulation treatment followed by rigorous fluid sampling was recommended to further support the above conclusions and improve the PI of ANP 70.

This Chapter is based on a conference paper (Ness et al., 2019).

Chapter 6 - THE IMPACT OF MEASUREMENT ERRORS

6.1 INTRODUCTION

Although variables such as CO_2, H_2S, alkalinity etc. described in Section 2.3.2 play a role in the prediction of pH dependent scales, it is important to understand the true impact each of these parameters in the final scale prediction results. In particular, the focus should be on understanding how field measurement errors may impact the final scale prediction results in various scenarios.

In the following calculations, a base case scenario is defined and then an error analysis run by changing only one variable at a time* whilst keeping all other data input fixed (*note that it is sometimes not possible to change just 1 variable as explained below). For all calculations the gas, oil, water compositions and rates at separator T and p are fixed; these are then equilibrated at reservoir conditions (with $CaCO_3$) and the equilibrated fluids are "brought" into the wellbore to obtain a scale prediction profile from the reservoir to the separator. All scale prediction results show cumulative $CaCO_3$ precipitation at every given point to remove the differences caused by selecting a variable number of calculation steps in the wellbore.

All of the calculations in this thesis are run using ScaleChem, a commercial integrated PVT + scale prediction software but they can be done applying any software of user's choice using the Heriot-Watt scale prediction workflow (Chapter 3). Although the absolute results may vary, trends and conclusions remain the same for any PVT and scale prediction software used as long as the correct procedure is followed (the numerical impact of different software choice is discussed in Chapter 7).

6.2 BASE CASE SCENARIO

The data for the base case scenario is shown in Table 6.1.

Separator Oil		Separator Gas		Separator Water	
Component	**Mole %**	**Component**	**Mole %**	**Component**	**mg/l**
H_2O	0.27	H_2O	2.57	Na^+	10,526
CO_2	0.20	N_2	1.35	K^+	210
H_2S	0.70	CO_2	2.15	Ca^{2+}	3164
C_1	2.89	H_2S	2.67	Mg^{2+}	517
C_2	1.61	C_1	70.93	HCO_3^-	144
C_3	2.87	C_2	9.12	HS^-	129
nC_4	2.91	C_3	5.83	H_2S	373
nC_5	2.81	Other gases	5.38	CO_2	123
nC_6	5.3			**Other Data Input**	
nC_7	11.70			T_{sep} (°C)	65
nC_8	11.29			p_{sep} (bar)	10
nC_9	5.59			T_{res} (°C)	90
nC_{10}	4.86			p_{res} (bar)	300
nC_{11}	4.06			GOR (scf/bbl)	1386
C_{12+}	40.62			Water cut	6%
Others	2.68			EOS	SRK

Table 6.1: Base case scenario input data.

This base case scenario is for a volatile oil with low water cut, relatively high CO_2 and H_2S concentration (respectively 2.2% and 2.7% in the gas phase at separator conditions). Sensitivity studies were also run for lower GOR hydrocarbons and for higher water cut wells. Unless otherwise stated, the *trends* for these other scenario and final conclusions are broadly similar to the base case scenario. The results for the base case scenario are shown in Figure 6.2 and Figure 6.3. The points in the system from reservoir to separator are identified by the labels Reservoir, Wellbore 1, Wellbore 2… Separator (Figure 6.1) and for each one the temperature and pressure (T and p) are specified (Table 6.2). In this scenario, gas breaks out at Wellbore 3 and the main $CaCO_3$

precipitation is predicted at separator conditions. The slight increase in Ca^{2+} concentration despite scale precipitation is caused by the water evaporation at separator T and p which concentrates ions in the aqueous phase. NOTE: Alkalinity is calculated using Equation (6.1) and does not include other species calculated by ScaleChem such as $NaHCO_3$, $MgCO_3$ etc. because in the following scenarios they change the absolute value but not the resulting trends and conclusions. The alkalinity is always reported as equivalent mg/l of bicarbonates HCO_3^-.

$$Alkalinity = m_{OH^-} + m_{HCO_3^-} + 2\,m_{CO_3^{2-}} + m_{HS^-} + 2\,m_{S^{2-}} + m_{A^-} - m_{H^+} \quad (6.1)$$

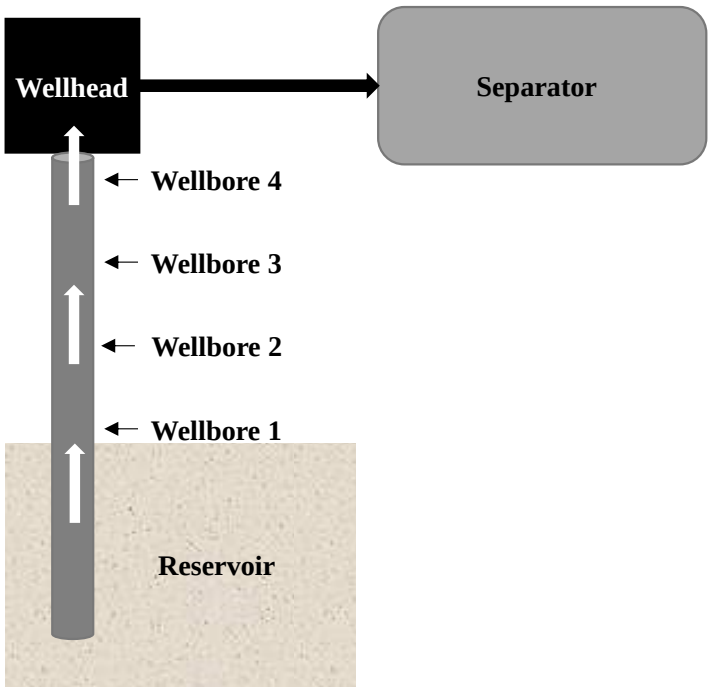

Figure 6.1: Wellbore schematic with selected calculation points.

Location	T (°C)	p (bar)
Reservoir	90	300
Wellbore 1	87	270
Wellbore 2	83	210
Wellbore 3	78	150
Wellbore 4	73	90
Separator	65	10

Table 6.2: Temperature and pressure profiles.

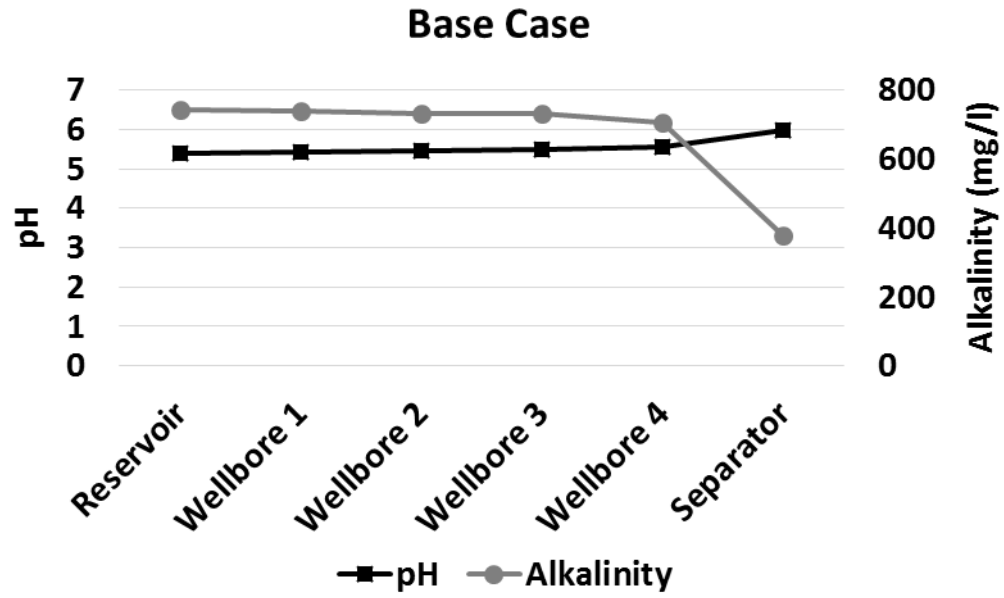

Figure 6.2: pH and alkalinity for base case scenario.

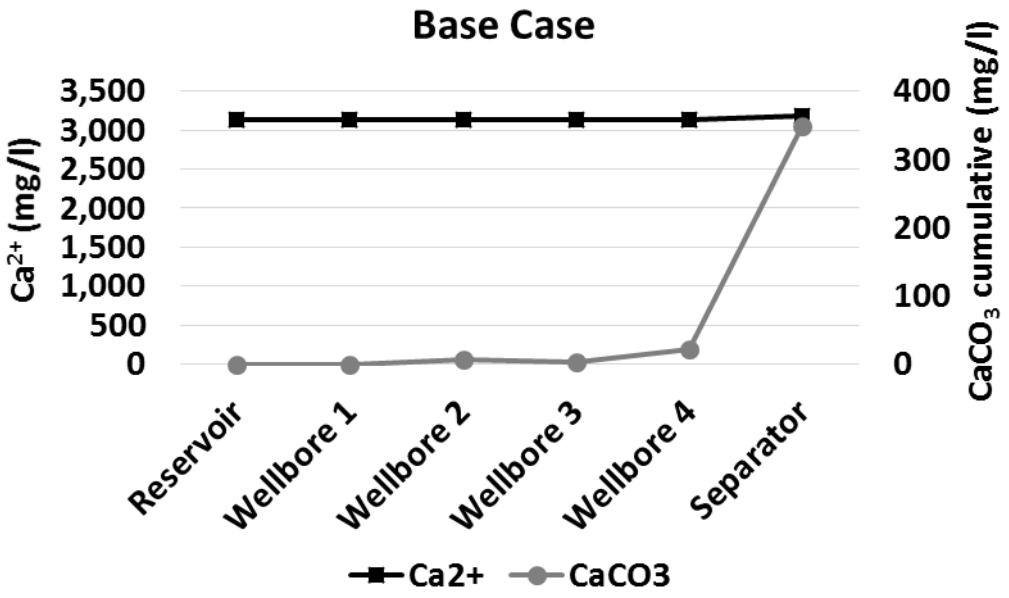

Figure 6.3: Ca^{2+} and cumulative $CaCO_3$ precipitation for the base case scenario.

These results show that calcium carbonate scale precipitates mainly at separator conditions where the pH increases due to a pressure drop and CO_2 loss to the hydrocarbon phase. Although scale precipitation is quite significant, the change in Ca^{2+} is barely noticeable because the Ca^{2+} is high (>3,000 mg/l).

6.2.1 Aqueous Iron (Fe^{2+})

The challenges of measuring dissolved iron in sour systems was addressed in Section 2.3.2. Although Fe^{2+} measurements in sour waters are highly unreliable, if the pH, aqueous sulphides and carbonates can be calculated correctly, it is possible to predict how much Fe^{2+} can be thermodynamically stable at the given conditions. This is here defined as the Maximum Dissolved Iron (MDI). If a higher concentration of total iron is present in the system (either from reservoir fluids, corrosion or other sources), scale will form. The fast reaction between Fe^{2+} and H_2S/HS^- (Rickard and Luther, 2007) and the high affinity between these ions means that when both Fe^{2+} and H_2S are present, there are three main scenarios of Fe^{2+}/FeS thermodynamic equilibrium:

- If the water pH is sufficiently low (normally caused by a high concentration of CO_2), it is possible to have stable Fe^{2+} in highly sour waters and no FeS precipitation. This is explained in details in a previous publication where results show that in produced water at pH≈3.5 and total aqueous sulphides >7,000 mg/l it is possible to have up to 30 mg/l of dissolved Fe^{2+} (Verri et al., 2017b);

- If the pH is higher, Fe^{2+} is in excess and H_2S is the limiting reagent, the available dissolved H_2S will react to form FeS and the remaining Fe^{2+} may remain dissolved as Fe^{2+} or form $FeCO_3$ if CO_2 is present.

- At higher pH values (say pH>5) and sulphide excess, virtually all of the Fe^{2+} precipitates as FeS and Fe^{2+} is essentially not present in the system.

In this base case scenario, pH and sulphide concentration are sufficiently high to cause all available Fe^{2+} to precipitate as FeS anywhere Fe^{2+} is present (from reservoir to

separator). For this reason, whatever concentration of Fe^{2+} is used at each selected point, it will all precipitate as FeS and the only difference will be the mass of precipitate.

6.2.2 Calcium Concentration (Ca^{2+})

Calcium, pH, alkalinity, bicarbonates and bisulphides are strongly linked together and in thermodynamic equilibrium scenarios one cannot be changed without impacting the others. This can be clearly seen from the chemical equations that govern aqueous sour carbonate systems shown in Equation (2.38) through (6.12).

$$H_2O \leftrightarrow OH^- + H^+ \tag{6.2}$$

$$CO_2 + H_2O \leftrightarrow H_2CO_3 \tag{6.3}$$

$$H_2CO_3 \leftrightarrow H^+ + HCO_3^- \tag{6.4}$$

$$HCO_3^- \leftrightarrow CO_3^{2-} + H^+ \tag{6.5}$$

$$H_2S \leftrightarrow HS^- + H^+ \tag{6.6}$$

$$HS^- \leftrightarrow S^{2-} + H^+ \tag{6.7}$$

$$HA \leftrightarrow A^- + H^+ \tag{6.8}$$

$$Ca^{2+} + CO_3^{2-} \rightarrow CaCO_3(s) \tag{6.9}$$

$$Fe^{2+} + CO_3^{2-} \rightarrow FeCO_3(s) \tag{6.10}$$

$$Fe^{2+} + S^{2-} \rightarrow FeS\,(s) \tag{6.11}$$

$$Alkalinity = m_{OH^-} + m_{HCO_3^-} + 2\,m_{CO_3^{2-}} + m_{HS^-} + 2\,m_{S^{2-}} + m_{A^-} - m_{H^+} \tag{6.12}$$

The connection between all these chemical species (through the complete set of equilibrium equations that must be honoured) is the reason why although only one input value is varied in this error analysis, all the other related values will adjust accordingly, as shown in the results below.

In these calculations, the gas phase CO_2 and H_2S concentrations are fixed and the corresponding aqueous concentrations are re-calculated according to the vapour-liquid equilibrium.

For the Ca^{2+} error analysis, the same input values are kept as for the base case and only the initial Ca^{2+} concentration at separator is varied. *This is equivalent to assuming that the measured Ca^{2+} value in produced water is incorrect or unreliable* and the impact of this input value on the final scale prediction profile must be established. A schematic of the calculation process is shown in Figure 6.4.

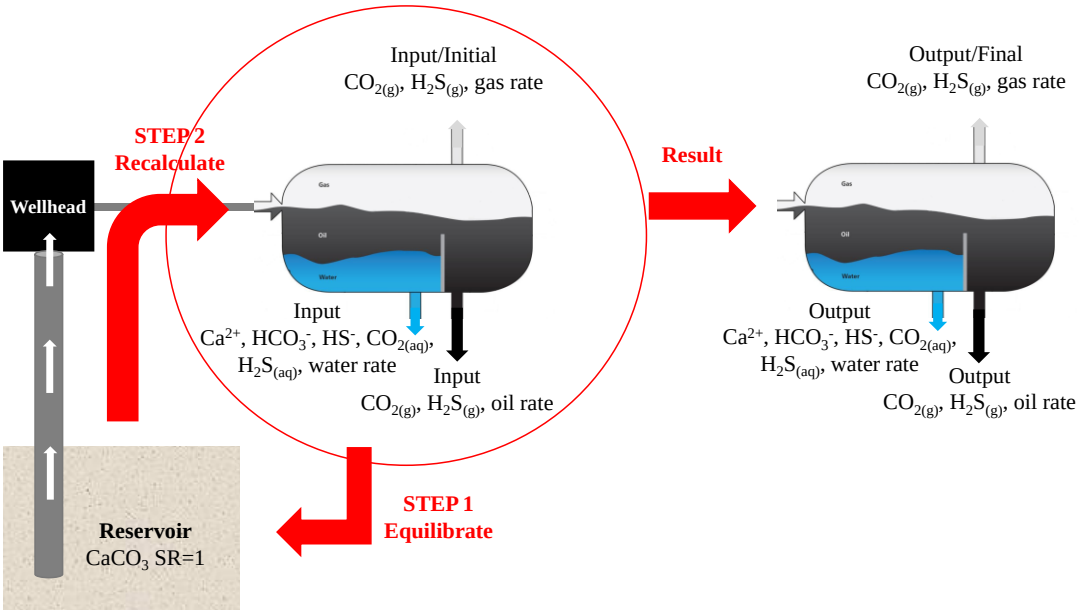

Figure 6.4: Schematics of data input/output and calculation process.

The cumulative $CaCO_3$ precipitation at separator is shown in Figure 6.5 for variable final separator Ca^{2+} concentrations.

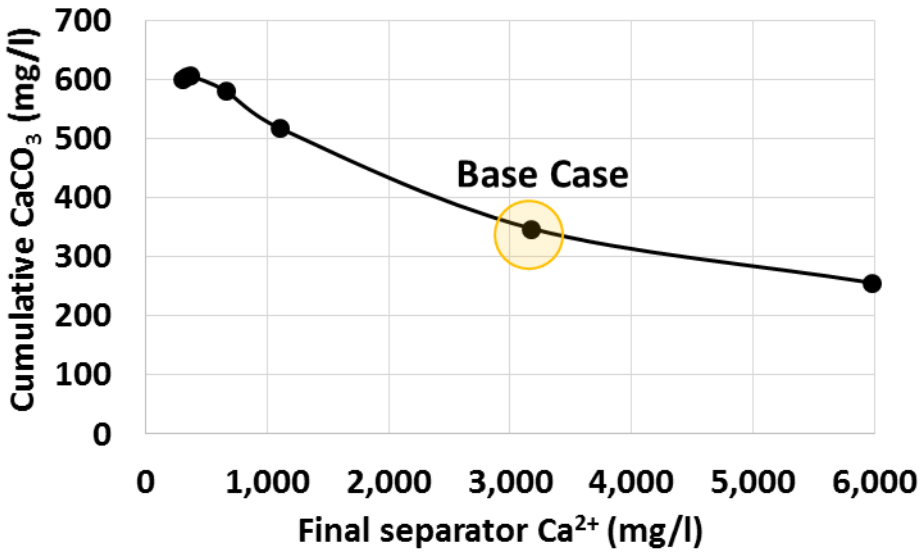

Figure 6.5: Cumulative $CaCO_3$ precipitation at separator for variable Ca^{2+} concentration (300-6,000 mg/l range).

Although Figure 6.5 shows that a large error in Ca^{2+} measurements can cause an equally significant difference in cumulative $CaCO_3$ precipitation, with relatively high Ca^{2+} concentrations as in this base case scenario, a measurement error of ±30% has a moderate impact on the final $CaCO_3$ precipitation (Table 6.3).

Final Ca^{2+}	**Cumulative $CaCO_3$**
Base Case (Ca^{2+}=3164 mg/l)	348 mg/l
+30% (Ca^{2+}=4113 mg/l)	-11% (309 mg/l)
+50% (Ca^{2+}=4746 mg/l)	-17% (288 mg/l)
-30% (Ca^{2+}=2215 mg/l)	+16% (403 mg/l)
-50% (Ca2+=1582 mg/l)	+31% (455 mg/l)

Table 6.3: Impact of Ca^{2+} measurement errors on cumulative $CaCO_3$ scale predictions.

The reason why the $CaCO_3$ precipitation decreases as separator Ca^{2+} increases is that, for a fixed gas phase CO_2 concentration (assumed in these calculations), the water alkalinity at equilibrium in the reservoir must be lower to be able to keep more Ca^{2+} in solution. This can be seen from the $CaCO_3$ solubility product shown in Equation (6.13)

where a higher Ca^{2+} concentration requires lower carbonates (CO_3^{2-}) hence lower alkalinity (Equation (6.12)). Finally, when this lower alkalinity water enters the wellbore it will precipitate less $CaCO_3$ in the production system.

$$K_{sp,CaCO_3} = m_{Ca^{2+}}\, m_{CO_3^{2-}}\, \gamma_{Ca^{2+}}\, \gamma_{CO_3^{2-}} \tag{6.13}$$

Figure 6.6 shows that if separator Ca^{2+} is lower than 360mg/l, the $CaCO_3$ precipitation decreases as Ca^{2+} decreases and this effect is due to stoichiometry where Ca^{2+} becomes the limiting reagent. This behaviour occurs in every system but the Ca^{2+} concentration at which the inversion starts happening is different for every fluid and mainly dependent on the gas phase CO_2 and H_2S concentration (Larsen et al., 2010).

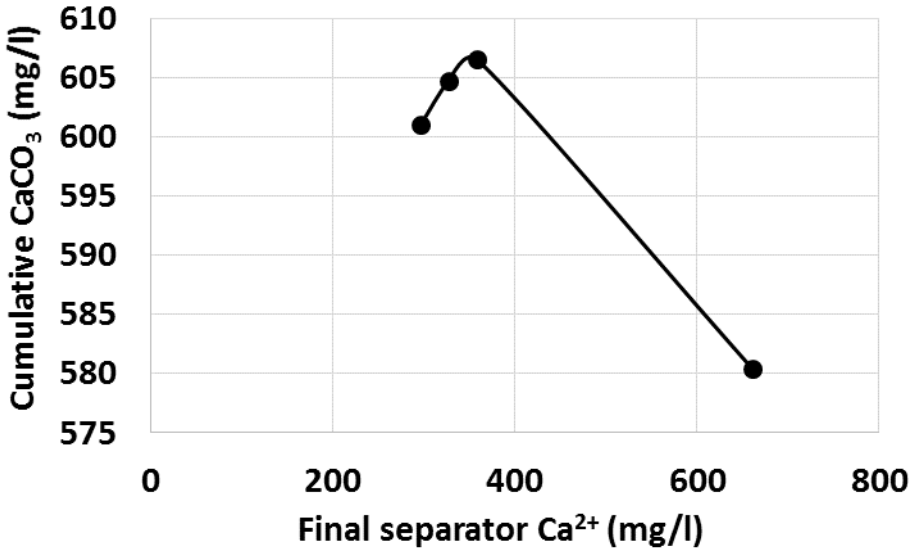

Figure 6.6: Cumulative $CaCO_3$ precipitation at separator for variable Ca^{2+} concentration (300-700 mg/l range).

As already mentioned, when the Ca^{2+} concentration is changed, other chemical properties such as alkalinity and pH must change because they are all interrelated. At equilibrium conditions, there is only one possible Ca^{2+}, alkalinity and pH combination for a given temperature, pressure and molecular CO_2 and H_2S (which are dictated by the

gas phase CO_2 and H_2S concentrations). The recalculated separator alkalinity and pH values for variable Ca^{2+} concentration are shown in Figure 6.7.

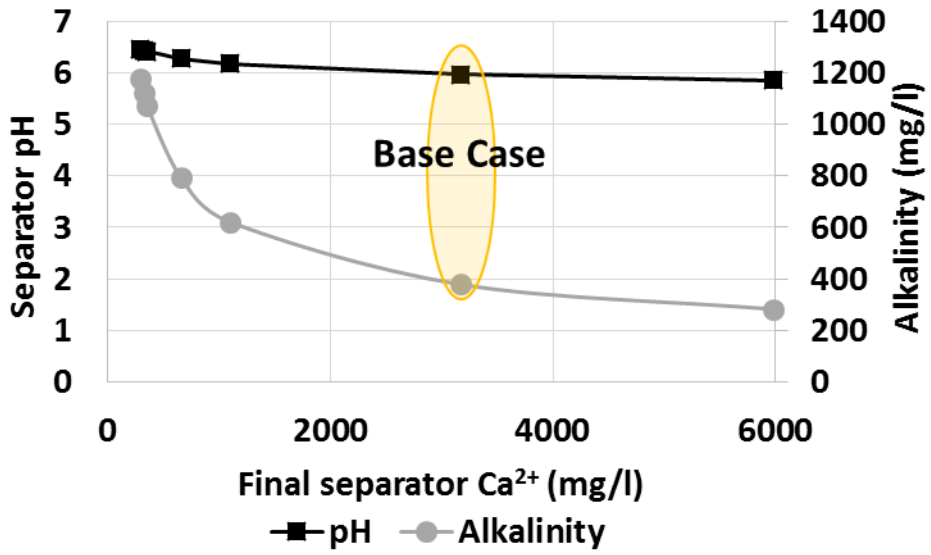

Figure 6.7: pH and alkalinity values at separator corresponding to variable Ca^{2+} concentrations.

The question is: which field data do we trust the most? If we can answer this question, all the corresponding system variables will be calculated as a results of the fixed, more reliable field data. In general, the field measured Ca^{2+} tends to be more reliable than pH and alkalinity although there can be exceptions. Finally, it is important to remember that these conclusions are true for equilibrium conditions. If the system is not at equilibrium or the aqueous phase is supersaturated (e.g. in the presence of scale inhibitor) comparing the calculated parameters with the expected values can give an indication of how far from equilibrium the system is.

6.2.3 Bicarbonates (HCO_3^-), Bisulphides (HS^-) and Alkalinity

If the separator Ca^{2+}, $CO_{2(g)}$ and $H_2S_{(g)}$ are fixed, only 3 scenarios for the input alkalinity value are possible, as follows:

1) Super saturation alkalinity (initial $CaCO_3$ SR>1): in this scenario, when the separator water is equilibrated, $CaCO_3$ drops out producing a water composition now in equilibrium with $CaCO_3$. The final Ca^{2+} and alkalinity will be lower than the initial values because of the scale precipitation.

2) Equilibrium alkalinity (initial $CaCO_3$ SR=1): in this scenario, the water is already at equilibrium with $CaCO_3$ for the given Ca^{2+}, $CO_{2(g)}$ and $H_2S_{(g)}$. This means that $CaCO_3$ is likely to have precipitated at separator conditions and the collected water sample (which gives us the input data) is in equilibrium with the solid.

3) Under saturation alkalinity ($CaCO_3$ SR<1): in this scenario, it is possible to have a different degree of under saturation depending on the input alkalinity. However, when the correct scale prediction workflow is used (obtain the reconstructed reservoir water composition and subsequently bring it up the wellbore to calculate the scale prediction profile) if $CaCO_3$ precipitates at separator conditions in the calculations it is not possible to reproduce this initial under saturated water composition but the final results is again the equilibrated water (same as scenario 1 and 2). Assuming that the calculations are carried out rigorously, this inconsistency could be due to wrong input data such as Ca^{2+} or gas phase composition, wrong number of calculation steps ($CaCO_3$ may have precipitated upstream of the separator at a T and p point not included in the calculations) or wrong T and p profiles.

The consequence of this, is that for a fixed separator Ca^{2+}, $CO_{2(g)}$ and $H_2S_{(g)}$, a large difference in initial alkalinity values results in similar final alkalinity and $CaCO_3$

precipitation because all cases converge to the separator water equilibrium value. This is shown in Figure 6.8.

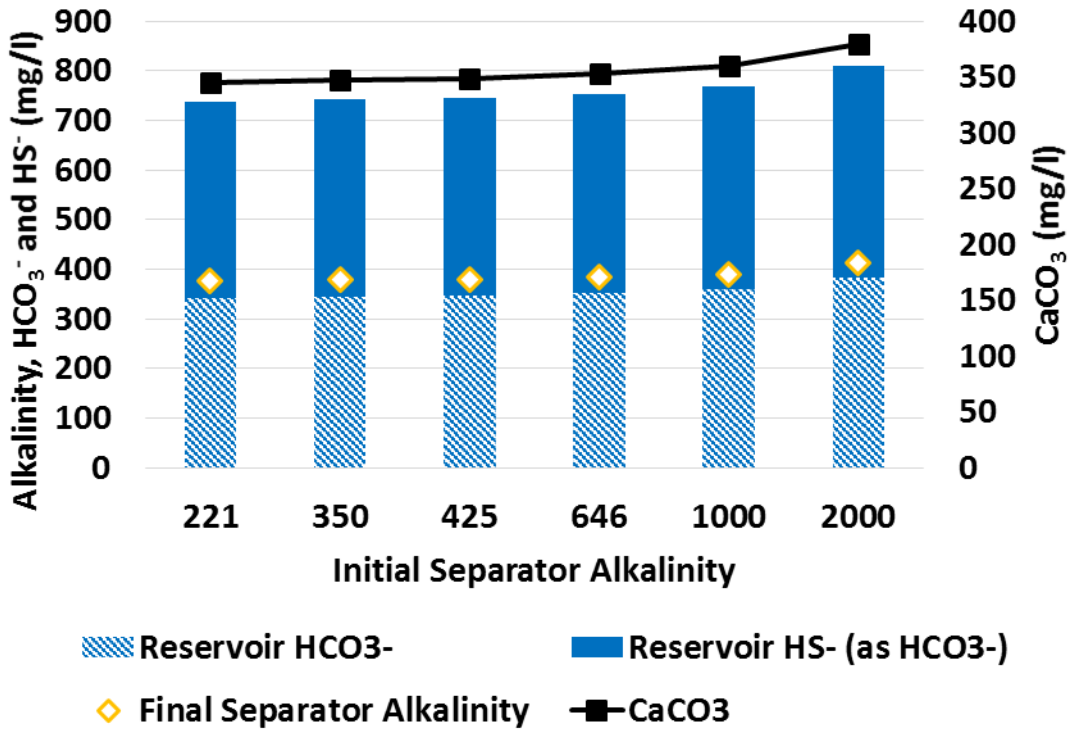

Figure 6.8: The impact of variable input HCO_3^- and HS^- on reservoir alkalinity and cumulative $CaCO_3$ precipitation.

If the reservoir water compositions is known instead of the separator water composition, the reservoir $CaCO_3$ equilibrium (SR=1) constrains the alkalinity to one unique value for a given reservoir Ca^{2+}, $CO_{2(g)}$ and $H_2S_{(g)}$ so this case is irrelevant for the error analysis.

As discussed above, calcium, pH, alkalinity, bicarbonates and bisulphides are strongly linked together and in thermodynamic equilibrium scenarios one cannot be changed without impacting the others. When the initial separator alkalinity is changed for a fixed initial separator Ca^{2+}, $CO_{2(g)}$ and $H_2S_{(g)}$ a different final Ca^{2+} concentration is obtained depending on the starting scenario (1, 2 or 3).

If the initial alkalinity is the one at equilibrium conditions, the initial and the final separator Ca^{2+} concentration will be the same. On the other hand, if the initial alkalinity is in the super saturated region the final separator Ca^{2+} concentration will be lower than the initial one to account for the $CaCO_3$ precipitation in the equilibration process (fluid recombination at reservoir conditions). Consequently, an initial alkalinity in the under saturated zone will produce a final separator Ca^{2+} concentration which is higher than the initial one because more Ca^{2+} can be stable in solution at those conditions (and so more $CaCO_3$ will dissolve in the reservoir equilibration process). The results are shown in Figure 6.9.

This connection between initial alkalinity and final Ca^{2+} provides a further constraint which limits the possible "true" results for a specific system's scale predictions.

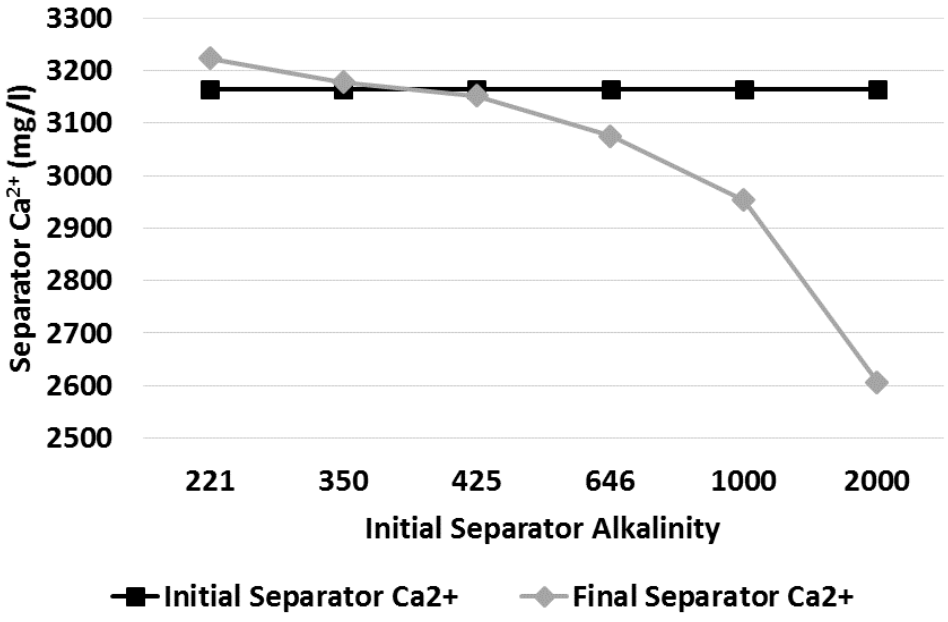

Figure 6.9: Variation between initial and final separator Ca^{2+} for different initial separator alkalinity.

6.2.4 Gas Phase CO_2 and H_2S

Gas phase CO_2 and H_2S concentrations are two of the most important field measurements for carbonate and sulphide scale predictions and they are fixed in these calculations. In other words, these two values are part of the "trusted" data input and the aqueous phase molecular CO_2 and H_2S are calculated based on the vapour/liquid equilibrium with the given gas phase concentrations (Verri et al., 2017a). However, in some scenarios these field measurements can be highly unreliable (or naturally very variable) and it is the aim of this study to understand what impact they can have on the final scale prediction profile.

If all H_2S is removed from the base case scenario, the impact of increasing CO_2 on the cumulative $CaCO_3$ precipitation at the separator can be calculated, as shown in Figure 6.10. The higher the CO_2 concentration, the higher the reservoir alkalinity (for which the main contributors are bicarbonates) and the more cumulative $CaCO_3$ precipitation is expected at the separator. This is true in reservoir containing carbonates where an increase in CO_2 causes a decrease in pH, more reservoir rock dissolution and ultimately increased reservoir alkalinity.

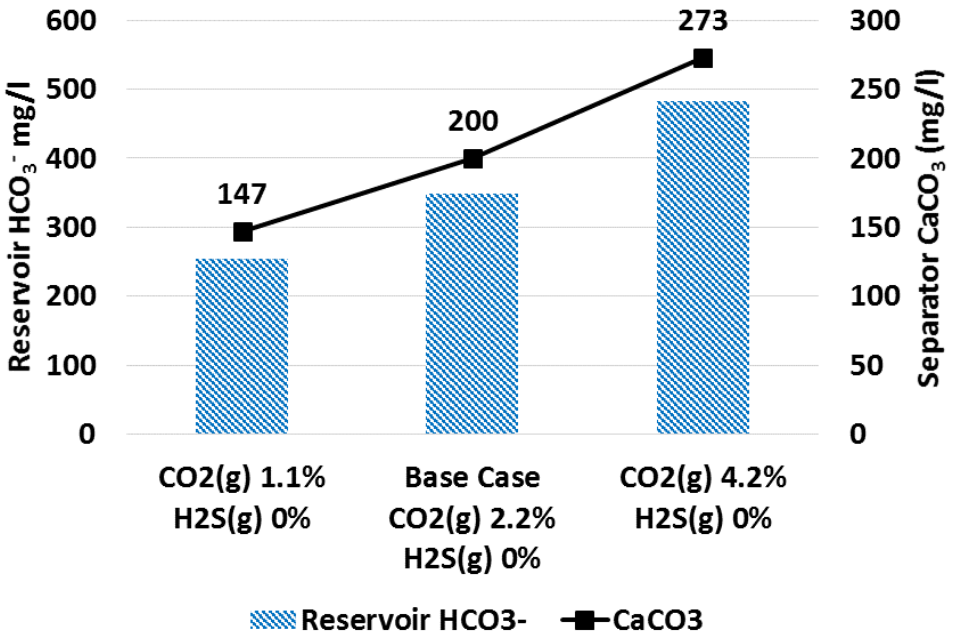

Figure 6.10: The impact of variable CO_2 concentration on the final scale predictions when H_2S is removed.

If the separator CO_2 concentration is fixed and the H_2S concentration varied, it can be seen that, as H_2S increases, the alkalinity also increases and so does the cumulative $CaCO_3$ precipitation at separator (Figure 6.11). Notice how the cumulative $CaCO_3$ precipitation at separator has increased >70% in the base case scenario when the original base case level of $H_2S_{(g)}$ concentration is added back.

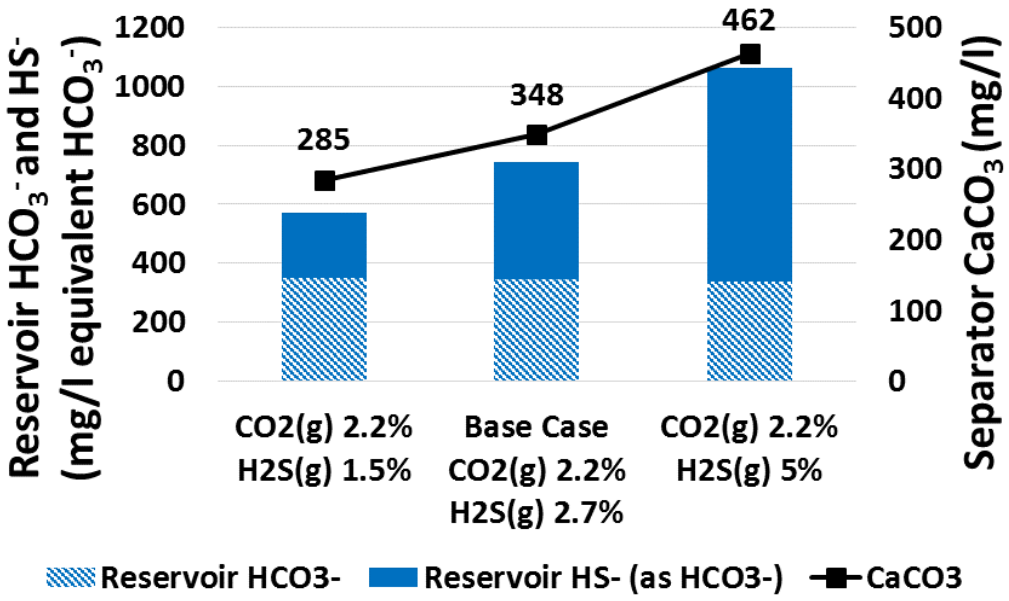

Figure 6.11: The impact of variable H_2S concentration on the final scale predictions for fixed $CO_{2(g)}$.

For higher H_2S concentrations, the alkalinity increases because the pH is almost unchanged and to maintain the dissociation equilibrium constant (Equation (6.14)) HS^- (the main contributor to alkalinity together with $HCO3^-$), must increase.

$$K_{a,1} = \frac{[HS^-] \times [H^+]}{[H_2S]} \tag{6.14}$$

The implications of these conclusions are important and have not yet been widely recognized or discussed in the literature. The presence and increase of H_2S in produced fluids has always been seen as a system integrity (corrosion) problem and a health and safety challenge, which it is of course. Associated FeS precipitation is also normally investigated when H_2S is present. However, it is clear that H_2S is relevant to $CaCO_3$ scale predictions because it affects reservoir alkalinity when carbonates are present. *In a souring reservoir containing carbonates, calcite scaling tendencies will become more severe (or appear for the first time) as H_2S increases because the reservoir produced brine alkalinity increases*. Moreover, *in a system containing H_2S, the study of carbonate*

scaling risk is incorrect unless the correct H_2S concentration is used in the scaling calculations.

The reality is that the input Ca^{2+} concentration is fixed but the final reservoir Ca^{2+} (in equilibrium with $CaCO_3$) changes when the $H_2S_{(g)}$ concentration is changed.

This higher Ca^{2+} and the increased alkalinity (caused by HS^-) produce the additional $CaCO_3$ precipitation in the wellbore. Again, in these calculations only one variable is changed in the data input but all these values are all connected and one cannot be changed without changing the other.

What happens when the H_2S concentration is fixed and the CO_2(g) concentration varies? This can be the case when the $CO_{2(g)}$ value is incorrect (or widely varying naturally) or in a sour field scenario where CO_2 water-alternating-gas (WAG) injection is being implemented. These findings are shown in Figure 6.12.

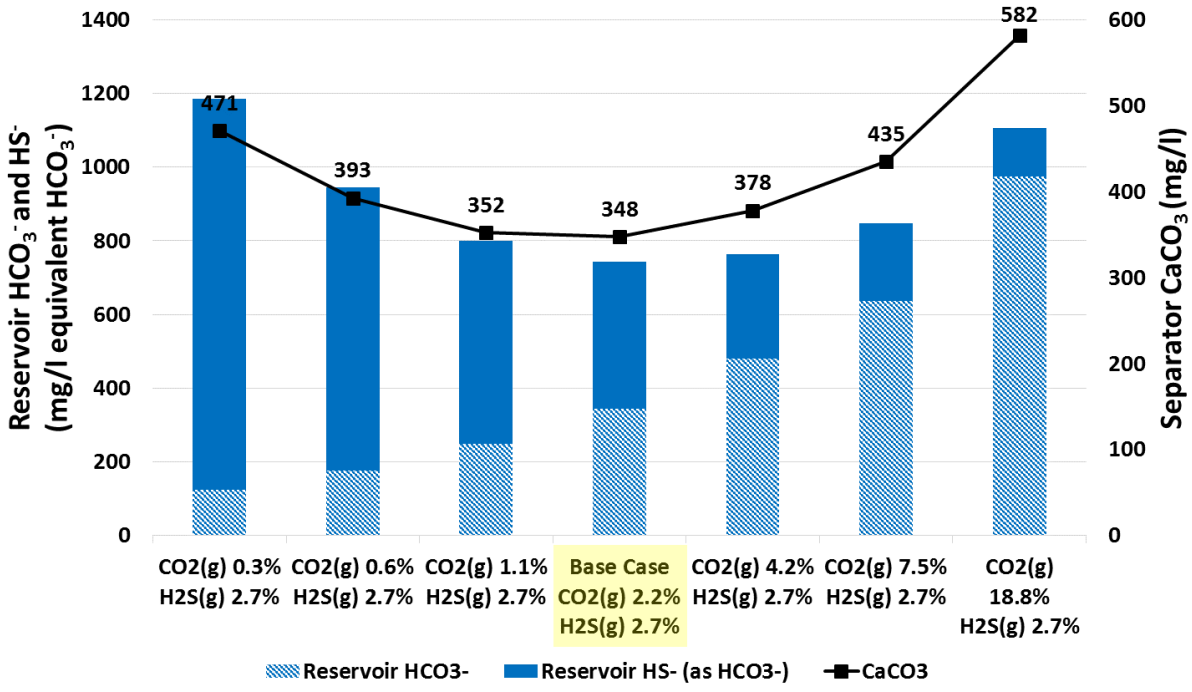

Figure 6.12: The impact of variable $CO_{2(g)}$ concentration on scale predictions for fixed $H_2S_{(g)}$.

If the H_2S gas concentration is fixed (at $H_2S_{(g)}$=2.7% mol) and the CO_2 concentration varied, there are two distinct and opposite effects on the water chemistry (where "→" denotes "leads to"):

1. Higher CO_2 → lower pH → more reservoir rock dissolution → more HCO_3^-→ higher alkalinity → more cumulative $CaCO_3$ precipitation at separator;

2. Higher CO_2 → lower pH → reduced HS^-/H_2S ratio → lower alkalinity → less cumulative $CaCO_3$ precipitation at separator.

Both effects occur in every scenario but effect 1 is predominant when $[HCO_3^-]/[HS^-]>1$ while effect 2 dominates the system when $[HCO_3^-]/[HS^-]<1$.

The selected example in Figure 6.12 shows that these results can be divided in two regions: for lower CO_2 concentration than the base case scenario (left of the base case scenario) effect 2 dominates whilst for higher CO_2 concentrations effect 1 is predominant.

These results clearly show that errors or natural variations in CO_2 levels have an impact on the final scale predictions, but that the net effect could be positive (less $CaCO_3$) or negative (more $CaCO_3$) depending on the [HCO3-]/[HS-] ratio.

In the given base case example, $CO_{2(g)}$ errors of ±50% have a small impact on the final cumulative $CaCO_3$ because we are at the "intersection" of effects 1 and 2 where $[HCO_3^-]/[HS^-]\approx1$. The further away from this intersection point, the more detrimental an error on $CO_{2(g)}$ is and the more important it becomes to have reliable field measurements.

Some of the key points that emerge from the above results can help minimise errors in pH dependent scale predictions:

- Accurate field sampling is required with particular focus on the gas phase composition (specifically CO_2 and H_2S) and the aqueous Ca^{2+} concentration;

- When H_2S is present in the system, it must always be included in the scale prediction modelling because it has a direct impact on $CaCO_3$ (not only on FeS);

- The sampling run at test separator should be done only when equilibrium conditions are reached;

- Previous publications show that a rigorous procedure is needed to use available field data and obtain the required software data input. Iteration calculations are also necessary to ensure the correct mass balance when non-integrated software packages are used;

- Tracking pH and alkalinity measurements can be a helpful tool to understand how far from saturation the system is. However, when looking only at thermodynamic calculations (no kinetics) and systems where reservoir fluids can be equilibrated with carbonates, pH and alkalinity are constrained at equilibrium conditions;

- Chapter 7 shows that PVT calculations play a key role in the final carbonate and sulphide scale predictions. For this reason, access to up-to-date PVT experimental data can significantly reduce scale prediction errors.

Nevertheless, due to the wide range of sources of errors, the methodical approach taken to investigate these errors informs the community that most models should be thought to create a range of probable outcomes, not a specific answer.

6.3 CONCLUSIONS

Carbonate and sulphide scales such as $CaCO_3$, $FeCO_3$ and FeS are pH dependent deposits and their formation is closely coupled together and impacted by a number of factors; this is already well known.

The main thrust of this Chapter is to examine the effects of measurement errors on the prediction of those scales.

A higher H_2S concentration always leads to an increase in alkalinity and an increase in cumulative $CaCO_3$ precipitation for reservoirs containing carbonate. Hence, in a souring reservoir, the carbonate scaling risk worsens. This also implies that if the effect of H_2S on carbonate scaling calculations is not taken into account, then all carbonate scale predictions may be unreliable.

Increasing the CO_2 concentration in the system in the presence of H_2S has *two opposing effects*. The first effect is that increasing CO_2 can cause more $CaCO_3$ precipitation due to increased HCO_3^- and alkalinity in the reservoir (when the fluids are equilibrated with calcite). The second effect is that increasing CO_2 may reduce the amount of deposited calcite in the presence of H_2S due to a shift in the $H_2S \leftrightarrow HS^-$ equilibrium towards H_2S which reduces reservoir alkalinity. Which of these two effects dominates depends on the $[HCO_3^-]/[HS^-]$ ratio in the specific system, which in turn depends on the CO_2/H_2S ratio.

For the examples presented, the following conclusions apply:

1. The three key measurements for reliable carbonate and sulphide scale predictions are Ca^{2+}, $CO_{2(g)}$ and $H_2S_{(g)}$.

2. Although the calcium ion concentration, [Ca^{2+}], can have a significant effect on the final amount of calcium carbonate precipitation, it is a fairly reliable field quantity to measure. Changing Ca^{2+} will also change the final alkalinity and pH thus constraining the possible "true" field measurements at equilibrium conditions.

3. There are three possible scenarios for the initial alkalinity value when the initial separator Ca^{2+}, $CO_{2(g)}$ and $H_2S_{(g)}$ are fixed: super saturation alkalinity, equilibrium alkalinity, under saturation alkalinity. Errors in the initial separator alkalinity have a negligible impact on the final scale prediction results because in the reservoir equilibration process, the recalculated alkalinities will all converge to the alkalinity equilibrium value. However, the final recalculated separator Ca^{2+} concentration will be different from the initial value and can be lower or higher depending on which of the three scenarios the initial alkalinity corresponds to.

Because of the difficulty of establishing the true solution Fe^{2+}, dissolved iron measurements can be best addressed using the concept of Maximum Dissolved Iron (MDI) described in a previous paper (Verri and Sorbie, 2017b).

This Chapter is based on a peer reviewed paper published in the course of this work (Ness and Sorbie, 2018a).

Chapter 7 - THE IMPACT OF SOFTWARE, EQUATIONS AND PARAMETERS CHOICE

7.1 INTRODUCTION

This Chapter presents the results of the impact of software, equations and parameters in previously discussed in Section 2.3.3 for some general scenarios (Ness and Sorbie, 2018b).

As mentioned previously, instead of trying the impossible task of decoupling each variable shown in Section 2.3.3, this work looks at the two properties that result from those variables and that allow us to compare different software in a clear and systematic manner: (a) volume and mole phase distribution and (b) CO_2 and H_2S partition coefficients.

The first part of this work (Paragraph 7.2) looks at the variability of CO_2 and H_2S partition coefficients in the following scenarios:

- Variable oil API and GOR (fixed software and EOS)
- Variable water cut and CO_2 concentration (fixed oil, software and EOS)
- Variable EOS (fixed oil)

The software used for this study are: Winprop (PVT only), HWPVT (Heriot-Watt version of the software HydraFlash, PVT only) and ScaleChem (integrated PVT + scale prediction). The scenarios we investigated are for generic oils and not from field examples. For this reason, the PVT model used was not tuned to match experimental data but was applied using the built in parameters for each software in order to show the differences in output which can be obtained.

The second part of this work (Paragraph 7.3) looks at the impact of partition coefficient variability on the final carbonate scale predictions which in all scenarios are calculated using ScaleChem aqueous phase model (by applying the Heriot-Watt scale prediction workflow described in Chapter 3). This study is not a "black box" software comparison exercise since it clearly demonstrates the connection between the aqueous and hydrocarbon phase thermodynamics, the scaling system and the final results.

Finally, one scenario is chosen to look at the impact that changing aqueous phase model (whilst keeping the same PVT results) has on carbonate scale predictions (Paragraph 7.4). The software used for this comparative analysis are ScaleChem, Multiscale and the in-house Heriot-Watt Scale predictions code (Silva, 2017).

7.2 VARIABILITY OF CO_2 AND H_2S PARTITION COEFFICIENTS

7.2.1 Partition Coefficients for Variable Oil API and GOR

The composition and properties of the 4 chosen oils are shown in Table 7.1 where GOR and API are taken from HWPVT sCPA PVT results.

Total Feed (mol%)	**Oil A**	**Oil B**	**Oil C**	**Oil D**
CH_4	28	49	52	48.2
CO_2	0.8	0.8	0.8	0.8
H_2S	0.6	0.6	0.6	0.6
C8	-	-	-	30.4
C16	5.6	1.6	1.6	-
C17	-	-	25	-
C22	15	28	-	-
C30	30	-	-	-
H_2O	20	20	20	20
GOR (scf/bbl)	204	670	970	1445
API	14	28	39	65
Water Cut (%)	1.8	3.3	4.5	7.2
$CO_{2(g)}$ @ std T and p	2.6%	1.6%	1.4%	1.6%
$H_2S_{(g)}$ @ std T and p	1.7%	1.1%	1.0%	1.1%

Table 7.1: Compositions and properties of 4 selected oils.

The results for K_{OW} (CO_2), K_{GW} (CO_2), K_{OW} (H2S) and K_{GW} (H_2S) for oil A, B, C and D at standard conditions (T=15.6°C and p=1 bar) obtained with HWPVT sCPA are shown in Figure 7.1.

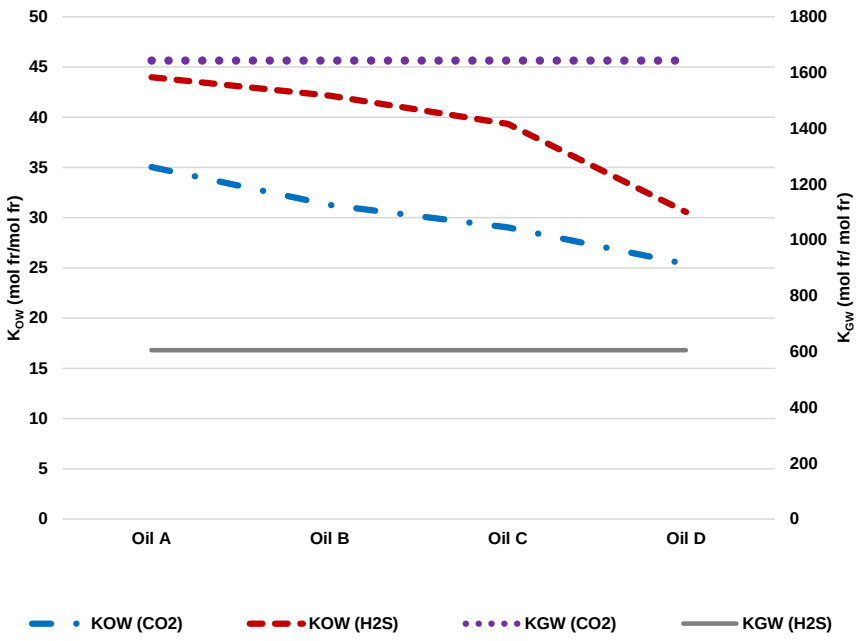

Figure 7.1: CO_2 and H_2S partition coefficients for Oil A, B, C and D at standard conditions.

From these results it is possible to draw the following conclusions:

- K_{GW} is clearly independent of the oil type because only the gas/water solubility of CO_2 and H_2S is considered in this parameter.

- K_{OW} decreases as the oil density decreases because less CO_2 and H_2S are soluble in lighter oils.

- K_{GW} (CO_2) >> K_{GW} (H_2S) which means that for a fixed gas phase concentration, H_2S is more soluble in water than CO_2.

- K_{OW} (H_2S) > K_{OW} (CO_2) because H_2S tends to partition into the oil more than CO_2.

7.2.2 Partition Coefficients for Variable Water Cut and CO_2 Concentration

The impact of variable water cut (from 1.8% to 50%) and CO_2 concentration (from 2.6% to 7.5%) on the CO_2 and H_2S partition coefficients using HWPVT sCPA and Winprop at variable temperature and pressure (T and p) was tested on *Oil A*. The results show that the variation in partition coefficients caused by a change in H_2O and CO_2 composition (and consequently in H_2S) is negligible and confirmed that K_{OW} and K_{GW} are mainly dependent on temperature and pressure.

An example in shown in Figure 7.2 for K_{OW} (CO_2) at 100 bar but the same overlapping results were obtained for K_{GW} (CO_2), K_{OW} (H_2S) and K_{GW} (H_2S) at 10, 50, 200 and 300 bar.

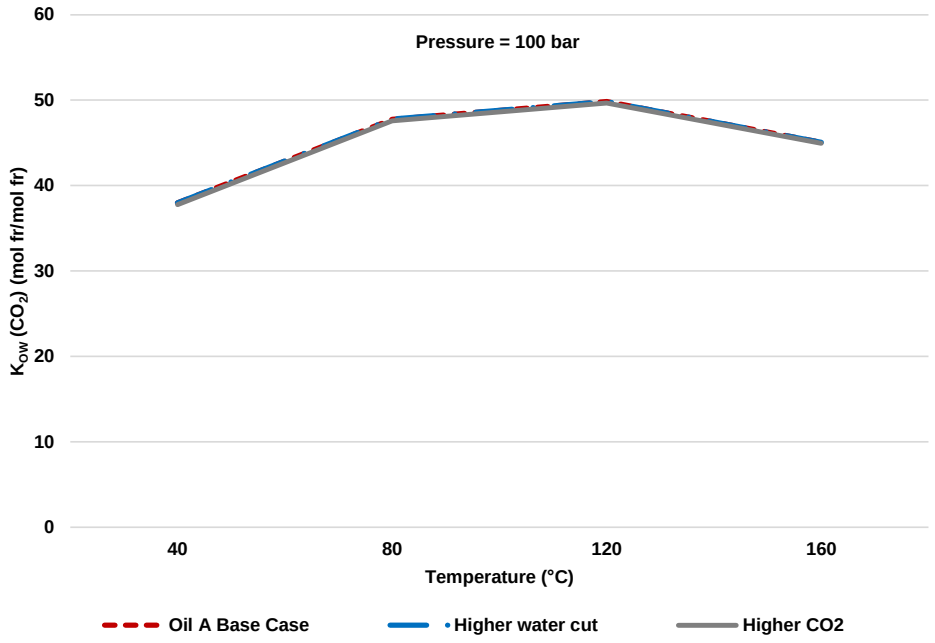

Figure 7.2: K_{OW} (CO_2) at 100 bar and variable temperature for Oil A, higher water cut scenario and higher CO_2 scenario.

7.2.3 Partition Coefficients for Variable Software and EOS

Oil B was selected to test the impact of variable software and EOS choice on the CO_2 and H_2S partition coefficients for temperatures between T = 40-160°C and pressure, p = 10-300 bar.

For this purpose each scenario was run using: HWPVT sCPA, HWPVT SRK, HWPVT PR, Winprop PR and ScaleChem (modified SRK, built in fixed EOS).

As mentioned previously, the scenarios investigated are for generic oils and not for field oil examples. For this reason the PVT models used were not tuned to match experimental data but the calculated partition coefficients are a direct result of the built in parameters for each software. The results for K_{OW} (CO_2), K_{GW} (CO_2), K_{OW} (H_2S) and K_{GW} (H_2S) are shown in Appendix 1 (Section 7.6). There is a significant discrepancy between the partition coefficients calculated using the different software packages and EOS models, and it is possible to make a few observations at this stage:

- Both K_{OW} and K_{GW} decrease as pressure increases because at higher pressure more CO_2 and H_2S partition into the water phase;

- K_{OW} (CO_2) increases with temperature up to a certain point and then it slightly decrease as temperature increases further;

- The opposite behaviour is observed for K_{OW} (H_2S) which remains almost constant or decreases as temperature increases;

- K_{GW} increase significantly with temperature at low pressure but does not change much at higher pressure (sometimes a gas phase is not predicted by the EOS to be present at higher pressure and we therefore cannot calculate K_{GW});

- The difference between calculated partition coefficients is significant not only when using different EOS models but also when using the same EOS in different software (see HWPVT PR and Winprop PR). This is because there are properties and parameters (i.e. critical T and p, binary interaction coefficients etc.) which can differ from one software to another and lead to different final partition coefficients. Full PVT software suites generally allow these parameters to be adjusted and this is normally done through data regression by matching PVT experimental data. However, this initial analysis is a straightforward comparison between software which uses built in values whilst field examples are shown in Chapter 4 and Chapter 5. These results obtained using different software do not mean that one answer is "wrong" and one is "right" but rather that they are both correctly calculated based on the given and built in data (which may, on the other hand, be more or less reliable).

It is difficult to clearly visualise and understand the range of values for partition coefficients at different conditions by simply looking at the graphs in Appendix 1 (Section 7.6). Therefore, to better show the variability of K_{OW} (CO_2), K_{GW} (CO_2), K_{OW} (H_2S) and K_{GW} (H_2S) for Oil B in the selected temperature and pressure range, it is possible to identify the minimum and maximum values for each partition coefficient and plot them against the corresponding T and p value as shown in Figure 7.3 through Figure 7.6. For some temperature and pressure combinations, two of the software used predict that a gas phase is not present and for this reason the values for K_{GW} (CO_2) and K_{GW} (H_2S) are missing in the graph.

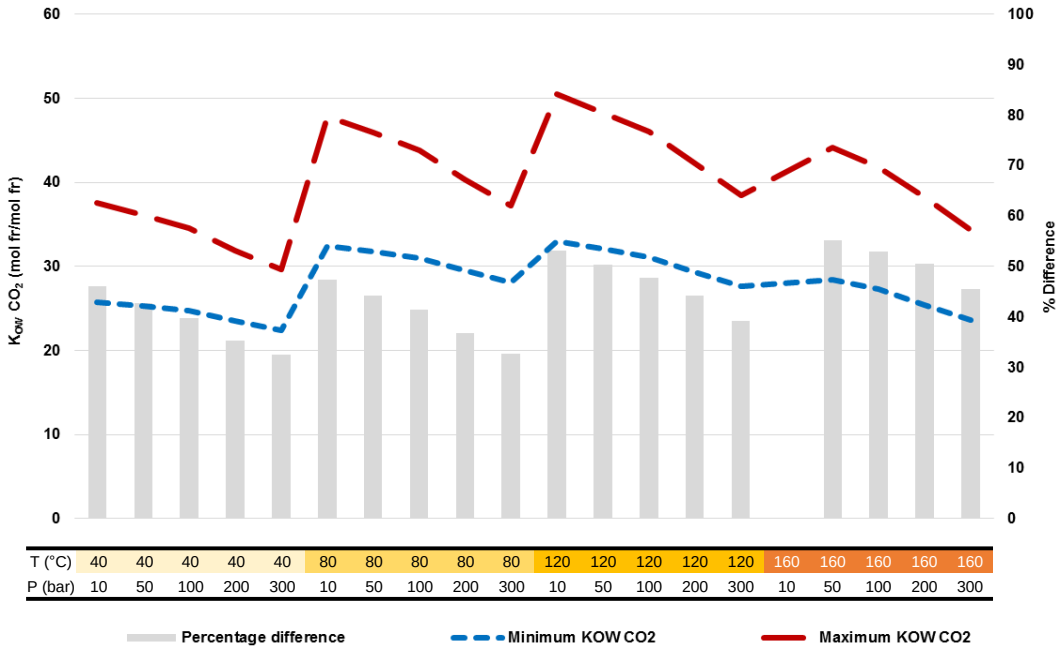

Figure 7.3: Minimum and maximum K_{OW} (CO_2) for oil B when comparing results from HWPVT, Winprop and ScaleChem.

- K_{OW} (CO_2) variability (Figure 7.3) ranges from 33% (at 300 bar and 40°C) to 55% (at 50 bar and 160°C) of the minimum value.

- The largest difference between minimum and maximum value is at lower pressure. However, notice that the *maximum* difference for K_{OW} (CO_2) is only slightly higher than the *minimum* difference for K_{OW} (H_2S) (Figure 7.5) clearly showing that there is a far bigger discrepancy for H_2S than CO_2.

- The difference decreases as pressure increases.

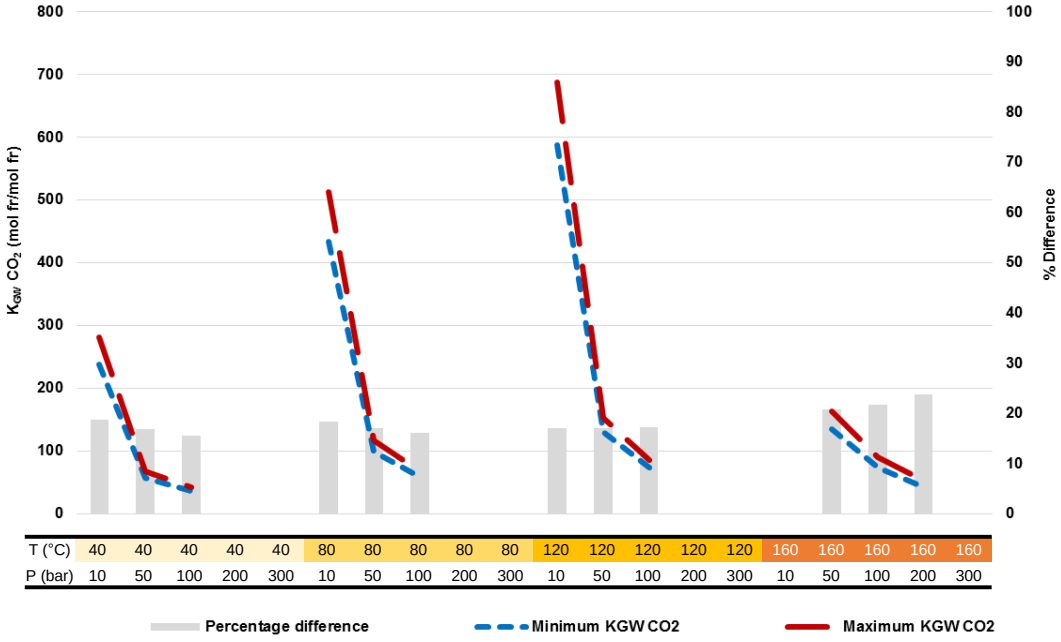

Figure 7.4: Minimum and maximum K_{GW} (CO_2) for oil B when comparing results from HWPVT, Winprop and ScaleChem.

- K_{GW} (CO_2) variability (Figure 7.4) is relatively small and ranges from 16% (at 100 bar and 40°C) to 24% (at 200 bar and 160°C) of the minimum value.

- Good quality experimental CO_2 gas/water solubility data is widely available and for this reason it is likely that all chosen software packages have a good database. Hence, the small discrepancy between minimum and maximum values.

- Gas is not present at higher pressures for some cases which is the reason for the missing values.

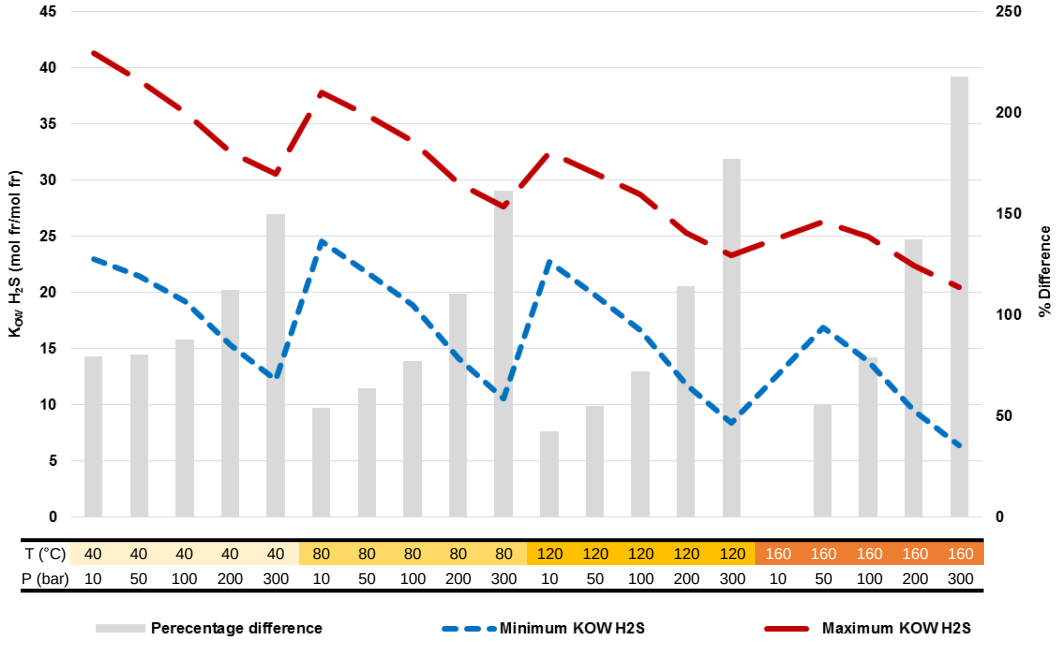

Figure 7.5: Minimum and maximum K_{OW} (H_2S) for oil B when comparing results from HWPVT, Winprop and ScaleChem.

- K_{OW} (H_2S) variability (Figure 7.5) ranges from 43% (at 10 bar and 120°C) to 218% (at 300 bar and 160°C) of the minimum value.

- The largest difference between minimum and maximum value is at higher pressure. There may be other explanations for this large discrepancy but the experimental database for H_2S solubility, particularly at high pressure is limited and this may play an important role in these results.

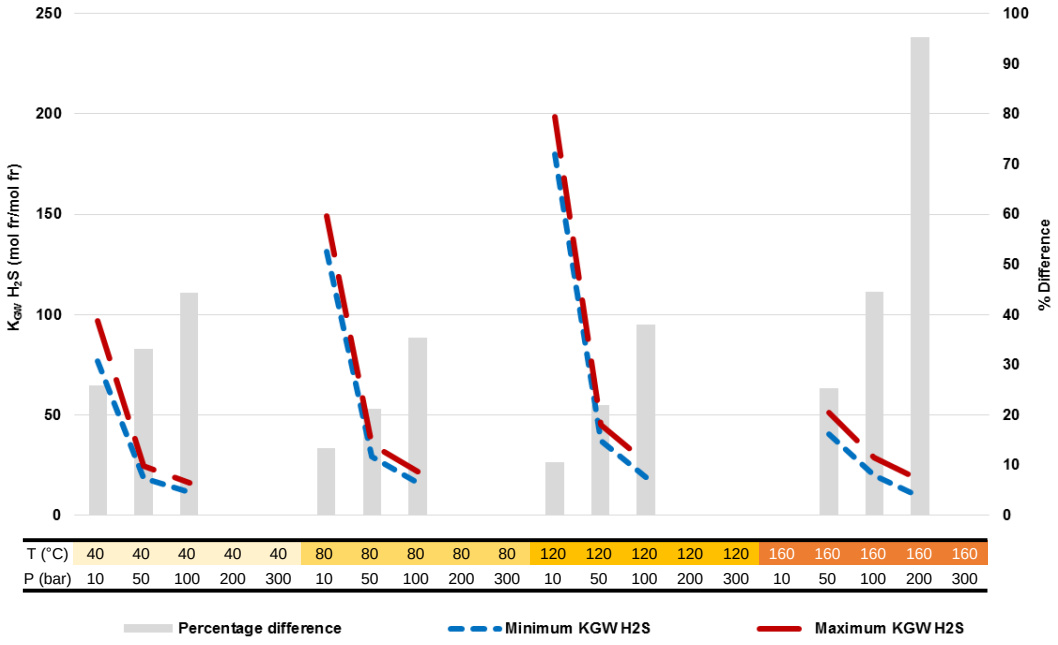

Figure 7.6: Minimum and maximum K_{GW} (H_2S) for oil B when comparing results from HWPVT, Winprop and ScaleChem.

- K_{GW} (H_2S) variability (Figure 7.6) ranges from 10% (at 10 bar and 120°C) to 95% (at 200 bar and 160°C) of the minimum value.

- The biggest difference between minimum and maximum value is at higher pressure as for K_{OW} (H_2S).

Now that the range of values for K_{OW} (CO_2), K_{GW} (CO_2), K_{OW} (H_2S) and K_{GW} (H_2S) is established for oil B at the selected T and p using the chosen software and EOS, the question is: what impact does this variability have on the final pH dependent scale predictions?

7.3 IMPACT OF PARTITION COEFFICIENTS ON CARBONATE SCALE PREDICTIONS

To test the impact of the variability of partition coefficients on carbonate scale predictions, one of the scenarios investigated for oil B was chosen: 120°C and 200 bar

for reservoir conditions and 80°C and 10 bar for topside conditions. The fluids are equilibrated with carbonate rock at reservoir conditions and using the HWU workflow (Chapter 3) the scaling potential at selected topside conditions was calculated.

The scale prediction model (aqueous phase model) used for these calculations is ScaleChem. The reservoir Ca^{2+} = 2,000 mg/l and the mole and volume phase distribution is taken from Winprop PR for all scenarios. Since Winprop predicts a gas phase to be present at reservoir conditions, a gas phase is always included in the reservoir.

There are two extreme scenarios for each T and p set:

- The first one is when minimum values for all partition coefficients K_{OW} (CO_2), K_{GW} (CO_2), K_{OW} (H_2S) and K_{GW} (H_2S) are used. This scenario gives the maximum water phase concentration of CO_2 and H_2S;

- The second scenario is when maximum values for all partition coefficients are used obtaining the lowest possible aqueous phase concentration of CO_2 and H_2S.

All other scenarios obtained varying only one partition coefficient at a time fall between these two extremes and they are not discussed here. Data for the two reservoir and topside scenarios is shown in Table 7.2.

	Reservoir Minimum	*Reservoir Maximum*	*Separator Minimum*	*Separator Maximum*
K_{OW} (CO_2)	29	42	32	48
K_{GW} (CO_2)	44	50	433	513
K_{OW} (H_2S)	12	25	25	38
K_{GW} (H_2S)	10	17	131	149
$CO_{2\,(aq)}$ (mg/l)	650	506	80	68
$H_2S_{\,(aq)}$ (mg/l)	1123	560	138	117
HCO_3^- (mg/l)	97	85	72	66
HS^- (mg/l)	136	77	52	48

Table 7.2: Partition coefficients and concentration of soluble carbonates and sulphides for reservoir and separator minimum and maximum scenarios.

There are 4 possible scenarios for scale prediction calculations:

1. "Reservoir minimum" conditions + "Separator minimum" conditions
2. "Reservoir minimum" conditions + "Separator maximum" conditions
3. "Reservoir maximum" conditions + "Separator minimum" conditions
4. "Reservoir maximum" conditions + "Separator maximum" conditions

This is shown schematically in Figure 7.7.

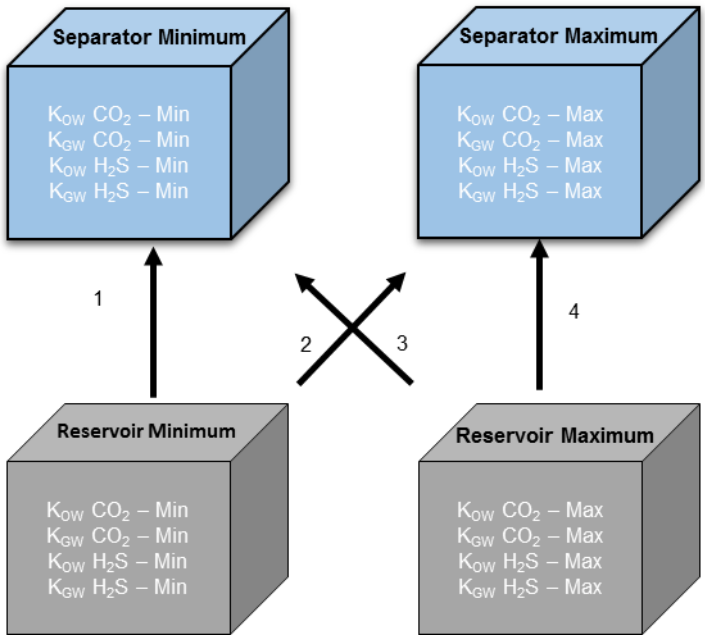

Figure 7.7: The 4 scale prediction scenarios investigated.

The results for all 4 scenarios are presented in Figure 7.8.

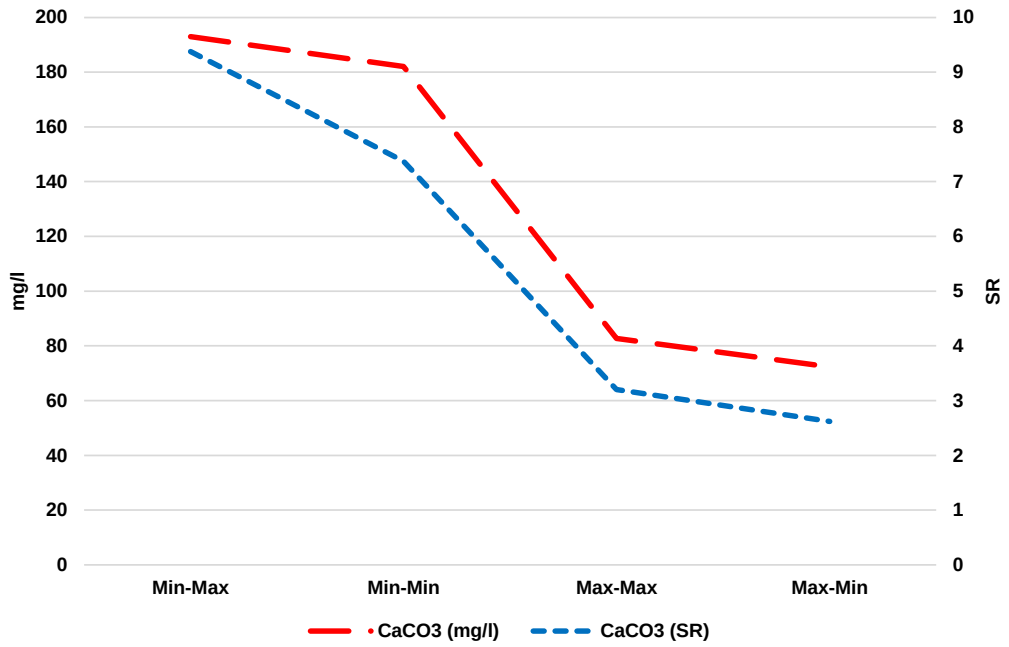

Figure 7.8: Scale prediction results for the 4 scenarios at topside conditions ($CaCO_3$ mass and saturation ratio).

It is clear how the variability of partition coefficients (caused by software, EOS and choice of parameters) has a major impact on the final carbonate scale prediction results.

In this scenario for Oil B at the given reservoir and topside T and p, using the same aqueous phase model (ScaleChem) the choice of PVT model (software, EOS and parameters) will dictate whether a mild or severe scale problem is predicted.

The worst scaling scenario is not surprisingly the one where the maximum concentration of $CO_{2(aq)}$ and $H_2S_{(aq)}$ is present in the reservoir (reservoir minimum) and the minimum concentration of $CO_{2(aq)}$ and $H_2S_{(aq)}$ is present at separator (separator maximum). This is because the release of CO_2 and H_2S to the gas phase is driving this carbonate scaling process and it is maximum in these conditions.

These results are very significant and clearly show:

- The importance of correctly understanding PVT calculations in the prediction of pH dependent scales;

- The impact of different PVT models on the final scale prediction results. In this scenario the same aqueous phase model was used but results obtained were completely different because of the PVT calculations (all included in the partition coefficients);

- The importance of being able to decouple PVT and aqueous phase models as showed in the HWU Workflow (Chapter 3) to test the impact of each model individually;

- The great value that accurate measurements of CO_2 and H_2S three phase distribution on actual field samples would have on the reliability of scale prediction.

The above results were obtained by independently changing CO_2 and H_2S partition coefficients and fixing the volumetrics from Winprop. The impact of PVT calculations for each individual software can be shown by using the corresponding partition coefficients and volumetrics, apply the HWU scale prediction workflow and use ScaleChem for the aqueous phase calculations. The results for these calculations are shown in Figure 7.9 for Winprop PR, ScaleChem and HWPVT sCPA and the conclusions above still apply.

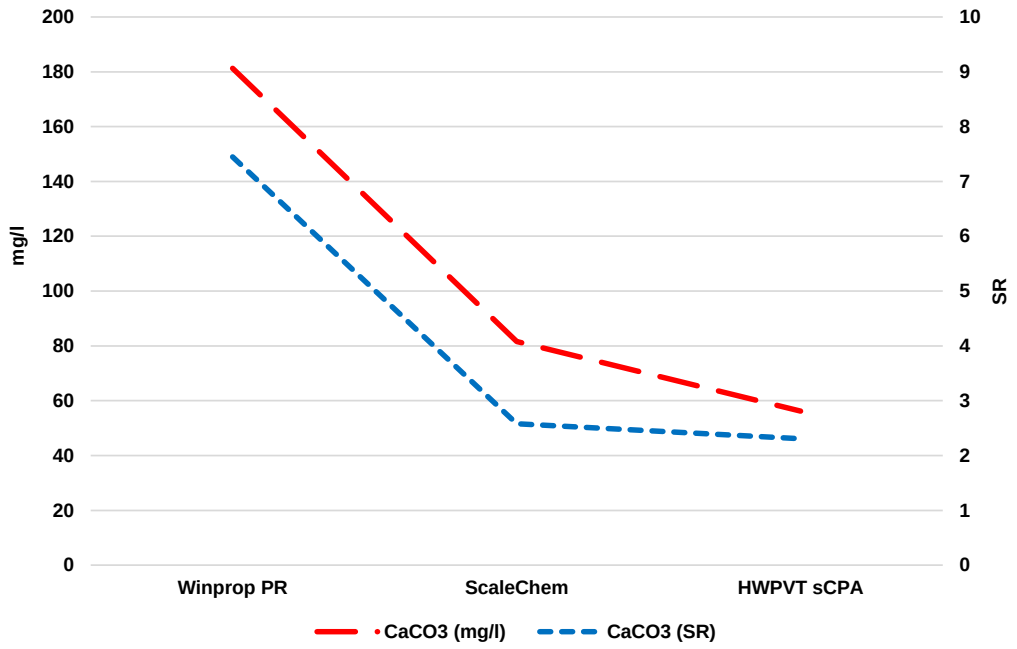

Figure 7.9: Scale prediction results for partition coefficients and volumetrics from Winprop PR, ScaleChem and HWPVT sCPA.

7.4 IMPACT OF VARIABLE AQUEOUS PHASE MODELS ON CARBONATE SCALE PREDICTIONS

The results shown in previous paragraphs highlight the significant impact of PVT on final scale predictions and how the choice of PVT software and EOS is key in determining the correct scaling tendencies.

To demonstrate that PVT calculations are the main contributor to differences in pH dependent scale predictions when using different software, this work also presents a comparison between predicted carbonate scaling tendencies for a fixed aqueous phase system (no gas or oil present) obtained using different aqueous phase models. The software used for this comparative analysis are ScaleChem, Multiscale and the in-house Heriot-Watt Scale predictions code (Silva, 2017).

The case selected for comparing different aqueous phase models is shown in Table 7.3 and is similar to the "Separator minimum" scenario in Table 7.2. However, since the conditions shown in Table 7.2 are for the equilibrated water at given T and p, in these calculations the concentration of bicarbonates and bisulphides was increased to obtain a supersaturated solution. This is necessary because here gas and oil phase are not present (aqueous phase only) and this is not an auto-scaling process (due to depressurization and repartitioning of CO_2 and H_2S in the oil and gas phase) like the one shown for reservoir to separator calculations.

Finally, different software require a different set of data input or use different variables to initiate the simulation. This information is shown in Table 7.3.

	Separator T	**Separator p**	**Initial Ca^{2+}**	**Initial CO_2**	**Initial H_2S**	**Initial HCO_3^-**	**Initial HS^-**
	°C	bar	ppm	ppm	ppm	ppm	ppm
ScaleChem	80	10	2000	80	130	150	100
HWU	80	10	2000	80	130	150	100
Multiscale	80	10	2000	-	-	-	-
	Initial Carbonates (as CO_2)	**Initial Sulphides (as H_2S)**	**Initial pH**	**Initial alkalinity (as HCO_3^-)**	**Type of calculation**		
	ppm	ppm		ppm			
ScaleChem	-	-	-	-	Concentration only		
HWU	-	-	7	-	Automatic		
Multiscale	188	233	-	335	Concentrations aqueous phase		

Table 7.3: Data input for ScaleChem, HWU model & Multiscale for aqueous model comparison.

The results obtained with each software are shown in Table 7.4.

	Final Ca^{2+}	Final CO_2	Final H_2S	Final HCO_3^-	Final HS^-	Final pH	$CaCO_3$ mass	$CaCO_3$ SR
	ppm	ppm	ppm	ppm	ppm		mg/l	
ScaleChem	1951	81	165	76	65	6.0	103	3.3
HWU	1956	82	166	81	65	5.9	110	3.7
Multiscale	1960	82	168	81	64	6.0	111	3.6
ScaleChem vs HWU	0.2%	0.8%	0.5%	6.1%	0.1%	2.7%	7.2%	11.1%
Multiscale vs HWU	0.2%	0.1%	0.9%	0.2%	0.7%	2.6%	0.6%	1.4%
Multiscale vs ScaleChem	0.4%	0.9%	1.4%	5.9%	0.8%	0.0%	7.3%	8.7%

Table 7.4: Final aqueous phase chemistry and absolute error % between the results obtained using the selected aqueous phase models.

The Heriot-Watt scale prediction model was optimised against Multiscale and not surprisingly the results obtained with these two aqueous phase models match particularly well.

The larger difference between results obtained with ScaleChem and HWU and Multiscale are possibly due to the fact that ScaleChem includes additional species in the calculations such as $CaHCO_3^+$ which will impact the final equilibrium values.

Nevertheless, all the results shown in Table 7.4 are in very good agreement and the discrepancy in calcium carbonate scale predictions is minimal. Most importantly, these values show that using different aqueous phase models has a relatively minor impact on calcium carbonate scale predictions compared to the effect of variable PVT models.

This aqueous phase model comparison was run using other temperature, pressure and concentration scenarios with difference in predicted $CaCO_3$ mass between 5% and 20%, consistently lower than the errors obtained with variable PVT software.

It is important to note that the results discussed in Section 4.3.5 show how different scale prediction software implement significantly different iron sulphide (mackinawite) solubility product, indicating that the choice of aqueous phase software plays an important role in iron sulphide scale predictions (unlike for calcium carbonate).

7.5 CONCLUSIONS

The variability of partition coefficients was investigated for different scenarios and some of the key findings are listed here:

- K_{GW} is independent of oil type (GOR and API).

- K_{OW} decreases as the oil density decreases because less CO_2 and H_2S are soluble in lighter oils.

- K_{GW} (CO_2) >> K_{GW} (H_2S) which means that for a fixed gas phase concentration, H_2S is more soluble in water than CO_2.

- K_{OW} (H_2S) > K_{OW} (CO_2) because H_2S tends to partition in oil more than CO_2.

- CO_2 and H_2S partition coefficients are mainly dependent on temperature and pressure and the compositional change (water cut, CO_2 and H_2S content) has a negligible impact on these values.

- Different software which use the same equation of state give different partition coefficient results because of other parameters which may be different (e.g. binary interaction coefficients).

The partition coefficient variability for Oil B using HWPVT, Winprop and ScaleChem ranges from 15% to 55% of the minimum value for CO_2 and is significantly greater for H_2S (10% to 218% of the minimum value). The large discrepancy between H_2S partition coefficients using different models is likely to be caused by the limited experimental solubility database available.

This partition coefficient variability has a significant impact on the final carbonate scale predictions which, in the example presented, can vary as much as 200% (mass of $CaCO_3$ predicted to precipitate) even when using the same aqueous phase model. Hence, a reliable PVT model which gives accurate CO_2 and H_2S partitioning results in the relevant temperature and pressure range is fundamental to obtain correct scale predictions. These results highlight the great value that real field data for CO_2 and H_2S partitioning can have, since this data would allow us to eliminate the great uncertainty which results from PVT calculations.

Finally, a comparison between different aqueous phase models (ScaleChem, Multiscale and the HWU scale prediction model) shows that although the predicted $CaCO_3$ scaling potential can be slightly different, these differences are minor compared the impact of variable PVT software. This reinforces the conclusion that reliable PVT calculations are fundamental to obtain accurate and reliable scale predictions.

7.6 APPENDIX 1

Figure 7.10 through Figure 7.13 show the results for K_{OW} (CO_2), K_{GW} (CO_2), K_{OW} (H_2S) and K_{GW} (H_2S) obtained using different software (HWPVT, Winprop and ScaleChem) and EOS (sCPA, SRK and PR).

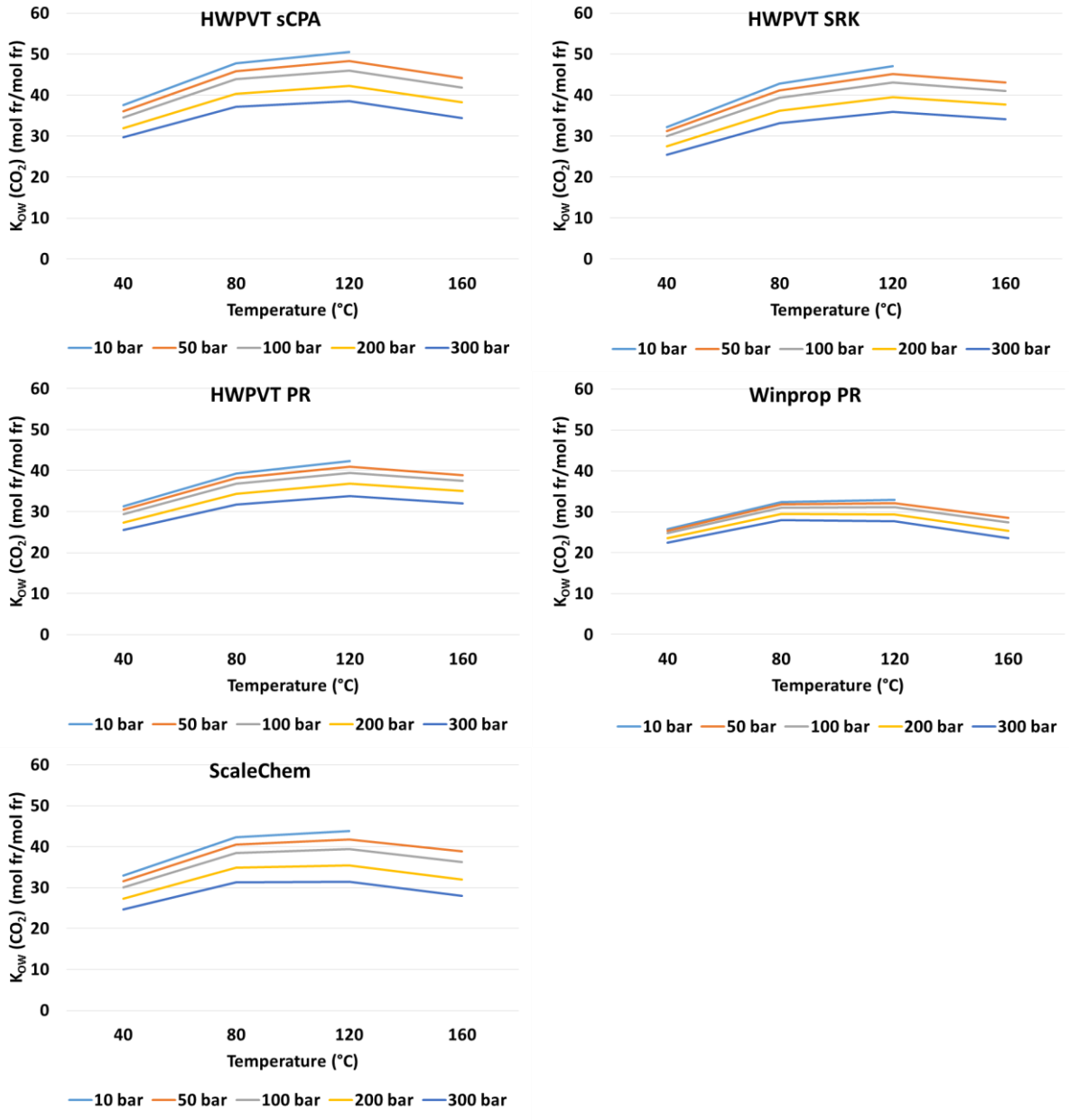

Figure 7.10: Oil/water CO_2 partition coefficient for Oil B calculated at variable temperature and pressure using different PVT software and EOS.

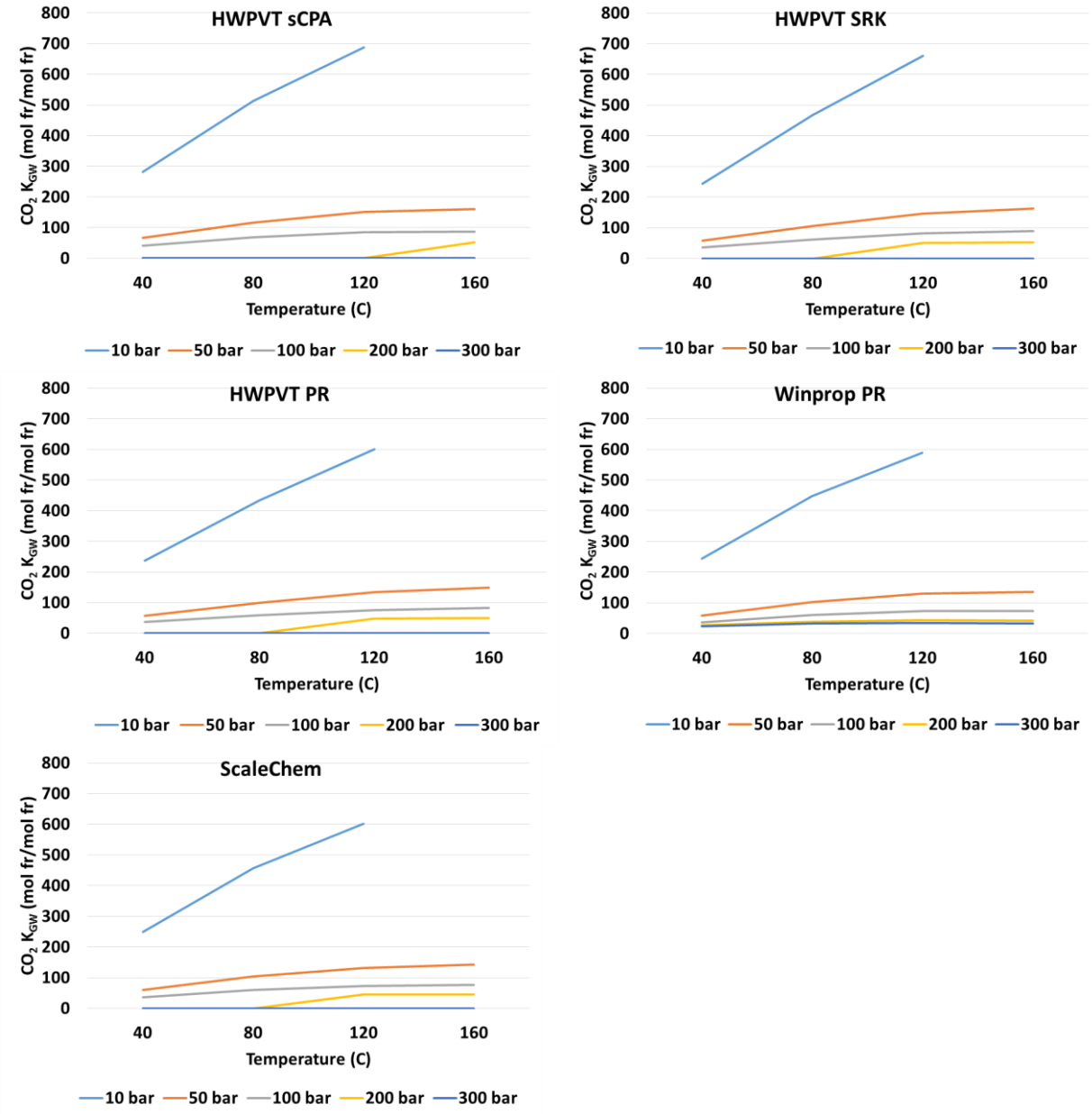

Figure 7.11: Gas/water CO_2 partition coefficient for Oil B calculated at variable temperature and pressure using different PVT software and EOS.

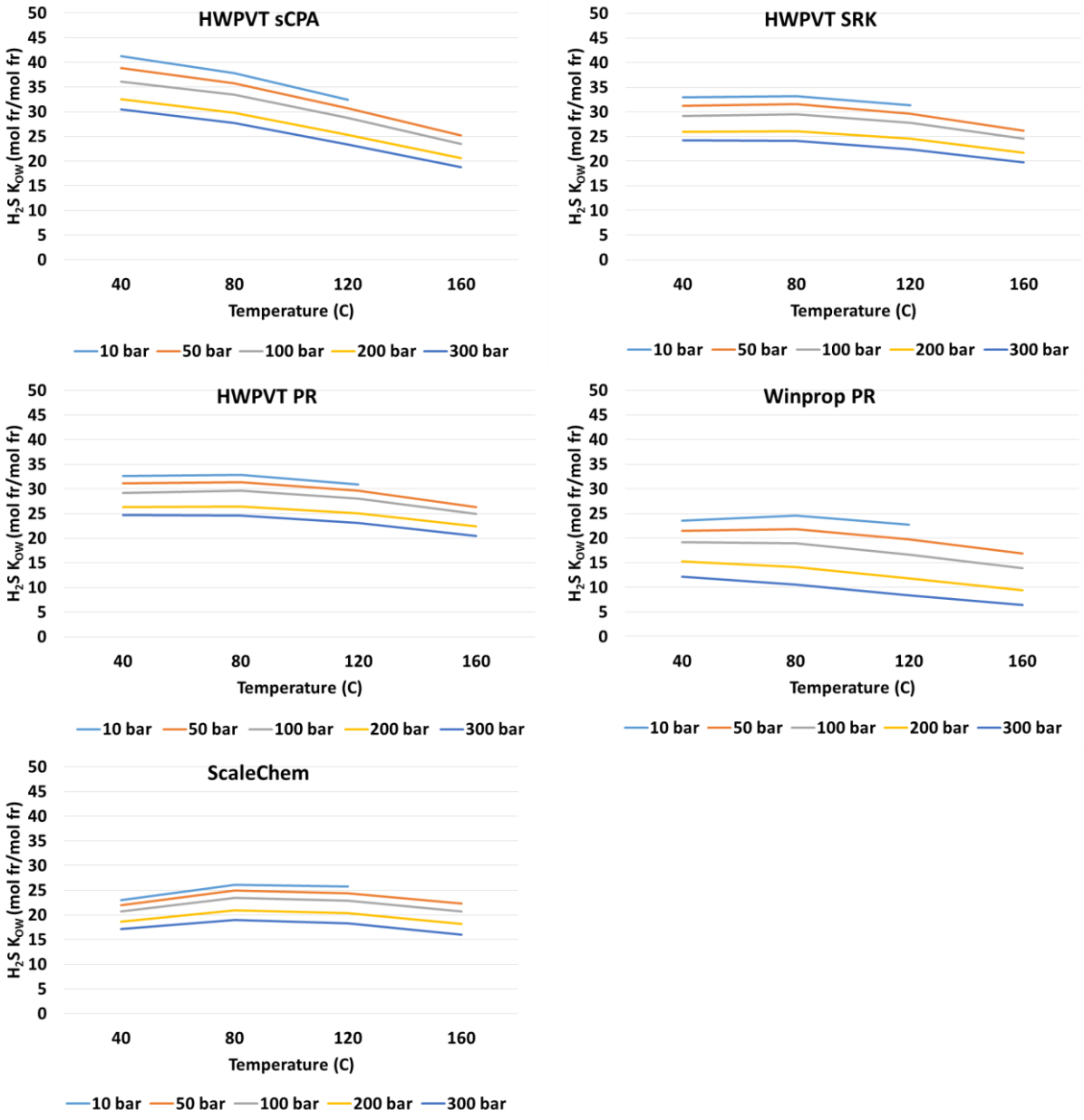

Figure 7.12: Oil/water H_2S partition coefficient for Oil B calculated at variable temperature and pressure using different PVT software and EOS.

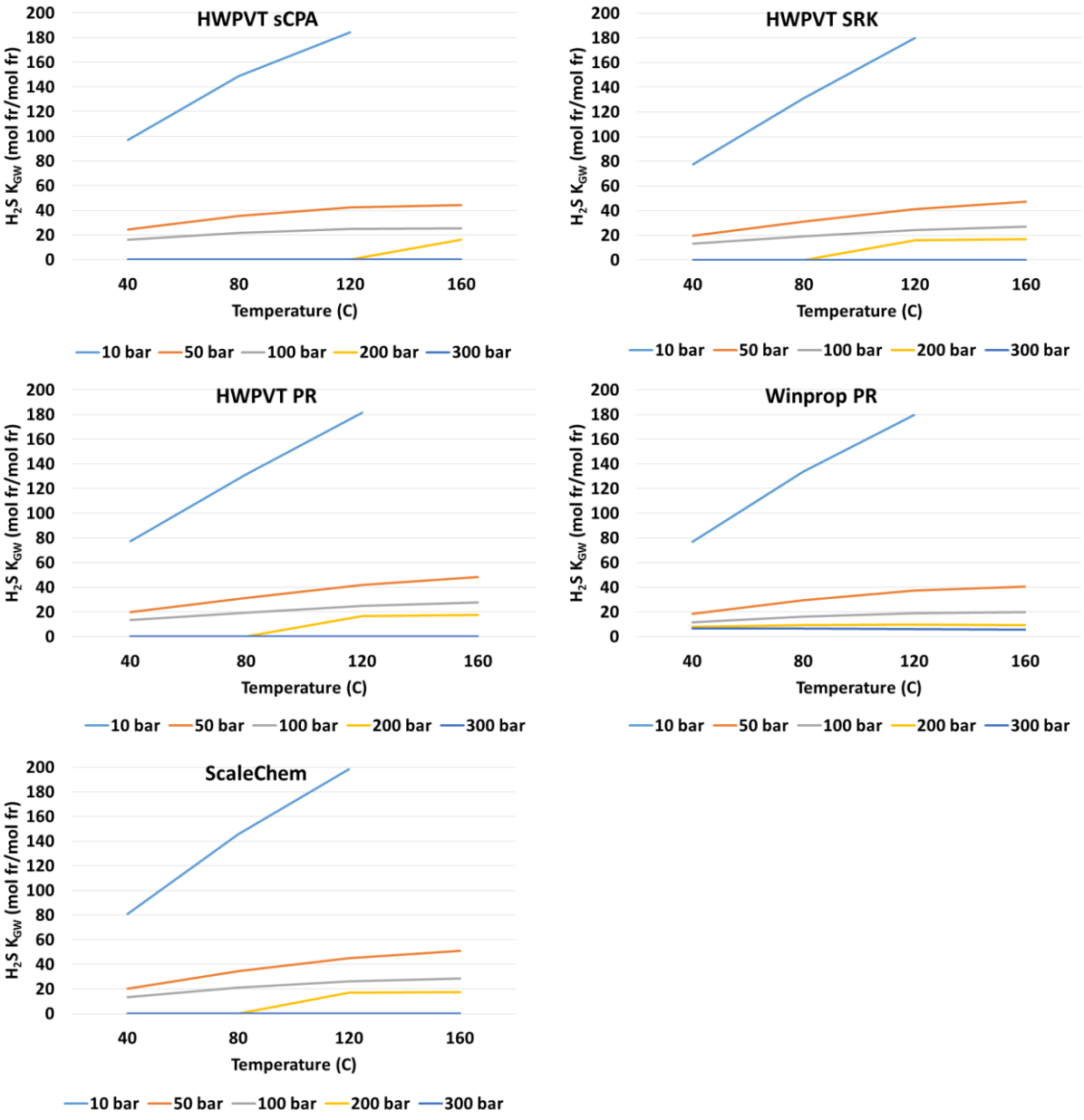

Figure 7.13: Gas/water H_2S partition coefficient for Oil B calculated at variable temperature and pressure using different PVT software and EOS.

Chapter 8 - CONCLUSIONS

8.1 CONTEXT OF THIS STUDY

This work was originally focused on iron sulphide (FeS) scale predictions but it quickly became clear that sulphides must be studied in combination with carbonates as they are both "pH-dependent" scales. Therefore, it is the entire coupled carbonate/sulphide system that governs the species available for scale formation. It was originally thought that the prediction of carbonate scale was a well-established and relatively routine procedure, but this turned out ***not*** to be the case. In discussion with some operating companies, it was claimed by some that they had a "correct" procedure for carrying out such calculations, but that these were not openly published. A thorough search showed that no rigorous procedure or workflow for carbonate scale prediction (in either "sweet" or sour systems) was in the public domain, as thus the first major task of this work was to develop one. Once this rigorous workflow was in place, then the correct modelling context was in place to model the iron sulphide system.

8.2 SUMMARY OF MAIN DEVELOPMENTS AND CONCLUSIONS

The main findings and conclusion of this work are as follows:

1. A rigorous procedure (workflow) for the prediction of carbonate and sulphide scales in oil and gas wells was developed (Verri et al., 2017a). This procedure involved taking available top side (separator) measurements of quantities and, with this feed composition, reconstructing the unique downhole chemistry of the aqueous phase (and the oil and gas). This downhole system, was then brought (numerically) "back up the wellbore" and the scale deposition profile was calculated. The final total system composition (oil, gas and brine composition) which reached the separator of course had

to agree with the input topside observations. The workflow was verified by taking a model case with perfect known data which was correctly reproduced by the workflow.

2. With this new workflow it is now possible to:

- Use commonly available field data to obtain scale prediction profiles from the near wellbore to the first stage of separation and further downstream if the phase separation is accounted for (mass balance). This is a very important feature because the software data input is not the same as the data readily available and iterative calculations must be performed to reconcile them;

- Use any selection of PVT and scale prediction software. This allows the user to choose from any available software and not have to compromise on PVT or scale prediction capabilities. It is recommended to use a full PVT software which implements SAFT type equations of state to better model CO_2 and H_2S partitioning;

- Calculate the reservoir water composition starting from the separator water chemistry assuming thermodynamic equilibrium is reached in the system;

- Calculate the full three phase volume and compositional changes from reservoir to separator.

3. This rigorous workflow was applied to two field scenarios to answer various important operational questions for each field. One was a field in the Middle East and the other was ion the North Sea, and each study is described in Chapter 4 and Chapter 5 respectively and in (Verri et al., 2017b, Ness et al., 2019).

4. There are significant challenges associated with the field measurement of dissolved iron required for iron sulphide scale predictions. To overcome the limitations of Fe^{2+} data in scale predictions, the concept of **Maximum Dissolved Iron** (MDI) was developed (Verri and Sorbie, 2017b) and applied to different field scenarios The maximum concentration of Fe^{2+} potentially present in the selected water gives an indication of whether iron may be produced from the reservoir, where most of the iron sulphide precipitation is expected to occur (providing Fe^{2+} availability) and provides a benchmark value to compare with field measurements and trends.

5. The impact of measurement errors or uncertainty around field data was studied to determine which input data is truly critical to carbonate and sulphide scale predictions (Ness and Sorbie, 2018a). It was shown that the most important field data for carbonate and sulphide scale predictions is Ca^{2+}, CO_2 and H_2S. Alkalinity and pH are calculated and constrained by these values. This does not mean that alkalinity and pH field measurements are to be disregarded but they can be used to compare with calculated data, estimate how close/far from equilibrium the system is, and to identify errors in field measurements etc.

6. It was found in this work that the presence of H_2S had an effect on the aqueous phase *Alkalinity*, and this rather surprising result had not previously been reported (Ness and Sorbie, 2017). The impact of H_2S on alkalinity and the effect of variable CO_2 concentration on H_2S speciation are critical to understand how varying one of these values changes the water chemistry. Whilst an increase in H_2S in a carbonate reservoir always corresponds to an increase in alkalinity and to more $CaCO_3$ precipitation in the well, an increase in CO_2 has two concurrent but opposing effects. When $[HCO_3^-]/[HS^-] > 1$ higher CO_2 causes more $CaCO_3$ precipitation in the wellbore due to the increased

reservoir rock dissolution and alkalinity. On the contrary, when $[HCO_3^-]/[HS^-]<1$ higher CO_2 causes less $CaCO_3$ precipitation in the wellbore as it shifts the HS-/H_2S equilibrium towards H_2S lowering alkalinity. This finding had hitherto not been reported and it was published from this work (Ness and Sorbie, 2018a).

7. The most widely used and well respected commercial software for scale prediction is an OLI product known as ScaleChem. However, ScaleChem has limited PVT model capabilities offering only a so called "modified" SRK (Soave-Redlich-Kwong) EOS which may not be sufficiently accurate to describe polar systems (CO_2 and H_2S). The research in this work has brought to light the impact of PVT modelling in carbonate and sulphide scale predictions. Using different PVT software, equations of state (EOS) and various input parameters can change scale prediction results very significantly and a specific EOS (SAFT type) may need to be used to model CO_2 and H_2S partitioning. The results presented show that there is a far greater discrepancy in scale prediction results when different PVT models are chosen compared to using different aqueous phase models for carbonates in particular, and by chemical coupling to the sulphide scale prediction.

8. For the prediction of iron sulphide (FeS) scale, the solubility product in scale prediction software can be very different and so the choice of aqueous phase model plays an important role on final sulphide scale prediction results. A detailed analysis of the ScaleChem model suggests that the effective solubility parameters used for sulphide scale predictions do not agree very well with published literature values. One consequence of this is that the quantities of free Fe^{2+} predicted in sour (H_2S rich) systems are too high.

9. Commercial integrated PVT and scale prediction software are more targeted to either one or the other set of calculations (i.e. PVT or aqueous chemistry). However, it is clear that both a robust PVT **and** scale prediction model must be used to obtain more reliable results. This is why one of the main goals of this research was to develop a workflow to study the impact of software choice and overcome this problem by allowing the use of ***any*** PVT and scale prediction software (integrated or standalone).

10. The results of this work strongly support the need for more experimental data to improve the database of both PVT and aqueous phase models used in scale predictions. This data includes but is not limited to three phase mutual CO_2 and H_2S solubility, improved iron sulphide solubility products and the thermodynamics of soluble iron sulphide species in produced water. Improving scale prediction software with a better experimental database is only part of the solution to improve scale prediction calculations. The application of a rigorous procedure (such as the one proposed in this work), good quality field data to use as software data input and a competent investigation of the specific field scenario is fundamental to obtain reliable results. Finally, scale predictions are not a "one -off" calculation but have to be reassessed every time a change in production conditions occurs. Hence, reviewing field data collected over time (e.g. produced fluids compositions) and field observations such as well response to the chemical treatment program contributes strongly to the improvement of scale prediction results.

8.3 FUTURE WORK

From the results of this work, it is clear that there are some important aspects of carbonate and sulphide scales that should be investigated further in order to improve scale predictions. These are:

(i) ***Coupling with a Corrosion Model:*** This would involve combining the study of bulk phase precipitation of FeS with surface corrosion reactions for iron sulphide scale. Corrosion plays a major role in the formation of iron sulphide in oil and gas wells and in many cases it is the main source of iron. Hence, a powerful iron sulphide scale prediction tool would combine full PVT and aqueous phase equations with a good corrosion model. However, there is still much debate on sour corrosion mechanisms and different corrosion models are likely to produce very different results. However, the Workflow described in this thesis would provide a reliable set of aqueous solution compositions as ***input*** for any corrosion model; and the model could in turn respond to any Fe^{2+} (or other species) produced by the corrosion model.

(ii) ***Inclusion of Kinetics:*** Introducing ***kinetics*** to scale prediction calculations is a topic that has been discussed for many years. However, the lack of reliable experimental data, the large number of variables impacting kinetics and the challenges in field data gathering for this purpose mean that the industry is still a long way away from being able to deliver very reliable kinetic scale predictions. Different software packages offer various options to attempt to account for kinetics, but the parameters required or the selection of reactions are still somewhat arbitrary and data is certainly lacking.

(iii) ***Different Forms of FeS:*** Work is required to try to understand the formation and transformation of different crystalline forms of iron sulphide (FeS) in oil and gas systems (mackinawite, pyrite, pyrrhotite etc.). The formation and transformation of different iron sulphide forms is associated with various parameters (watercut, amount of H_2S in the gas, etc.) and is certainly affected by kinetics. Hence, the goal of predicting different forms of iron sulphide in real field scenarios presents very similar challenges to that of introducing kinetics in pH-dependent scale predictions.

(iv) ***Dissolved Fe Species:*** The role of dissolved iron species was studied and described in the literature review of this thesis. However, the role of these species in oil and gas system brines needs further study. Although dissolved iron sulphide species have been investigated in marine environments, it is not clear what role these compounds play in oil and gas wells and whether their presence could actually impact Fe^{2+} availability in the reaction of iron sulphide precipitation. If the system of equations could be more clearly defined, then these could relatively straightforwardly be included in current scale prediction codes. This activity could also greatly assist with the problem of interpreting "total Fe" reported in oilfield data, as discussed in the literature review in Chapter 2.

(v) ***Define "correct" PVT model:*** considering the major impact that PVT models have on pH-dependent scale predictions, defining the correct PVT to use is an important step forward in this field. Together with gathering 3-phase mutual CO_2/H_2S solubility experimental data to improve PVT modelling, a comparison between the modelling results and field data is necessary. However, there are additional challenges with field sample collection and analysis (particularly of CO_2 and H_2S in gas/oil/water at variable temperature and pressure) that also need to be addressed.

Chapter 9- REFERENCES

AFTEN, C. W. & ROBERTS, G. *New Compounds for Hydrogen Sulfide Scavenging and Iron Sulfide Control*, SPE International Symposium on Oilfield Chemistry, SPE-141286-MS, 2011, The Woodlands, Texas, USA

AL-HARBI, B. G., GRAHAM, A. J. & SORBIE, K. S. *Iron Sulphide Inhibition and Interaction with Zinc and Lead Sulphide*, SPE International Oilfield Scale Conference and Exhibition, SPE-190743-MS, 2018, Aberdeen, Scotland, UK

AL-HUMAIDAN, A. Y. & NASR-EL-DIN, H. A. *Optimization of Hydrogen Sulfide Scavengers Used During Well Stimulation*, SPE International Symposium on Oilfield Chemistry, 1999, Houston, Texas

AMEND, J. P., EDWARDS, K. J. & LYONS, T. W. 2004. *Sulfur Biogeochemistry - Past and Present*, Boudler, CO, The Geological Society of America.

ANDERKO, A. & SHULER, P. J. 1997. A Computational Approach to Predicting the Formation of Iron Sulfide Species Using Stability Diagrams. *Computers & Geosciences.*

BAHADORI, A. 2014. Corrosion Inhibitor Evaluations. *Corrosion and Materials Selection: A Guide for the Chemical and Petroleum Industries.* John Wiley & Sons, Ltd.

BANAŚ, J., LELEK-BORKOWSKA, U., MAZURKIEWICZ, B. & SOLARSKI, W. 2007. Effect of CO_2 and H_2S on the Composition and Stability of Passive Film on Iron Alloys in Geothermal Water. *Electrochimica Acta.*

BELZILE, N., CHEN, Y. W., CAI, M. F. & LI, Y. 2004. A Review on Pyrrhotite Oxidation. *Journal of Geochemical Exploration.*

BRANKLING, D., BAYMAN, M. & JENVEY, N. *Formation and Control of the Vaterite Scale Polymorph of Calcium Carbonate in the Galley Field Development*, International Symposium on Oilfield Scale, SPE-68304-MS, 2001, Aberdeen, United Kingdom

BREZINSKI, M. *Chelating Agents in Sour Well Acidizing: Methodology or Mythology*, SPE European Formation Damage Conference, SPE-54721-MS, 1999, The Hague, Netherlands

BROWNLEE, J. K., DOUGHERTY, J. A., SAIMA, T. & HAUSLER, R. H. 2000. Solving Iron Sulfide Problems in an Offshore Gas Gathering System. *Corrosion.*

BRUNNER, E., PLACE, M. C., JR. & WOLL, W. H. 1988. Sulfur Solubility in Sour Gas. *Journal of Petroleum Technology.* Society of Petroleum Engineers.

BURGER, E. & JENNEMAN, G. *Forecasting the Effects of Reservoir Souring From Waterflooding a Formation Containing Siderite*, Proceedings of SPE International Symposium on Oilfield Chemistry, SPE-121432-MS, 2009, The Woodlands, TX

BURGER, E. D., JENNEMAN, G. E. & CARROLL, J. J. *On the Partitioning of Hydrogen Sulfide in Oilfield Systems*, SPE International Symposium on OIlfied Chemistry, SPE-164067-MS, 2013, Texas, USA

CALSEP. 2015. *PVTsim NOVA* [Online]. Available: https://www.pvtsimnova.com/ [Accessed].

CMG. 2017. *Winprop* [Online]. Available: http://www.cmgl.ca/winprop [Accessed].

COLE, J., NEBRIJA, E. L., SAGGAF, M. M., AL-SHABEEB, A. N., DEN BOER, L. & DOYEN, P. M. 2003. Integrated 3D Reservoir Modeling for Permian Khuff Gas Development in Ghawar Field, Saudi Arabia. *The Leading Edge.*

COLLINS, I. R. & JORDAN, M. M. 2003. Occurrence, Prediction, and Prevention of Zinc Sulfide Scale Within Gulf Coast and North Sea High-Temperature and High-Salinity Fields. *SPE Production & Facilities.*

COOMBE, D., HUBERT, C. & VOORDOU, G. *Mechanistic Modelling of H2S Souring Treatments by Application of Nitrate or Nitrite*, Canadian International Petroleum Conference, 2013, Calgary, Alberta

CSÁKBERÉNYI-MALASICS, D., RODRIGUEZ-BLANCO, J. D., KIS, V. K., REČNIK, A., BENNING, L. G. & PÓSFAI, M. 2012. Structural Properties and Transformations of Precipitated FeS. *Chemical Geology.*

DANESH, A. 1998. *PVT and Phase Behaviour of Petroleum Reservoir Fluids*, Elsevier.

DAVISON, W. 1991. The Solubility of Iron Sulphides in Synthetic and Natural Waters at Ambient Temperature. *Aquatic Science.*

DAVISON, W., PHILLIPS, N. & TABNER, B. J. 1999. Soluble Iron Sulfide Species in Natural Waters: Reappraisal of Their Stoichiometry and Stability Constants. *Aquatic Sciences.*

DEAN, J. A. 1999. *Handbook of Chemistry*.

DICKSON, A. G. 1981. An Exact Definition of Total Alkalinity and a Procedure for the Estimation of Alkalinity and Total Inorganic Carbon From Titration Data. *Deep Sea Research Part A. Oceanographic Research Papers.*

DOS SANTOS, L. C., ABUNAHMAN, S. S., TAVARES, F. W., RUIZ AHÓN, V. R. & KONTOGEORGIS, G. M. 2015. Cubic Plus Association Equation of State for Flow Assurance Projects. *Industrial & Engineering Chemistry Research.* American Chemical Society.

EVANS, P. & DUNSMORE, B. *Reservoir Simulation of Sulfate Reducing Bacteria Activity in the Deep Sub-Surface*, CORROSION 2006, NACE-06664, 2006, San Diego, California

EXPRO. 2015. *MultiScale* [Online]. Available: http://multiscale.no/downloads/brochures-and-data-sheet/ [Accessed].

FADAIRO, A. A., AKO, C. H. & FALODE, O. A. *Elemental Sulphur Induced Formation Damage Management in Gas Reservoir*, SPE International Conference on Oilfield Scale, SPE-154980-MS, 2012, Aberdeen, UK

FANG, H., BROWN, B., YOUNG, D. & NEŠIĆ, S. *Investigation of Elemental Sulfur Corrosion Mechanisms*, NACE Corrosion, NACE 11398, 2011,

FIROOZABADI, A. 1999. *Thermodynamics of Hydrocarbon Reservoirs*, McGraw Hill.

FLEMING, N., RAMSTAD, K., ERIKSEN, S. H., MOLDRHEIM, E. & JOHANSEN, T. R. 2007. Development and Implementation of a Scale-Management Strategy for Oseberg Sør. *SPE Production & Operations.* Society of Petroleum Engineers.

FORD, W. G. F., WALKER, M. L., HALTERMAN, M. P., PARKER, D. L., BRAWLEY, D. G. & FULTON, R. G. *Removing a Typical Iron Sulfide Scale: The Scientific Approach*, SPE Rocky Mountain Regional Meeting, SPE-24327-MS, 18-21 May 1992, Casper, Wyoming

FRIEDMAN, G. & SCHULTZ, D. 1994. Precipitation of vaterite ($CaCO_3$) during oil field drilling. *Mineralogical Magazine.*

GAO, S., JIN, P., BROWN, B., YOUNG, D., NESIC, S. & SINGER, M. 2017. Corrosion Behavior of Mild Steel in Sour Environments at Elevated Temperatures. *CORROSION*.

GARZON, F. O., NASR-EL-DIN, H. A., AL-MUTAIRI, S. H. & AL-HARITH, A. *Lessons Learned From Repickling Old / Sour Gas Wells*, SPE Middle East Oil and Gas Show and Conference, SPE-105633-MS, 2007, Manama, Bahrain

GILBERT, P. D., GRECH, J. M. & TALBOT, R. E. *Tetrakishydroxymethylphosphonium sulfate (THPS) for dissolving iron sulfides downhole and topside - A study of the chemistry influencing dissolution*, CORROSION 2002, 2002, Denver, Colorado

HAJJ, H. E., PENG, Y., FAN, C., ALBURAIKAN, R., LEAL, J. & CHANG, F. *A Systematic Approach to Dissolve Iron Sulfide Scales*, SPE Middle East Oil & Gas Show and Conference, 2015, Manama, Bahrain

JACOBS, I. C. & THORNE, M. A. *Asphaltene Precipitation During Acid Stimulation Treatments*, SPE Formation Damage Control Symposium, 1986, Lafayette, Louisiana

JASINSKI, R., FLETCHER, P., TAYLOR, K. & SABLEROLLE, W. *Calcite Scaling Tendencies for North Sea HTHP Wells: Prediction, Authentication and Application*, SPE Annual Technical Conference and Exhibition, SPE-49198-MS, 1998, New Orleans, Louisiana

JOHNSON, R. J., FOLWELL, B. D., WIREKOH, A., FRENZEL, M. & SKOVHUS, T. L. 2017. Reservoir Souring – Latest developments for application and mitigation. *Journal of Biotechnology*.

JORDAN, M. M., SJURSAETHER, K., EDGERTON, M. C. & BRUCE, R. *Inhibition of Lead and Zinc Sulphide Scale Deposits Formed During Production From High Temperature Oil and Condensate Reservoirs*, SPE Asia Pacific Oil & Gas Conference, 2000, Brisbane, Australia

KAASA, B. 1998. *Prediction of pH, Mineral Precipitation and Multiphase Equilibria During Oil Recovery*. Doctor of philosophy, Norwegian University of Science and Technology.

KAASA, B. & OSTVOLD, T. *Alkalinity in Oil Field Waters. What Alkalinity is and How it is Measured.*, International Symposium of Oilfield Chemistry, SPE-37277-MS, 1997, Houston, Texas

KAASA, B. & OSTVOLD, T. *Prediction of pH and Mineral Scaling in Waters With Varying Ionic Strenght Containing CO_2 and H_2S for*

0<T(C)<200 and 1<P(bar)<500, NACE Corrosion, NACE-98062, 1998, San Diego, California

KAN, A. T. & TOMSON, M. B. *Scale Prediction for Oil and Gas Production*, International Oil and Gas Conference and Exhibition in China, SPE-132237-MS, 2010, Beijin, China

KO, S., WANG, X., KAN, A. T. & TOMSON, M. B. *Identification of Novel Chemicals for Iron Sulfide Scale Control and Understanding of Scale Controlling Mechanism*, SPE International Conference on Oilfield Chemistry, SPE-193550-MS, 2019, Galveston, Texas, USA

KONTOGEORGIS, G. M. & FOLAS, G. K. 2009. Thermodynamic Models for Industrial Applications: From Classical and Advanced Mixing Rules to Association Theories. Wiley.

KONTOGEORGIS, G. M. & FOLAS, G. K. 2010a. Applications of CPA to the Oil and Gas Industry. *Thermodynamic Models for Industrial Applications.* John Wiley & Sons, Ltd.

KONTOGEORGIS, G. M. & FOLAS, G. K. 2010b. *Thermodynamic Model for Industrial Applications*, Wiley.

KRAUSKOPF, K. B. 1995. Solution-Mineral Equilibria Part 1: Carbonates. *Introduction to Geochemistry.* McGraw Hill.

KUNANZ, H., WÖLFEL, S. & LEOBEN, M. *Scale Removal with Ultrasonic Waves*, SPE International Oilfield Scale Conference and Exhibition, SPE-169770-MS, 2014, Aberdeen, Scotland

KVAREKVAL, J., NYBORG, R. & CHOI, H. 2003. Formation of multilayer iron sulfide films during high temperature CO_2/H_2S corrosion of carbon steel. *Corrosion 2003.*

LARSEN, T., OSTVOLD, T. & MCCARTNEY, R. A. Understanding $CaCO_3$ Precipitation during Oil Recovery. Oilfield Chemistry Symposium, 2010 Geilo, Norway.

LEAL, J., SOLARES, J. R., NASR-EL-DIN, H. A., FRANCO, C., GARZON, F., MARRI, H. M., AQEEL, S. A. & IZQUIERDO, G. *A Systematic Approach To Remove Iron Sulphide Scale : A Case History*, SPE Middle East Oil and Gas Show and Conference, SPE 105607-MS, 2007, Manama, Bahrain

LEHMANN, M. & FIROUZKOUHI, F. *A New Chemical Treatment to Inhibit Iron Sulfide Deposition*, SPE International Oilfield Scale Conference, SPE-114065-MS, 2008, Aberdeen, UK

LEWIS, A. E. 2010. Review of Metal Sulphide Precipitation. *Hydrometallurgy.* Elsevier B.V.

LOPEZ, T. H., YUAN, M., WILLIAMSON, D. A. & PRZYBYLINSKI, J. L. *Comparing Efficacy of Scale Inhibitors for Inhibition of Zinc Sulfide and Lead Sulfide Scales*, SPE Oilfield Scale International Symposium, 2005, Aberdeen, UK

MA, J., FUSS, T. & SHI, J. *Iron Sulfide Scale Deposition in Deep Sour Reservoirs*, SPE International Conference and Exhibition on Formation Damage Control, SPE-179009-MS, 2016, Lafayette, LA

MACKAY, E. J., MATHARU, A. P., SORBIE, K. S., JORDAN, M. M. & TOMLINS, R. *Modeling of Scale Inhibitor Treatments in Horizontal Wells: Application to the Alba Field*, SPE Formation Damage Control Conference, SPE-39452-MS, 1998, Lafayette, Louisiana

MCCARTNEY, R. A., DUPPENBECKER, S. S. & CONE, R. *Constraining the Conditions of Scale Deposition in a Gas Condensate Well: A Case Study*, SPE International Oilfield Scale Conference and Exhibition, SPE-169804-MS, 2014, Aberdeen, Scotland

MIRZA, M. S. & PRASAD, V. *Scale Removal in Khuff Gas Wells*, Middle East Oil Show and Conference, 1999, Bahrain

MURPHY, R. & STRONGIN, D. R. 2009. Surface Reactivity of Pyrite and Related Sulfides. *Surface Science Reports.* Elsevier B.V.

NACE. *Monitoring Corrosion in Oil and Gas Production with Iron Counts*, SP0192-2012, 2012,

NANCOLLAS, G. H. & SAWADA, K. 1982. Formation of Scales of Calcium Carbonate Polymorphs: The Influence of Magnesium Ion and Inhibitors. *Journal of Petroleum Technology.* Society of Petroleum Engineers.

NASR-EL-DIN, H. A. & AL-HUMAIDAN, A. Y. *Iron Sulfide Scale: Formation Removal and Prevention*, International Symposium on Oilfield Scale, 2001, Aberdeen, United Kingdom

NASR-EL-DIN, H. A., AL-HUMAIDAN, A. Y., MOHAMED, S. K. & AL-SALMAN, A. M. *Iron Sulfide Formation in Water Supply Wells With Gas Lift*, SPE International Symposium on Oilfield Chemistry, SPE-65028-MS, 2001, Houston, TX

NESS, G. & SORBIE, K. S. The Impact of Reservoir Souring on Calcium Carbonate Scaling Risk. Reservoir Microbiology Forum, 2017 London, UK. Energy Institute.

NESS, G. & SORBIE, K. S. 2018a. The Impact of Field Measurements and Data Handling Procedures on Carbonate and Sulphide Scale Predictions. *SPE Production & Operations.*

NESS, G. & SORBIE, K. S. *Rigorous Carbonate and Sulphide Scale Predictions: What Really Matters?*, SPE International Oilfield Scale Conference and Exhibition, SPE-190726-MS, 2018b, Aberdeen, Scotland, UK

NESS, G., SORBIE, K. S., LUGO, N. & KELLY, C. *The Impact of H_2S on Carbonate Scaling risk. A Field Case Study.*, SPE International Conference on Oilfield Chemistry, SPE-193583-MS, 2019, Galveston, TX

NING, J., ZHENG, Y., YOUNG, D., BROWN, B. & NESIC, S. *A Thermodynamic Study of Hydrogen Sulfide Corrosion of Mild Steel*, CORROSION 2013, NACE-2013-2462, 2013, Orlando, Florida

OKOCHA, C., KAISER, A., WYLDE, J., PETROZZIELLO, L., HAEUSSLER, M., KAYSER, C., CHEN, T., QIWEI, W., CHANG, F. & KLAPPER, M. *Review of Iron Sulfide Scale: The Facts & Developments and Relation to Oil and Gas Production*, SPE Kingdom of Saudi Arabia Annual Technical Symposium and Exhibition, SPE-192207-MS, 2018, Dammam, Saudi Arabia

OLAJIRE, A. A. 2015. A Review of Oilfield Scale Management Technology for Oil and Gas Production. *Journal of Petroleum Science and Engineering.*

OLI. 2016. *ScaleChem* [Online]. Available: https://www.olisystems.com/oli-studio-scalechem [Accessed 20/08/2019].

PANTHI, S. R. Carbonate Chemistry and Calcium Carbonate Saturation State of Rural Water Supply Projects in Nepal. International Water Technology Conference, 2003 Egypt.

PAULO, J., MACKAY, E. J., MENZIES, N. & POYNTON, N. *Implications of Brine Mixing in the Reservoir for Scale Management in the Alba Field*, SPE International Symposium on Oilfield Scale, SPE-68310-MS, 2001, Aberdeen

PEDERSEN, K. S. & CHRISTENSEN, P. L. 2007. *Phase Behavior of Petroleum Reservoir Fluids*, CRC Press - Taylor & Francis Group.

PLELLIS, C. 2012. Occurrence of Pyrophoric Iron Immune to Chemical Washing in Vacuum Distillation Columns. *Journal of Loss Prevention in the Process Industries.* Elsevier Ltd.

PRZYBYLINSKI, J. L. *Iron Sulfide Scale Deposit Formation and Prevention under Anaerobic Conditions Typically Found in the Oil Field*, SPE International Symposium on Oilfield Chemistry, SPE-65030-MS, 2001, Houston, Texas

RAHIM, Z., AL-ANAZI, H., AL-KANAAN, A. & AZIZ, A. A. *Successful Exploitation of Khuff-B Low Permeability Gas Condensate Reservoir through Optimized Development Strategy*, SPE/DGS Saudi Arabia Section Technical Symposium and Exhibition, SPE-136953-MS, 2010, Al-Khobar, Saudi Arabia

RAMACHANDRAN, S., AL-MUNTASHERI, G., LEAL, J. & WANG, Q. *Corrosion and Scale Formation in High Temperature Sour Gas Wells : Chemistry and Field Practice Existing Knowledge about FeS Scales*, SPE International Symposium on Oilfield Chemistry, SPE-173713-MS, 2015a, The Woodlands, Texas, USA

RAMACHANDRAN, S., GUPTA, A., AL-MUNTASHERI, G., LEAL, J. & SYAFIL, I. *Analysis of High Temperature Sour Gas Wells to Mitigate Corrosion and Scale Formation*, SPE Saudi Arabia Section Annual Technical Symposium and Exhibition, SPE-178001-MS, 2015b, Al-Khobar, Saudi Arabia

RICKARD, D. 1989. Experimental Concentration-Time Curves for the Iron(II) Sulphide Precipitation Process in Aqueous Solutions and Their Interpretation. *Chemical Geology.*

RICKARD, D. 1995. Kinetics of FeS Precipitation: Part 1. Competing Reaction Mechanisms. *Geochimica et Cosmochimica Acta.*

RICKARD, D. 2006. The Solubility of FeS. *Geochimica et Cosmochimica Acta.*

RICKARD, D. & LUTHER, G. W. 2007. Chemistry of Iron Sulfides. *Chemical Reviews.*

ROBINSON, D. B. & PENG, D. Y. 1978. *The Characterization of the Heptanes and Heavier Fractions for the GPA Peng-Robinson Programs*, Gas Processors Association.

ROYAL INSTITUTE OF TECHNOLOGY, K. 2013. *MINTEQ* [Online]. Available: https://vminteq.lwr.kth.se/ [Accessed 20/08/2019].

SALMA, T. *Cost Effective Removal of Iron Sulfide and Hydrogen Sulfide from Water Using Acrolein*, SPE Permian Basin Oil and Gas Recovery Conference, SPE-59708-MS, 2000, Midland, Texas

SAVIN, A. J., ADAMSON, B., WYLDE, J. J., KERR, J. R., KAYSER, C. W. & TRALLENKAMP, T. *Sulfide Scale Control : A High Efficacy Breakthrough Using an Innovative Class of Polymeric Inhibitors*, SPE International Oilfield Scale Conference and Exhibition, SPE-169777-MS, 2014, Aberdeen, Scotland

SHENG, J. 2013. *Enhanced Oil Recovery Field Case Studies*, Gulf Professional Publishing.

SILVA, D. 2017. *Mineral Scale Prediction Modelling: Precipitation of $CaCO_3$ Scale in CO_2-Water Alternating Gas Production System.* PhD Petroleum Engineering, Heriot-Watt University.

SILVA, D., SORBIE, K. S., G., N. & MACKAY, E. J. *Carbonate and Sulphide Scale Prediction Modelling in Auto-Scaling Processes,* SPE Oilfield Scale Conference, SPE-190711-MS, 2018, Aberdeen, Scotland

STANDLEE, S., EFIRD, K. D. & SPILLER, D. *Under Deposit Corrosion from Iron Sulfide*, Corrosion 2011, NACE-11266, 2011, Houston, TX

SUN, W. & NEŠIĆ, S. 2009. A Mechanistic Model of Uniform Hydrogen Sulfide/Carbon Dioxide Corrosion of Mild Steel. *CORROSION.*

SUN, W., NEŠIĆ, S. & PAPAVINASAM, S. *Kinetics of Iron Sulfide and Mixed Iron Sulfide/Carbonate Scale Precipitation in CO_2/H_2S Corrosion,* CORROSION 2006, NACE-06644, 2006, San Diego, California

SUN, W., NEŠIĆ, S., YOUNG, D. & WOOLLAM, R. C. 2008. Equilibrium Expressions Related to the Solubility of the Sour Corrosion Product Mackinawite. *Industrial and Engineering Chemistry Research.*

SVENNINGSEN, G., PALENCSAR, A. & KVAREKVAL, J. *Investigation Of Iron Sulfide Surface Layer Growth In Aqueous H_2S/CO_2 Environments,* Corrosion 2009, NACE-09359, 2009, Atlanta, GA

TANG, Y., VOELKER, J., KESKIN, C., XU, Z.-G., HU, B. & JIA, C. *A Flow Assurance Study on Elemental Sulfur Deposition in Sour Gas Wells,* SPE Annual Technical Conference and Exhibition, SPE-147244-MS, 2011, Denver, CO, USA

VAN DER STAR, W. R. L., LATIL, M.-N., VAN DER ZON, W., INEKE, E., MARCELLIS, F., VAN EIJDEN, J., BAAIJENS, T., BOL, G. & LOMANS, B. P. Microbial Induced Carbonate Precipitation as a Sand Control Measure for Oil Wells. Reservoir Microbiology Forum, 2017 London, UK. Energy Institute.

VERINK JR., E. D. 2011. Simplified Procedure for Constructing Pourbaix Diagrams. *Uhlig's Corrosion Handbook.* John Wiley & Sons.

VERRI, G. & SORBIE, K. S. *The Impact of Field Measurements, Data Handling Procedures and Software Selection on Carbonate and Sulphide Scale Predictions,* SPE Symposium: Production

Enhancement and Cost Optimisation, SPE-189218-MS, 7-8 November 2017 2017a, Kuala Lumpur, Malaysia

VERRI, G. & SORBIE, K. S. *Iron Sources in Sour Wells: Reservoir Fluids or Corrosion?*, NACE Corrosion, 2017b, New Orleans

VERRI, G., SORBIE, K. S. & SILVA, D. 2017a. A Rigorous General Workflow for Accurate Prediction of Carbonate and Sulphide Scaling Profiles in Oil and Gas Wells. *Journal of Petroleum Science and Engineering.*

VERRI, G., SORBIE, K. S., SINGLETON, M. A., HINRICHSEN, C., WANG, Q., CHANG, F. F. & RAMACHANDRAN, S. 2017b. Iron Sulphide Scale Management in High H_2S and CO_2 Carbonate Reservoirs. *SPE Production & Operations.* Society of Petroleum Engineers.

VERRI, G., SORBIE, K. S., SINGLETON, M. A., SILVA, D., HINRICHSEN, C., WANG, Q. & CHANG, F. F. 2017c. A New Approach to Combined Sulphide and Carbonate Scale Predictions Applied to Different Field Scenarios. *SPE Production & Operations.*

VETTER, O., BENT, M. & KANDARPA, V. 1987. Three-Phase PVT and CO2 Partitioning. *SPE California Regional Meeting.*

VETTER, O. J. & FARONE, W. A. *Calcium Carbonate Scale in Oilfield Operations*, SPE Annual Technical Conference and Exhibition, SPE-16908-MS, 1987, Dallas, Texas

WALKER, M., DILL, W. & BESLER, M. 1990. Iron Control Provides Sustained Production Increase In Wells Containing Sour Gas. *Journal of Canadian Petroleum Technology.*

WANG, Q., AJWAD, H., SHAFAI, T. & LYNN, J. D. *Iron Sulfide Scale Dissolvers : How Effective Are They?*, SPE Saudi Arabia Section Technical Symposium and Exhibition, SPE-168063-MS, 2013a, Al-Khobar, Saudi Arabia

WANG, X., QU, Q., BERRY, S. & CUTLER, J. *Iron Sulfide Removal : A Nonacidic Alternative to Hydrochloric Acid Treatment*, SPE European Formation Damage Conference & Exhibition, SPE-165199-MS, 2013b, Noordwijk, The Netherlands

WARREN, E. A. & SMALLEY, P. C. 1994. *North Sea Formation Waters Atlas*, Geological Survey.

WHITSON, C. H. & KUNTADI, A. *Khuff Gas Condensate Development*, International Petroleum Technology Conference, IPTC-10692-MS, 2005, Doha, Qatar

WOLTHERS, M., CHARLET, L., VAN DER LINDE, P. R., RICKARD, D. & VAN DER WEIJDEN, C. H. 2005. Surface Chemistry of Disordered Mackinawite (FeS). *Geochimica et Cosmochimica Acta.*

WOLTHERS, M., VAN DER GAAST, S. J. & RICKARD, D. 2003. The Structure of Disordered Mackinawite. *American Mineralogist.*

WOOLLAM, R., TUMMALA, K., VERA, J. & HERNANDEZ, S. *Thermodynamic Prediction of $FeCO_3$/FeS Corrosion Product Films*, Corrosion 2011, NACE-11076, 2011, Houston, TX

WYLDE, J. J. *Sulfide Scale Control in Produced Water Handling and Injection Systems : Best Practices and Global Experience Overview*, SPE International Oilfield Scale Conference and Exhibition, SPE-169776-MS, 2014, Aberdeen, Scotland

WYLDE, J. J., DUTHIE, A. W. & MCALLISTER, H. *Root Cause Failure Analysis and Mitigation of Iron Sulfide Scale Deposition in the BP Bruce Produced Water Reinjection Plant*, CORROSION 2008, 2008, New Orleans, Louisiana

WYLDE, J. J., OKOCHA, C., BLUTH, M., SAVIN, A. & ADAMSON, B. *Iron Sulfide Inhibition : Field Application of an Innovative Polymeric*, SPE International Symposium on Oilfield Chemistry, 2015, The Woodlands, Texas, USA

WYLDE, J. J., OKOCHA, C., SMITH, R., MAHMOUDKHANI, A. & KELLY, C. J. *Dissolution of Sulfide Scale: A Step Change With a Novel, High Performance, Non-Mineral Acid Chemical*, SPE International Oilfield Scale Conference and Exhibition, SPE-179880-MS, 2016, Aberdeen, Scotland, UK

WYLDE, J. J., TURNER, N., AUSTILL, M., OKOCHA, C. & OBEYESEKERE, N. *Development, Testing and Field Application of a Novel Combination Foamer-Iron Sulfide Scale Inhibitor-Corrosion Inhibitor in East Texas*, SPE International Conference on Oilfield Chemistry, SPE-184584-MS, 2017, Montgomery, Texas, USA

WYLDE, J. J. & WINNING, I. G. *Challenges and Solutions Associated With the Development of an Iron Scale Dissolver Chemistry*, Corrosion, NACE 04730, 2004, New Orleans, Louisiana

ZHAO, J., JIN, L. Z., ZHANG, X. K. & LI, Q. M. 2011. Spontaneous Combustion Tendency of Sulfide Ores: A Perspective From TPO Data and Adsorption Properties. *Procedia Engineering.*

ZHENG, Y., NING, J., BROWN, B. & NEŠIĆ, S. 2015a. Electrochemical Model of Mild Steel Corrosion in a Mixed H_2S/CO_2 Aqueous

Environment in the Absence of Protective Corrosion Product Layers. *CORROSION*.

ZHENG, Y., NING, J., BROWN, B., YOUNG, D. & NESIC, S. *Mechanistic Study of the Effect of Iron Sulfide Layers on Hydrogen Sulfide Corrosion of Carbon Steel*, Corrosion 2015, NACE-2015-5933, 2015b, Dallas, TX